SAND2018-2505R

SANDIA REPORT

SAND201X-XXXX
Unlimited Release
March 8, 2018

SunShot Innovator in Residence Final Report

Dr. Jeff Koplow

Prepared by
Sandia National Laboratories
Albuquerque, New Mexico 87185 and Livermore, California 94550

Sandia National Laboratories is a multimission laboratory managed and operated by National Technology and Engineering Solutions of Sandia, LLC, a wholly owned subsidiary of Honeywell International, Inc., for the U.S. Department of Energy's National Nuclear Security Administration under contract DE-NA0003525.

Issued by Sandia National Laboratories, operated for the United States Department of Energy by National Technology and Engineering Solutions of Sandia, LLC.

Available to DOE and DOE contractors from
U.S. Department of Energy
Office of Scientific and Technical Information
P.O. Box 62
Oak Ridge, TN 37831

Telephone: (865) 576-8401
Facsimile: (865) 576-5728
E-Mail: reports@osti.gov
Online ordering: http://www.osti.gov/scitech

Available to the public from
U.S. Department of Commerce
National Technical Information Service
5301 Shawnee Rd
Alexandria, VA 22312

Telephone: (800) 553-6847
Facsimile: (703) 605-6900
E-Mail: orders@ntis.gov
Online order: http://www.ntis.gov/search

SAND201X-XXXX
March 8, 2018
Unlimited Release

SunShot Innovator in Residence Final Report

Dr. Jeff Koplow
Energy Innovation Department
Sandia National Laboratories
P.O. Box 969
Livermore, CA 94551

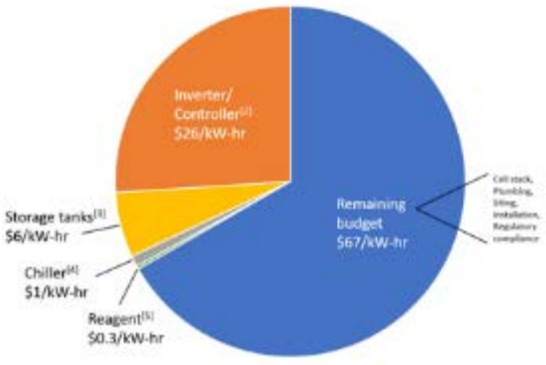

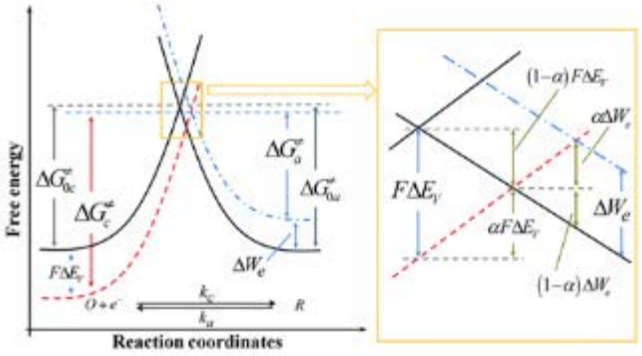

Lu et al., Phys. Chem. Chem. Phys., 2016, **18**, 4721-4727.

ACKNOWLEDGMENTS

The author wishes to acknowledge support from DOE's Solar Energy Technology Office and the Sunshot program. The author further wishes to acknowledge his Sandia colleagues Dr. Wayne Staats, Dr. Arthur Kariya, and Mr. Justin Vanness, each of whom made significant contributions to cell construction and design, and techno-economic analysis, and Kent Smith, who assisted with many aspects of mechanical fabrication. I would also like to express my sincerest gratitude to Dr. LeRoy Whinnery, who coordinated the subject matter expert briefing series in Year 2, and Dr. Jerry Simmons who strongly advocated for follow-on support of this work.

TABLE OF CONTENTS

FIGURES

EXECUTIVE SUMMARY

This report describes the development of Radical-Ion Flow Battery (RIFB) technology for electrochemical grid storage, and solar thermochemical cycles for conversion of concentrated solar energy to stored chemical energy. The Radical-Ion Flow Battery stores energy via electrolysis of a molten salt electrolyte such as $NaNO_2$ into an alkali metal and nitrogen dioxide, both of which can be stored as liquids in non-pressurized tanks. The use of extremely facile ion-radical single electron transfer reactions at both electrodes that entail no breaking of covalent bonds is directed towards minimizing thermodynamic irreversibility in the charge/discharge cycle, and eliminating the need for catalytically active electrode materials. Both kinetics and mass transport are also facilitated by the absence of diluent species; the battery electrolyte and active chemical ingredient are one and the same. Our underlying strategy for low-cost scalability is the use of only earth abundant starting materials (NaCl, N_2, O_2, and steel). The underlying strategy for avoiding the problem of capacity fade over 10,000 charge/discharge cycles is the use of extremely simple chemistry. It is argued that operation at elevated temperature is highly advantageous for very large-scale batteries from the standpoint of battery heat-sinking, access to ultrahigh conductivity electrolytes, and increased electrochemical kinetic rate constants. Numerous practical considerations, such as seals, insulators, and electrical feedthroughs are examined in detail, as are questions related to low-cost mass production and battery techno-economic analysis.

We also examine a novel thermochemical cycle for conversion of water and oxygen to hydrogen peroxide. Hydrogen peroxide has an energy storage density of 2.7 MJ/liter and has the further advantages that it can be used to directly drive heat engines such as gas turbines, or used to generate electricity in membrane-less fuel cells. This solar thermochemical cycle also has the benefits of earth abundant materials, environmentally friendly chemistry, and low peak process temperature (850 °C). Prior art solar thermochemical cycles operating at much higher temperatures encounter numerous engineering challenges that tend to drive up cost and lower thermodynamic efficiency.

The structure of this report is intended to take the reader along the actual R&D path traversed during the course of this work, including refutation of early hypotheses, strategic pivots, and periodic points of reckoning to refine and/or redirect research strategy. Our intention is to show how the innovation process unfolds (and sometimes fails), rather than presenting only a highly polished distillation of final results.

1. INTRODUCTION

The goal of the SunShot Innovator in Residence program was to apply a multidisciplinary problem solving methodology to outstanding problems in the field of solar energy, wherein (a) problem solving goals are selected on the basis of market need in a manner that is technology agnostic, (b) questions related to real-world practicality are used as a powerful down-select tool in the ideation process, and (c) the broad subject matter expertise available at the national labs is strongly leveraged to quickly overcome R&D obstacles as they emerge. Many of the avenues for exploration in solar energy are self-evident, such as rethinking strategies for making PV panels as efficient as possible. Other topics that received consideration included the question of how to best manage production intermittency, optimizing extraction of power from large ensembles of PV panels at different operating points, opportunities for fundamental advances in dc-dc and dc-ac conversion technology (efficiency, cost, grid compatibility, etc.), rethinking aspects of PV panel and PV inverter thermal management, new panel deployment concepts to increase energy yield and reduce cost/complexity, methodologies for improving modularity and reducing installation/servicing costs, targeted efforts to eliminate the need for costly and/or unreliable components, improved thermodynamic cycles for CSP, high performance refractory and thermal reservoir materials for CSP, the application of CSP to thermochemical production of chemical fuels, potential high-value commercial applications for high-power, high-spatial-coherence ultraviolet light collected at CSP facilities, effective use of stranded capacity to supply power to non-time-sensitive applications such as desalination and electrolytic refining, and novel manufacturing processes for major system components. The project was divided into three execution phases: 1) literature and prior art review followed by prioritization of problem solving objectives, 2) ideation of novel technology solutions, and 3) research and development of proposed technology solutions subject to real-world techno-economic constraints.

As will be discussed shortly, we determined that grid storage was the most important remaining challenge hindering proliferation of solar energy technology. Much of the technical discussion that follows falls within the realm of chemistry; this was driven by the problem-solving needs of grid-scale energy storage, which we initially approached in a technology agnostic manner. Although it had been many years since our group had worked on any chemistry related R&D, quantitative analysis of application requirements – in particular cost and scalability – unambiguously indicated that energy storage in the form of chemical bonds provided the most realistic pathway to addressing the challenge of renewable power intermittency.

2. SSIR IDEATION PHASE

The ideation phase of the inaugural SSIR Project began in October of 2015. Early-stage work entailed an extensive overview of the field of solar power and an in-depth investigation of customer needs. The overarching goal of this project was to create whatever non-incremental technological breakthroughs are needed to allow renewable energy (principally solar power) to become a pillar of our energy economy. Referring to Figure 1, an underlying assumption of this work is that the only realistic pathway to rapid adoption of renewables is strong and permanent market price signaling. We must work with deliberate speed to reach an end-state scenario in which it becomes conventional wisdom that renewable energy is highly competitive in many applications. Given the tremendous progress to date in PV solar and wind technologies (Figure 2), there appeared to be three remaining areas in which game-changing technological innovation

was required to shift private-sector investment strategy to a more diverse range of energy sources:

1) Grid storage (principally to address intermittency of renewables)
2) Transmission (connection of remotely located renewables to the grid)
3) Vehicle battery technology (or synthetic fuels created from renewable energy)

SunShot Innovator in Residence Program

Overarching goal: Create whatever non-incremental technological breakthroughs are needed to allow solar power to displace fossil fuels as the basis of our energy economy.

Underlying assumption: The only realistic pathway to rapid adoption of renewables is strong and permanent market price signaling.

Buy-in objective: It must become conventional wisdom that fossil fuels are too expensive to compete with renewable energy.

Technology assessment: Tremendous progress to date in PV solar and wind. Three remaining areas in which game-changing technological innovation is required to shift private-sector investment strategy away from fossil fuels in favor of renewables:

1) Grid storage (principally to address intermittency of renewables)
2) Transmission (connection of remotely located renewables to the grid)
3) Vehicle battery technology (or synthetic fuels created from renewable energy)

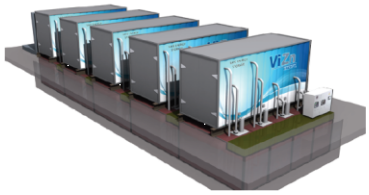

The grid storage problem

The long distance transmission problem

The EV battery problem

Figure 1: Guiding principles adopted by PI at the outset of the SSIR program.

The onset of cost-competitive renewables is real:

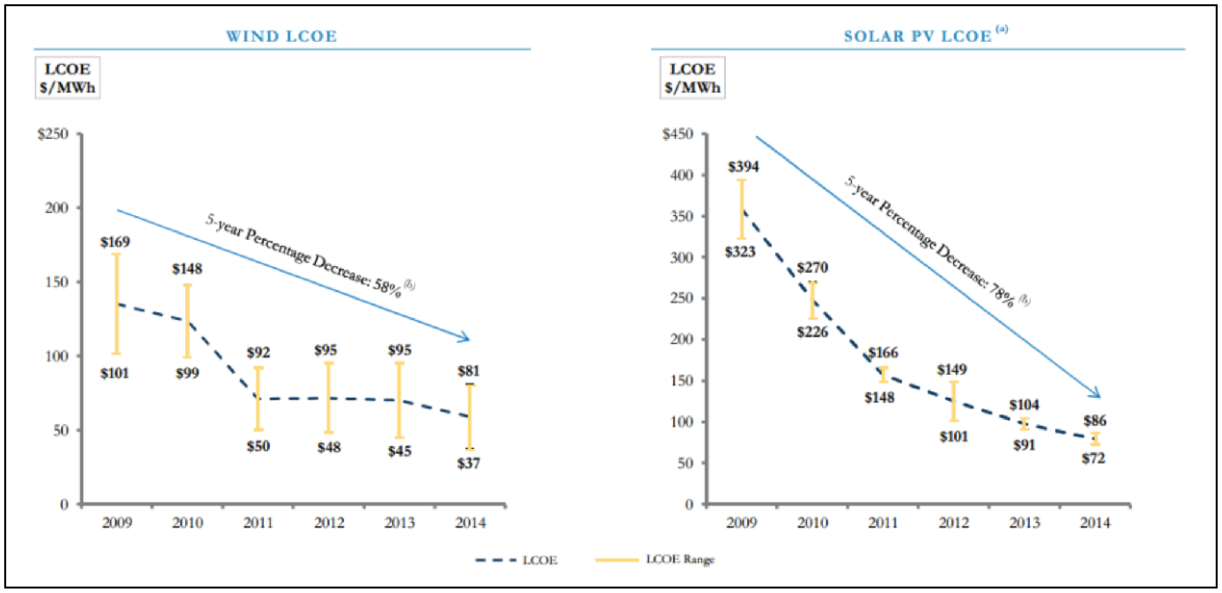

Wind may play a comparable role to solar power.

TRL development of a revolutionary advance in grid storage could be underwritten by both industries.

Figure 2: Longstanding uncertainty about the cost-competitiveness of renewable energy is fading quickly.

The first several months of the project explored two alternative Grid/Transmission/Vehicle technology pathways.

A) Solar-thermal-chemical-based: Thermal energy is used to directly drive non-spontaneous chemical reactions to create either stable chemical reagents that can be (1) efficiently converted to electricity on demand, and/or (2) used directly as fuel by the transportation sector.

B) Battery-based: Conversion of electricity generated by renewables to energy-dense electrochemical reagents that can later be converted back to electrical power, and that may also be transported economically to demand centers prior to being converted back to electrical power.

2.1. Solar thermal energy conversion exploratory work

Concentrating solar thermal power (CSP) has two intrinsic advantages over photovoltaic solar power:

1) Energy capture efficiency: Substantially all of the incident solar radiation that is collected by a device such as a concentrating solar mirror array can be converted directly to heat (e.g. on an optically absorbing surface). In contrast, the market average for energy conversion efficiency is 12-18% for current generation PV panels.[1]
2) Upfront cost: The per unit area manufacturing cost for mirrors used for concentrating solar power can be substantially lower than that of photovoltaic panels.

Assuming that some form of heat engine is used to convert the collected thermal energy into electrical power, there are however substantial penalties imposed by Carnot efficiency considerations, radiative losses associated with operation at high temperature, and numerous sources of parasitic loss in any real-world heat engine; the best solar-to-electrical conversion efficiencies achieved to date are of order 30% for parabolic-dish/Stirling-engine systems. Accordingly, increasing the efficiency with which collected thermal energy may be converted to electricity is a fundamentally important goal.

As is well known from the prior art, utility scale storage of renewable energy is another major difficulty that confronts intermittent renewables such as solar power and wind. An inability to store renewable energy that is generated on an intermittent basis substantially reduces the value of the power that is generated, limits market penetration of renewables, introduces significant uncertainty from the standpoint of investment ROI, necessitates costly countermeasures, and reduces the efficiency with which transmission lines, transformers, and other components of electrical grid are used.

As alluded to above, the other major challenge that confronts that confronts the energy industry is transportation fuel. In some applications, the ultimate goal is to largely eliminate the consumption of fossil fuels for transportation in favor of battery powered vehicles (wherein the electrical power for battery charging is provided by renewables), or vehicles that are powered from chemical fuels that are synthesized from raw materials such as water or carbon dioxide, using energy from renewable sources. The emergence of a practical and efficient route to renewable synthetic fuels could be used to supplement fossil fuels in the transportation sector, and it would also address the grid storage problem. If one or more synthetic fuels could be developed that are compatible with cheap and highly efficient fuel cell technology, this could be of great technological importance; combustion of fuels in traditional heat engines has many drawbacks, most notably intrinsic limitations on efficiency, mechanical complexity, maintenance requirements, and emissions. Important objectives therefore include:

1) A practical and cost-effective route to renewable synthetic fuels.
2) Generation of chemical fuels in the form of easily stored liquids.
3) Renewable liquid chemical fuels that are compatible with existing infrastructure.
4) Renewable liquid chemical fuels that can be converted to electrical power on demand at high efficiency.

The prior art on the subject of solar-to-fuel conversion is very extensive. At present, the only method that has been prototyped on a significant scale entails the use of renewable electrical power for electrolysis of water to generate hydrogen gas. The most obvious disadvantages of electrolytic hydrogen generation are that it consumes electrical power (e.g. from photovoltaic

solar plants), which is a far more valuable commodity than thermal power (e.g. such as that obtained from combustion or concentrating solar arrays), and that hydrogen fuel is difficult to store, especially in the context of transportation applications.

Nonetheless, the vast majority of the prior art in solar-to-fuel conversion technology focuses on thermochemical, electrochemical, and/or photochemical reduction of water and/or carbon dioxide. These approaches do not provide a straightforward route to the end goal of a practical liquid fuel. This is due to both the availability of water and carbon dioxide as readily available chemical feedstock, and also that the first step of cost effectively converting solar radiation to any form of chemical fuel, regardless of that fuel's logistical desirability, is an extremely challenging goal in and of itself. Accordingly, there is an extensive body of research on the subject of converting H_2 and CO to methanol and other candidate synthetic liquid fuels, and work directed towards storing H_2 in the form of condensed-phase chemical compounds such as metal hydrides.

A survey of the extensive literature on solar thermal chemical cycles investigated over the past few decades contains lessons learned that can roughly be translated into a set of design rules for new candidate solar thermal cycles.

1) It is imperative that the peak process temperature of any proposed solar thermal cycle be kept as low as possible. Much of the prior art contemplates using concentrated solar power to drive endothermic chemical reactions at temperatures upwards of 1400 °C. The use of such high process temperatures is highly counterproductive from the standpoint of (a) radiative losses, which scale as T^4, (b) requirements for exotic/expensive materials, and (c) the complexity of optical hardware needed to achieve high CSP concentration ratios.
2) It is imperative that the number of steps in any proposed chemical cycle be kept as small as possible, with the exception of steps that are trivial to carry out at very high yield, or multiple steps that can be carried out as a single concerted process.
3) If possible, it is desirable have only a single high-temperature endothermic reaction involving chemically benign constituents to provide the thermodynamic driving force for the reaction cycle. Having only one high temperature process can significantly simplify plant design.
4) It is important to avoid the use of reactants that are expensive, toxic, and/or difficult to work with. An exception may be granted for carbon monoxide because of its fundamental importance to the problem at hand, and other toxic species that are only formed as short-lived intermediates that are easy to contain, incapable of causing long term contamination of equipment, and have a short atmospheric lifetime.
5) It is desirable to minimize the use of reactions in which thorough mixing of the reactant species is intrinsically difficult to achieve. It is desirable to have reactants comprise "highly miscible" species, wherein the definition of miscible here is extended to mean chemical constituents that readily mix at all relevant length scales, thereby minimizing requirements for specialized apparatuses adapted to promoting interaction of reactants.
6) To the extent that reactants comprise chemical constituents that are recycled on a continuous basis, the process of separating these constituents for reuse must be simple and non-energy-intensive.

7) It is very important to avoid the use of reactions that are prone to unwanted side reactions.
8) It is desirable to choose reactions whose equilibrium constants are large enough that complete chemical conversion from reactants to products occurs automatically.
9) It is advisable to avoid reaction steps that require rapid quenching of the product species to avoid back reaction to the original starting products. For example, thermal dissociation of many oxides results in gas phase products that readily recombine upon exiting the reactor.
10) In many instances, it desirable to extract the products from a high temperature reactor in a manner that requires recuperation of some of the heat to achieve as high a cycle efficiency as possible. But it must also be kept in mind that in practice, many recuperator designs are complex/expensive and not particularly efficient. We should therefore consider the merit of high temperature reaction steps whose products have low heat capacity, in which case recuperation is less of a concern.
11) It is extremely important to avoid reactions that suffer from problems associated with chemical poisoning or deactivation of surface reaction sites. This is a critically important consideration, because reaction cycles that are sensitive to trace impurities and/or dependent on maintaining specific micro-morphology at reaction sites are vulnerable to deactivation over the course of thousands of successive reaction cycles.
12) Any reaction step that proposes some form of heterogeneous catalysis should very carefully scrutinized from the standpoint of catalyst longevity. If there are any plausible routes to catalysis deactivation, simple and powerful countermeasures such as restoration of a pristine surface by baking out at high temperature must be in place.

One way to look at the above design rules is to consider them a list of problem solving constraints that make finding an appropriate thermochemical cycle a difficult or impossible task. However, the above list of design rules can be used as a powerful down-select tool that can be used to quickly eliminate hundreds of candidate reactions that might otherwise prove to be ultimately impractical.

2.2. Proposal for a $H_2O + ½ O_2 \rightarrow H_2O_2$ thermochemical cycle

Having used the design rules above as a down-select tool, we will describe two novel proposed thermochemical energy cycles investigated in early Year 1. In the interest of brevity, we will not enumerate the dozen or so other less promising novel thermochemical cycles investigated. Indeed, the shortcomings of the less promising thermochemical cycles also contributed to the above design rules and precautions.

The first thermochemical cycle we describe entails the conversion of water and oxygen into hydrogen peroxide:

reaction 1: $2\ Na_2O_2 + 4\ H_2O \rightarrow 4\ NaOH + 2\ H_2O_2$
reaction 2: $4\ NaOH + 4\ CO_2 \rightarrow 4\ NaHCO_3$
reaction 3: $4\ NaHCO_3 + \Delta \rightarrow 2\ Na_2O + 4\ CO_2 + 2\ H_2O$
reaction 4: $2\ Na_2O + O_2 \rightarrow 2\ Na_2O_2$
———————————————————————————
net reaction: $2\ H_2O + O_2 \rightarrow 2\ H_2O_2$

wherein the symbol "Δ" denotes the input of heat into an endothermic reaction.
Hereafter we will refer to the above set of reactions as the "hydrogen peroxide solar thermal chemical cycle".

The product of the above reaction (H_2O_2) is a thermodynamically unstable chemical species:

$\Delta H^o = \Delta H^o_f$ (products) - ΔH^o_f (reactants)
ΔH^o = [2 (-191.17)] – [2 (–285.83) + 0] = +189.32 kJ
ΔS^o = [2 (+143.9)] – [2 (+69.91) + (+205.03)] = -57.05 J K^{-1}
ΔG^o = [2 (-134.03)] – [2 (–237.18) + 0] = +206.30 kJ

	ΔH^o_f (kJ mol^{-1})	ΔG^o_f (kJ mol^{-1})	ΔS^o_f (J mol^{-1} K^{-1})
H_2O (l)	-285.83	-237.18	+69.91
H_2O_2 (aq)	-191.17	-134.03	+143.9
O_2 (g)	0	0	+205.03

that is capable of storing a considerable amount of energy in liquid form at ambient temperature and pressure on an indefinite basis. In the above equations, numerical quantities such as ΔH^o = +189.32 kJ are meant to indicate that 189.32 kJ of heat are absorbed when 2 moles of H_2O (l) and 1 mole of O_2 (g) are combined to form 2 moles of H_2O_2 (l). It will be further understood that strictly speaking, the above thermodynamic calculations apply to the special case of all reactants and products in their standard state (e.g. 1 atmosphere pressure, 25 °C). For present purposes, such an assumption provides a reasonable basis for numerical calculations.

The chemical feedstock for the above reaction cycle comprises water and oxygen, both of which are readily available. The only product of the above thermochemical cycle is hydrogen peroxide; all other chemical species are intermediates that may be recycled on an indefinite basis. The products of H_2O_2 exothermic decomposition are water and oxygen, both of which are environmentally benign. Additional advantages of hydrogen peroxide as an energy storage medium are (a) the decomposition reaction is very easy to control, (b) it is readily adaptable to simple high-efficiency gas turbine driven generators, and (c) hydrogen peroxide is also a very promising candidate for simple membrane-less fuel cells (please see Figure 3 for example).

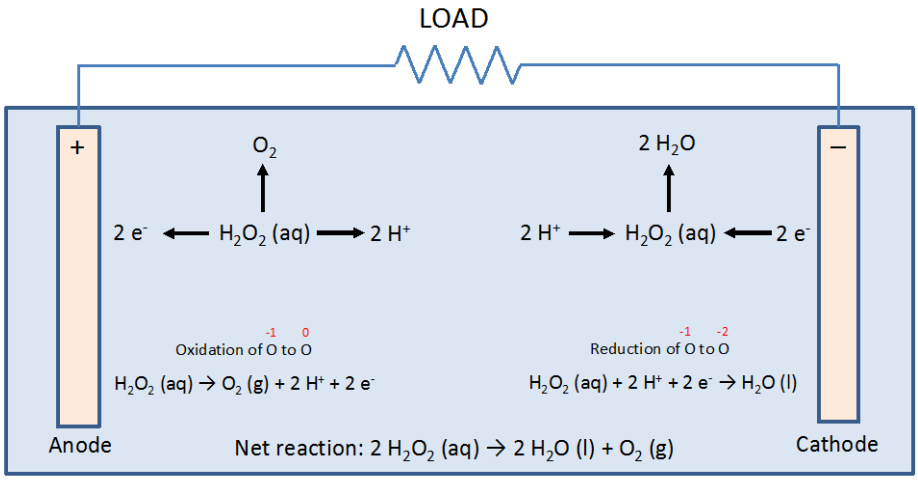

Figure 3: The hydrogen peroxide fuel cell is unusual in that it can implemented without an ion-selective membrane. This is a very attractive attribute from the standpoint of cost, performance, and long-term reliability.

storage medium	energy density by volume (MJ/liter)	energy density by mass (MJ/kg)
gasoline	44.4	32.4
hydrogen peroxide	2.7	3.8
lithium ion battery	0.46 - 0.72	0.83 - 3.6

The above energy density data[2] clearly indicate that hydrogen peroxide would be practical for grid storage from the standpoint of energy density because its energy density is higher than lithium-ion batteries, which are considered viable for grid storage in some installations. It is conceivable that the practicality and cost-effectiveness of H_2O_2 for utility-scale grid storage may exceed that of systems based on lithium batteries, and recently proposed systems based on anthraquinone redox reactions.[3]

Moreover, hydrogen peroxide may turn out to be practical for transportation applications as well. For example, assuming an on-board fuel cell efficiency of order 50%, the data in the above table indicate that H_2O_2 provides a factor of 2 to 3 improvement in volumetric energy density relative to the lithium ion batteries used in current generation electrical vehicles. It is also plausible that a simple piston or gas turbine engine based on thermal decomposition of H_2O_2 into high-pressure, high-temperature steam could be operated at an efficiency of 30%, which would still provide a 1.5 to 2X volumetric energy density advantage over lithium ion batteries.

Hydrogen peroxide is an important industrial chemical whose physical properties and handling precautions are well understood. To date hydrogen peroxide has been used as an energy storage medium in only specialty applications such as rockets, thrusters, torpedoes, and jet packs (typically in concentrations ranging from 70 to 98%[4]). If solar thermal production of H_2O_2 on a large scale proves to be feasible, the extraordinary simplicity of the hydrogen peroxide monopropellant decomposition reaction promises to make it adaptable to, and easy to optimize for, an extremely wide range of energy sector applications. In addition, concentrated hydrogen

peroxide is easy to store at ambient temperature and pressure in thin-walled tanks fabricated from chemically compatible materials such as polyethylene and aluminum. In practice, to avoid decomposition, trace quantities of chemical inhibitors such urea, sodium phosphate, or sodium stannate are typically added to provide long shelf life and reduce sensitivity to incidental contamination.

At this point it should be noted that in principle, the proposed thermochemical cycle could be carried out by an alternate method: directly converting NaOH to Na_2O by thermal dissociation. Writing out all of the steps of the thermodynamic cycle formally, we have:

reaction 1: $2\ Na_2O_2\ (s) + 4\ H_2O\ (l) \rightarrow 4\ NaOH\ (aq) + 2\ H_2O_2\ (aq)$
reaction 2: $4\ NaOH\ (aq) + \Delta \rightarrow 4\ NaOH\ (s)$
reaction 3: $4\ NaOH\ (s) + \Delta \rightarrow 2\ Na_2O\ (s) + 2\ H_2O\ (g) \uparrow$
reaction 4: $2\ H_2O\ (g) \rightarrow 2\ H_2O\ (l)$
reaction 5: $2\ Na_2O\ (s) + O_2\ (s) \rightarrow 2\ Na_2O_2\ (s)$
———————————————————————————————
net reaction: $2\ H_2O\ (l) + O_2\ (g) \rightarrow 2\ H_2O_2\ (l)$

The hypothetical reaction 3 above, involving direct thermal dissociation of sodium hydroxide, is predicted to be highly endothermic, but also accompanied by a large increase in entropy.

$4\ NaOH\ (s) + \Delta \rightarrow 2\ Na_2O\ (s) + 2\ H_2O\ (g) \uparrow$
$\Delta H^o = [2\ (-414.22) + 2\ (-241.82)] - [4\ (-425.61)] = +390.36\ kJ\ mol^{-1}$
$\Delta S^o = [2\ (+75.06) + 2\ (+188.72)] - [4\ (+64.46)] = +269.72\ J\ mol^{-1}\ K^{-1}$
$\Delta G^o = [2\ (-375.48) + 2\ (-228.59)] - [4\ (-379.53)] = +309.98\ kJ\ mol^{-1}$

Thus, in principle it might be possible for the above reaction to occur as written if anhydrous sodium hydroxide (NaOH (s)) can be brought to sufficiently high temperature. But in practice, NaOH (s) is observed to boil at 1388 °C at atmospheric pressure without chemical decomposition. Given that atmospheric pressure dissociation occurs in the gas phase at some temperature greater than 1388 °C, we may conclude that from a practical point of view the process temperature for direct dissociation of NaOH is prohibitively high. Moreover, even if this reaction were successfully carried out in the gas phase, separation of the resulting products would be very difficult.

On the other hand, a desirable feature of the NaOH to Na_2O conversion reaction is that because it so thermodynamically unfavorable, this single reaction can provide the thermodynamic driving force for the remainder of the thermochemical cycle as well as that required to produce a thermodynamically unstable product (H_2O_2) with a relatively high energy density.

The solution to the NaOH thermal dissociation concerns is to divide the process into a two-step reaction involving carbon dioxide:

$4\ NaOH + 4\ CO_2 \rightarrow 4\ NaHCO_3$
$4\ NaHCO_3 + \Delta \rightarrow 2\ Na_2O + 4\ CO_2 + 2\ H_2O$

wherein CO_2 is consumed in the first step and regenerated in the second step. Reaction 1, the formation of sodium bicarbonate from sodium carbonate and carbon dioxide, is spontaneous at room temperature and convenient to carry out. Reaction 2 actually occurs in two steps:

$2\ NaHCO_3\ (s) + \Delta \rightarrow Na_2CO_3\ (s) + CO_2\ (g) \uparrow + H_2O\ (g) \uparrow$
$2\ Na_2CO_3\ (s) + \Delta \rightarrow Na_2O\ (s) + CO_2\ (g) \uparrow$

The first of these two decomposition reactions proceeds readily at 200 °C. For the latter reaction, evolution of CO_2 (g) from Na_2CO_3 (s) is observed to occur at ~850 °C at atmospheric pressure. Accordingly, conversion of sodium bicarbonate to sodium oxide can be carried out as a single concerted process at 850 °C.

850 °C is a very manageable reaction temperature for a solar thermal reactor. This is very important from the standpoint of reducing T^4 radiative losses, the cost/complexity of reactor construction, and the degree of solar concentration required to achieve peak process temperature. Indeed, the degree of solar concentration required is significant from the standpoint of heliostat and mirror array cost/complexity.

In addition, it should be noted that the sodium carbonate dissociation step could be carried out at lower temperature by reducing the partial pressure of carbon dioxide well below 1 atmosphere (e.g. by dilution of the CO_2 effluent, or operation at reduced pressure) if deemed worthwhile. Finally, in certain embodiments extraction of hot Na_2O powder generated in the final reaction step from the reaction vessel is conducted in a manner that a substantial quantity of the heat contained therein is recovered for use in portions of the thermochemical cycle (i.e. for providing process heat to other parts of the cycle).

In the proposed reaction scheme, CO_2 also plays another important role, namely to neutralize NaOH generated by the hydrogen peroxide forming reaction:

$2\ Na_2O_2 + 4\ H_2O \rightarrow 4\ NaOH + 2\ H_2O_2$

For example, let us assume we maintain a partial pressure of 1 atmosphere of carbon dioxide by purging the reaction vessel with CO_2. For $P_{CO2} = 1$ atm, the dissociation constants of the various species present are such that:

$[H^+] = 1.3 \times 10^{-4}$ M
$[OH^-] = 7.7 \times 10^{-11}$ M
$[HCO_3^-] = 1.3 \times 10^{-4}$ M
$[CO_3^{2-}] = 5.6 \times 10^{-11}$ M

$[Na^+]$ is limited to $<< 1.3 \times 10^{-4}$ M because of the scarcity of anions present. This implies that the resulting hydrogen peroxide solution will be contaminated with only traces of sodium salt. The small amount of $NaHCO_3$ present may be converted to sodium phosphate by the addition of a small amount of phosphoric acid (with evolution of CO_2 gas). As mentioned earlier, trace

quantities of chemical inhibitors such as sodium phosphate are typically added to hydrogen peroxide solutions to ensure long shelf life and reduce sensitivity to incidental contamination.

Let us now examine the issue of preventing H_2O_2 product decomposition in further detail. In a long obsolete process for generating hydrogen peroxide in the laboratory, the reaction:

$2\ Na_2O_2 + 4\ H_2O \rightarrow 4\ NaOH + 2\ H_2O_2$

was typically carried out in ice cold dilute sulfuric acid to keep both the temperature and pH of the reaction mixture low enough to prevent decomposition of the H_2O_2 product into H_2O and O_2. This is unfortunate, because it would be much more convenient to react a stoichiometric quantity of water with sodium peroxide directly, wherein separation of the resulting products, NaOH (s) and H_2O_2 (l) would be trivial. But as noted above, the heat generated by this exothermic reaction, in conjunction with the high pH imparted by the presence of NaOH, creates conditions conducive to decomposition of hydrogen peroxide into water and oxygen gas. On the other hand, when the reaction is carried out in dilute sulfuric acid, the result is a dilute solution of hydrogen peroxide in water. If the desired result is concentrated hydrogen peroxide (which it is in the present instance), additional steps such as vacuum distillation and drying over a suitable desiccant would be required. The elimination of such additional steps and the energy burden of distillation and/or dehydration would be highly desirable in the context of an industrial scale chemical process.

Accordingly, it is desirable to eliminate such additional purification steps while preventing decomposition of the valuable H_2O_2 product. Let us assume for the sake of discussion that we desire the output of such a solar thermal plant to comprise a 90% hydrogen peroxide solution in water. It will be understood that the figure "90%" is merely used for the purpose of the present discussion. It remains to be seen what concentration of hydrogen peroxide should be targeted for such an installation in practice. In an embodiment of the subject inventions(s), the hydrogen peroxide forming reaction may be carried out by adding an incremental quantity of water to a much larger existing volume of 90% hydrogen peroxide, after which the stoichiometric equivalent increment of Na_2O_2 powder required to restore the solution to 90% hydrogen peroxide concentration is dispersed into the reaction volume. In such a reaction scheme, the large volume of H_2O_2 present would not participate in the reaction, but it would serve to dilute the reactants (thereby avoiding concentrated generation of heat) and absorb whatever heat is generated by the $Na_2O_2 + H_2O$ reaction with a relatively small temperature rise in the reactant/product mixture. In addition to providing high heat capacity, the large volume of the reaction mixture would facilitate the use of a high-surface-area heat exchanger that could likely employ simple convective cooling by ambient air.

Sodium bicarbonate precipitate would then be collected from the bottom of the reaction vessel and later converted back to sodium oxide in the solar furnace. The very small quantity of hydrogen-peroxide solution that would be lost in the form of damp sodium bicarbonate powder would be decomposed in the solar furnace.

The above approach eliminates the need for post-reaction purification of hydrogen peroxide to achieve the target concentration of 90%, addresses the problem of NaOH neutralization, and

consolidates H_2O_2 producing reaction and the NaOH carbonation into a single process. Moreover, carrying out the NaOH + CO_2 reaction in solution facilitates complete mixing of the reacting species, as opposed to attempting to react a heterogeneous mixture of CO_2 (g) and NaOH (s).

Let us now write out the formal thermochemical cycle for H_2O_2 production according to the above description:

reaction 1: $4\ CO_2\ (g) + 4\ H_2O\ (l) \rightarrow 4\ H_2CO_3\ (aq)$
reaction 2: $2\ Na_2O_2\ (s) + 4\ H_2CO_3\ (aq) \rightarrow 4\ NaHCO_3\ (s)\downarrow + 2\ H_2O_2\ (aq)$
reaction 3: $4\ NaHCO_3\ (s) + \Delta \rightarrow 2\ Na_2O\ (s) + 4\ CO_2\ (g)\uparrow + 2\ H_2O\ (g)\uparrow$
reaction 4: $2\ H_2O\ (g) \rightarrow 2\ H_2O\ (l) + \Delta$
reaction 5: $2\ Na_2O\ (s) + O_2\ (g) \rightarrow 2\ Na_2O_2\ (s)$

———————————————————————————————

net reaction: $2\ H_2O\ (l) + O_2\ (g) \rightarrow 2\ H_2O_2\ (aq)$

Reaction 1, dissolution of carbon dioxide gas in water to form carbonic acid, is conveniently carried out at or near room temperature.

$4\ H_2CO_3\ (aq) \leftarrow 4\ CO_2\ (g) + 4\ H_2O\ (l)$
$\Delta H^o = [4\ (-699.95)] - [4\ (-393.51) + 4\ (-285.83)] = -82.44\ kJ$
$\Delta S^o = [4\ (+187.4)] - [4\ (+213.63) + 4\ (+69.91)] = -384.56\ J\ K^{-1}$
$\Delta G^o = [4\ (-623.08)] - [4\ (-394.36) + 4\ (-237.18)] = +33.84\ kJ$

The dissolution of 4 moles of CO_2 in water releases 82.44 kJ of heat, of which presumably none can be recuperated or converted to useful work in a practical plant design. It will be noted that the slightly positive value of ΔG^o does not imply that the forward reaction will not be observed at 25 °C, but rather, that the equilibrium constant for formation of H_2CO_3 is somewhat less than unity. As H_2CO_3 is consumed by reaction with NaOH, more CO_2 will enter solution to maintain this equilibrium.

Reaction 2, conversion of sodium peroxide to hydrogen peroxide, is favorable from both the standpoint of enthalpy and entropy:

$4\ NaHCO_3\ (s)\downarrow + 2\ H_2O_2\ (aq) \leftarrow 2\ Na_2O_2\ (s) + 4\ H_2CO_3\ (aq)$
$\Delta H^o = [4\ (-470.1) + 2\ (-191.17)] - [2\ (-515.0) + 4\ (-285.83)] = -89.4\ kJ$
$\Delta S^o = [4\ (+48.1) + 2\ (+143.9)] - [2\ (+95.0) + 4\ (+69.91)] = +10.6\ J\ K^{-1}$
$\Delta G^o = [4\ (-419.2) + 2\ (-134.03)] - [2\ (-451.0) + 4\ (-237.18)] = -94.1\ kJ$

and may be conveniently be carried out at or near room temperature (e.g. in accordance with the methods described above). The 89.4 kJ of heat released into the reaction mixture must be disposed of, and presumably none of it can be recuperated or converted to useful work in a practical plant design.

Reaction 3 is the highly endothermic $NaHCO_3$ thermal decomposition step, which may be carried out at ~850 °C, and is what provides the thermodynamic driving force for the thermochemical cycle as a whole.

$2\ Na_2O\ (s) + 4\ CO_2\ (g) \uparrow + 2\ H_2O\ (g) \uparrow \ \leftarrow \ 4\ NaHCO_3\ (s) + \Delta$
$\Delta H^o = [2\ (-414.22\ ) + 4\ (-393.51) + 2\ (-241.82)] - [4\ (-948.0)] = 905.9\ kJ$
$\Delta S^o = [2\ (+75.06) + 4\ (+213.63) + 2\ (+188.72)] - [4\ (+102.0)] = 974.1\ J\ K^{-1}$
$\Delta G^o = [2\ (-375.48) + 4\ (-394.36) + 2\ (-228.59)]] - [4\ (-852.0)] = 622.4\ kJ$

Step 4, condensation of water vapor, is exothermic

$2\ H_2O\ (l) \ \leftarrow \ 2\ H_2O\ (g) + \Delta$
$\Delta H^o = 2\ (-285.83) – 2\ (241.82) = -88.02\ kJ$
$\Delta S^o = 2\ (+69.91) – 2\ (+188.72) = -237.62\ J\ K^{-1}$
$\Delta G^o = 2\ (-237.18) – 2\ (228.59) = 17.18\ kJ$

Step 5, oxidation of sodium oxide to sodium peroxide, is exothermic:

$2\ Na_2O_2\ (s) \ \leftarrow \ 2\ Na_2O\ (s) + O_2\ (g)$
$\Delta H^o = \ [2\ (-515.0)] - [2\ (-414.22) + (0)] = -201.6\ kJ$
$\Delta S^o = \ [2\ (+95.0)] – [(2\ (+75.06) + (+205.03)] = -165.2\ J\ K^{-1}$
$\Delta G^o = [2\ (-451.0)] – [2\ (-375.48) + (0)] = 151.0\ kJ$

Reaction 4, oxidation of sodium oxide to sodium peroxide, is thermodynamically favorable below the decomposition temperature of Na_2O_2 (675 °C), and may be conveniently carried out at 250 to 350 °C. The partial pressure of oxygen may be elevated to assist completion of reaction 1 if necessary. In certain embodiments, extraction of hot Na_2O_2 powder generated in reaction 1 is conducted in a manner that a substantial quantity of the heat contained therein is recovered for use in the thermochemical cycle, rather than directly released into the environment.

It will be understood that substantially all of the carbon dioxide and sodium used in the proposed thermochemical cycle can be recycled. Water and oxygen are the only consumables and hydrogen peroxide is only product. In addition to the fact that the initial capital expenditure for sodium (e.g. as sodium bicarbonate) and carbon dioxide is expected to be low, the proposed reaction sequence also has the advantage that none of its constituents have high toxicity. It will also be noted that none of the above reactions suffer from problems associated with chemical poisoning or deactivation of surface reaction sites that have hampered many of the metal oxide reaction cycles explored in the prior art. This is a critically important consideration, because reaction cycles that are sensitive to trace impurities and dependent on maintaining specific micro-morphology at reaction sites are vulnerable to deactivation over the course of successive reaction cycles.

During the course of this investigation, a 2014 paper from by Miyaoka et al. was found that suggests exploitation of the alkali metal oxide to peroxide reaction for generation of hydrogen via water splitting.[5] What is distinct about the thermochemical cycle proposed here is that (a) our

objective is the conversion of water and oxygen to hydrogen peroxide, and (b) the use of CO_2 to both reduce peak process temperature of the cycle and control the pH of the H_2O_2 synthesis reaction:

$$2\ Na_2O_2 + 4\ H_2O \rightarrow\ 4\ NaOH + 2\ H_2O_2$$

to prevent decomposition of hydrogen peroxide.

2.3. Potential exploitation of Reppe chemistry

The other novel thermochemical cycle examined early in Year 1 is directed towards conversion of CO_2 and H_2O into C_2H_2 (acetylene gas):

$$8\ Na\ (l) + 6\ CO_2\ (g) \rightarrow 4\ Na_2CO_3\ (s) + 2\ C\ (s)$$
$$Na_2CO_3\ (s) + 2\ C\ (s) \rightarrow 2\ Na\ (l) + 3\ CO\ (s)$$
$$4\ Na(l) + 3\ CO\ (g) \rightarrow Na_2C_2\ (s) + Na_2CO_3\ (s)$$
$$Na_2C_2\ (s) + 2\ H_2O\ (g) \rightarrow 2\ NaOH\ (s) + C_2H_2\ (g)$$
$$2\ NaOH + 2\ CO_2\ (g) \rightarrow 2\ NaHCO_3\ (s)$$
$$4\ Na_2CO_3\ (s) \rightarrow 4\ Na_2O + 4\ CO_2\ (g)$$
$$2\ NaHCO_3\ (s) \rightarrow Na_2O + 2\ CO_2\ (g) + H_2O$$
$$5\ Na_2O\ (s) + \Delta \rightarrow 10\ Na\ (s) + 2½\ O_2\ (g)$$

$$2\ CO_2\ (g) + H_2O\ (g) \rightarrow C_2H_2\ (g) + 2½\ O_2\ (g)$$

The objective of this proposed cycle is to exploit classical Reppe chemistry for the production of liquid hydrocarbon fuels:

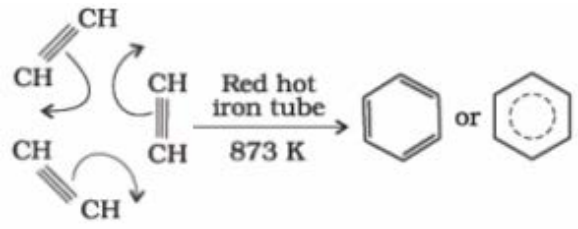

Other species such as cyclooctatetraene may be generated by such acetylene polymerization reactions, and subsequent hydrogenation reactions can easily be carried out if desired. Because of the large number of steps in the above thermochemical cycle, a strategic decision was made to defer further technical due diligence on the acetylene-to-syn-fuel cycle. Exploratory work in the area of grid storage battery technology needed to get underway given the rapid pace of developments in PV Solar technology and the relative ease with which battery storage can be merged with existing infrastructure. It is nonetheless a recommendation of this report that both of these two proposed thermochemical cycles be further investigated.

2.4. Investigation of electrochemistry prior art to date

Electrochemical storage, and in particular, battery technologies potentially applicable to the problem of grid storage, were also investigated. As shown in Figure 4, assuming that electricity will be generated by solar and wind and distributed via transmission lines, an electrical battery

that is cost effective and has high round-trip efficiency is a highly desirable form of grid storage. Modularity and ease of deployment are also desirable characteristics. Special geological siting requirements (e.g. compressed air storage), relatively low round-trip energy storage efficiency (e.g. thermal storage), and poor scalability (e.g. flywheels) must be considered potential disqualifiers.

Figure 4: The logistics of candidate energy storage technologies are central to the soundness of their value proposition.

The prior art contains thousands of electrochemical devices, most of which are classified as batteries, flow batteries, or fuel cells. In a conventional battery, electrical current is generated by a thermodynamically favorable redox reaction that is carried out as two separate anode/cathode half reactions. The chemical reagents for the redox reaction, as well the two electrodes and an ion-conducting electrolyte are all contained within the enclosure comprising the battery. Many such batteries contain additional components as well, such as separators to prevent inadvertent contact between the closely spaced anode and cathode surfaces. Storage batteries may be rechargeable (e.g. a lithium ion battery) or non-rechargeable (e.g. a Zn-MnO_2 Leclanche cell). The energy storage capacity of such a device is limited by the quantity of electrochemically active reagents stored within the enclosed volume that defines the battery. In the case of a flow battery, the vast majority of the two electrochemically active reagents may be stored in external tanks rather than within the battery itself. The reactants are then fed into the electrode/electrolyte/electrode region of the battery on an as needed basis. A well-known example of such a device is the vanadium redox flow battery which has been investigated for the

application of grid storage. A grid storage battery is a large-scale electrical storage device capable of sourcing/sinking substantial quantities of electrical power to/from the electrical grid; grid storage is critically important for effective integration of intermittent renewable energy sources such as solar and wind power. Finally, the fuel cell is a device that operates on a similar principle to the flow battery, but one of the two chemical reactants is usually oxygen, and the other is a chemical species typically classified as a fuel, such as hydrogen (H_2), methane (CH_4), methanol (CH_3OH), etc. Referring now to Figure 5, in such a fuel cell, a combustion reaction that is normally carried out in a flame such as:

$2\ H_2 + O_2 \rightarrow 2\ H_2O$

is instead carried out in an electrochemical cell in the form of two physically separate half reactions. For example, in an acid electrolyte fuel cell:

hydrogen electrode $2\ H_2 \rightarrow 4\ H^+ + 4\ e^-$

oxidation of elemental hydrogen to H^+

oxygen electrode $O_2 + 4\ H^+ + 4\ e^- \rightarrow 2\ H_2O$

reduction of elemental oxygen to O^{2-}

In the above example, protons that are generated at the hydrogen electrode and consumed at the oxygen electrode are transported through the electrolyte, in the interior of the fuel cell. The electrons generated at the hydrogen electrode and consumed at the oxygen electrode travel through an external circuit, such as the filament of an incandescent light bulb. The net chemical reaction is the same as that which occurs within a hydrogen/oxygen flame. But in the case of a fuel cell, the free energy of the reaction:

$2\ H_2 + O_2 \rightarrow 2\ H_2O$

is directly furnished in the form of electrical power rather than heat. When compared to using a hydrogen/oxygen flame to drive a heat engine (e.g. a gas turbine or internal combustion engine) to produce mechanical work that is then used to impart rotation to an electrical generator, the fuel cell has in principle two major advantages. The first of these is the absence of moving parts, noise, etc. The second advantage is that heat engines are subject to the Carnot efficiency limit, whereas fuel cells are not. In other words, a fuel cell allows electrical power to be generated from chemical potential in a much more direct fashion than a heat engine, and in principle it has the potential to carry out the chemical reaction in question as a thermodynamically reversible process in which none of the chemical potential is converted to waste heat.

For example, a combustion reaction such as:

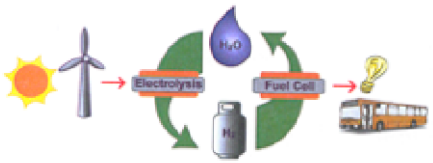

$2\ H_2 + O_2 \rightarrow 2\ H_2O$

can be carried out in an electrochemical cell in the form of two physically separate half reactions as a reversible thermodynamic cycle. For instance, in an acid electrolyte fuel cell:

hydrogen electrode $2\ H_2 \rightarrow 4\ H^+ + 4\ e^-$ ***oxidation of elemental hydrogen to*** H^+

oxygen electrode $O_2 + 4\ H^+ + 4\ e^- \rightarrow 2\ H_2O$ ***reduction of elemental oxygen to*** O^{2-}

Unlike a heat engine, no Carnot efficiency limitation, and (nominally) no moving parts.

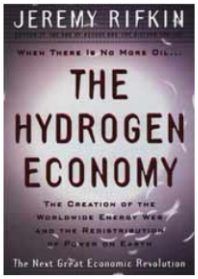

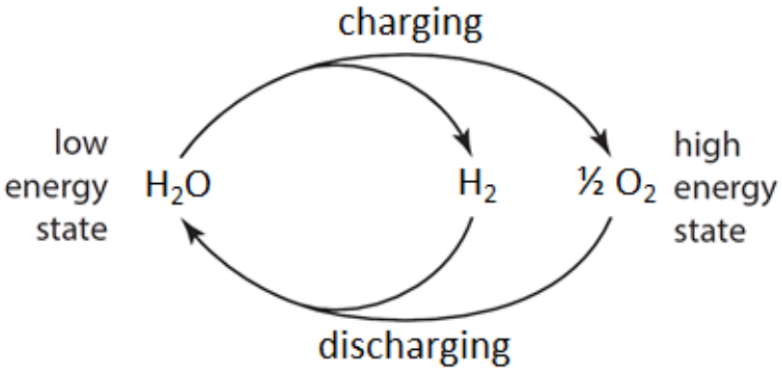

Figure 5: Electrochemical reactions can in principle achieve the desired power and energy density using earth abundant materials.

Referring to Figure 6, reason that fuel cells have yet to displace devices such as internal combustion engines in the vast majority of practical applications is that physical implementation of a device that carries out a combustion reaction such as $2\ H_2 + O_2 \rightarrow 2\ H_2O$ as a purely electrochemically process is fraught with numerous technical difficulties. In many instances, the technical obstacles that arise in the implementation of fuel cells, or analogues of such technical problems, also arise in batteries and flow batteries. The prior art is therefore principally concerned with novel approaches to circumventing such technical difficulties.

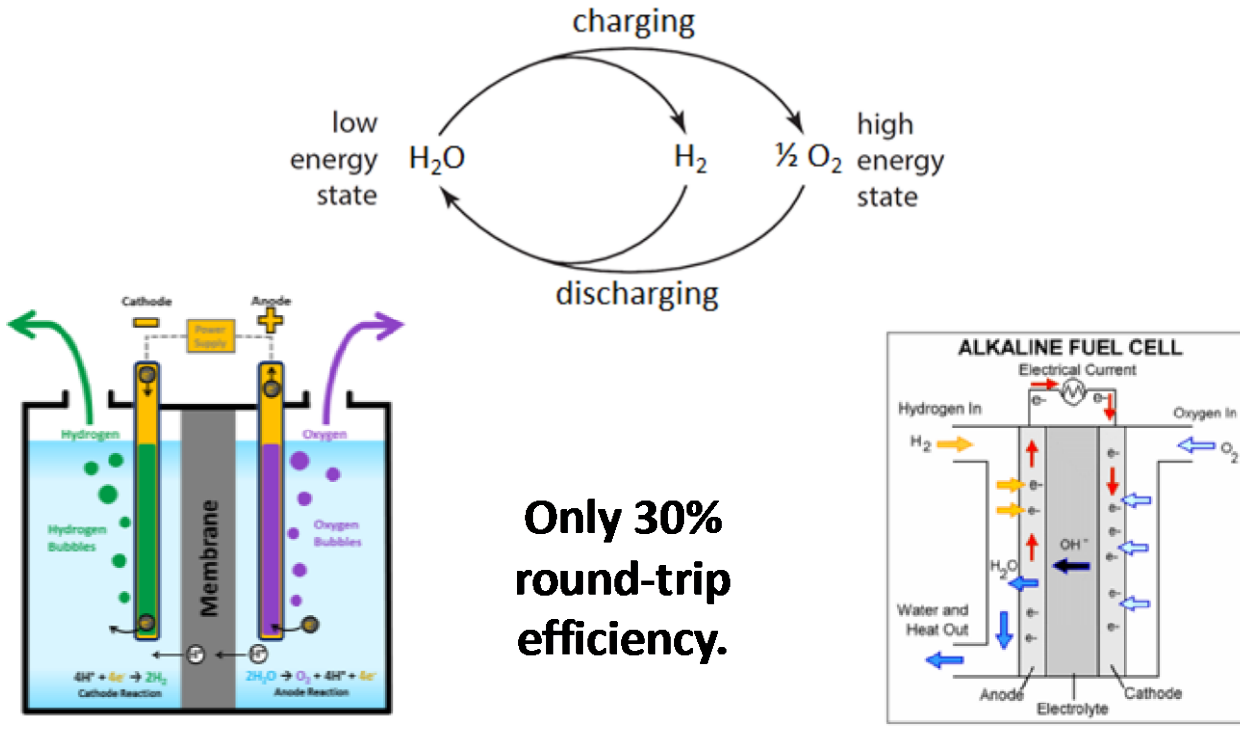

Storage of compressed gas is also economically unattractive.

Figure 6: Implementation of electrochemical reactions in real-world devices is often fraught with technical difficulty.

For example, in the case of a hydrogen/oxygen fuel cell, although the thermodynamics of the chemical reaction 2 H_2 + O_2 → 2 H_2O are extremely favorable, the chemical kinetics of the two redox half reactions occurring at the anode and cathode are a significant limitation. This is especially the case with the O_2 half-reaction at the cathode, which has very high activation energy. The usual approach to counteract such slow electrode kinetics is to coat the electrodes with catalytically active chemical species such as platinum (so as to reduce the activation energy barrier), make the surface area of the electrode as large as possible, and to apply an overvoltage to speed up the rate of the electrochemical reaction. But the use of exotic materials such as platinum, palladium, glassy carbon, etc. is in many cases cost prohibitive. A further constraint is that candidate materials must be electrically conductive (or somehow blended with electrically conductive materials). While there are numerous ways of increasing the effective surface area of the electrode (e.g. by roughening the surface, corrugating the surface, etc. subject to limitations associated with trapping of gas bubbles), there are nearly always practical limitations regarding the total amount of volumetric space available (e.g. in a cell phone battery, or car battery). Finally, the additional overvoltage we must supply to force the electrochemical reaction to occur at a reasonably fast rate amounts to a source of thermodynamic irreversibility. Thus, as illustrated in Figure 7, in practice we might observe experimentally that electrolysis of water (to produce hydrogen and oxygen) in such a fuel cell requires 1.8 to 2.0 V under standard state conditions (unless we are willing to tolerate extremely sluggish operation at very low operating current), far in excess of the 1.23 V predicted on the basis of the free energy for the chemical reaction:

$2\ H_2 + O_2 \rightarrow 2\ H_2O \quad E^\circ = 1.23\ V$

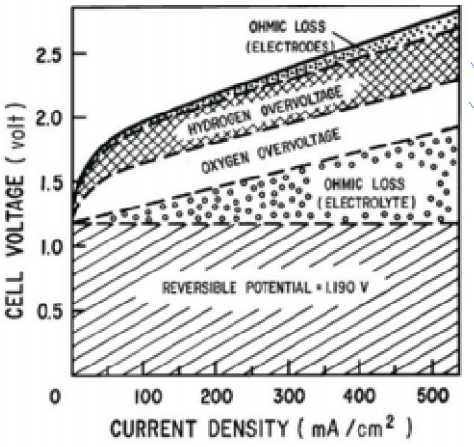

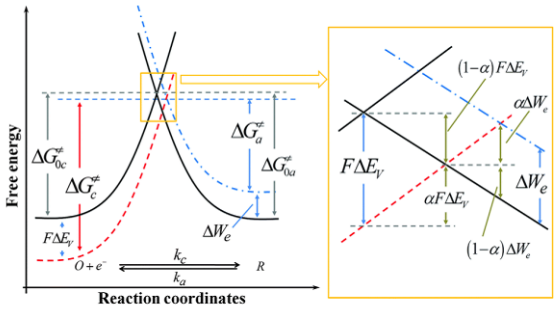

We can apply an overvoltage to improve chemical kinetics by lowering the activation energy barrier.

Schematic diagram of triple phase boundary (TPB).

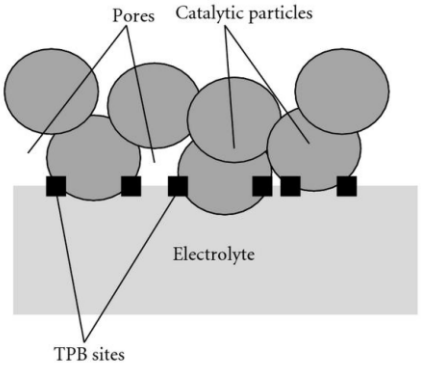

Hypothesized oxygen reduction reaction at a platinum electrode

Hypothesized dissociative ORR reaction mechanism

$$O_2 + Pt \longrightarrow PtO_2$$
$$PtO_2 + H^+ + e^- \longrightarrow PtOOH$$
$$PtOOH + H^+ + e^- \longrightarrow H_2O + PtO$$
$$PtO + H^+ + e^- \longrightarrow PtOH$$
$$PtOH + H^+ + e^- \longrightarrow Pt + H_2O$$

But I thought $2\ H_2 + O_2 \rightarrow 2\ H_2O$ was supposed to be a simple reaction... and you're also requesting Pt electrodes?

Figure 7: Where is all the thermodynamic irreversibility coming from?

Zooming in on the electrode/reagent interaction at a microscopic scale, yet another problem that adversely affects the kinetics of a device such as a hydrogen fuel cell is that the reactions in question occur at a triple phase boundary between the electrode, electrolyte, and gas-phase reactant (H_2 or O_2).[6] In other words, the electrochemical reaction only occurs in the immediate vicinity of where a spherical gas bubble makes tangential contact with the surface of the electrode, and where there is adequate access to electrolyte, as depicted in Figure 8. This means that at any given instant in time, the vast majority of the electrode surface is not actually participating in the electrochemical reaction. If on the other hand, only a two-phase boundary is required, all regions of the electrode surface could be simultaneously active. This would greatly improve the kinetics of the half reaction occurring at the electrode, and drastically reduce the amount of overvoltage required to achieve a given operating current (or alternatively, drastically increase the power density of such a device).

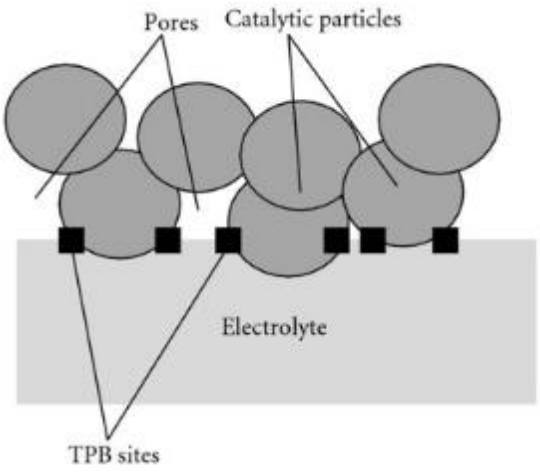

Figure 8: The triple-phase boundary problem. The electrochemical reaction only occurs in the immediate vicinity of where a spherical gas bubble makes tangential contact with the surface of the electrode, and where there is adequate access to electrolyte. Only a small portion of the electrode surface is active at any given time. *Fuel Cell Fundamentals*, R. O'Hayre, S. Cha, W. Colella, and F. Prinz, John Wiley and Sons (2006).

Referring to Figure 9, yet another obstacle to favorable electrode kinetics concerns the nature of the transition state reaction complex for each half reaction. For example, in the case of a hydrogen fuel cell, important questions include:

1) Does formation of the transition state reaction complex involve breaking a strong covalent bond such as that found in O_2?
2) Does formation of the transition state reaction complex involve making and breaking multiple chemical bonds, or just one?
3) For a reaction such as $2\ H_2 + 4\ OH^- \rightarrow 4\ H_2O + 4e^-$, such as that found in an alkaline-electrolyte hydrogen fuel cell, how many molecules/ions must be brought together to form the transition state reaction complex, and how precise must the geometry of the reaction complex be?
4) For a reaction such as $O_2 + 4\ H^+ + 4e^- \rightarrow 2\ H_2O$, such as that found in an acid-electrolyte hydrogen fuel cell, how many steps are involved in the oxidation reduction reaction (ORR) mechanism, and which step is rate limiting?

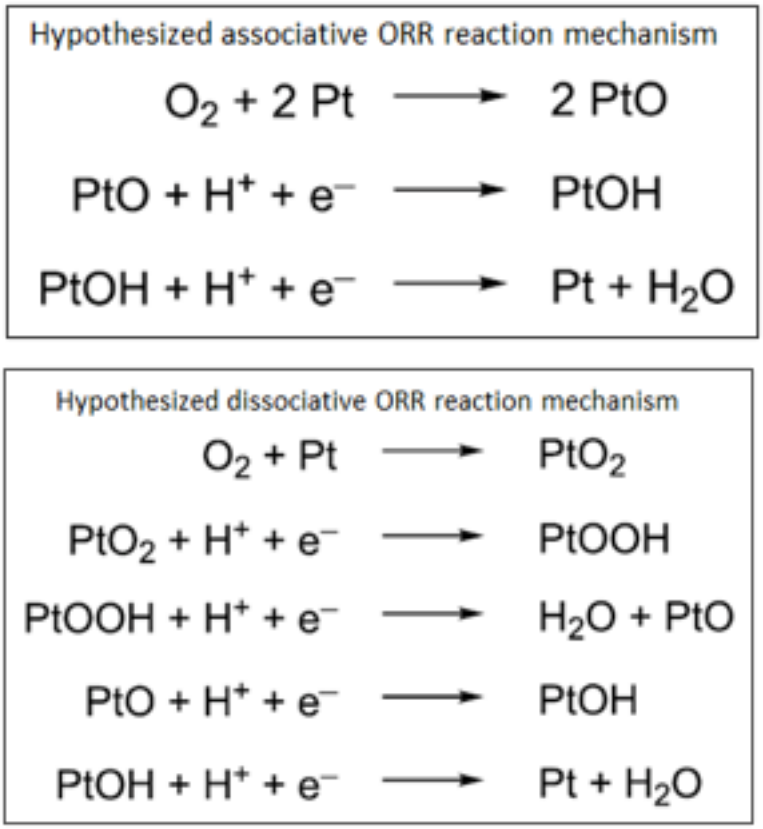

Figure 9: Examples of hypothesized mechanisms for oxygen reduction reactions at a Pt electrode. A. Gómez-Marín, R. Rizo and J. Feliu, "Some reflections on the understanding of the oxygen reduction reaction at Pt(111)", Beilstein J. Nanotechnology, Vol. 4, 956–967 (2013).

As discussed in Figure 10, such questions illustrate the complexity of reagent/electrode interactions, and the numerous potential opportunities for electrochemical kinetic bottlenecks.

Sluggish ion transport: ohmic loss in the electrolyte

Sluggish electron transport: ohmic loss in electrode structures

Sluggish electrochemical kinetics at electrode/electrolyte interface

a) Low effective electrode area due to triple phase boundary

b) Low probability of reaction complex formation

c) High activation energy for breaking of strong covalent bonds

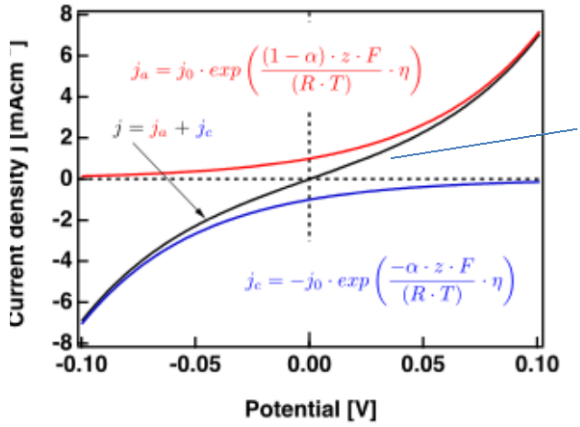

Butler-Vollmer Equation:

$$j = j_0 \cdot \left\{ \exp\left[\frac{\alpha_a z F \eta}{RT}\right] - \exp\left[-\frac{\alpha_c z F \eta}{RT}\right] \right\}$$

If the exchange current density (j_o) is low, then high overvoltage (η) is required.

High overvoltage implies high irreversibility.

Figure 10: Slow kinetics indirectly results in poor efficiency. High round-trip efficiency can be had if we're willing to operate at impractically low current densities. But under practical operating conditions, efficiency penalties arise from the effects below.

Figure 11 summarizes technologically important fuel cell architectures developed to date. The primary distinction between these different fuel cell technologies is the type of electrolyte employed, and each type of fuel cell is typically referred to by its acronym: AFC (alkaline fuel cell), PEMFC (proton exchange membrane fuel cell), DMFC (direct methanol fuel cell), PAFC (phosphoric acid fuel cell), MCFC (molten carbonate fuel cell), SOFC (solid oxide fuel cell). In each case, the job of the electrolyte is to transmit a specific ionic species that is generated by one of the electrode half reactions and consumed by the other. The electrolyte must transmit such ions under the influence of an electrical field with as little electrical resistance as possible, but at the same time not transmit electrons. Referring to Figure 12, the choice of electrolyte has a direct bearing on (1) what type of oxidation-reduction reactions may be contemplated for such a fuel cell, (2) what type of electrode materials may be used in such a fuel cell, and (3) the operating temperature range of such a fuel cell. These three factors in turn influence whether or not some form of catalyst is required at either or both electrodes to ensure adequately fast electrochemical kinetics and adequately small overvoltage. One broad theme that emerges in fuel cell technology is that high temperature operation is typically conducive to fast chemical kinetics (which may eliminate the need for expensive catalysts such as platinum) and high electrolyte conductivity. On the other hand, operation at high temperature (e.g. 550 – 650 °C in the case of the molten carbonate fuel cell and 800 – 1000 °C in the case of the solid oxide fuel cell) imposes numerous technical difficulties with materials compatibility, corrosion, seals, etc. and also places a practical lower limit on the size of a fuel cell; small fuel cells have high surface-area-to-volume ratios such that the efficiency penalty associated with thermal losses for operation at high temperature may be prohibitive. Finally, some of the fuel cell architectures listed in Figure 11 are

very vulnerable to poisoning by chemical impurities such as sulfur and/or products of side reactions such as carbon monoxide. Additional challenges include reactant/product mass transport rate limitations, and the prevention of "crossover" of fuel and oxidant through the electrolyte, which results in "chemical short circuiting" of the electrochemical cell. Each of the above concerns and tradeoffs are germane to the discussion that follows.

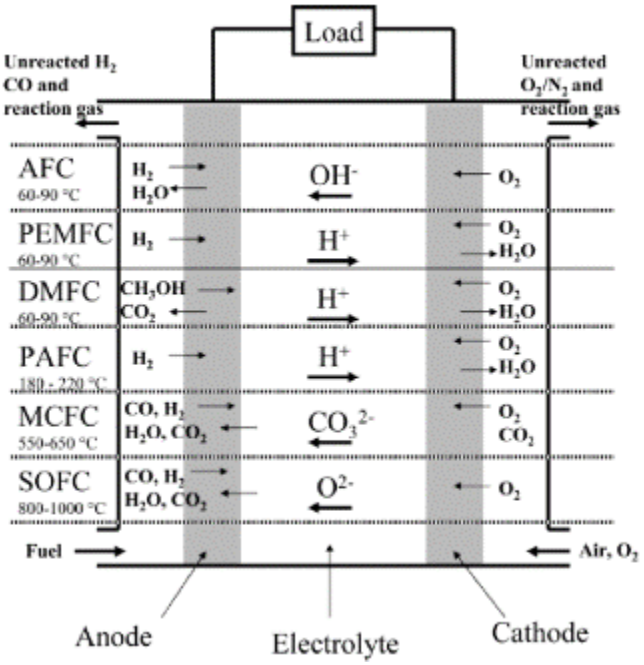

Figure 11: Summary of the reactions and processes that occur in various fuel cell systems. M. Winter, R. Brodd, "What are batteries, fuel cells, and supercapacitors?", Chemical Reviews, Vol. 104, No. 10 (2004).

advantages	disadvantages	comments
	Alkaline (AFC)[a]	
mechanically rechargeable low-cost KOH electrolyte	limited activated life intolerant of impurities in gas streams CO_2 and CO pure H_2 only suitable fuel	original development >30 years ago Apollo fuel cell operates at room temp to 80 °C demo in vehicles in the 1970s
	Polymer Electrolyte Membrane Fuel Cell (PEMFC)	
nonvolatile electrolyte few materials problems CO_2 rejecting electrolyte pressure differential between anode and cathode polymer electrolyte	expensive catalysts required CO a strong poison H_2O management essential high-cost electrolyte pure H_2 only suitable fuel oxygen kinetics are slow intolerant of impurities limited life water management essential	operates best at 60−90 °C originally developed for space by GE hydrogen fuel (re-formed hydrocarbons, pure H_2, MH storage) main development efforts for automotive and stationary applications
	Direct Methanol Fuel Cell (DMFC)	
direct fuel conversion slow electrode kinetics improved wt and vol polymer electrolyte	stable reaction intermediates high catalyst loadings water management essential low overall efficiency methanol hazardous	operates best at 60 to 90 °C) same construction as PEMFC methanol fuel eliminates reformer lower current capability methanol crossover reduces efficiency needs new membrane, higher efficiency high catalyst loadings main effort for portable electronic devices
	Phosphoric Acid Fuel Cell (PAFC)	
CO_2 rejecting electrolyte high fuel efficiency	H_2 only suitable fuel anode CO catalyst poison O_2 kinetics hindered low conductivity electrolyte high-cost catalysts limited life	operates best at ~200 °C stationary energy storage (nominal units, 250 kW) available commercially
	Molten Carbonate Fuel Cell (MCFC)	
fast electrode kinetics high efficiency CO/CH_4 usable fuel direct reforming feasible high-grade heat available	materials problems and life low sulfur tolerance high ohmic electrolyte low tolerance to sulfur need to recycle CO_2 limited life	operates best at 550 °C nickel catalysts, ceramic separator membrane hydrocarbon fuels re-formed in situ several large demonstration units significant government support
	Solid Oxide Fuel Cell (SOFC)	
high grade heat available fast electrode kinetics in situ reforming feasible no electrolyte management high system efficiency tolerant of impurities	high fabrication costs severe materials constraints high electrolyte conductivity	operates at 900 °C conducting ceramic oxide electrodes hydrocarbon fuels re-formed in situ least sensitive to sulfur, etc.

[a] Metal air batteries with replaceable anodes are often considered to be a fuel cell but are not considered here.

Figure 12: Advantages and disadvantages of various fuel cell systems. M. Winter, R. Brodd, "What are batteries, fuel cells, and supercapacitors?", Chemical Reviews, Vol. 104, No. 10 (2004).

Another fundamental difficulty that is encountered in electrochemical devices concerns non-ideal processes that adversely affect longevity. Consider for example the familiar lead acid battery used in the automotive industry. The lead acid battery is based on disproportionation of lead (II) sulfate into lead (IV) oxide and elemental lead in a sulfuric acid electrolyte:

$$2PbSO_4(s) + 2\ H_2O(l) \rightarrow Pb(s) + PbO_2(s) + 2H_2SO_4\ (aq)$$

During discharge of the lead acid battery, the half reaction occurring at the (-) electrode is:

$$PbSO_4\ (s) + H^+ + 2\ e^- \rightarrow Pb\ (s) + HSO_4^-\ (aq)$$

and the half reaction occurring at the (+) electrode is:

$$PbSO_4\ (s) + 2\ H_2O\ (l) \rightarrow PbO_2\ (s) + HSO_4^-\ (aq) + 3\ H^+\ (aq) + 2\ e^-$$

The concentration of H_2SO_4 used in lead acid batteries, commonly referred to as "battery acid", is approximately 30%. As shown in Figure 13, the ionic conductivity of the aqueous H_2SO_4 electrolyte peaks at a sulfuric acid concentration of ~30%.[7] Electrolyte conductivity is of paramount importance in most batteries because resistive losses in the battery amount to another source of thermodynamic irreversibility. The series resistance of the electrolyte can also be the limiting factor that determines the power density of battery, because it dictates how much current can be drawn from the battery before the onset of excessive voltage droop. For the same reason, the ionic resistance of the electrolyte may also impose limitations on how quickly such a battery can be recharged. Some batteries therefore use electrolyte additives to reduce internal resistance,

but the addition of any chemical additive opens up new possibilities for chemical side reactions, materials incompatibility, etc.

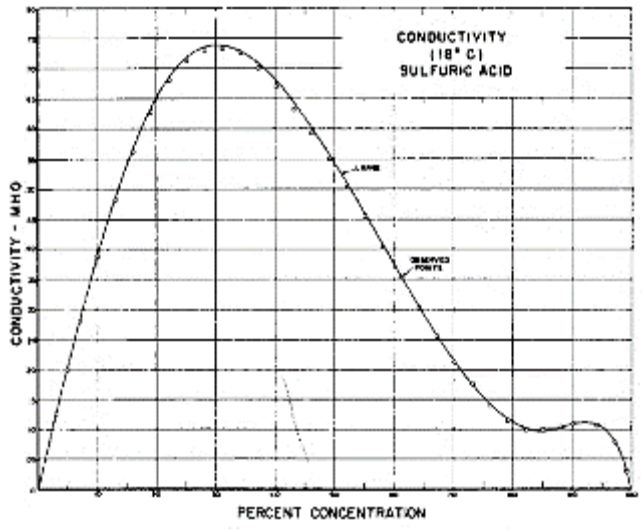

Figure 13: Electrical conductivity of aqueous sulfuric acid as a function of H_2SO_4 concentration at 18 °C. H. Darling, "Conductivity of Sulfuric Acid Solutions", Journal of Chemical Engineering Data, Vol. 9, No. 3, pg. 421 (1964).

Despite the extreme maturity of lead acid battery technology, they suffer from a number of non-idealities that are also representative of nuisance problems encountered in other battery chemistries. One such problem is sulfonation, the tendency of finely divided amorphous lead sulfate to crystallize into large, electrochemically inert crystals. This process gradually reduces the energy capacity of a lead acid battery. Another problem, especially in stationary power applications, is electrolyte stratification. As noted above, it is desirable to maintain the concentration of sulfuric acid at approximately 30% to minimize electrolyte resistance. But H_2SO_4 has a much higher density than H_2O, and tends "settle out of solution", creating a concentration gradient in the electrolyte wherein the H_2SO_4 solution in the upper portion of the battery is too weak, and the H_2SO_4 solution in the lower portion of the battery is too strong. Figure 14 attempts to summarize these observations.

Many battery chemistries also suffer from structural deterioration over time because the one or more of the solid components within the batteries undergo volumetric changes during charging/discharging. Cyclic mechanical stress of such components can be very problematic if the materials in question are brittle. For example, in devices such as lithium ion batteries (Figure 15) that rely on intercalation of Li^+ ions in rigid materials such as graphite, electrochemical swelling caused by intercalation of lithium ions can be problematic.

Based on disproportionation of lead (II) sulfate into lead (IV) oxide and elemental lead in a sulfuric acid electrolyte:

$2\ PbSO_4\ (s) + 2\ H_2O\ (l) \rightarrow Pb\ (s) + PbO_2\ (s) + 2H_2SO_4\ (aq)$

During discharge of the lead acid battery, the half reaction occurring at the (-) electrode is:
$PbSO_4\ (s) + H^+\ (aq) + 2\ e^- \rightarrow Pb\ (s) + HSO_4^-\ (aq)$

and the half reaction occurring at the (+) electrode is:

$PbSO_4\ (s) + 2\ H_2O\ (l) \rightarrow PbO_2\ (s) + HSO_4^-\ (aq) + 3\ H^+\ (aq) + 2\ e^-$

Battery acid is the gold standard for electrolyte conductivity ($0.73\ \Omega^{-1}\ cm^{-1}$) and enables very high current density

Battery acid is vulnerable to stratification

Capacity fade is inevitable due to sulfonation, the gradual conversion of fine grained $PbSO_4$ into large, electrochemically inert crystals.

Lead is heavy, relatively expensive, and not environmentally friendly.

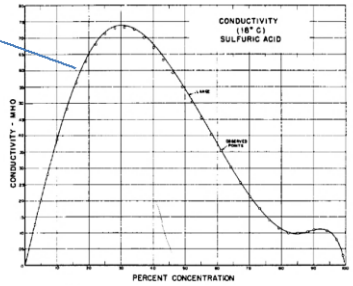

Figure 14: What can be learned from the venerable lead-acid battery?

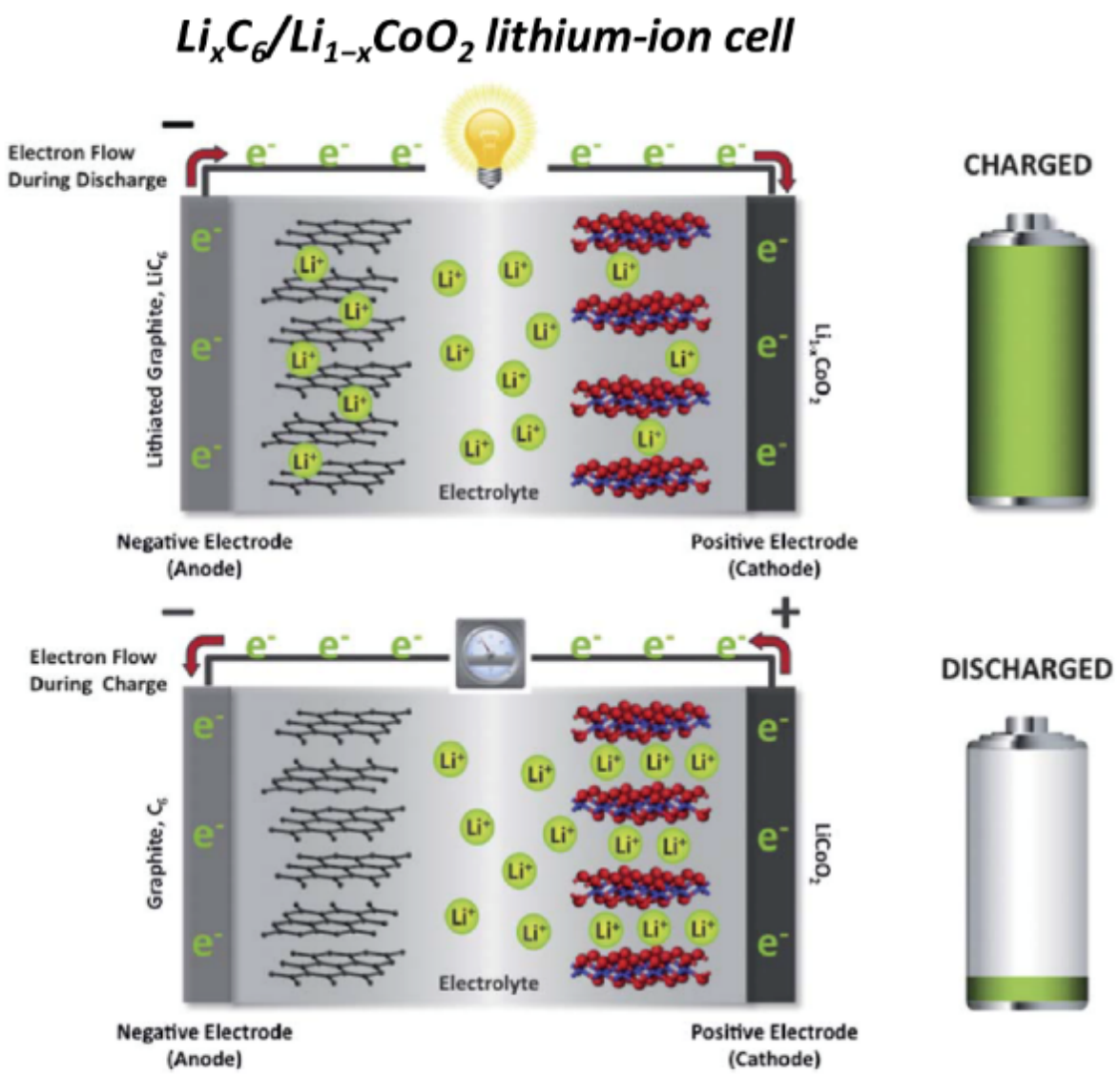

A schematic illustration of the working principles of a $Li_xC_6/Li_{1-x}CoO_2$ lithium-ion cell. During discharge, lithium ions diffuse from a lithiated graphite (Li_xC_6) structure (the anode) into a delithiated $Li_{1-x}CoO_2$ structure (the cathode) with concomitant oxidation and reduction of the two electrodes, respectively. The reverse process occurs during charge. M. Thackeray, C. Wolverton and E. Isaacs, "Electrical energy storage for transportation—approaching the limits of, and going beyond, lithium-ion batteries", Energy Environ. Sci. 5, 7854 (2012).

Figure 15: What valuable lessons can be learned from Li-ion batteries?

Gradual loss of battery capacity also commonly results from deposition of electrochemically inert material onto the surfaces of one or both electrodes. The following account of capacity fade in Li ion batteries is reproduced from an article entitled, "What causes Li ion to die?"[8]

During charge, lithium gravitates to the graphite anode (negative electrode) and the voltage potential changes. Removing the lithium again during discharge does not reset the battery fully. A film consisting of lithium atoms forms on the surface of the anode called solid electrolyte interface (SEI). Composed of lithium oxide and lithium

carbonate, the SEI layer grows as the battery cycles. The film gets thicker and eventually forms a barrier that obstructs interaction with graphite. The cathode (positive electrode) develops a similar restrictive layer known as electrolyte oxidation. Dr. Dahn stresses that a voltage above 4.10V/cell at high heat causes this, a demise that can be more harmful than cycling. The longer the battery stays in this condition, the worse the degradation gets. The build-up can result in a sudden capacity loss that is difficult to predict by cycling alone. This phenomenon had been known for some years but measuring the coulombic efficiency can verify these effects in a more scientific and systematic manner.

The chemical complexity of lithium ion batteries, many of which for example contain upwards of 5 electrolyte additives,[9] manifests itself in the form of other degradation processes observed over the life of the battery as well. Commonly these include: (1) chemical reduction of the electrolyte (which is typically an alkyl carbonate) by the anode, (2) chemical oxidation of the electrolyte by the cathode, (3) thermal decomposition reactions of the electrolyte and/or electrolyte additives, (4) internal short circuits (e.g. due to dendritic growth), (5) and irreversible plating of lithium metal during rapid recharging or charging at low temperatures.

Such problems were summed up recently in remarks from Dr. George Crabtree, Director of the Joint Center for Energy Storage Research (JCESR) at Argonne National Laboratories[10]:

Almost everything you've tried in Li-ion has failed, and it failed not because it was a bad idea, it failed because there are a lot of side reactions in a battery that take place, and those side reactions sometimes consume the active ingredient or the electrolyte and limit the lifetime. So for a variety of reasons that have nothing to do with the quality of the original idea, most things fail. And that means you have to have backup plans.

Finally, many high-performance battery chemistries suffer from intrinsic safety problems (see for example, Figure 16).[11] In the case of Li-ion batteries for example, overcharging can eventually result in venting of the battery enclosure, often accompanied by discharge of flame.[12] Discharging a Li-ion battery too deeply can also result in serious problems. Copper from the anode collector can migrate into the electrolyte where it can form dendrites resulting in internal short circuits. This presents the risk of fire if someone subsequently attempts to recharge such a battery. Figure 17 outlines some of the other non-ideal properties that make it difficult for Li-ion batteries to compete for bulk grid storage.

During discharge of a $Li_xC_6/Li_{1-x}CoO_2$ lithium-ion cell, Li^+ ions diffuse from a lithiated graphite (Li_xC_6) structure (the anode) into a delithiated $Li_{1-x}CoO_2$ structure (the cathode) with concomitant oxidation and reduction of the two electrodes, respectively. The reverse process occurs during charge.

But things can also go wrong:

A schematic illustration of thermal runaway in a lithium-ion battery. R. Whitwam, "Doping lithium-ion batteries could prevent overheating and explosion", www.extremetech.com, June 25, 2015.

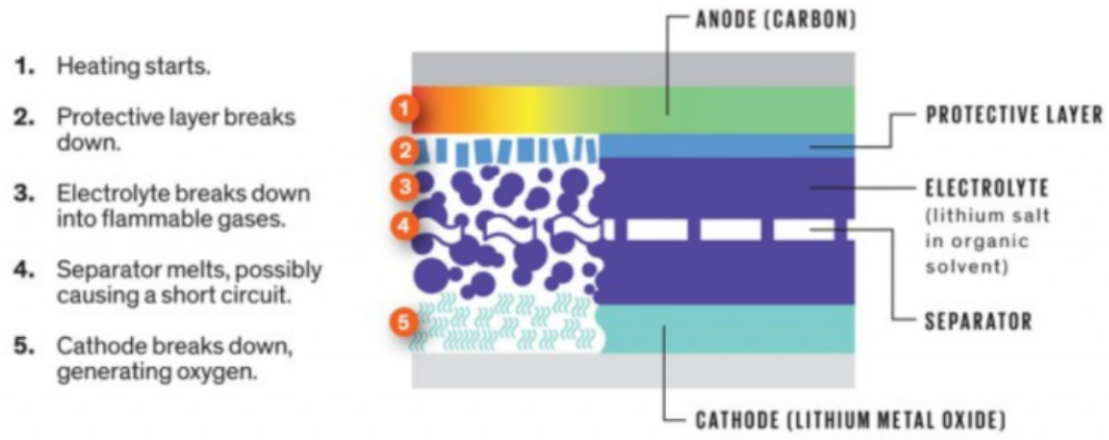

Figure 16: Thermal runaway is a grave concern for bulk energy storage because so much energy is stored in one place.

Other Li-ion battery problems:

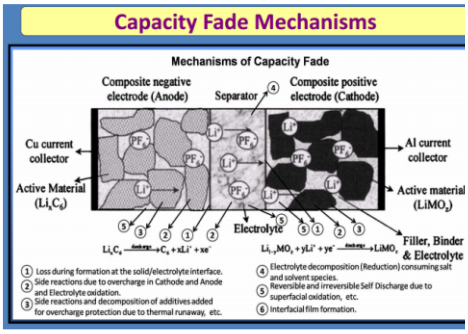

Capacity fade due to deposition of electrochemically inert material (Li_2O and Li_2CO_3) onto the surfaces of one or both electrodes.

Structural deterioration of electrodes subject due to volumetric changes during charging/discharging cycles.

Chemical complexity (up to 5 electrolyte additives)

- chemical reduction of the electrolyte (which is typically an alkyl carbonate) by the anode,
- chemical oxidation of the electrolyte by the cathode,
- thermal decomposition reactions of the electrolyte and/or electrolyte additives,
- internal short circuits (e.g. due to dendritic growth of Li or Cu),
- irreversible plating of Li metal during rapid recharging or charging at low temperatures.

Such problems were summed up recently in remarks from Dr. George Crabtree, Director of the Joint Center for Energy Storage Research (JCESR) at Argonne National Laboratories:

Almost everything you've tried in Li-ion has failed, and it failed not because it was a bad idea, it failed because there are a lot of side reactions in a battery that take place, and those side reactions sometimes consume the active ingredient or the electrolyte and limit the lifetime. So for a variety of reasons that have nothing to do with the quality of the original idea, most things fail. And that means you have to have backup plans.

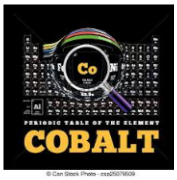

Material abundance is a further problem, particularly with regard to cobalt.

Figure 17: The requirement for 10,000 charge/discharge cycles is problematic for Li-ion batteries.

While the above discussion draws on representative examples of battery pathologies observed in familiar lead acid and Li-ion batteries, it is by no means exhaustive. Many analogous degradation processes and failure modes are associated with other battery chemistries. The above discussion is not intended to detract in any way from the remarkable achievements of those who developed these successful prior art technologies. The issue at hand is that bulk grid storage represents a fundamentally different application space with a different ordering of priorities.

A simple but important observation is that the potential for undesired/unintended chemical reactions increases rapidly as the number of chemical ingredients is increased. For example, consider the problem of two chemical species that turn out to be chemically incompatible with each other. If three chemical reagents are present, there are three possible permutations for pair-wise chemical incompatibility. The addition of a fourth reagent increases the number of pair-wise permutations to six. Five chemical reagents yields ten pairwise permutations, and n reagents yields n!/[2(n - 2)!] potential pair-wise incompatibilities. Battery chemistry is a striking example of the law of unintended consequences. It could therefore be argued that greater emphasis should be placed on seeking out battery chemistries that are as simple as possible.

However, there are numerous challenges that confront any candidate battery chemistry, any one of which can render such a battery architecture unviable, or only competitive in niche applications. From a market acceptance standpoint, a truly competitive battery technology for an

application such as grid storage must be easy to manufacture, very inexpensive, and extremely reliable. Other constraints are logistical in nature, such as the inconvenience of a battery chemistry that requires the maintenance of very hot or cold temperatures. For batteries of extremely large size, such as those intended for grid storage, it is important to have a battery architecture that is easy to decommission, and whose contents may be fully recycled. Other design challenges pertain to electrical performance, such as adequately high energy density and adequately high electrical conductivity of the anode, cathode, and electrolyte materials. Limited solubility of active reagents in the electrolyte may also pose a problem from the standpoint of energy and power density. A further requirement for good electrical performance is to avoid the problem of reactant depletion and product accumulation to the fullest extent possible; mass transport of electrochemical reactants and products to and from the electrochemical reaction zone must be extremely facile.

The chemical constituents of a proposed battery (or flow battery or fuel cell) may be prohibitively expensive and/or prohibitively toxic. In some cases, one or more chemical constituents may be too corrosive to be used in conjunction with non-exotic structural materials, seals, etc. Some electrochemical systems that look good on paper exhibit extreme sensitivity to chemical impurities in practice. This is problematic not only because any such device is vulnerable to the introduction of contaminants during its construction and operating lifetime; the upfront cost of high-purity reagents can in some cases be orders of magnitude more expensive than their standard-purity counterparts. If at all possible, we should avoid the use of any exotic materials (e.g. for catalysts) and steer clear of electrode structures that rely on complex and/or delicate micromorphology, nanomaterials, etc. As noted earlier, the intercalation-based electrode structures used in Li-ion batteries, for example, are vulnerable to structural degradation during charging and recharging, and this degradation can be accelerated if the charging/discharging process is not carefully controlled. It would be far more preferable to have a battery that is highly insensitive to the manner in which it is charged and discharged. Again, this suggests that the chemistry of the electrodes and electrolyte should be as simple as possible, and we further note that simple chemistry is very valuable from the standpoint of reducing the complexity of engineering optimization and effective focusing of limited R&D resources.

Lastly, we must be cognizant of past instances of (1) performance claims for new battery technologies that have later proved to be irreproducible, (2) manipulation of performance specifications to portray candidate battery technologies in as positive a light as possible, and (3) the degree of difficulty involved in achieving the economies of scale required to succeed in applications such as grid storage. It is therefore desirable to devise a cost-effective battery technology that not only performs extremely well, but for which the underlying reasons for high performance and excellent reliability are in no way mysterious or a matter of speculation to the scientific and engineering community. And ideally, the low cost, extreme scalability, and low technical risk (e.g. of capacity fade several years after commissioning) of a proposed battery technology should be self-evident to those who might underwrite investment in this new technology as well.

2.5. Compiling the list of design rules and precautions

It is argued here that an attempt to devise a battery architecture suitable for bulk grid storage should begin not with a specific chemistry in mind, but with a gathering of fundamental observations. As you will see, some of these “insights” are seemingly trivial, and yet taken

together, they form a blueprint for rethinking the problem of grid storage from first principles. To give a concrete example, let us consider what general conclusions can be drawn from the 30% efficient H_2/O_2 regenerative fuel cell discussed earlier. Referring now to Figure 18, what precautionary principles and design rules might we be able to derive from the example of H_2/O_2 regenerative fuel cell? It is apparent that we should endeavor to steer clear of:

1) Electrochemical half-reactions having high activation energy.
2) Electrochemical half-reactions involving low-probability reaction complexes.
3) Electrochemical half-reactions that require exotic catalysts (e.g. Pt, Pd).
4) Electrochemical half-reactions that incur the triple phase boundary kinetic penalty.
5) Electrolytes with intrinsically poor ionic conductivity.
6) Electrode structures* with intrinsically high electrical resistivity.
7) Requirements for storing compressed gas.

*both the electrode material and electrode aspect ratio are important

Given all of the above drawbacks, it might seem like a waste of time to consider what does work well in the H_2/O_2 regenerative fuel cell grid storage scheme, but let's do it anyway. Where did the H_2/O_2 regenerative fuel cell score points?

1) Earth abundant chemical reagents.
2) Environmentally friendly chemical reagents.
3) Absence of unwanted side reactions (more about this shortly).
4) No kinetic penalty for dilution; the electrolyte is the chemically active reagent.

Items 1, 2, 3 in the above list are elementary observations, but we must admit that cheap ingredients that are environmentally benign and have very simple chemistry are outstanding qualities that we should strive to emulate. Item 4 in the above list is also an elementary observation, but one that is usually overlooked. The concentration of water in the electrolyte of an acidic or alkaline H_2/O_2 regenerative fuel cell is of order 50 M. The rate of a chemical reaction is the product of a rate constant and the chemical activities of the reagents present. The fact that the electrolyte and the electrochemically active ingredient are one and the same is an enormous advantage, not only from the standpoint chemical kinetics, but also from the standpoint of diffusive transport. Moreover, the phase change upon electrolysis of H_2O to H_2 and O_2 gas provides an extremely effective and fully passive mechanism for preventing the build-up of reaction products that would otherwise gather in the vicinity of the electrode/electrolyte interface. There is a lot to admire, even if sluggish kinetics and cost/complexity of hydrogen storage are deal breakers.

It is apparent that we need to steer clear of:

Electrochemical half-reactions having high activation energy.
Electrochemical half-reactions involving low-probability reaction complexes.
Electrochemical half-reactions that require exotic catalysts (e.g. Pt, Pd).
Electrochemical half-reactions that incur the triple phase boundary kinetic penalty.
Electrolytes with intrinsically poor ionic conductivity.
Electrode structures* with intrinsically high electrical resistivity.
Requirements for storing compressed gas.

*both the electrode material and electrode aspect ratio are important

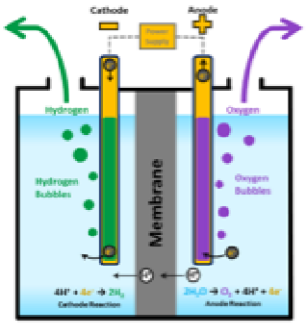

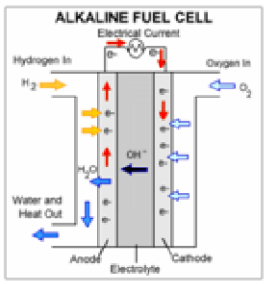

But where did the H_2/O_2 regenerative fuel cell score points?

Earth abundant chemical reagents.
Environmentally friendly chemical reagents.
No kinetic penalty for dilution; the electrolyte *is* the active chemically reagent.
Absence of unwanted side reactions (more about this shortly).

Figure 18: Stepping back to make fundamental observations can sometimes provide unexpected insights.

Figure 19 provides a complete list of pitfalls compiled in the course of this study that we will be striving to avoid. Some of these pitfalls are not fatal, although many of them are. Some pitfalls pertain to technical feasibility, while other pertain to techno-economic viability. With all of these considerations in mind, are we ready to attempt to design an alternative battery architecture? I would argue no. We need to consider all of the application requirements. This includes stringent application requirements that will render most candidate battery chemistries immediately non-viable, but it also includes physical and techno-economic scaling laws that can be uniquely leveraged in this unusual application.

Further updated list of pitfalls:

Complex reaction mechanisms
Breaking of strong covalent bonds
Triple phase boundary kinetic penalty
Reagent dilution kinetic penalty
Exotic electrode materials
Storage of compressed gas
Poor electrolyte conductivity
High resistance electrode structures
Unwanted side reactions that result in degradation
Chemical reagents having persistent toxicity
Non-earth-abundant chemical reagents (cost and scalability)
Electrolyte stratification
Low gravimetric storage density
Capacity fade (grid storage requires 10,000 charge/discharge cycles)
Vulnerable/delicate electrode morphology
Chemical complexity (n!/[2 (n - 2)!] pair-wise permutations)

Figure 19: Considerations that must simultaneously be kept in mind in the search for a suitable battery chemistry.

Referring now to Figure 20, if we know a priori that we are going to be building very large batteries in extremely large quantities, what issues assume the greatest importance? Well, first and foremost, they had better be extremely cheap. Simplicity and earth abundant materials should be foremost considerations. A related issue is scalability. A battery design that works well at small size but can't be scaled up to something the size of a shipping container is going to have a difficult time competing in the bulk grid storage arena. Safety is also critically important, because we're talking about storing a lot of energy in one place. It's one thing if a lithium-ion laptop battery catches fire. The specter of a multi-million-dollar Li-ion battery the size of small building burning out of control is another matter. The reagents used inside the battery had better be environmentally friendly and/or recyclable, because we're planning to build an enormous number of these batteries and some day they will need to be decommissioned. The environmental impact of mineral extraction also looms large because of the staggering quantity of materials involved. Then there is the issue of industrial capacity of existing supply chains. If we need to ramp up production of such batteries on a massive scale over the course of a decade, will sourcing the necessary materials by difficult or involve economic disruption of existing markets?

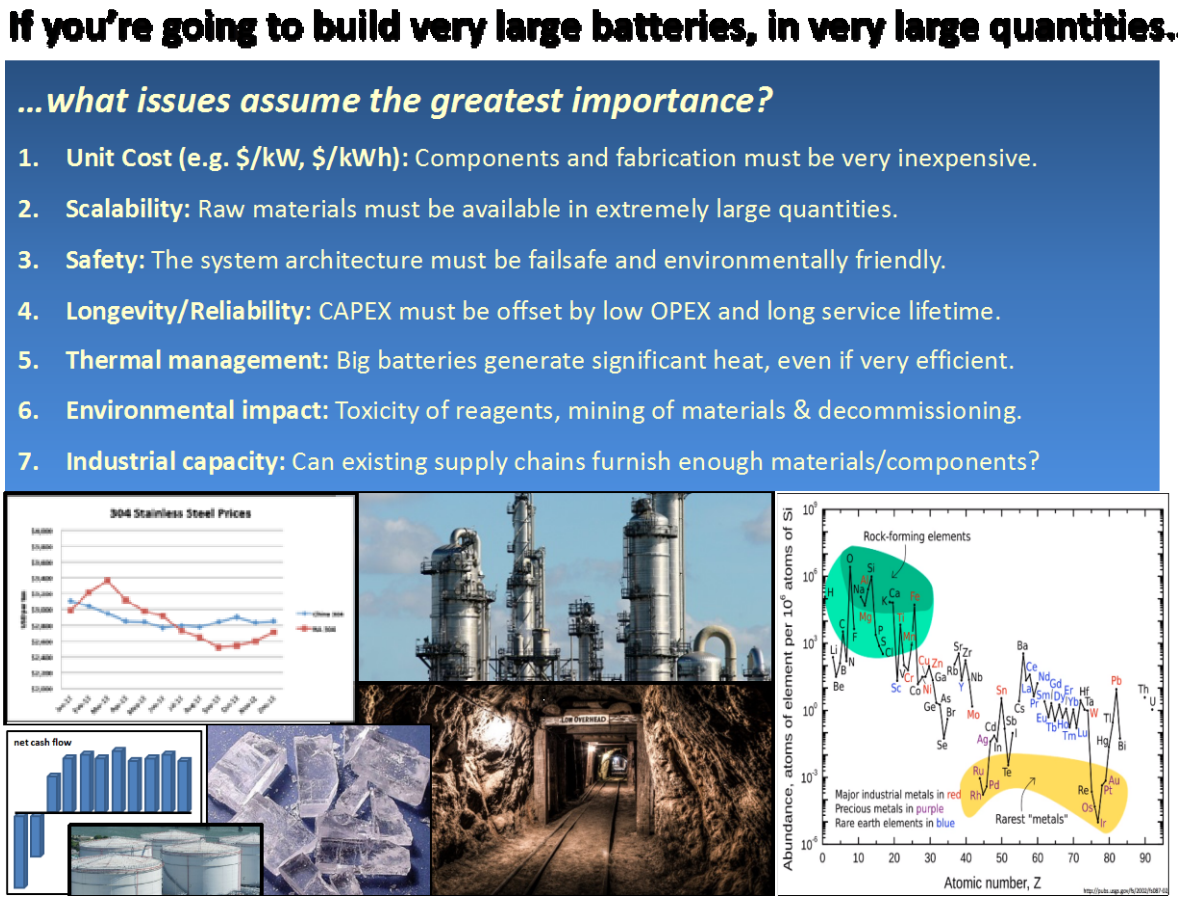

Figure 20: Problem solving hints are often hiding inside the application space. Some are obvious, but some are not.

Next, we must consider the subject of battery thermal management from first principles. Let us imagine a 10-MW/100-MW-hr battery the size of a shipping container that is connected to the grid to buffer the diurnal variability of Solar PV. At any given time, as much as 10 MW of electrical power is either entering (charging) or exiting (discharging) this battery. Even if the charging and discharging efficiency of such a battery is as high as 95%, at any given time we have as much as 500 kW of waste heat being generated inside a volume the size of a shipping container. This heat has to be removed, and the gold standard for practicality in heat sinking is air cooling. Our battery must therefore be equipped with an air-cooled heat exchanger capable of exporting 500 kW of heat to the surrounding air. Having spent many years building and designing heat exchangers,[13] it was surprising to learn that the issue of heat sinking is discussed relatively infrequently in publications concerned with grid-scale electrochemical storage. Heat exchanger hardware can be quite expensive, bulky, and complicated. When contemplating heat-sinking at the 500-kW level, it is very important to remember that the amount of heat that can be rejected is proportional to product of heat-exchanger thermal conductance and ΔT, where $\Delta T = T_{hot} - T_{ambient}$ is the driving force for heat transfer. From an engineering standpoint, reductions in heat-exchanger thermal resistance tend to be hard-won, which strongly suggests that such a battery should be intentionally be designed to operate well above ambient temperature. This is the only viable approach to rejecting 500 kW of heat to the surrounding air without a large and expensive heat exchanger. And the imperative to design for high-temperature operation goes

hand-in-hand with the L^2 scaling law that governs conductive cooling of large objects to their surroundings illustrated in Figure 21. In the case of an electrochemical cell the size of an automotive battery, operation at high temperature is extremely undesirable because a great deal of energy (relative to that stored in the battery) will be expended keeping the battery hot. The situation is completely reversed for the case of battery the size of shipping container. Keeping such a battery well above ambient temperature requires very little heat and very little thermal insulation because of the L^2 scaling law of Figure 21. On the contrary, the main challenge to operating a battery the size of shipping container, even it has very high round trip efficiency, is keeping it from overheating (and doing so without an expensive and complicated heat exchanger). Thus, much of the thermal management intuition gathered from the prior art in electrochemical cells is potentially very misleading in the present context. Perhaps instead, we should be thinking about the potential advantages that can be leveraged if we commit ourselves to high-temperature operation, with the understanding that temperatures must not be so high that conventional low-cost engineering materials are unsuitable.

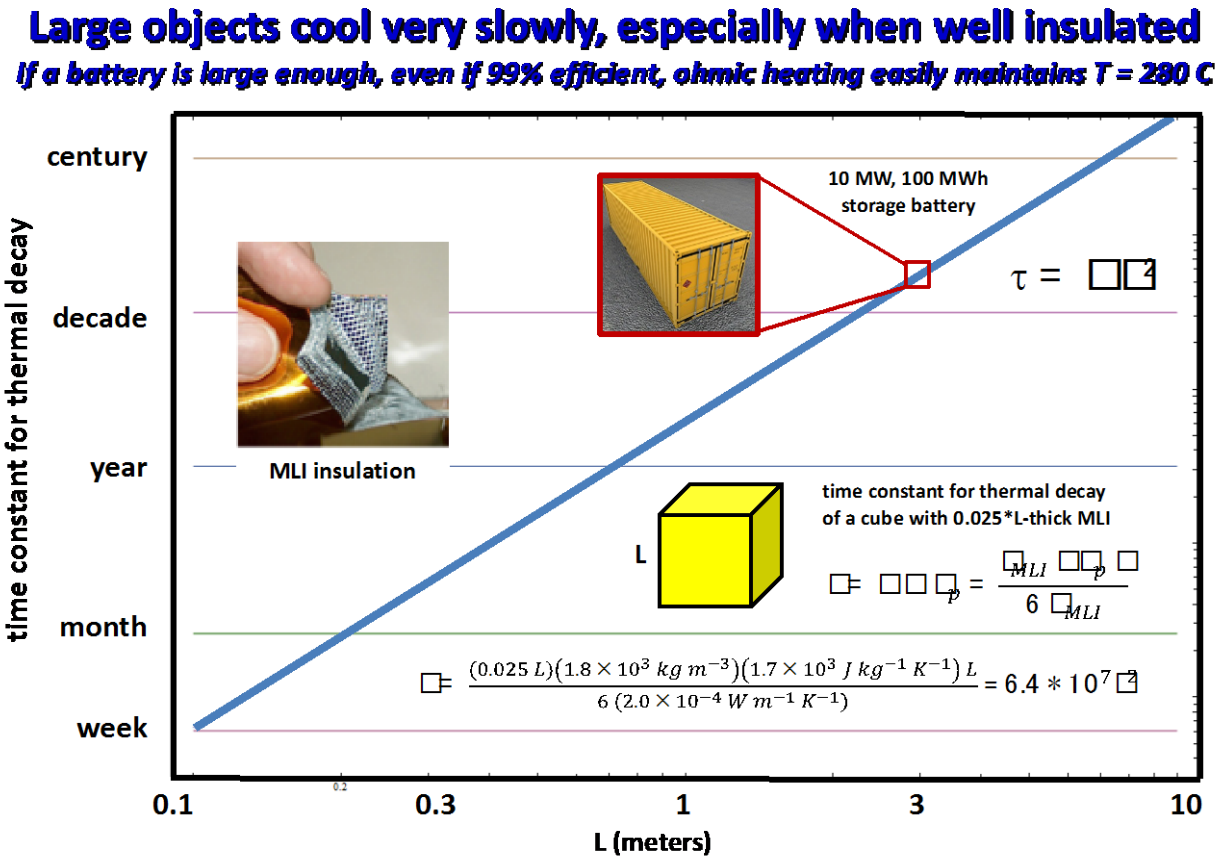

Figure 21: The magnitude of the L^2 effect described below is very counterintuitive. It can also be valuably exploited.

We have attempted to capture this and other fundamental design considerations in Figure 22. We assert that a competitive battery technology for bulk grid storage would be based on a flow battery architecture, because scaling up energy storage only requires more reagent and larger storage tanks, and because a flow battery eliminates the need to co-locate large quantities of chemically reactive species (safe storage requires physical separation of reactants).

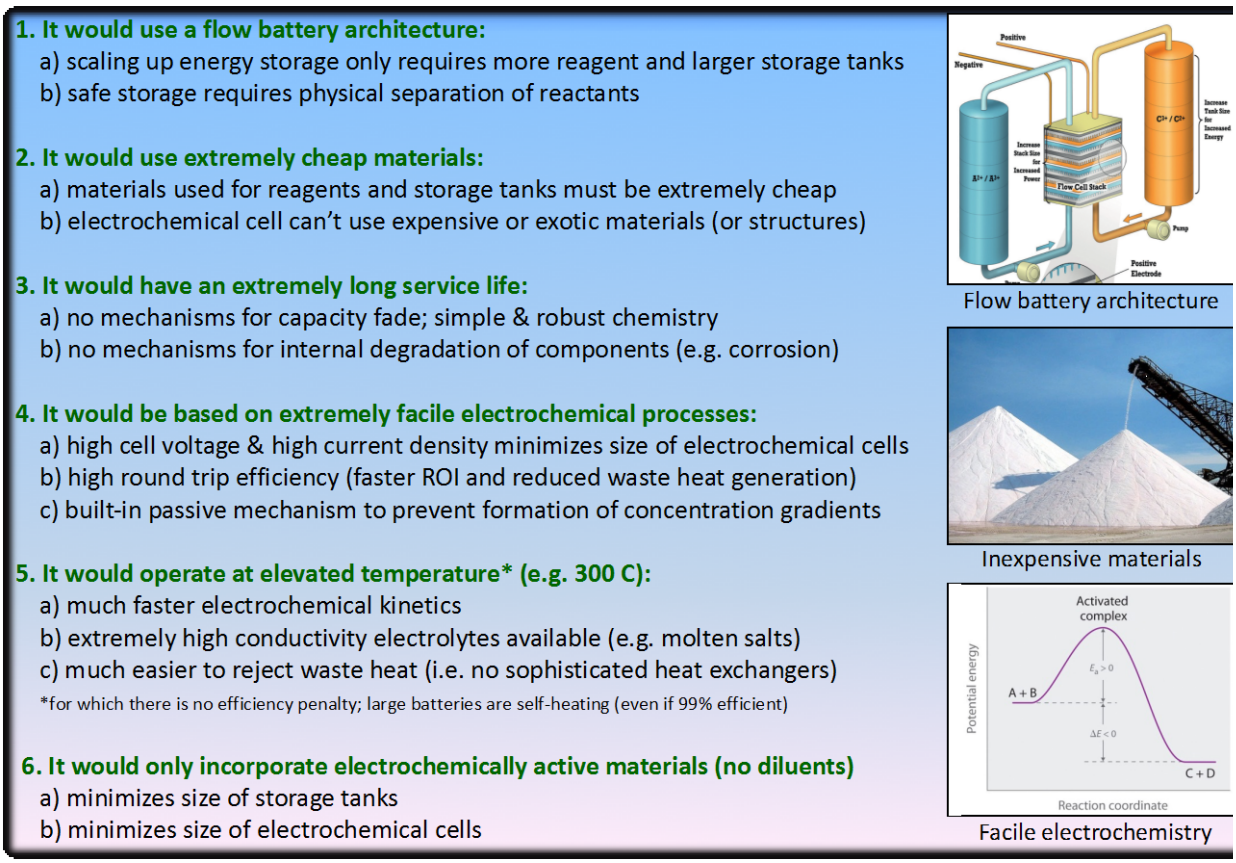

Figure 22: Bringing the design process into clearer focus. Can we be more specific about what system architecture characteristics we should be aiming for?

As discussed earlier, we further assert that such a battery would use extremely cheap materials, not only for the chemical reagents and electrochemical cell, but for the storage tanks and plumbing as well. Such battery must also have an extremely long service life (e.g. 30 years) to meet requirements for cost amortization. We should therefore be looking for battery chemistries that have no known mechanisms for capacity fade, which most likely means simple and robust chemistry. There must be no mechanisms for internal degradation of components (e.g. corrosion) over a 30-year timeframe as well.

As articulated in Figure 22, we assert that such a battery would be based on extremely facile electrochemical processes; sluggish electrochemistry invariably results in significant efficiency penalties and interferes with our ability to shrink the electrochemical cell portion of the flow battery down in size to minimize cost. High roundtrip efficiency also implies faster ROI and reduced waste heat generation. Along similar lines, high cell voltage is very desirable to minimize current density, which affects both the size of electrochemical cells and I^2R losses. Referring now to Figure 23 – also relevant to the issue of facile charging/discharging – ideally, we'd like to have a built-in passive mechanism to prevent formation of concentration gradients, and avoid reliance on diffusive transport and the resultant overvoltage efficiency penalties.

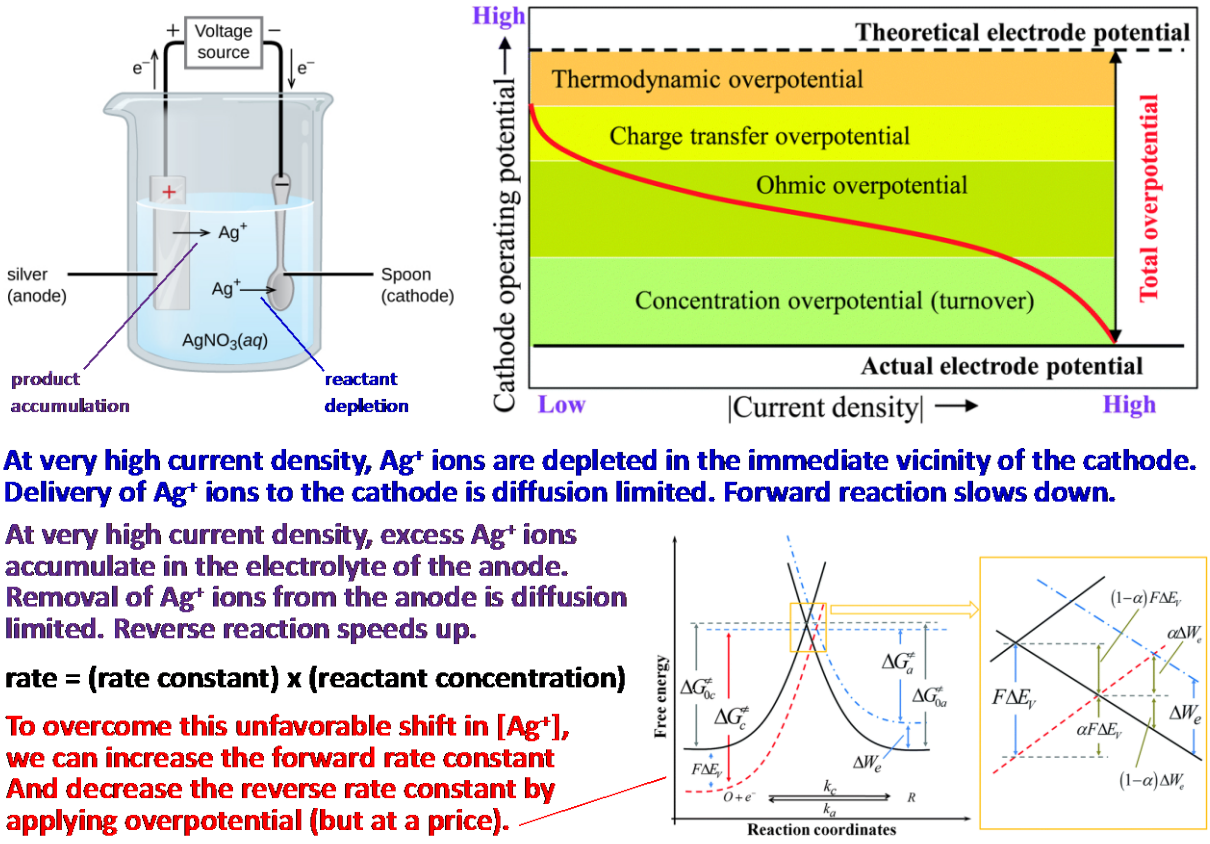

Figure 23: At high current density, the onset of an additional overvoltage term is observed. How do we combat this effect?

This brings us to high-temperature operation (e.g. 300 °C), a design strategy which if employed carefully makes it not only easier to reject waste heat, but also provides for much faster electrochemical kinetics and access to electrolytes having extremely high conductivity, such as molten salts. Again, it must be emphasized that there is no energy efficiency penalty for maintaining such batteries at elevated temperature; above the size of a cubic meter, such batteries are self-heating and do not require additional heat to maintain their temperature.

Finally, we contend that such a battery would only incorporate electrochemically active materials (no diluents), which not only improves chemical kinetics and mass transport as noted earlier, but also minimizes the size of storage tanks, electrochemical cells, and plumbing.

All of the above considerations are very instructive, but we would be remiss if we did not also ask ourselves one additional fundamental question. What does an extremely facile electrochemical half-reaction look like? Referring to Figure 24, the exchange current density (j_o) is equivalent to the chemical kinetic rate constant of a half reaction. Observed values of j_o for well-known half reactions vary from 10^{-20} A cm^{-2} to 10^{-1} A cm^{-2}. This 19-order-of-magnitude range in rate constants suggests that we would be well advised to understand what factors contribute to high values of exchange current density. In classical electrochemistry, the half reaction $Ag^+ + e^- \leftrightarrow Ag$ (j_o = 0.15 A cm^{-2}) is a well-known example of a high j_o electrochemical process. What is it that is unique about the $Ag^+ + e^- \leftrightarrow Ag$ half-reaction for the silver spoon being electroplated in Figure 24? The first important point is that the half-reaction in question is

a single electron transfer reaction. Furthermore, other than the need for the Ag^+ ion to shed a coordination sphere of surrounding H_2O molecules, it is for all intents and purposes, a single-step reaction mechanism. The activation energy for this reaction is very low because there is no breaking of chemical bonds, and the rate is fast in part because of no significant motion of nuclei. Finally, there is no triple phase boundary penalty; all portions of the electrode surface are simultaneously active. What about the electron configuration of the electrochemically active species? The electron configuration for elemental silver is:

Ag: [Kr] $4d^{10}$ $5s^1$

The 4d orbitals are completely filled, but there is a single unpaired electron in the 5s orbital. This single unpaired electron is chemically analogous to free radical species, which are well known for their high reactivity. The question of whether it is an incorrect use of terminology to think of elemental silver as a “free radical” is certainly very valid, but as we move further up the periodic table, we find perhaps more valid analogies. Consider the classical “harpoon mechanism” for the reaction of sodium metal with a diatomic halogen. As the Na atom ([Ar] $3s^1$) approaches the highly electronegative halogen molecule, it’s single unpaired 3s electron is drawn in the direction of the halogen molecule; in effect there is a Coulombic attraction between the two species that provides a higher than gas kinetic collision rate. While it must be remembered that the notion of designating all species having open shell electron configurations as “free radicals” is limited in its significance – much as the “harpoon mechanism” is merely a model and not a complete depiction of the chemical physics that govern such reactions – the notion that such “radical-ion” electron transfer reactions are likely to be extremely facile is reasonable to hypothesize.

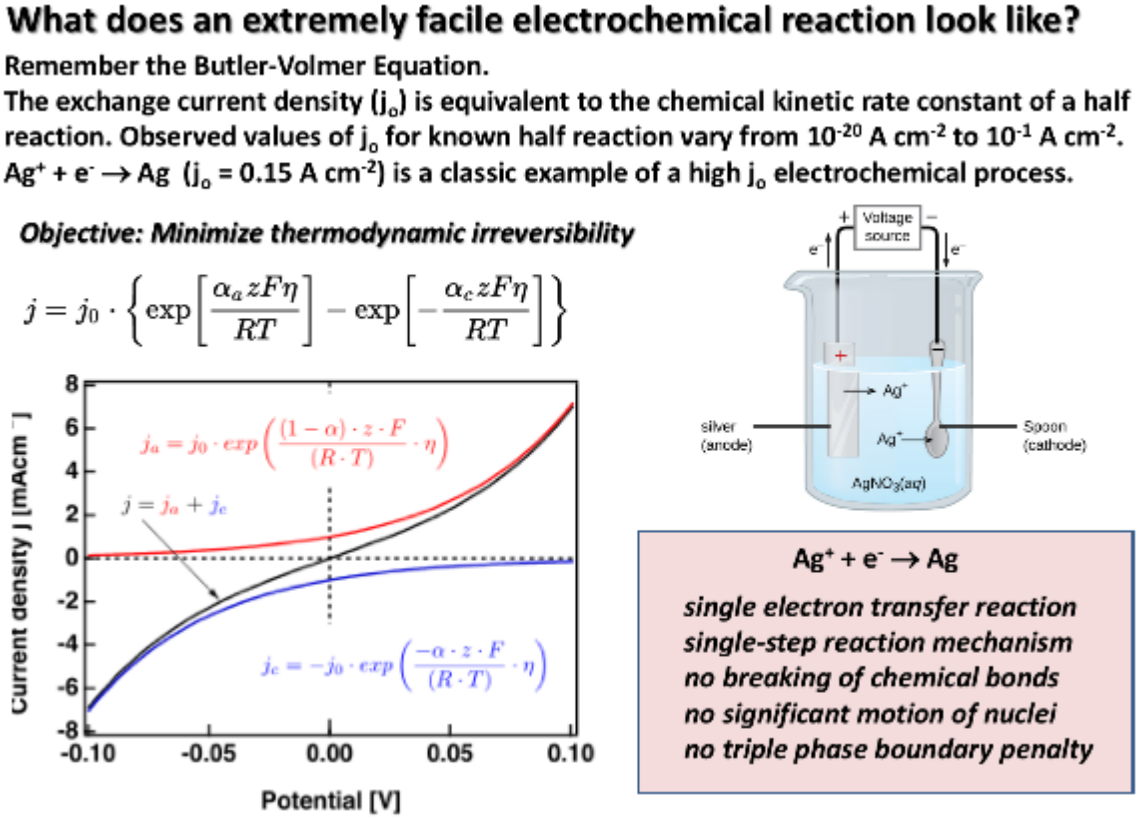

Figure 24: Despite a very long history of battery innovation, this fundamental question is an important one to ask.

Such considerations are manifested in the classical sodium sulfur battery, invented over 50 years ago and still the subject of extensive research today. Referring to Figure 25, in the sodium sulfur battery the half reaction at the inner electrode is the simple 1e$^-$ process $Na \leftrightarrow Na^+ + e^-$. The molten sodium metal (melting point of 97 °C) is sequestered from the electrolyte by an ionically conductive material such as sodium beta alumina (Na-β-Al_2O_3) which forms a hermetic enclosure but is capable of conducting Na^+ ions with low ohmic resistance under an applied electric field. A review of the extensive literature on sodium sulfur batteries is rather striking in that the vast majority of papers focus on one of two topics:

1) Nuisance problems on the sulfur side of the battery related to corrosion, seal and insulator degradation, and non-ideal electrochemical processes, and
2) Improvements in Na^+ ion conducting materials such as Na-β-Al_2O_3, and NASICON.

Rarely is there any mention of the $Na \leftrightarrow Na^+ + e^-$ half reaction. The reason for this is that the $Na \leftrightarrow Na^+ + e^-$ half reaction does its job. It's a simple observation, but an important one. The $Na \leftrightarrow Na^+ + e^-$ half reaction provides an excellent approximation to a thermodynamically reversible process. This is consistent with literature measurements of the exchange current density for molten sodium chloride, which reaches an astronomical 100 A cm^{-2} at 820 °C, and doubles when the temperature is further increased by 100 °C.[14] It is also consistent with the hand waving argument that a sodium atom has a single unpaired electron in its outer shell that is easily removed and renders a highly stable Na^+ ion. Maybe we should be thinking about how to construct an electrochemical cell that employs ultrafast radical-ion half reactions on both sides of

the battery. If both the ion and radical at the electrode/electrolyte interface are stable species, separated by little or no activation energy barrier, we ought to observe extremely facile kinetics at both electrodes.

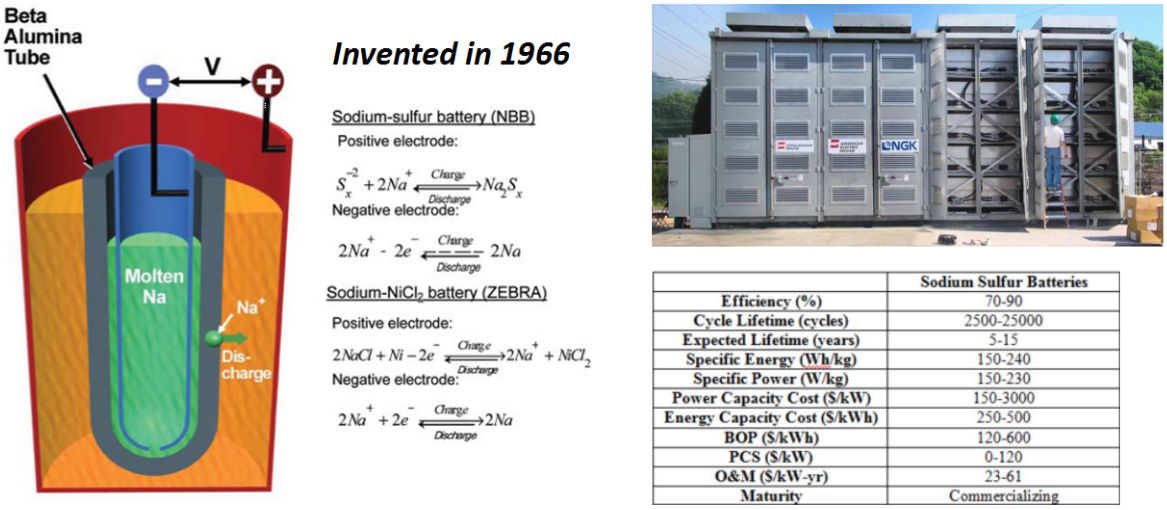

	Sodium Sulfur Batteries
Efficiency (%)	70-90
Cycle Lifetime (cycles)	2500-25000
Expected Lifetime (years)	5-15
Specific Energy (Wh/kg)	150-240
Specific Power (W/kg)	150-230
Power Capacity Cost ($/kW)	150-3000
Energy Capacity Cost ($/kWh)	250-500
BOP ($/kWh)	120-600
PCS ($/kW)	0-120
O&M ($/kW-yr)	23-61
Maturity	Commercializing

...the sodium side of which exhibits exemplary behavior.

Na → Na⁺ + e⁻ is actually a radical-ion half reaction.

Na-β-Al$_2$O$_3$ has remarkably high conductivity for Na⁺ ions (0.24 Ω^{-1} cm^{-1} @ 300 C).

The sulfur side does not exhibit exemplary behavior (corrosion, seals, overvoltage).

These nuisance problems have prevented proliferation of NaS battery technology.

Nonetheless, companies such as NGK has expended enormous resources on NaS.

Note the use of elevated (but manageable) temperature to speed chemical kinetics.

Figure 25: An analogy can be found in the classic sodium sulfur battery.

3. THE RADICAL-ION FLOW BATTERY (RIFB) CONCEPT

With the above considerations in mind, we now describe what we will be referred to hereafter as the Radical-Ion Flow Battery (RIFB). In an effort to make the discussion that follows more concrete, we will use utility-scale grid storage as the representative application for the proposed technology, and we will use a representative embodiment of the Radical-Ion Battery based on sodium nitrite ($NaNO_2$) to provide an overview. The description of this representative embodiment/application is in no way meant to be limiting. As discussed later, a very wide range of other embodiments and applications are contemplated.

Referring to Figure 26, the active portion of the electrochemical cell comprises an outer cylindrical container fabricated from a material such as stainless steel, that serves as both an electrode and a containment vessel for the electrolyte, wherein the electrolyte comprises molten $NaNO_2$ maintained at a temperature of 300 °C, that surrounds a hollow cylindrical enclosure (fabricated from a sodium-ion-selective membrane material such as sodium-beta-alumina) containing molten sodium metal, wherein the sodium metal functions as a second electrode. As illustrated in Figures 27 and 28, the system as a whole further comprises an external reservoir of molten sodium metal, an external reservoir of nitrogen dioxide, and an external reservoir of

molten $NaNO_2$. During charging/discharging of the battery, the two electrochemical half reactions are:

Charging half reactions:

Na^+ (molten) + e^- (cationic electrode) → Na (liquid) *Na^+ ions are sourced from the electrolyte*

NO_2^- (molten) → NO_2 (gas) + e^- (anionic electrode) *NO_2^- ions are sourced from the electrolyte*

Discharging half reactions:

Na (liquid) → Na^+ (molten) + e^- (cationic electrode) *Na^+ ions are sinked to the electrolyte*

NO_2 (gas) + e^- (anionic electrode) → NO_2^- (molten) *NO_2^- ions are sinked to the electrolyte*

In the interest of clarity, we have introduced the notation "cationic electrode" and "anionic electrode" above. A tremendous amount of confusion arises in the prior art in conjunction with the terms "anode" and "cathode". Sometimes the anode and cathode of a device is defined in terms of electrical polarity, while in other instances anode/cathode designations are assigned according to whether oxidation or reduction is taking place. Moreover, the above criteria may be reversed depending on whether a battery, fuel cell, etc. is being charged or discharged. To make the situation even more confusing, the direction that electrons flow is opposite to the direction that conventional electrical current flows. To avoid this confusion and to provide a clear mental picture of the embodiments described herein, we will use the terms cationic electrode and anionic electrode. Whether the electrochemical cell is being charged or discharged, the cationic electrode is the electrode that sources (sinks) cations from (to) the electrolyte, and the anionic electrode is the electrode that sources (sinks) anions from (to) the electrolyte. In colloquial terms, we might say that the cationic electrode "transacts business with cations" and the anionic electrode "transacts business with anions". To further clarify the above description, Figure 29 provides a schematic diagram of a planar version of such an electrochemical cell, and Figure 30 explicitly illustrates the electron transfer processes entailed in the four half reactions (two for charging and two for discharging).

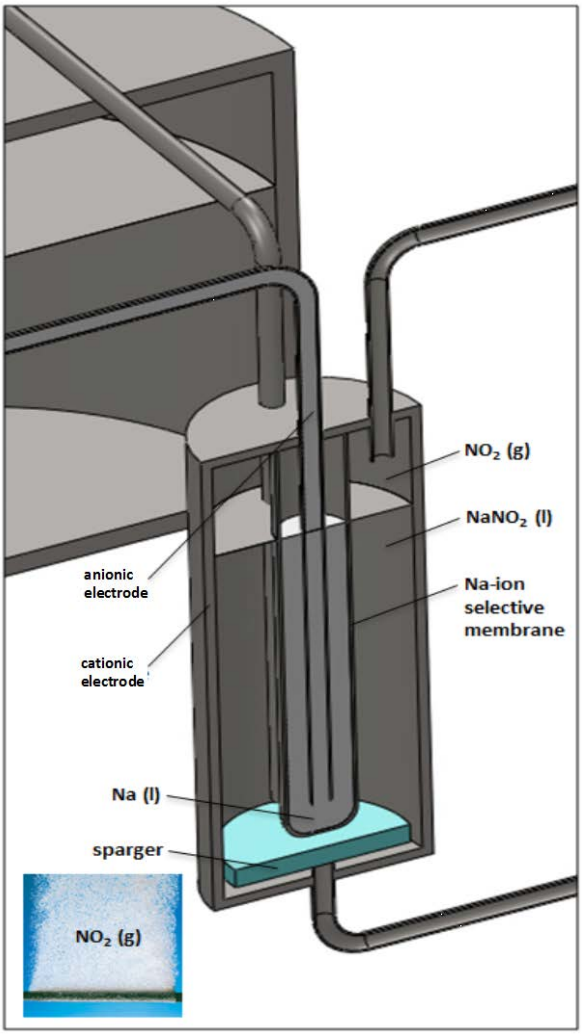

Figure 26: One possible instantiation of the electrochemically active portion of a $NaNO_2$-based radical-ion battery.

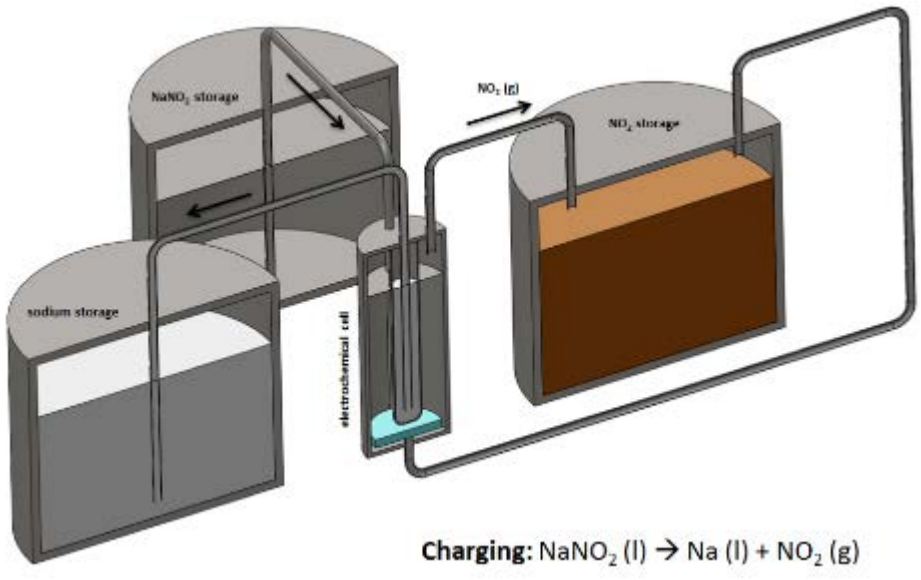

Figure 27: One possible instantiation of a $NaNO_2$-based radical-ion battery shown during electrical charging.

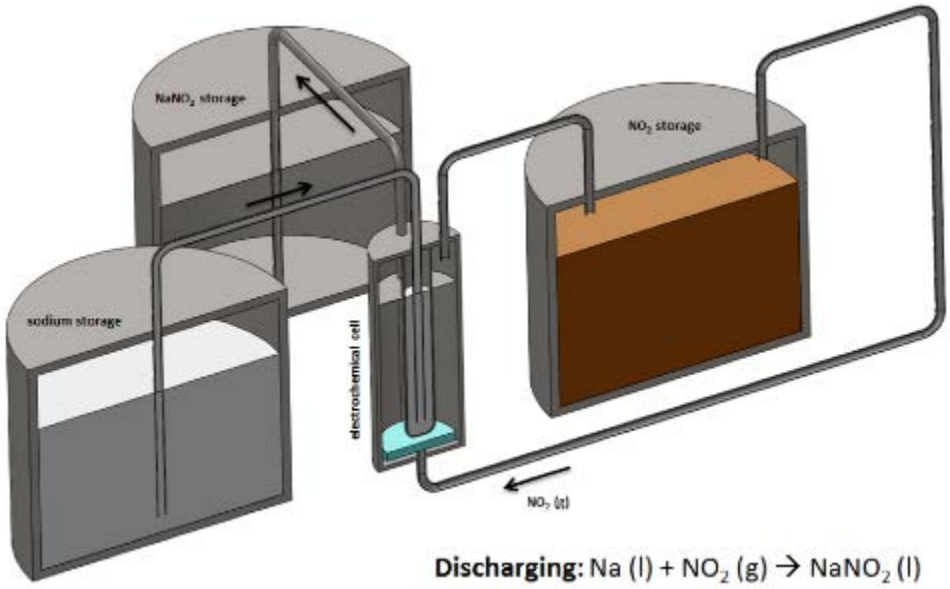

Figure 28: One possible instantiation of a $NaNO_2$-based radical-ion battery shown during electrical discharging.

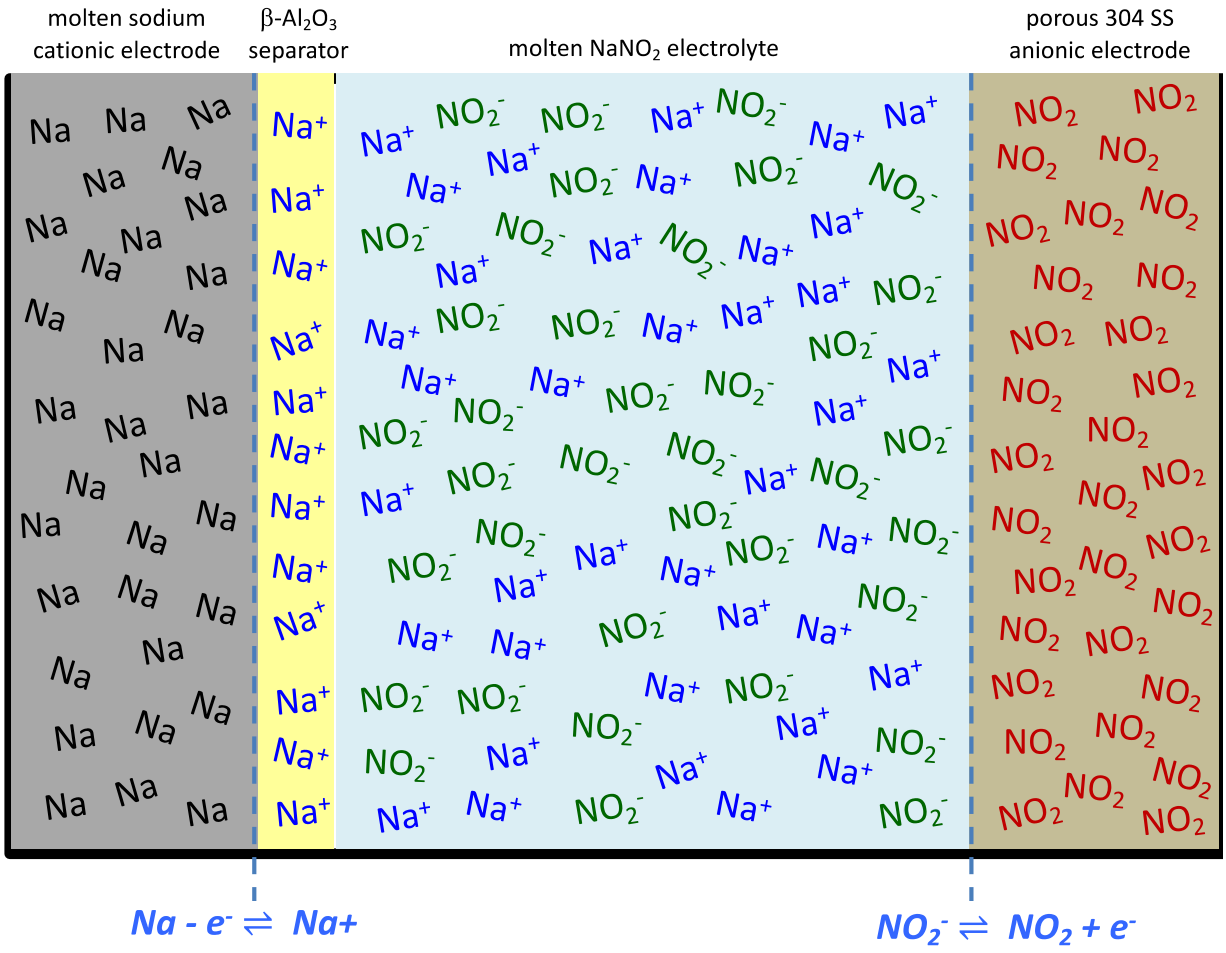

Figure 29: Schematic diagram of planar Radical-Ion Flow Battery.

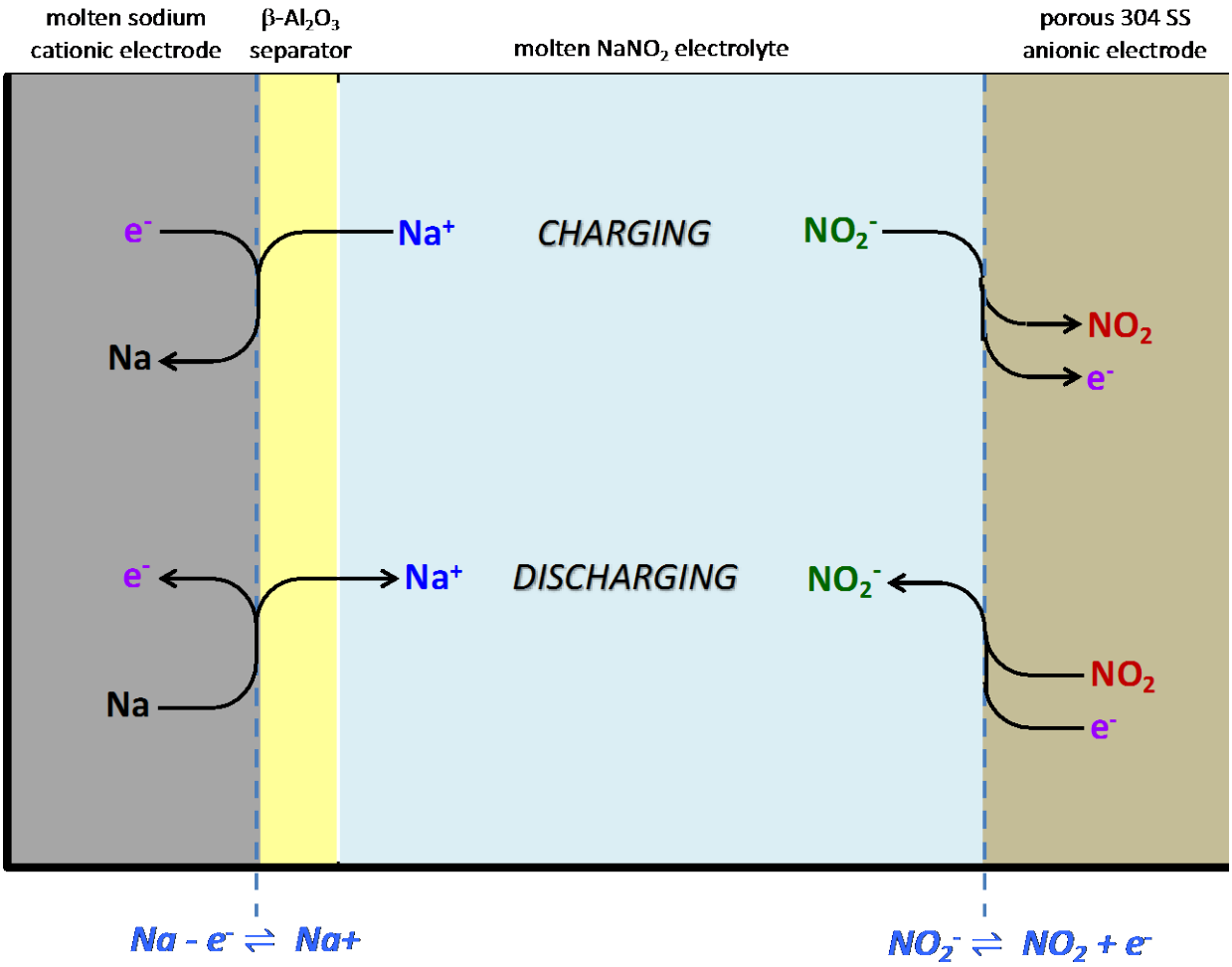

Figure 30: Schematic diagram of charging and discharging half reactions.

Using tabulated thermodynamic data for the standard free energy of formation for each of the reagents:[15]

$\Delta G_f°(Na) = 0$ kJ mol^{-1}

$\Delta G_f°(NO_2) = +51.9$ kJ mol^{-1}

$\Delta G_f°(NaNO_2) = -284.6$ kJ mol^{-1}

we calculate the change in free energy for the Na + NO_2 → $NaNO_2$ reaction under standard state conditions to be:

$\Delta G° = -336.5$ kJ mol^{-1}

from which we calculate a standard state electrochemical potential of:

$$E° = \frac{\Delta G_f°}{n\,F} = \frac{336500\ J\ mol^{-1}}{96485\ C\ mol^{-1}} = 3.49\ V$$

At elevated temperature the free energy required to dissociate $NaNO_2$ into Na and NO_2 is somewhat lower. Based on heat capacity data for Na, NO_2, and $NaNO_2$,[16] [17] in Figure 31 we

have calculated the molar enthalpies, molar entropies, ΔH, ΔS, and ΔG for the reaction $NaNO_2$ → Na + NO_2, and the temperature dependence of the electrochemical cell voltage, all as a function of temperature. The step-like features in some of these plots correspond to solid-to-liquid phase transitions. The cell voltage at the nominal operating temperature of 300 °C is 3.01 V, with a temperature coefficient of -1.4 mV K^{-1}. As shown in Figure 32, the thermodynamics for partitioning of NO_x into NO and NO_2 is not a problem at the operating temperatures contemplated; even at 300 °C, 80% of NO_2 generated by electrolysis remains in the form of NO_2.

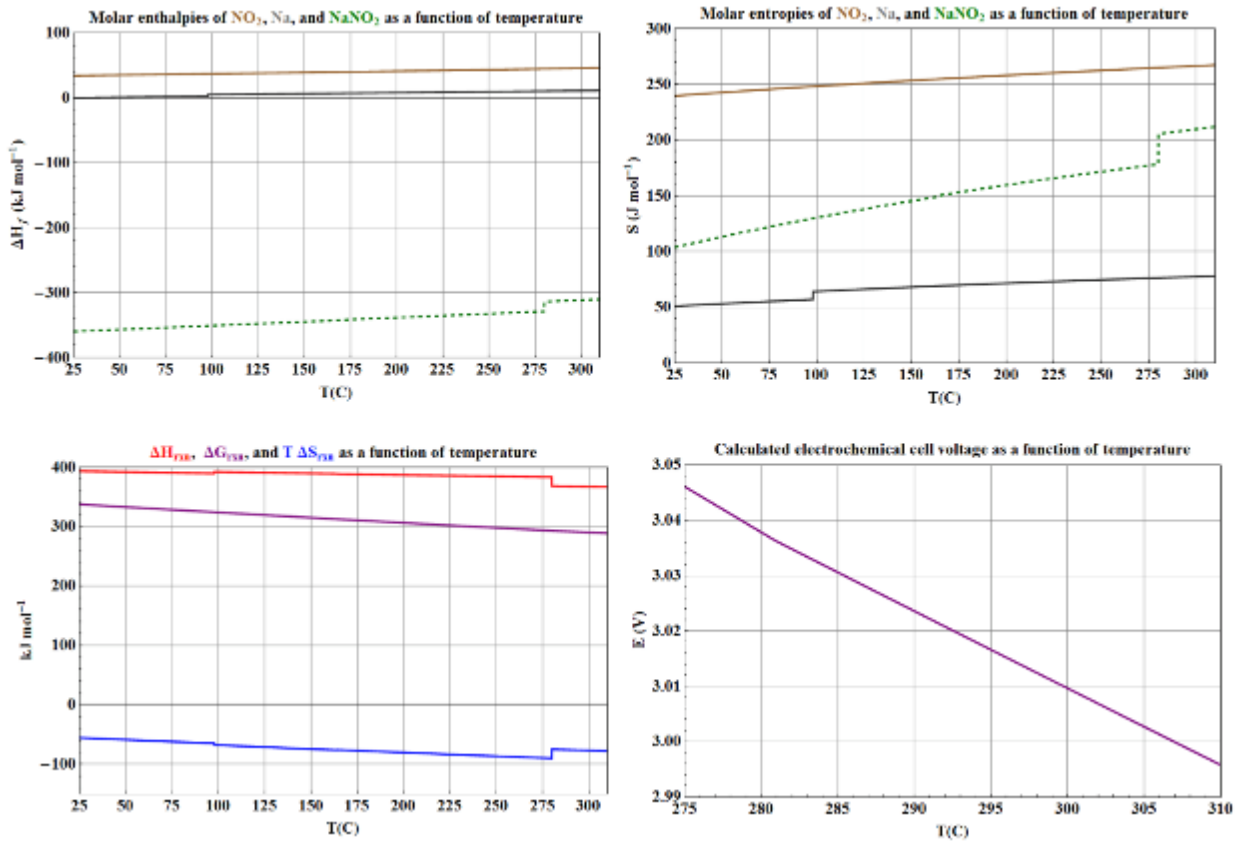

Figure 31: Crunching the numbers: molar enthalpies (ΔH), molar entropies (ΔS), and Gibbs free energy (ΔG) of reagents, and electrochemical cell voltage for $NaNO_2$ → Na + NO_2 reaction as a function of temperature. The nominal cell voltage at 280 C is 3.04 V. High cell voltage keeps I^2R losses to a minimum.

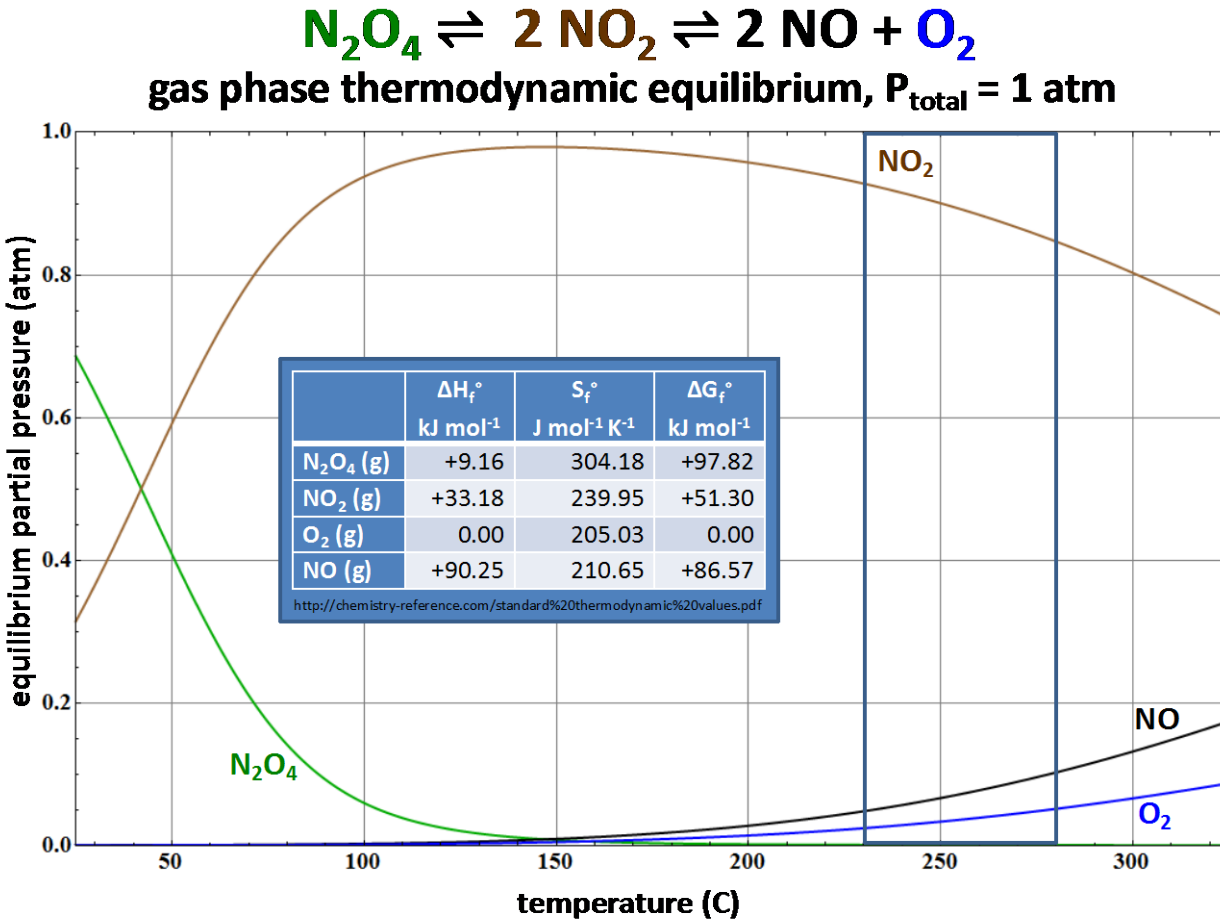

Figure 32: Thermal dissociation of NO_2 is not a major concern under contemplated operating conditions.

Referring now to Figure 33, it will be noted that both electrode processes comprise simple electron transfer reactions that involve no bond breaking or displacement of nuclei (other than a change of O-N-O bond angle from 115° to 134°),[18] and that both half reactions involve an ion and a free radical. The unpaired electrons of free radical species such as Na and NO_2 tend to be chemically labile, and unlike neutral molecules such as H_2, O_2, H_2O, etc. ionic species such as Na^+ and NO_2^- readily accept and donate electrons, respectively. The use of radical/ion electron-transfer reactions at both electrodes is directed towards providing unusually favorable electrochemical reaction kinetics. The very low activation energy of radical/ion electron transfer reactions, in addition to the fact that each half reaction presumably entails a single-step, unimolecular process, further suggests that exotic catalysts such as platinum, palladium, etc. will not be necessary to achieve low overvoltages and high current density.[19] As mentioned earlier, eliminating the need for expensive/exotic catalyst materials is a very important objective. And as will be discussed later, one point that is often overlooked is that the presence of such potent catalysts increases the likelihood of undesired side reactions that prove detrimental to the longevity and reliability of a proposed electrochemical cell. Moreover, to the extent that a radical-ion redox half-reaction such as $NO_2^- \rightarrow NO_2 + e^-$ exhibits relative indifference to the

material chosen for the electrode, it also implies that constraints on the chemical purity of the electrode surfaces and reagents are likely to be relaxed.

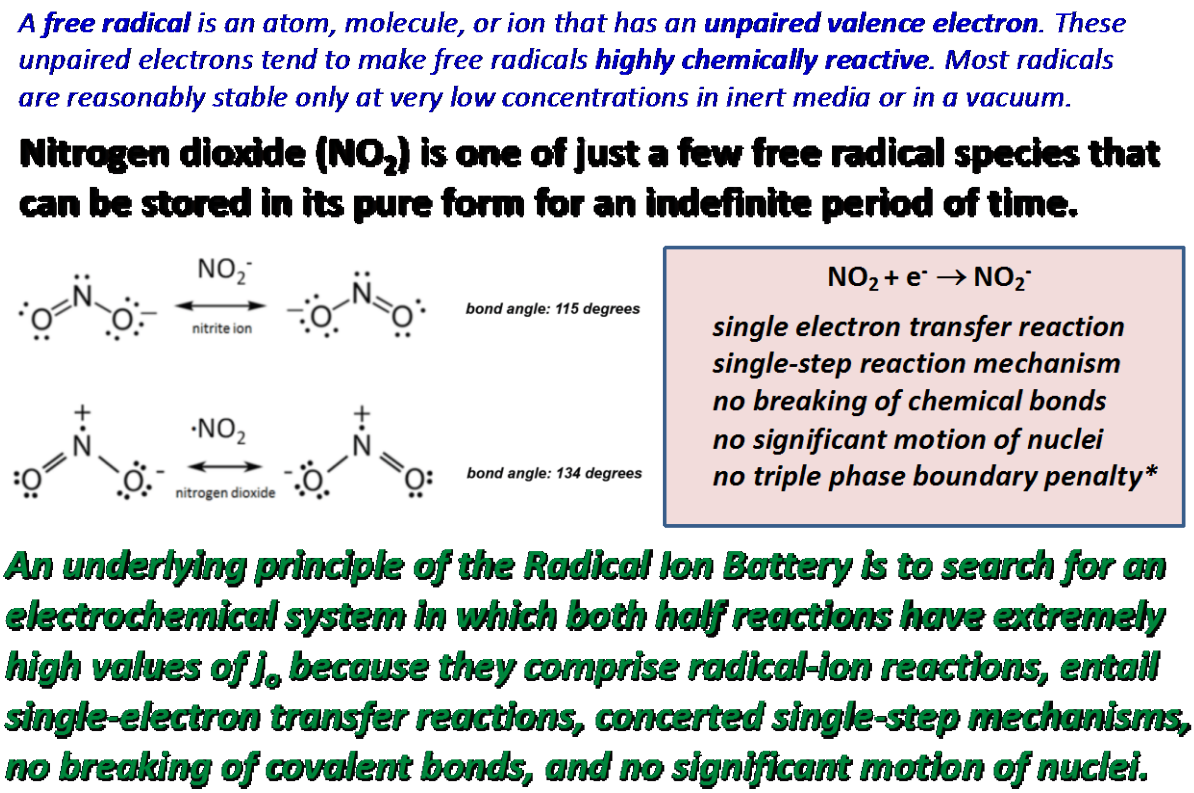

Figure 33: What's going on at the anionic electrode?

The fact that the electrolyte and the electrochemically active species transported through the electrolyte are one and the same is also extremely favorable from the standpoint of reaction kinetics (due to concentration effects) and transport (due to the very short distance Na^+ and NO_2^- ions are required to move within the electrolyte to reestablish electrostatic equilibrium). Referring to Figure 34, another important aspect of the proposed electrochemical cell concerns facile reactant/product transport. Because NO_2 is evolved as buoyant gas bubbles, NO_2 gas generated during the charging reaction is rapidly removed from the vicinity of the anionic electrode, rather than accumulating in the surrounding electrolyte. In the case of the cationic electrode, accumulation of Na in electrolyte adjacent to the electrode is a non-issue because Na and Na^+ are rigorously separated by the ion-selective membrane. In fact, the presence of this ion-selective barrier is the only reason the reaction $NaNO_2 \rightarrow Na + NO_2$ can be carried out. In the absence of such a barrier, sodium metal would immediately react with the electrolyte to form oxides of sodium.

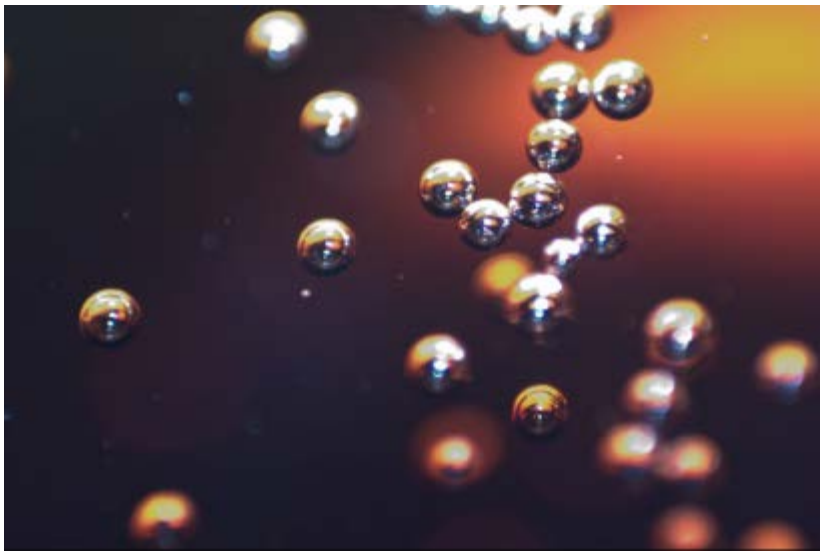

Figure 34: Nitrogen dioxide bubbles in molten $NaNO_2$.

Note, it is important to make a clear distinction between half reactions at the anionic electrode involving stable free radical species such as NO_2, and chemical species such as diatomic chlorine (Cl_2). While individual chlorine atoms have unpaired electrons by virtue of having an odd number of valence electrons, atomic chlorine is not a stable free radical that persists indefinitely under the conditions found in such an electrochemical cell. Rather, atomic chlorine atoms rapidly combine to form diatomic chlorine, a stable covalently bonded molecule with a bond energy of 240 kJ mol^{-1}.[20] The strong covalent bond found in Cl_2 (and other such halogen species) represents a significant kinetic impediment to the electrochemical half-reaction at the anionic electrode. In marked contrast, the electrochemical half reaction involving the interconversion of NO_2 and NO_2^- at the anionic electrode presumably entails a single-step, unimolecular process involving no bond breaking or significant displacement of nuclei, and has very low activation energy. Beyond the halogens, it will be understood that there are many chemical species that may be converted to free radicals under appropriate conditions, but that do not furnish significant steady state concentrations of free radicals under the conditions found in such an electrochemical cell.

3.1. Scalabilty considerations

Yet another critically important attribute of the proposed technology is the extreme abundance of the constituents required to fabricate such batteries. The net reaction for the synthesis of $NaNO_2$ on an industrial scale is:

$2\ NaCl + N_2 + 2\ O_2 \rightarrow 2\ NaNO_2 + Cl_2$

Sodium chloride may be prepared from sea water, salt lakes, or NaCl mineral deposits. Nitrogen and oxygen can be sourced from the atmosphere. In practice, the above synthesis process may be carried out as follows:

Reaction

2 [2 NaCl (aq) + 2 H_2O → 2 NaOH (aq) + H_2 (g) + Cl_2 (g)]	chlor-alkali process	A
2 [2 H_2O (l) → O_2 (g) + 2 H_2 (g)]	electrolysis of water	B
2 [N_2 (g) + 3 H_2 (g) → 2 NH_3 (g)]	Haber-Bosch process	C
1 [4 NH_3 (g) + 5 O_2 (g) → 4 NO (g) + 6 H_2O (l)]	combustion of NH_3	D
1 [2 NO (g) + O_2 (g) → 2 NO_2 (g)]	oxidation of nitric oxide	E
2 [2 NaOH (aq) + NO_2 (g) + NO (g) → 2 $NaNO_2$ (aq) + H_2O (l)]	$NaNO_2$ synthesis	F
2 [2 NaCl + N_2 + 2 O_2 → 2 $NaNO_2$ + Cl_2]	$NaNO_2$ production, Cl_2 by-product	

It will be understood that the above reaction scheme is one of several possible routes to industrial scale synthesis of $NaNO_2$. In this particular scheme, 1/3 of the H_2 required for synthesis of NH_3 is derived from the chloralkali process, and 2/3 is provided by electrolysis of water. Reaction steps A, B, and C are non-spontaneous chemical reactions that require the input of energy. Reaction steps D, E, and F are spontaneous chemical reactions.

Another outstanding attribute of this system is the very high ionic conductivity of the electrolyte. The ionic conductivity of molten sodium nitrite at 300 °C is 1.40 Ω^{-1} cm^{-1}, which is nearly twice the conductivity of battery acid (0.73 Ω^{-1} cm^{-1}, please see Figure 13). [21] And unlike battery acid, molten sodium nitrite is a pure substance, and therefore does not suffer from problems with electrolyte stratification. As a further basis of comparison, the best electrolytes in fuel cells have conductivities of order 0.1 Ω^{-1} cm^{-1},[22] and typical conductivities of electrolyte mixtures used in lithium ion batteries are ~0.01 Ω^{-1} cm^{-1} at room temperature (increasing by approximately 30–40% at 40 °C and decreasing slightly at 0 °C).[23] Very high electrolyte conductivity in conjunction with highly favorable reaction kinetics, high output voltage (~3.0 V), and the absence of diluents or other host species should equate to very high power density. The relatively low molecular weight of $NaNO_2$ potentially translates to high gravimetric energy density as well.

Let us now calculate the theoretical energy density of the proposed battery system in its fully charged state. The combined molar volume of Na (s) and NO_2 (l) is:

$$V = \frac{M_{Na}}{\rho_{Na}} + \frac{M_{NO2}}{\rho_{NO2}} = \frac{22.99\ g\ mol^{-1}}{0.927\ g\ cm^{-3}} + \frac{46.01\ g\ mol^{-1}}{1.448\ g\ cm^{-3}} = 56.57\ cm^3\ mol^{-1}$$

and the combined molar mass of Na (s) and NO_2 (l) is simply the molecular weight of $NaNO_2$, which is 69.00 gm mol^{-1}. Assuming an open circuit voltage of 3.01 V, and $\Delta G = n\ F\ E$, this corresponds to theoretical gravimetric and volumetric energy densities of 1.17 kW-hr kg^{-1} and 1.45 kW-hr $liter^{-1}$, respectively.

As with other battery chemistries, the actual gravimetric and volumetric energy densities that can be obtained in practice depend on the balance of plant required, and the extent to which the battery contains electrochemically inactive ingredients (see for example Figure 35). It should also be recognized that the importance of a performance metric such as energy density is

application dependent (contrast for example, utility-scale grid storage with electric vehicles), and if applied improperly, can be misleading. Nonetheless, as discussed later, in some potential applications preliminary figures for theoretical energy density are relevant and informative.

For example, the above figures allow us to formulate an estimate of how much $NaNO_2$ would be needed to meet the demand for grid storage worldwide in a future energy economy based solely on renewable energy (Na and NO_2 are then generated from $NaNO_2$ during operation of the battery). The total rate of energy consumption worldwide, seasonally and diurnally averaged, is of order 20 TW.[24] Referring now to Figure 36, in a renewable energy scenario based purely on solar energy, the amount of energy storage (E) we would need to address the diurnal variability of solar power production is of order one third of total daily energy consumption.

$$E = \frac{(2.0 \times 10^{13}\ J\ sec^{-1})\ (3600\ \mathrm{sec}\ hr^{-1})(24\ hr\ day^{-1})}{3} = 5.8 \times 10^{17}\ J$$

The mass of $NaNO_2$ we would need to construct to construct such a grid storage system is:

$$m = \frac{(5.8 \times 10^{17}\ J)}{(1.17\ kWhr\ kg^{-1})\ (3.6 \times 10^{6}\ J\ kWhr^{-1})(1000\ kg\ MT^{-1})} = 140 \text{ million metric tons}$$

We further note that the above figure of 140 million metric tons is probably an overestimate of the amount of raw material required, because it is very likely that a future all renewable energy economy, if it can be made to happen, would primarily comprise a mixture of wind and solar. This is significant in that many studies have shown that a mixture of solar and wind power tends to cancel out some of the diurnal variability that either energy source would impose otherwise.[25] Lastly, the above calculation is also conservative in that it assumes zero base load electricity production from sources such as hydroelectric power, geothermal power, nuclear power, etc.

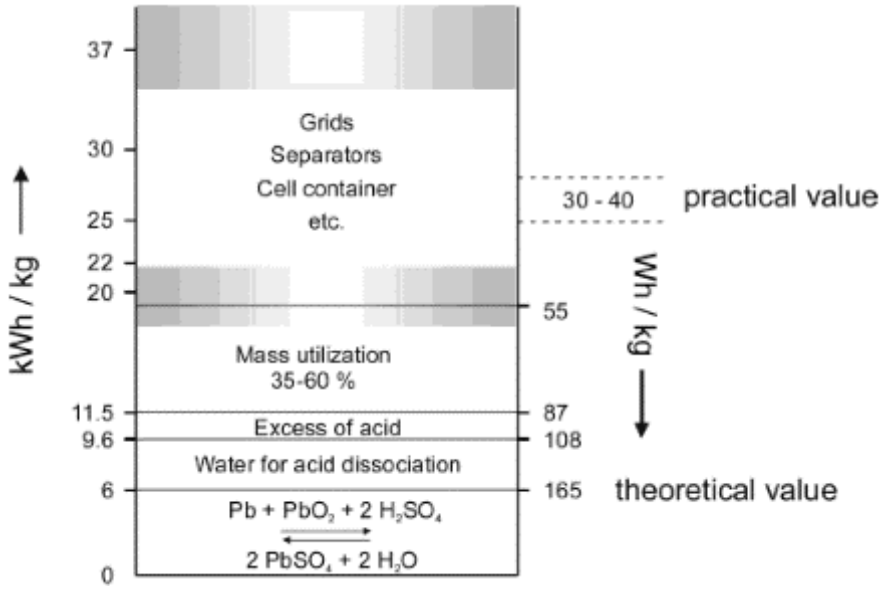

Figure 35: Depiction of the components of a lead acid battery showing the differences between theoretical and practical energy density of a lead acid battery. M. Winter, R. Brodd, "What are batteries, fuel cells, and supercapacitors?", Chemical Reviews, Vol. 104, No. 10 (2004).

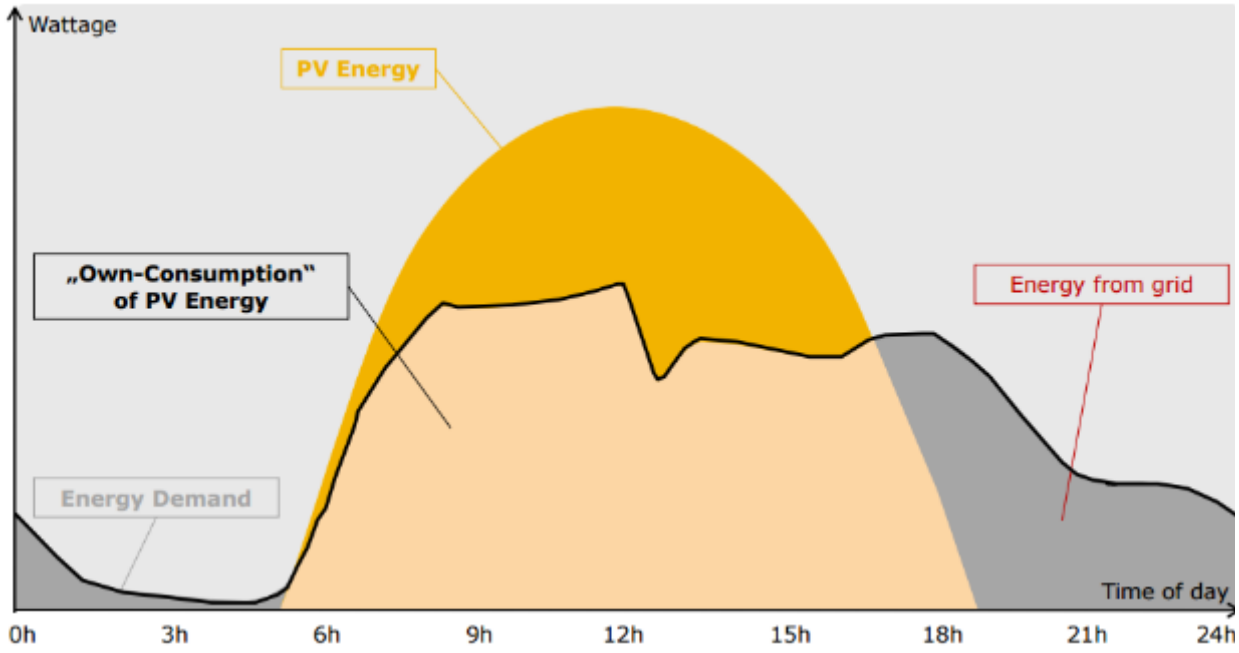

Figure 36: Simulation of grid storage capacity requirements over a single diurnal cycle assuming a renewable energy system based on PV solar power only. T. Grigoleit, "Energiewende in Germany: from generation to integration", Energy, Environment and Resources, July 2014. http://www.gtai.de/GTAI/Content/EN/Meta/Events/Invest/2014/Reviews/Powerhouse/Media/grigoleit-seattle.pdf

To determine whether the above chemical processes could be carried out at sufficient scale to address worldwide requirements for energy storage, there are four questions that must be answered:

1) Would the energy consumption of $NaNO_2$ synthesis from raw materials be prohibitive?
2) Are adequate quantities of chemical feedstock available?
3) Can our existing chemical industry handle the required manufacturing throughput?
4) Are there waste disposal challenges, and if so, are they manageable and affordable?

Regarding question #1, the change in free energy for the reaction:

$2\ NaCl + N_2 + 2\ O_2 \rightarrow 2\ NaNO_2 + Cl_2$

is

$\Delta G = [2\ \Delta G_f°(NaCl) + \Delta G_f°(N_2) + \Delta G_f°(O_2)] – [2\ \Delta G_f°(NaNO_2) - \Delta G_f°(Cl_2)]$

$\Delta G = [(2\ mol)\ (-384.1\ kJ\ mol^{-1}) + 0 + 0] – [(2\ mol)\ (-284.6\ kJ\ mol^{-1}) - 0] = 199\ kJ$

Thus in theory, synthesizing 1 mole of $NaNO_2$ from NaCl, N_2, and O_2 requires 100 kJ of energy. The corresponding figure for 140 million metric tons of $NaNO_2$ is:

$\Delta G = (1.00 \times 10^5\ J\ mol^{-1})(\ 1.4 \times 10^{14}\ gm)/(69.0\ gm\ mol^{-1}) = 2.0 \times 10^{17}\ J$

If $NaNO_2$ could be synthesized at 100% efficiency, this would translate to about 3 hours of electricity consumption:

$$\tau = \frac{2 \times 10^{17}\ J}{2 \times 10^{13}\ J\ sec^{-1}} = 1 \times 10^{4}\ sec$$

In reality, the energy efficiency with which electrical power can be converted into $NaNO_2$ starting from NaCl, O_2, and N_2 is far lower. But given that the above figure is in no way prohibitive, let us undertake the corresponding calculation for real-world $NaNO_2$ production.

As noted earlier, the above reaction scheme for bulk synthesis of $NaNO_2$ is one of several possible. In our present energy economy, the hydrogen required for industrial scale synthesis of ammonia is derived from natural gas, rather than from electrolysis, which is somewhat more costly because of the large quantities of electrical power consumed by electrolysis (see Figure 37). Therefore, for the purposes of this calculation, we will assume that ammonia production is carried out using the existing infrastructure for ammonia production based on natural gas, and that both the H_2 and Cl_2 generated as by-products of the chloralkali process are sold into existing markets to defray some of the cost of $NaNO_2$ synthesis. Accordingly, the natural-gas-based form of the Haber-Bosch process currently practiced can be considered a replacement for reactions B and C above.

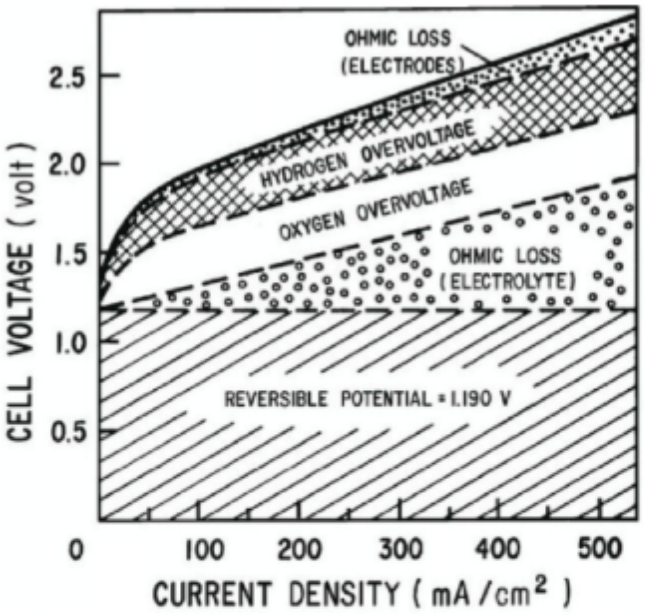

Typical operating voltage: 1.8 to 2.2 V

I. Abe, "Alkaline Water Electrolysis", Energy Carriers and Conversion Systems, Vol. 1: http://www.eolss.net/sample-chapters/c08/e3-13-03-02.pdf

1. 5.3 kWhr m^{-3} used for this calculation
2. volume measured at 0 C
3. density measured at 0 C

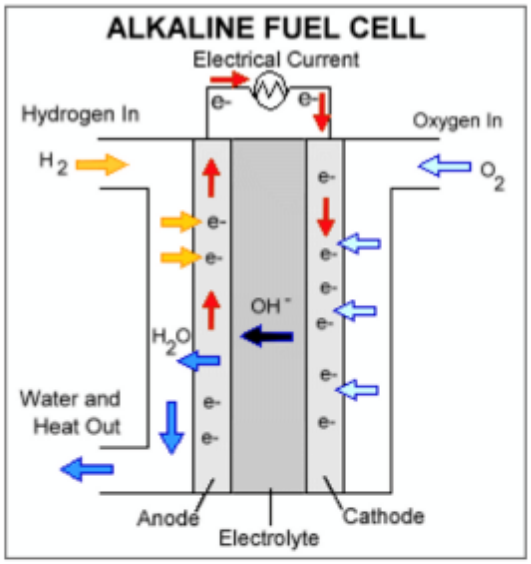

http://energy.gov/eere/fuelcells/types-fuel-cells

ε = 4.3-5.3 kWhr m^{-3} of H_2 [1, 2]
ρ = 89.9 gm m^{-3} of H_2 at 0 C [3]
$\varepsilon = 2.1 \times 10^5$ J gm^{-1}
M_{H2} = 2.02 gm mol^{-1}
$\varepsilon = 4.3 \times 10^5$ J mol^{-1} of H_2

Figure 37: Production of H_2 by electrolysis of water requires an estimated energy input of 430 kJ mol^{-1}.

Referring to Figure 38, real-world production of Cl_2 by the chloralkali process requires an estimated energy input of 890 kJ mol^{-1}, and yields 2 moles of NaOH plus 1 mole of H_2. Referring now to Figure 39, each mole of NH_3 requires an energy input of 490 kJ, so we have:

2 [2 NaCl (aq) + 2 H_2O → 2 NaOH (aq) + H_2 (g) + Cl_2 (g)] 1880 kJ

2 [N_2 (g) + 3 H_2 (g) → 2 NH_3 (g)] 1960 kJ

A combined energy input of 3840 kJ therefore produces 4 moles of $NaNO_2$. Thus the energy required for industrial-scale synthesis of $NaNO_2$ amounts to 960 kJ mol^{-1}. To synthesize 140 million metric tons (1.4×10^{14} gm) of $NaNO_2$, the required energy input is:

$\varepsilon = (1.4 \times 10^{14} \text{ gm})\ (9.6 \times 10^{5} \text{ J mol}^{-1})/(69.0 \text{ gm mol}^{-1}) = 1.9 \times 10^{18}$ J

which corresponds to about 1 day of electricity production:

$\tau = (1.9 \times 10^{18} \text{ J})/(2.0 \times 10^{13} \text{ J sec}^{-1}) = 9.5 \times 10^{5}$ sec = 27 hr

The above calculations indicate that the one-time expenditure of energy required to synthesize $NaNO_2$ for construction of a radical-ion battery grid storage network is insignificant in the context of equipment intended to last for 30 years (1×10^{4} diurnal charging cycles). Incidentally, these calculations further indicate that the estimated net energy efficiency for industrial synthesis of $NaNO_2$ is about 10% (100 kJ mol^{-1} theoretical, 960 kJ mol^{-1} actual).

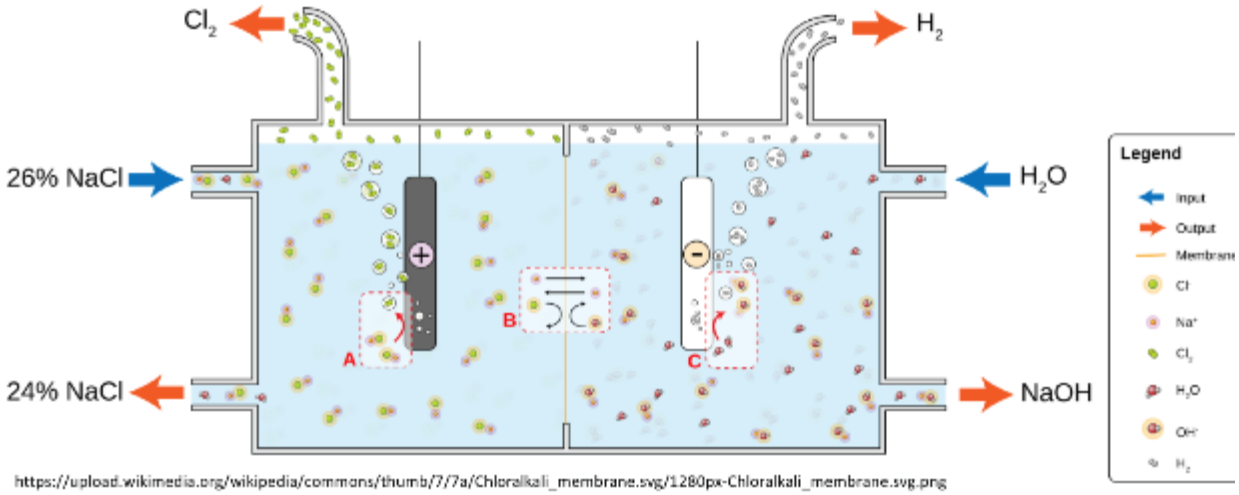

https://upload.wikimedia.org/wikipedia/commons/thumb/7/7a/Chloralkali_membrane.svg/1280px-Chloralkali_membrane.svg.png

Electricity Consumption by Production Process

kWh (AC)/t Cl2	Mercury	Diaphragm	Membrane
Electricity process	3360	2720	2650
Electricity utilities	200	250	140
Calorific (steam)		610	180
Total	3560	3580	2970
Ratio to mercury		similar	~ 17% lower

$\varepsilon = 3500$ kWhr MT^{-1} of Cl_2

$\varepsilon = 12600$ J gm^{-1} of Cl_2

$M_{Cl2} = 70.9$ gm mol^{-1}

$\varepsilon = 8.9 \times 10^{5}$ J mol^{-1} of Cl_2

http://siteresources.worldbank.org/INTPOPS/Resources/SimonWorldChlorineCouncil.pdf

Figure 38: Production of Cl_2 by the chloralkali process requires an estimated energy input of 890 kJ mol^{-1}.

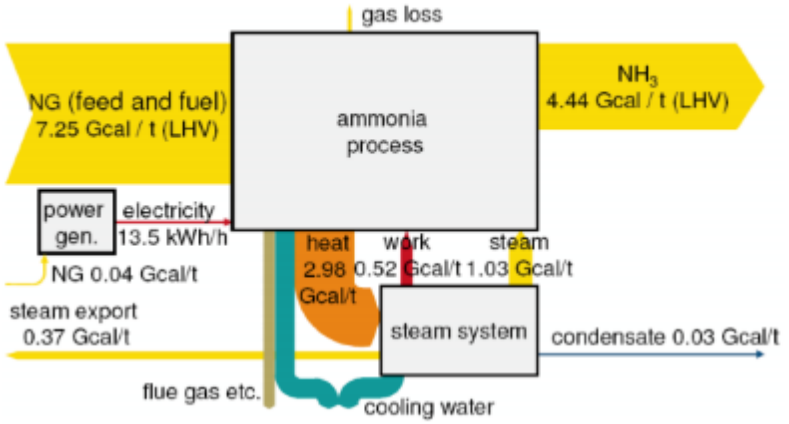

http://www.thyssenkrupp-industrial-solutions.com/fileadmin/documents/publications/Nitrogen-Syngas-2011/Low_Energy_Consumption_Ammonia_Production_2011_paper.pdf

"Low Energy Consumption Ammonia Production: Baseline Energy Consumption, Options for Energy Optimization", Kl. Noelker, J. Ruether, Uhde GmbH, Dortmund, Germany, Submitted for the Nitrogen + Syngas Conference 2011, Duesseldorf

Stream	Consumption or credit
feed and fuel	7.25 Gcal/t
Electricity	0.04 Gcal/t
steam export	–0.37 Gcal/t
Total	6.91 Gcal/t

$\varepsilon = 6.91 \times 10^9$ cal MT^{-1} of NH_3
$\varepsilon = 2.89 \times 10^4$ J gm^{-1} of NH_3
$M_{NH3} = 17.0$ gm mol^{-1}
$\varepsilon = 4.92 \times 10^5$ J mol^{-1} of NH_3

Figure 39: Production of NH_3 by the Haber Bosch process requires an estimated energy input of 490 kJ mol^{-1}.

Given that the energy required for $NaNO_2$ synthesis does not constitute an obstacle, we must now consider questions related to the chemical industry supply chain. Scarcity of raw materials is a non-issue for the radical-ion battery because world supplies of sodium, nitrogen, and oxygen are, for all intents and purposes, unlimited. Synthesis of 140 million metric tons of $NaNO_2$ requires 47, 28, and 47 million metric tons of sodium, nitrogen, and oxygen, respectively. The mass of the hydrosphere is estimated to be 1.4×10^{18} metric tons, 97% of which is sea water having an average concentration of sodium ions of 1.08% by mass. Thus the total mass of sodium in the ocean is of order 1.5×10^{16} metric tons, 8 orders of magnitude greater than that required to synthesize 140 million metric tons of $NaNO_2$. The mass of the atmosphere is estimated to be 5.15×10^{15} metric tons, of which 4.02×10^{15} metric tons comprises nitrogen, and 1.08×10^{15} comprises oxygen. The corresponding figures for N_2 and O_2 required for $NaNO_2$ synthesis are roughly 8 orders of magnitude lower (2.8×10^7 metric tons of nitrogen and 4.7×10^7 metric tons of oxygen, respectively).

Abundant raw material is a necessary but not sufficient criterion for feasibility, however. We must further examine whether production of 140 million tons of $NaNO_2$ (e.g. between now and 2030) would be a manageable burden for the existing chemical industry. Current figures for worldwide production of NaCl are approximately 300 million metric tons per year, which corresponds to 120 million metric tons of sodium per year. An additional burden of ~3.1 million metric tons of sodium per year between now and 2030 would therefore only constitute a 3% perturbation in NaCl production. Worldwide production of NH_3 is currently of order 200 million metric tons per year, which corresponds to 160 million metric tons of nitrogen. An additional throughput of ~1.9 million metric tons of nitrogen per year between now and 2030 would therefore constitute a 1.2% perturbation to NH_3 production. The worldwide production of Cl_2 by

the chloralkali industry is of order 70 million metric tons per year. This implies that the sodium throughput of the chloralkali industry is currently 28 million metric tons per year. An additional processing burden of ~3.1 million metric tons of sodium per year represents an 11% perturbation to the chloralkali industry. As discussed below, the current growth rates of these industries indicate that such production burdens should be easily manageable in the coming years. Finally, we note that the list of materials used to fabricate the Na-β-Al_2O_3 ion exchange membranes, of which much lower quantities would be required, does not include any rare elements either.

Lastly, we examine the question of waste generation/disposal. Cl_2 is generated as a by-product of $NaNO_2$ synthesis, as is H_2. There is already a great deal of demand for these industrial chemicals, such that an 11% increase in their production by the chloralkali industry would not be expected to cause a significant market dislocation. The chlorine production industry, for example, is currently projected to have 4.9% compound annual growth through 2019.[26] For hydrogen production, the compound annual growth through 2019 is projected at 5.9%, and only ~4% of hydrogen generation is sourced from the chloralkali process. Thus an 11% increase in H_2 from chloralkali production can easily be absorbed at current market prices. We may therefore conclude that large scale production of $NaNO_2$ for applications such as grid storage will not generate by-products that need to be disposed of, significantly alter existing markets in the chemical industry, or place chemical production capacity under significant strain. This analysis is summarized in Figure 40.

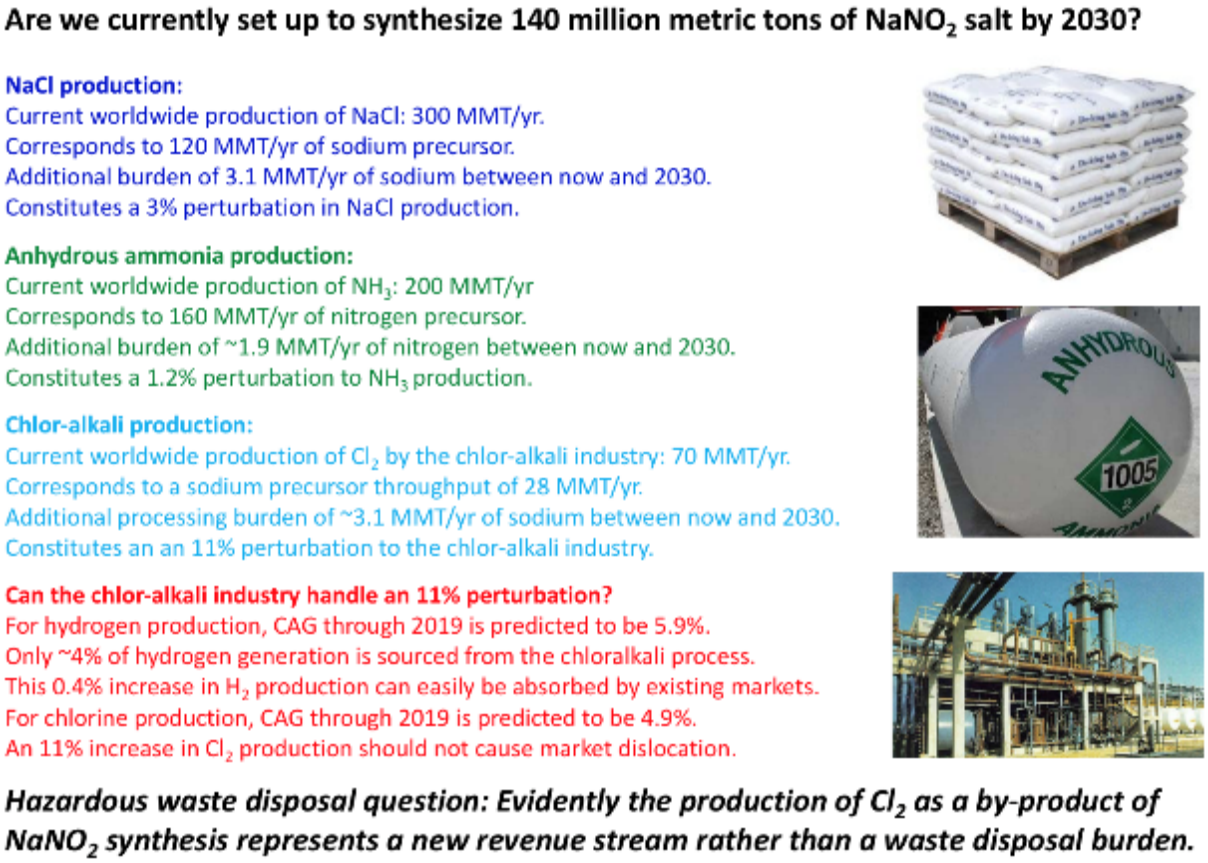

Figure 40: Investigating the production capacity of our existing chemical industry infrastructure.

3.2. Preliminary consideration of side reactions, capacity fade, and self-discharge

Returning now to the internal operation of the radical-ion battery, another critically important feature of the proposed battery technology is the small number of permutations for possible side reactions. The only chemical species present in the electrochemical cell are Na, Na^+, NO_2^-, and NO_2. The elemental sodium, while very reactive, is sequestered from the other chemical constituents by the ion-selective membrane. The operating temperature of the electrochemical cell is too low to cause thermal decomposition of the sodium nitrite melt, which only leaves the possibility of unwanted chemistry between the species Na^+, NO_2^-, and NO_2. By definition, the reaction of $Na^+ + NO_2^- \rightarrow NaNO_2$ is not relevant above the melting point of $NaNO_2$ (271 °C). The reaction $NO_2^- + NO_2 \rightarrow NO_2 + NO_2^-$ is irrelevant because it is a null process. There does not appear to be evidence to date of a significant $Na^+ + NO_2$ reaction channel either (which is not surprising given that $Na^+ + NO_2^-$ does not occur at these temperatures). Dimerization of NO_2 into N_2O_4 is only observed at much lower temperature and/or higher pressure than 300 °C at 1 atm. Although we do expect extensive dimerization of NO_2 into N_2O_4 within the NO_2 (l) storage tank, this dimerization reaction is readily reversible. At ~300 °C, NO_x decomposition processes such as $2\ NO_2 \rightarrow N_2 + 2\ O_2$ are thermodynamically favorable, but not kinetically viable. And although we anticipate that a minor fraction of the NO_2 generated in the charging half reaction will be converted to NO and O_2 as a result of thermal decomposition at ~300 °C, such a reaction also constitutes a null process because NO and O_2 will quickly revert back to NO_2 at lower temperature en route to the NO_2 storage vessel.

This is also true of the reaction $NO_2^- + NO_2 \rightarrow NO_3^- + NO$. To the extent that this reaction occurs, NO evolved may readily be converted back to NO_2 by exposure to O_2 (e.g. generated in the 3rd reaction step below) and the nitrate ion can be electrochemically oxidized in a manner analogous to the nitrite ion at the anionic electrode to yield NO_2 and O_2. But there is a potential efficiency penalty associated with the reaction $NO_2^- + NO_2 \rightarrow NO_3^- + NO$. Consider the following sequence of reactions:

$NO_2^- \rightarrow NO_2\ (g) + e^-$	electrolysis of $NaNO_2$ ($E° = 3.49$ V)
$NO_2^- + NO_2\ (g) \rightarrow NO_3^- + NO\ (g)$	unwanted side reaction occurring in melt
$NO_3^- \rightarrow NO_2\ (g) + ½\ O_2\ (g) + e^-$	electrolysis of $NaNO_3$ ($E° = 4.32$ V)
$NO\ (g) + ½\ O_2\ (g) \rightarrow NO_2\ (g)$	recombination of NO + ½ O_2 in the gas phase
---	---
$2\ NO_2^- \rightarrow 2\ NO_2\ (g) + 2\ e^-$	net conversion of 2 moles of NO_2^- to NO_2 (g)

The numerical values of E° for electrolysis of $NaNO_2$ and $NaNO_3$ shown above are derived later. In the above sequence of reactions, it requires 3.49 eV + 4.32 eV = 7.81 eV to convert 2 NO_2^- ions to 2 NO_2 molecules (and their corresponding Na^+/Na counterparts). In the absence of this unwanted side reaction, the process $2\ [NO_2^- \rightarrow NO_2\ (g) + e^-]$ would only require 3.49 eV + 3.49 eV = 6.98 eV. Thus the unwanted side reaction $NO_2^- + NO_2\ (g) \rightarrow NO_3^- + NO\ (g)$ potentially imposes an efficiency penalty of 10.6% during the round trip charging/discharging process. But the scientific literature contains a wide range of early fundamental studies

pertaining to the electrolysis of various molten salts, one of which in 1970 specifically investigated whether the speculated $NO_2^- + NO_2$ (g) $\rightarrow NO_3^- + NO$ (g) reaction is operative in molten nitrite.[27] For example, one way to test for this hypothesized side reaction is to electrolyze molten sodium nitrite at a potential too low to electrolyze sodium nitrate and wait to see whether nitrate ion is formed. The authors of the above study did not observe a significant effect. In addition, they ruled out a speculative electrode reaction $2\ NO_2^- \rightarrow NO_3^- + NO + e^-$.

Thus we conclude:

1) If it occurs, the $NO_2^- + NO_2$ (g) $\rightarrow NO_3^- + NO$ side reaction doesn't have the potential to permanently alter the chemical composition of the electrochemical cell.
2) If this side reaction does occur to a small extent, we will incur a correspondingly small fraction of the 10.6% penalty discussed above. Future experimental work should be directed towards determining whether any measureable efficiency penalty due to the above reaction can be detected in practical electrochemical cells.
3) NO_2 (g) dissolved in molten nitrite likely has a "limited shelf life". This is potentially an important consideration if we wish to pre-dissolve NO_2 (g) in the electrolyte prior to discharge in an effort to improve electrode reaction kinetics (discussed later).

Finally, we note that the absence of potent catalysts such as platinum in the proposed electrochemical cell reduces the probability that thermodynamically favorable processes such as $2\ NO_2 \rightarrow N_2 + 2\ O_2$ will occur unexpectedly via heterogeneous catalysis.

Another important point is that both of the electrochemical half-reactions include built-in purification processes that occur automatically as the chemical reagents are cycled between the charged and discharged state. For example, imagine that such an electrochemical cell is commissioned in its fully discharged state, wherein the only reagent present in significant quantity is molten $NaNO_2$. Let us then fully charge the battery. At the cationic electrode, Na^+ ions are transported through the ion-selective membrane, collected in the form of pure sodium metal, and then transferred to the Na storage vessel. At the anionic electrode, NO_2 gas bubbles out of the molten electrolyte and is deposited into the NO_2 storage vessel. In the case of sodium, the process is somewhat reminiscent of converting sea water to pure water by reverse osmosis through a semi-permeable membrane, and the net effect is similar to the electrochemical refining of impure copper into pure copper by a process that is sometimes referred to as "electrowinning". In the case of NO_2, the purification process is more analogous to distillation. Exploitation of such in situ distillation processes to remove ppb levels of transition metal impurities was critically important to the successful development of low-loss optical fibers in the early 1970s, and may contribute to ease of implementation in the case of radical-ion battery technology. Once the charging process is complete, whatever residue is left behind may be removed from the electrolyte compartment if desired. One special case is the nitrate ion impurity, which may instead be electrochemically converted at the anionic electrode. To the extent that the process $NO_3^- \rightarrow NO_2 + \frac{1}{2}\ O_2 + e^-$ does occur, it has the effect of converting traces of $NaNO_3$ present in the desired starting material to $NaNO_2$ (wherein the small quantities of O_2 gas generated could simply be vented after the NO_2 is cold-trapped in the NO_2 storage reservoir). Accordingly, we expect that the starting material for construction of the proposed electrochemical cell could be in the form of $NaNO_2$ or $NaNO_3$ salt, whichever is more convenient or readily available, and that purity requirements are unlikely to be stringent.

We also anticipate that unlike many battery chemistries, self-discharge is unlikely to be a problem. Although sodium metal has significant solubility in molten sodium nitrite, in the proposed electrochemical cell, sodium metal is sequestered from the electrolyte by the ion-selective membrane (e.g. sodium-beta-alumina ceramic). This physical barrier only allows passage of sodium ions under the influence of an electrical field; elemental sodium cannot leach into the electrolyte. Dendritic growth at the cationic electrode is precluded not only by the presence of the membrane, but also by the fact that sodium metal (m.p. 97 °C) is a liquid at the operating temperature of the electrochemical cell. We further expect no mechanism for dendrite formation (or metal deposition of any kind) at the anionic electrode either where the NO_2^-/NO_2 interconversion process takes place.

3.3. Preliminary consideration of cell implementation options

Another potentially compelling attribute of the proposed battery architecture is that it may be possible to configure all of the electrochemical reactions in question as two-phase processes. This is self-evident in the case of the cationic electrode, where Na metal and Na ions are the only species present. At the anionic electrode, the charging half reaction $NO_2^- \rightarrow NO_2 + e^-$ also comprises a simple two-phase interaction at the electrode surface. An important point, however, is that the discharging half reaction at the anionic electrode, $NO_2 + e^- \rightarrow NO_2^-$ can also be carried out as a two-phase process because NO_2 is substantially soluble in molten sodium nitrite. From the standpoint chemical kinetics, this is a much more favorable situation than attempting to promote a three-phase electrolyte/NO_2(g)/electrode interaction by bubbling NO_2 gas in close proximity to the electrode/electrolyte interface; to some degree a three-phase process would likely constitute a kinetic bottleneck. Rather, the proposed system can be operated like a flow battery in which molten electrolyte containing predissolved nitrogen dioxide is delivered to the surface of the anionic electrode, and in which the entire electrolyte reservoir (as opposed to just the electrode region) may be used as a sparging vessel to promote dissolution of NO_2 gas in the molten electrolyte. In some embodiments this may done by simply bubbling NO_2 (g) through the molten electrolyte reservoir, wherein the mean bubble diameter is chosen to be small enough to provide sufficiently fast dissolution kinetics; bubble size affects both the surface-area-to-volume ratio of the NO_2/electrolyte interface and the bubble residence time (which is inversely proportional to the upward terminal velocity of the buoyant gas bubbles). In further embodiments, other techniques may be used to promote saturation (or supersaturation) of the electrolyte with NO_2 gas. For example, pressurization may be used in a manner analogous to forced carbonation of water with CO_2 gas.

An alternative approach to promoting the kinetics of NO_2 dissolution in molten $NaNO_2$ would be to exploit the extremely high surface-area-to-volume ratio of nascent bubble formation during the charging reaction at the anionic electrode; in the early stages of bubble formation, the very small diameter of such nascent bubbles implies an extremely high surface-area-to-volume ratio. Taking this idea a step further, during the charging reaction, as NO_2 is formed at the electrolyte/electrode interface, the NO_2 evolved may either form a bubble or enter solution. The later outcome may be promoted by ensuring that the electrolyte is adequately circulated to prevent saturation with NO_2 gas in the vicinity of the anionic electrode. Bubble-free operation has the further advantage that occlusion of the electrode surface by adherent gas bubbles, which adversely effects electrode kinetics, is avoided. During periods of rapid charging, however, the rate at which NO_2 is evolved may exceed the rate at which it can be absorbed (solvated) by the electrolyte. For this reason, it may prove advantageous to exploit solvation of NO_2 as it is

evolved at the anionic electrode in conjunction with NO_2 (g) sparging of the molten electrolyte reservoir and/or other methods described earlier.

Alternatively, a more conventional approach, in which the $NO_2 + e^- \rightarrow NO_2^-$ half reaction is carried out at a triple-phase boundary (electrolyte/NO_2/electrode), may be used. For example, the aforementioned stainless steel electrode could be fabricated from sintered stainless steel particles to create a porous, high-surface-area-to-volume structure, including a hollow interior that functions as an NO_2 gas manifold. NO_2 gas bubbling out of such a porous structure would naturally form a large number of electrolyte/NO_2(g)/electrode triple-phase boundary sites that are automatically replenished as NO_2 (g) is consumed. Numerous designs for electrodes adapted to promoting such triple-phase electrolyte/gas/electrode interactions are known from the prior art.

In practice, it may prove advantageous to employ all three of the above mechanisms:

1) NO_2 (g) sparging of the molten $NaNO_2$ electrolyte reservoir,
2) solvation of nascent NO_2 bubbles as they are evolved at the anionic electrode, and
3) the use of a porous NO_2 (g) bearing electrode made of sintered metal (or other structure adapted to promoting the triple-phase electrolyte/gas/electrode interaction),

to ensure optimal handling of different operating regimes (e.g. fast charging vs. trickle charging). Having said that, we anticipate that the ability to predissolve large quantities of NO_2 (g) in the electrolyte prior to a discharge cycle, so as to allow the discharging half-reaction at the anionic electrode to be carried out as a two-phase process, may:

1) be the preferred mode of operation for minimizing irreversibility at the anionic electrode, and
2) facilitate very high discharge rates (e.g. very high power density) in applications that occasionally demand high bursts of current.

On the other hand, we must include the caveat that as discussed earlier, limitations to the "shelf life" of NO_2 dissolved in molten NO_2^- may have a bearing on successful application of such a pre-dissolution strategy (although perhaps less so for some of the lower operating temperature embodiments discussed later). It may also turn out that the kinetics of predissolution are too slow to support operation at high discharge current densities. In the event that the potential benefits of predissolution cannot be realized in practice, it is important to recognize that there is a long history of fuel cell systems capable of operating at high discharge current density despite reliance on triple phase boundary kinetics at one or both electrodes.

As implied in the above discussion, the anionic electrode must be adapted to efficient operation for both the charging half-reaction:

$NO_2^- \rightarrow NO_2$ (g) + e^-

and the discharging half-reaction:

NO_2 (g) + $e^- \rightarrow NO_2^-$

In the event that engineering conflicts or undesirable performance tradeoffs arise in the design of an electrode optimized for both of these processes, in some applications we contemplate the use

of separate, individually optimized, anionic electrode structures adapted for optimal charging and discharging performance, respectively. It will also be understood that multiple electrodes may be used, as may composite electrode structures comprising high-electrical-conductivity structures adapted to minimization of electrode resistive losses, in conjunction with other specialized structures, such as coatings adapted to improve electrode kinetics, prevent corrosion, etc.

Further embodiments are contemplated in which the use of low-melting electrolyte mixtures, elevated pressure, or both is used to increase the solubility of NO_2 in the electrolyte. In related embodiments the use of low-melting electrolyte mixtures, elevated pressure, or both is used to render NO_2 a liquid rather than a gas in one or more portions of the electrochemical cell. In one such embodiment, liquefied NO_2 is delivered through a porous anionic electrode. In another embodiment, NO_2 (l) and the molten electrolyte comprise partially or fully miscible liquids. In yet another embodiment, the electrochemically active portion of the electrolyte (e.g. $NaNO_2$ in a $Na/NaNO_2/NO_2$ radical-ion battery) is liquefied and dissociated into free ions by dissolution in a solvent, rather than by melting. In one such embodiment, NO_2 (l), which is a well-known aprotic solvent that exists in equilibrium with its dimer N_2O_4, is used for this purpose. This could entail the use of NO_2 (l) at a pressure of 1 atm, in which case the boiling point of NO_2 is 21 °C, or the use of elevated pressure to enable operation at higher temperatures. For example, at a pressure of 20 atm, the boiling point of NO_2 is of order 100 °C.[28] In yet another embodiment, NO_2 generated by the charging reaction (e.g. $NaNO_2 \rightarrow Na + NO_2$), is stored in the electrolyte rather than in a separate reservoir.

3.4. Storage and safety considerations

The ease with which the chemical reagents in question can be stored is critically important. Hydrogen, for example, can be readily generated by electrolysis of water (albeit at only ~70% efficiency),[29] but is very difficult to store economically. A closely related consideration is safety. Storing large quantities of chemically energetic reagents is potentially very dangerous.

From the standpoint of economical storage, ideally the reagents in question would be pumpable liquids that can be stored at atmospheric pressure in containers of relatively lightweight construction, and fabricated from inexpensive materials (e.g. steel). From the standpoint of safety, we would like such storage systems to be failsafe (e.g. in the event of a sustained power outage), and we must avoid the use of chemical reagents having persistent toxicity with respect to personnel or the environment. As outlined below, all of the reagents in the proposed $NaNO_2$-based system meet this requirement.

Referring to Figure 41, sodium nitrite is a stable non-volatile solid that is easily contained. $NaNO_2$ exhibits moderate toxicity, but spills can be easily cleaned up without specialized equipment, and any residue may be neutralized through simple inorganic reactions such as:

$NH_4Cl\ (aq) + NaNO_2\ (s) \rightarrow NaCl\ (aq) + 2\ H_2O\ (l) + N_2\ (g)$

Sodium metal can be conveniently stored as a solid at room temperature, as a liquid above 97 °C, and is chemically compatible with materials such as stainless steel. The biggest risk associated with accidental release of sodium metal is fire, via either reaction with oxygen or water. Environmental toxicity is not a significant concern because sodium readily converts to sodium hydroxide (NaOH) and subsequently sodium bicarbonate ($NaHCO_3$) upon exposure to the atmosphere. From the standpoint of safety, the most important objective is to prevent a situation

in which a large quantity of sodium metal gains access to a large quantity of water or air, generating large quantities of heat and/or hydrogen gas, that would set the stage for a runaway process in which the entire reservoir of sodium metal is consumed by fire. This objective can be achieved by storing sodium metal in underground tanks beneath an inert fill material such as dry soil or sand. In the event of a breach, the rate at which fugitive sodium could gain access to air or water would be very limited, thereby preventing buildup of heat. Thus if we were to punch a hole in an underground storage tank containing liquid sodium metal (e.g. stored at 100 °C), in the presence of dry fill material such a storage container would likely exhibit a self-healing property in which liquid sodium would quickly freeze upon contact with the fill medium, and then gradually form a chemically inert "scab" of sodium hydroxide and/or sodium bicarbonate by reacting with small quantities of air/humidity present. In a worst case scenario, the fact that the sodium reservoir is buried well underground would only permit a "slow burn", providing ample time to pump much of the remaining liquid sodium to another storage container. We could also equip the site with cylinders of compressed inert gas such as nitrogen that could be vented at a moment's notice to the base of the fill column, forcing inert gas to percolate up through a granular fill material such as dry sand.

Figure 41: Nitrogen dioxide, sodium metal, and sodium nitrite.

Nitrogen dioxide gas is quite toxic, but on the other hand, it is not persistent in the environment or in the human body. From the standpoint of safety, the situation that must be avoided is the release of a large plume of NO_2 into the surrounding atmosphere that would endanger people in the vicinity of such a facility. Fortunately, NO_2 can be liquefied at atmospheric pressure at temperatures below 21.2 °C (70.2 °F), thereby eliminating scenarios in which large quantities of

NO_2 gas rapidly escape because the NO_2 storage vessel is under positive pressure. On the contrary, liquefied NO_2 could be stored as a liquid in a failsafe manner in underground storage tanks that are passively maintained at the temperature of the surrounding soil (see Figure 42). In the event of a leak, there would be ample time to pump the contents of the damaged NO_2 tank to another container. In addition, the density of NO_2 gas is significantly greater than air, which causes it to settle and hug the ground. Accordingly, such a tank could be surrounded by a berm to contain fugitive NO_2 that might percolate upward through the fill medium in the event of a breach, equipped with a NO_x sensor to activate a chemical neutralization system (e.g. an alkaline aqueous mist). At the same time a pump could be actuated to transfer the contents of the damaged storage vessel to an adjacent tank.

NO_2 can be stored as a liquid at in underground storage vessels.
Vessel temperature is passively regulated by the surrounding soil.
No pressurization is required.
NO_2 can therefore be stored in a failsafe storage condition.
No compressors are required (cold trapping and vapor flashing)

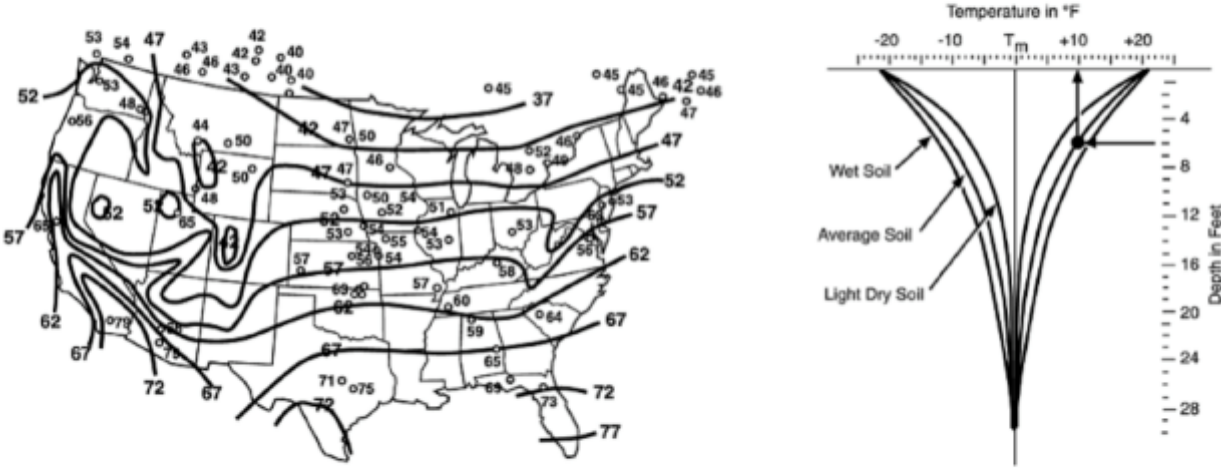

Mean annual earth temperature observations at individual stations, superimposed on well water temperature contours.

Amplitude of seasonal soil temperature change as a function of depth below ground surface.

http://www.builditsolar.com/Projects/Cooling/EarthTemperatures.htm

Figure 42: NO_2 can be stored in an inexpensive and failsafe manner.

As noted earlier, NO_2 exists in chemical equilibrium with its dimer, N_2O_4, which shifts in favor of N_2O_4 at low temperature and/or high pressure. Accordingly, the terms NO_2 and N_2O_4 are sometimes used loosely and interchangeably in situations where both species actually coexist. Alternatively one may encounter the notation "NO_2/N_2O_4". In the context of the present discussion, it will be understood that any reference to NO_2 (g), NO_2 (l), and NO_2 (s) represents simplified notation, wherein it is understood that the material in question may comprise some or substantially all of the NO_2 dimer, N_2O_4 (e.g. when liquefied).

Returning to the question of NO_2 storage and referring back to Figure 42, it will be noted that in some geographic regions, the soil temperature may be comparable to or slightly in excess of the

boiling point of NO_2 (l). Under such circumstances, a container of NO_2 (l) would be expected to maintain a gentle boil. In some embodiments, this NO_2 boil-off may simply be diverted to a molten $NaNO_2$ reservoir for predissolution. In other embodiments suppression of boiling may exploit the fact that NO_2 (l) is a fairly effective aprotic solvent, such that one or more solute additives may be added to affect NO_2 (l) boiling point elevation. In various embodiments, such boiling point elevation additives may comprise solutes that exhibit no chemical reactivity towards NO_2 and/or solutes having very low vapor pressure (e.g. inorganic salts), such that substantially pure NO_2 (g) may be withdrawn from the NO_2 reservoir without concern for contamination by such solutes. In other embodiments a cooling system such as a heat pump may be used for thermal management of the NO_2 reservoir. This may include cooling or freezing a portion of the NO_2 (l) reservoir during periods of excess electricity production; the freezing point of NO_2 (l) is -11.2 °C (11.8 °F). A well-insulated vessel containing a mixture of NO_2 liquid and NO_2 “ice” would therefore be expected to remain in the condensed phase for an extended period of time.

It will further be understood that in some embodiments, pressurization, instead of or in addition to cooling, may be used to facilitate NO_2 storage. For example, depending on the application and the size of the NO_2 reservoir, it may prove advantageous to store NO_2 in pressurized containers without any form of temperature control. Alternatively, a stream of NO_2 gas (such as that generated by boil off) may be pressurized, allowed to cool and subsequently liquefy, and then added to the NO_2 storage vessel so as to affect refrigeration. In other embodiments, electrolytic production of NO_2 during the charging process may be used to pressurize the NO_2 gas reservoir as an alternative to a compressor.

Both NO_2 and sodium metal have another desirable property, namely that all traces of material may be removed from the storage container by heating the walls of the tank and cold trapping the Na or NO_2 vapor. This would facilitate periodic inspection of tanks, which is desirable from the standpoint of preventing breaches of containment and gathering data regarding what if any unexpected tank degradation mechanisms may be operative under certain circumstances.

The other potential vulnerability that must be managed concerns the possibility of a breach at the ion-selective electrode. For example, consider the example of an electrochemical cell that uses a ceramic sodium-beta-alumina membrane. In the event that the ceramic membrane is compromised (e.g. by a hairline fracture), we must consider the prospect of a violent chemical reaction in which the molten sodium metal comes into contact with the molten $NaNO_2$ electrolyte. In the event that such a breach occurs, we anticipate that the resulting change in cell voltage would be immediately detected and the electrolytic cell would promptly be shut down by closure of valves and opening of electrical connections. Other counter measures such as rapid draining of the electrolyte might also be employed. But this is not the primary concern. The primary concern is that if a sufficiently large quantity of sodium comes into contact with the electrolyte, enough heat may be generated to further damage the ceramic membrane, accelerating combustion and resulting in a runaway process.

To make such a system failsafe, we contemplate providing sufficient separation of the electrochemical cell (e.g. by distance and/or containment structures) and reactant reservoirs that a complete and catastrophic failure of the electrochemical cell would not result in damage to the reactant reservoirs. The electrochemical cell could also be located underground surrounded by inert fill material (or in some other secondary containment vessel) to prevent access to

atmospheric oxygen, which could otherwise accelerate combustion. But another potent countermeasure would be to keep the quantity of sodium metal residing in the electrochemical cell to an absolute minimum at all times. In principle, only a relatively thin coating of sodium metal on one side of the sodium-beta-alumina membrane is required for the electrochemical cell to function properly. For example, the sodium-beta-alumina membrane may comprise a planar surface of horizontal orientation whose top surface is wetted with a thin layer of sodium metal. The thickness of the sodium layer may be maintained by an active control system, or passively regulated by the presence geometric constraints (e.g. a planar metal plate located above the planar sodium-beta-alumina plate, spaced a short distance apart). In a similar manner, coaxial metal and sodium-beta-alumina tubes having a predetermined gap distance could be used to accomplish the same objective. In an alternative embodiment, the appreciable vapor pressure of sodium metal at the operating temperature of the electrochemical cell could be exploited, wherein sodium vapor rather than molten sodium metal, would be delivered to the sodium side of the sodium-beta-alumina membrane (e. g. equipped with a current collecting wire mesh), thereby keeping the amount of sodium metal present to an absolute minimum. Although the use of sodium vapor would reduce the chemical activity of Na at the sodium-beta-alumina membrane (see Figure 43), in some applications the resulting kinetic and thermodynamic penalties may not be prohibitive in quantitative terms (e.g. because of other rate limiting processes).

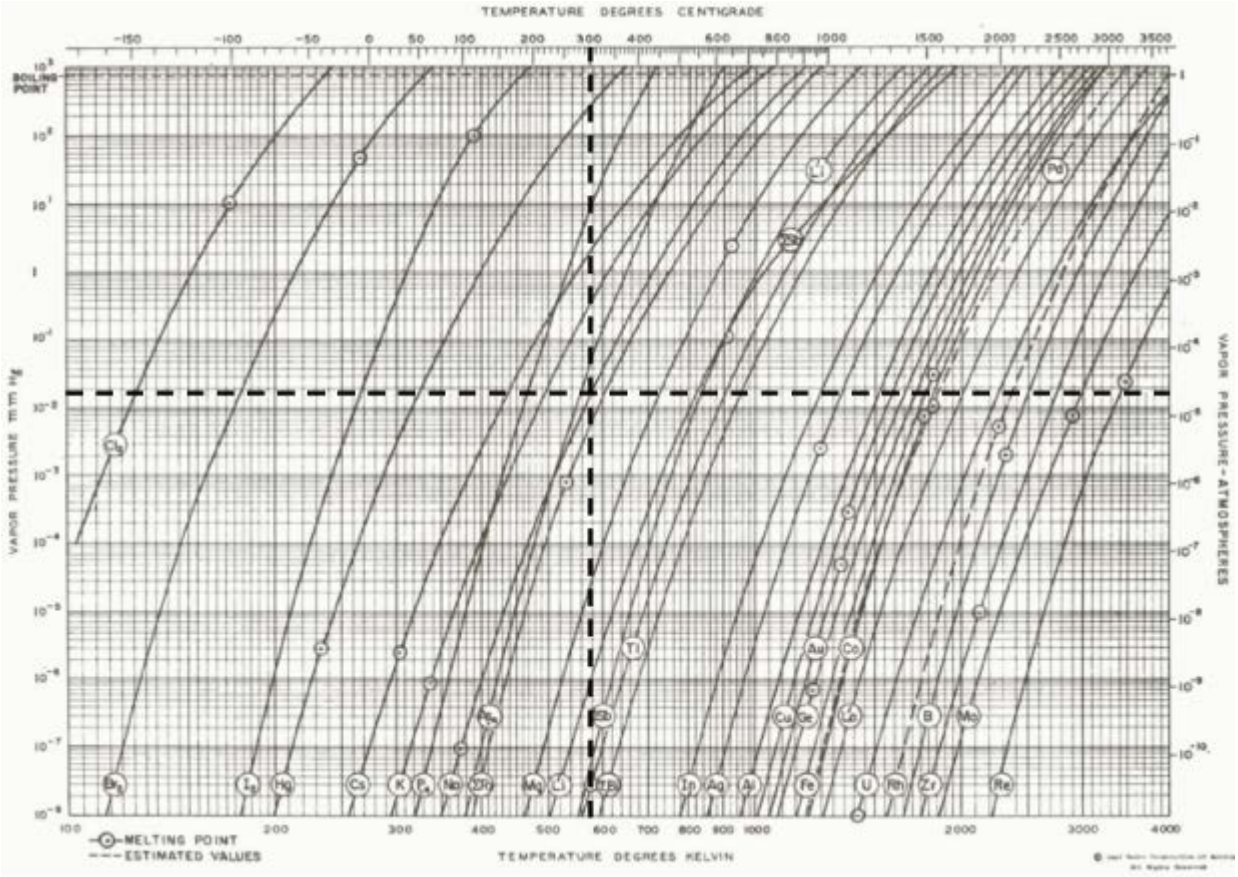

Figure 43: At 300 C, the vapor pressure of sodium metal is of order 2.3 x 10^{-5} atm. Elemental vapor data obtained from http://www.powerstream.com/vapor-pressure.htm

3.5. The transmission problem

As noted earlier, in some potential applications, preliminary figures for theoretical energy density can be both relevant and informative. Consider for example, the case of a utility-scale solar or wind power installation situated in a location that is not connected to rest of the electrical grid by high-capacity electrical transmission lines, but is located near a railroad. In a proposed embodiment, sodium metal and liquefied NO_2 generated at a geographically remote site is shipped by rail in tanker cars to one or more destinations having electrical transmission lines of appropriate capacity, where the electrochemical reaction $Na + NO_2 \rightarrow NaNO_2$ is used to generate electrical power. The same railway would then be used to ship the resulting $NaNO_2$ back to the remote site (e.g. in granular or molten form) to complete the cycle. Whether or not such a scheme could provide a cost effective means to sidestep the transmission line problem depends in large part on the theoretical energy density of the electrochemical reaction $Na + NO_2 \rightarrow NaNO_2$.

To make a preliminary assessment of such a proposal, it is instructive to look the coal industry. The vast majority of coal mined in the U.S. is used to generate electricity, and coal fired power plants currently provide ~40% of all electricity generated.[30] In many cases, the locations of large deposits of high-quality coal do not coincide with the geographic locations of major population centers. As shown in Figure 44, in the coal industry this geographic disparity between supply and demand often amounts to many hundreds of miles. In some instances it has proven economical to construct remote “mine mouth” coal-fired power plants connected to population centers by high capacity electrical transmission lines. But as explained below, in many instances this approach is not economically viable.

Figure 44: Much of the coal mined in the U.S. is transported several hundred miles by rail to coal fired electrical power generation plants located on the outskirts of population centers. Powder River Basin graphic from http://thinkprogress.org/climate/2011/03/26/207755/why-are-obama-and-salazar-pushing-a-massive-expansion-of-coal-mining/

We tend to think of coal fired power plants as having two inputs, coal and atmospheric oxygen, and two outputs, electrical power and CO_2 emissions. In reality the situation is more complicated. Vast quantities of water[31] are required to operate coal-fired power plants and significant quantities of ash, particulates,[32] sulfur dioxide,[33] and heavy metals[34] are produced as by-products. In some instances, where cheap coal and cheap water happen to be co-located, the construction of dedicated transmission lines may be given serious consideration. But in most cases, it has proven more practical to transport coal by rail to population centers or other major grid tie points having ample access to water, and forgo the construction of coal-fired power plants in remote locations. Thus as shown in Figure 44, coal that is mined in rural Wyoming may be transported by rail to a location as far away as Georgia, more than 1500 miles away. The same freight train then makes the return trip from Georgia to Wyoming empty (or in some cases, lightly loaded with coal ash). Note that a further consideration is the substantial transmission losses that would be incurred for such long distance of electrical transmission lines, which are typically of order 1.5% per 100 miles.[35]

It is fortunate for the coal industry that the economics of coal transport by rail as a substitute for high capacity electrical transmission lines turned out to be viable. Otherwise much of the inventory of coal in countries such as the U.S. would be stranded from the standpoint of utility-scale electrical power generation. That the transport of coal by rail over very long distances is economically viable reflects several factors: 1) rail transport is very energy efficient (1 gallon of

diesel fuel may be used to transport a ton of cargo a distance of order 450 miles[36] due to low rolling resistance, low aerodynamic drag, and the relatively high efficiency of large diesel engines); 2) coal, which for all intents and purposes is pure carbon, has very high energy density; (3) atmospheric oxygen provides 73% by mass of the reactants required for the combustion reaction $C + O_2 \rightarrow CO_2$; and (4) the capital investment for construction railroads, while large, does not in practice turn out to be prohibitive when appropriately amortized.

Let us now examine the question of coal transport by rail in more quantitative terms. According to the U.S. Energy Information Administration (EIA), one ton of coal burned in a modern coal-fired power plant generates 1.90 MW-hr of electricity.[37] If we assume an average capacity of a modern coal gondola car is 120 tons, [38] and the average length of a coal freight train is 120 cars,[39] this corresponds to 27.4 GW-hr of electricity per train load of coal. Thus a single daily shipment of coal could be used to operate a power plant with an average output power of order 1 GW. This is the yard stick we will need to use to conduct a preliminary assessment of Na/NO_2 rail transport.

In the case of renewables such as solar and wind, the regulatory hurdles to construction of new long-distance electrical transmission lines are often formidable. In contrast, the vast majority existing railroad right-of-ways were established 50 to 150 years ago, and are therefore not a source of contention. Moreover, there is ample precedent for shipment of bulk quantities of hazardous materials such as molten sodium and liquefied nitrogen dioxide by rail. Evidently, the engineered safety systems required for safe transport of such hazardous cargo, which have gradually evolved over the past 150 years, do not represent an added financial burden that is prohibitive. In fact, this has proven to be case for rail transport of a wide variety of hazardous substances, many of which are considerably more dangerous than sodium metal and nitrogen dioxide. Well known examples include chlorine, anhydrous ammonia, ethylene oxide, vinyl chloride, anhydrous hydrogen fluoride, anhydrous hydrogen chloride, hydrogen cyanide, nitrosyl chloride, methyl bromide, sulfur dioxide, sulfur trioxide, phosgene, methyl mercaptan, hydrogen sulfide, bromine, phosphorus trichloride, fuming nitric acid, fuming sulfuric acid, concentrated hydrogen peroxide (52%), liquid hydrogen, acetylene, liquid oxygen, liquefied petroleum gas, diioscyanate, titanium tetrachloride, dimethyl sulfate, ethyl trichlorsilane, chlorosulfonic acid, acetone cyanohydrin, and molten sulfur (maintained at 140 °C). In today's highly litigious environment, the existence of such precedents is important. Permitting and other regulatory barriers are far less of a challenge if the safety, economics, and legality of undertaking such industrial activities are not open to idle speculation.

3.6. The rolling pipeline model

Referring to Figure 45, in the U.S. molten sodium metal is transported by rail in DOT 105J300W tank cars having a name plate capacity of 33,600 gallons, with 5% outage (also known as ullage) to allow for thermal expansion of the liquid contents.[40] Liquefied nitrogen dioxide is transported in DOT 105A500W tank cars with a name plate capacity of 20,500-gallons and a required outage of 2% (Figure 45).[41] [42]

Figure 45: Top: DOT 105J300W tank car used for transport of molten sodium. Nameplate capacity = 33,600 gallons. Required outage for transport of molten sodium: 5%. Bottom: DOT 105A500W tank car used for transport of liquefied nitrogen dioxide. Nameplate capacity = 20,500 gallons. Required outage = 2%.

The stoichiometry of the $Na + NO_2 \rightarrow NaNO_2$ reaction dictates:

$n_{Na} = n_{NO2}$

where n is the number of moles of each reagent. In terms of the number of rail cars used for each reagent (N), the volumetric capacity of each rail car (V), the fill factor (f), reagent density (ρ), and molar mass of each reagent (M), the above expression can be written:

$$\frac{N_{Na} V_{Na} f_{Na} \rho_{Na}}{M_{Na}} = \frac{N_{NO2} V_{NO2} f_{NO2} \rho_{NO2}}{M_{NO2}}$$

We then impose a further constraint on the number of train cars allowed per train:

$N_{Na} + N_{NO2} = N_{tot}$

where $N_{tot} = 120$ is proposed for the purpose of comparison to the coal industry. The theoretical ratio of Na rail cars to NO_2 rail cars is:

$$\frac{N_{Na}}{N_{NO_2}} = \frac{V_{NO_2} f_{NO_2} \rho_{NO_2} M_{Na}}{V_{Na} f_{Na} \rho_{Na} M_{NO_2}} = \frac{(20{,}500\ gal\ car^{-1})\,(0.980)\,(1.88\ g\ cm^{-3})\,(23.0\ g\ mol^{-1})}{(33{,}600\ gal\ car^{-1})\,(0.950)\,(0.927\ g\ cm^{-3})\,(46.0\ g\ mol^{-1})} = 0.638$$

For a 120-car train we find:

$$N_{NO_2} = N_{tot}\left(\frac{N_{NO_2}}{N_{NO_2}+N_{Na}}\right) = \frac{N_{tot}}{1+\frac{N_{Na}}{N_{NO_2}}} = \frac{N_{tot}}{1+\frac{V_{NO_2} f_{NO_2} \rho_{NO_2} M_{Na}}{V_{Na} f_{Na} \rho_{Na} M_{NO_2}}} = \frac{120}{1+0.638} = 73.3 \approx 73$$

The stoichiometry of the Na + NO_2 → $NaNO_2$ reaction therefore dictates that we have 73 NO_2 rail cars and 47 Na rail cars in a 120 car train.

We can now determine the amount of stored energy carried by such a Na/NO_2 train load. The total volume of the Na/NO_2 payload is:

$$V_{payload} = [(20{,}500\ gal\ car^{-1})(0.98)(73\ cars) + (33{,}600\ gal\ car^{-1})(0.95)(47\ cars)]\ (3.79\ l\ gal^{-1})$$

$$V_{payload} = 1.12 \times 10^7\ liters$$

The total energy of the 120 car payload is therefore:

$$E_{payload} = (1.45 \times 10^3\ W\ hr\ liter^{-1})(1.10 \times 10^7\ liters) = 1.60 \times 10^{10}\ W\ hr$$

The 16.0 GW-hr figure calculated for a 120-car train carrying Na/NO_2 is 58% of the 27.4 GW-hr figure we calculated for a 120-car coal train (despite the enormous advantage that coal enjoys because 73% of the mass of reactants required for the chemical reaction C + O_2 → CO_2 comprises ambient atmospheric oxygen that need not be transported). Thus a single daily shipment of Na + NO_2 could be used to operate a power plant with an average output power of order half a GW. We therefore conclude that the high energy density of the Na + NO_2 → $NaNO_2$ reaction may make it feasible to circumvent the transmission problem that currently confronts renewables such as solar and wind by using rail in a manner analogous to the coal industry.

There are of course additional details that must be considered with regard to such a proposal. Some of these are relatively minor, and clearly will not alter the conclusion that there is roughly parity between the energy content of a rail shipment containing coal and a rail shipment containing Na/NO_2. For example, the efficiency with which the electrochemical reaction Na + NO_2 → $NaNO_2$ may be carried out in practice is somewhat less than 100% (although on theoretical grounds, we predict very low overpotentials for the radical-ion reactions at both electrodes, and therefore very high charge/discharge efficiency). We also note that the mass of the Na/NO_2 payload:

$$m = (2.18 \times 10^{10}\ W\ hr)/(1.17 \times 10^3\ \text{W-hr kg}^{-1}) = 1.86 \times 10^7\ \text{kg} = 20{,}500\ \text{tons}$$

is 42% larger than the 14,400 ton coal payload referred to earlier, which would result in somewhat higher fuel costs. We must also take into consideration the energy penalty of heat losses if we propose to ship one or more reagents above ambient temperature in thermally insulated tank cars. We will later examine such heat loss effects in quantitative terms. In a real world application it may be preferable to operate separate Na and NO_2 rail shipments to provide an added margin of safety in the event of a derailment. But once again, we anticipate that the added cost of such measures would be incremental.

On the other hand, such a feasibility analysis should also include the economic benefits of drastically reduced CO_2 emissions, drastically reduced water consumption, the elimination of unwanted byproducts such as sulfur dioxide, heavy metals, particulates, and coal ash, elimination of soil remediation projects at the mine site, etc. Such an economic analysis might also include

the cost savings realized by reclaiming steel and other materials from obsolete rolling stock and rails should a gradual transition from coal to renewable energy take place.

One first-order consideration we have yet to address regarding shipment of Na/NO_2 by rail, however, is the return trip. As mentioned earlier, in the coal industry the returning freight train comprises empty cars, or in some cases, gondola cars lightly loaded with coal ash. In the case of Na/NO_2 by rail, the entire mass of the Na and NO_2 reagents must be returned in the form of sodium nitrite, instead of just empty tank cars. Moreover, we must consider the possibility that rail tanker cars suitable for transport of molten sodium and liquefied nitrogen dioxide may, for one or more reasons, be unsuitable for transporting $NaNO_2$. A worst-case analysis would therefore assume that the Na/NO_2 train would have to be returned empty (analogous to what is done in the coal industry), and an additional train of comparable capacity would be required to haul $NaNO_2$ (and returned empty) in the opposite direction.

Alternatively, it may prove feasible to repurpose the Na and NO_2 tanker cars for $NaNO_2$ transport. The molar volume of $NaNO_2$ is 31.8 cm^3, whereas the combined molar volumes of Na + NO_2 amounts to 56.6 cm^3. The fact that the molar volume of $NaNO_2$ is only 56% that of Na + NO_2 separately, in addition to the fact that tank car outage is expected to be unnecessary for transport of granular $NaNO_2$, suggest that a randomly packed polydispersed mixture of granulated/powdered $NaNO_2$ could be fit into the available volume of the Na and NO_2 tank cars. Alternatively, the $NaNO_2$ payload could be loaded into the cars in molten form, and either allowed to solidify (or partially solidify), or kept molten at ~275 °C for the duration of the return trip.

In any scenario involving the reuse of Na and NO_2 rail cars for return transport of $NaNO_2$, we must be able to purge substantially all of the Na and NO_2 from each tanker car prior to introducing $NaNO_2$. In particular, molten $NaNO_2$ and molten Na metal are known to react violently. A reaction such as:

$$2\ Na + 2\ NaNO_2 \rightarrow Na_2O + 2\ NO$$

also converts elemental Na to electrochemically inactive oxide species such as Na_2O, will result in net loss of NO_2 if the NO evolved is not recovered, and would likely cause spattering of molten material. There is also potential for NO_x termination reactions that result in irreversible formation of N_2.

In the case of NO_2, it should be straightforward to empty the tanker car gravimetrically or under positive pressure, and then remove residual traces of NO_2 by evaporation, cold trapping, etc. In the case of molten sodium, it also conceivable that one or more simple methods may be implemented for complete removal of residual sodium metal. Perhaps the simplest approach is the use of gravimetric draining (e.g. sloped surfaces that lead to a drain) in conjunction with a super-hydrophobic interaction between the container's wall and its liquid contents. Referring to Figure 46, the exploitation of super-hydrophobic surface interactions to facilitate removal of all traces of liquid via simple gravimetric drainage, while somewhat counterintuitive, is well known.[43] Although a somewhat arbitrary definition, a contact angle of greater than 150° is often used to designate the transition from hydrophobic to super-hydrophobic wetting behavior. The super-hydrophobic interaction is such that residual liquid assumes the shape of nearly spherical droplets that roll along the super-hydrophobic surface like miniature ball bearings. In the case of liquid sodium, there are a number of common materials that naturally exhibit very high wetting

angles. Nickel-coated surfaces, for example, are super-hydrophobic with respect to liquid sodium metal at temperatures below 360 °C.[44] Alternatively, the use of granulated $NaNO_2$ could be used to prevent wetting of the tank car's interior surfaces by sodium nitrite.

Figure 46: Examples of super-hydrophobic surfaces on steel and copper that provide for perfect gravimetric drainage. M. Qu, B. Zhang, S. Song, L. Chen, J. Zhang, X. Cao, 2007 Fabrication of Superhydrophobic Surfaces on Engineering Materials by a Solution-Immersion Process. Advanced Functional Materials, 17, 593-596.

In a longer term scenario, if radical-ion battery technology demonstrates its ability to address the grid storage and transmission problems that currently confront renewable energy, it might prove technically and economically feasible to develop a single type of rail car that can be used to transport (and conveniently purge) molten sodium, liquid nitrogen dioxide, and molten sodium nitrite. For example, it might prove possible to implement a coating that is super-hydrophobic with respect to both molten sodium and molten sodium nitrite and also non-reactive with respect to nitrogen dioxide. Alternatively, we might be able to use a coating material such as nickel that is super-hydrophobic with respect to molten sodium nitrite and non-reactive with respect to nitrogen dioxide, wherein molten sodium nitrite is gravimetrically drained, and residual traces of solidified $NaNO_2$ are removed by dissolution in water. Note that molten sodium nitrite has a viscosity of only 3.0 centipoise at 300 °C[45] and therefore drains in a manner similar to water (for comparison, water has a viscosity of 1.0 centipoise and isopropyl alcohol has a viscosity of 2.0 centipoise at room temperature).

Comparing the transport costs of $Na/NO_2/NaNO_2$ and coal entails considering two possible scenarios:

1) Transportation costs are nearly double that of coal because separate trains are required for the fronthaul (Na/NO_2) and backhaul ($NaNO_2$) journeys; on average 50% of the rolling stock travels empty.
2) The same train cars may be used for the fronthaul and backhaul journeys.

Referring to Figure 47, the breakdown of expenses for rail transport are such that the incremental cost of running a return train fully loaded rather than empty may only amount to 30%. Let us imagine that an in depth analysis determines that the incremental cost for scenario 1 is 80% and

the incremental cost of scenario 2 is 30%, relative to the baseline case of single train that travels one direction fully loaded and the other direction empty. The relative impact of such cost increments depends on whether transport costs are at present a minor or major component of the overall cost of coal generated electricity. According to the EIA, the estimated average cost to transport of coal by rail in the U.S. was $17.25 per short ton in 2010.[46] The EIA also currently estimates the levelized cost of energy for conventional coal power plants to be 9.5 cents per kW-hr.[47] Earlier we noted that one ton of coal burned in a modern coal-fired power plant generates 1.90 MW-hr of electricity.[48] Accordingly, the revenue from electricity sales per ton of coal is:

$R = (1.90 \times 10^3 \text{ kW-hr/ton})(\$0.095/\text{kW-hr}) = \$180/\text{ton}$

Apparently the transportation cost of coal is of order 10% of coal generated electricity revenue. This indicates that increasing transportation costs by 30% to 80% under scenarios 1 and 2, while not insignificant, should not fundamentally alter the economics of the proposed "rolling pipeline" transmission model.

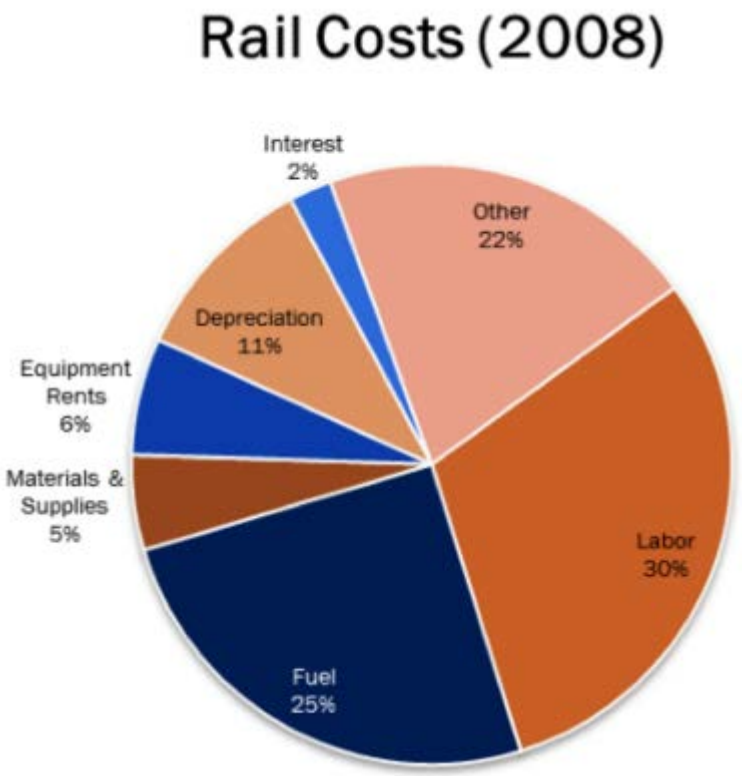

Figure 47: Breakdown of costs for rail freight shipment.
http://www.c2es.org/technology/factsheet/FreightTransportation

Thermal management considerations also exert an influence how rail transport would best be implemented. Consider for example, the question of whether to transport $NaNO_2$ as a granular solid or molten liquid form. As mentioned earlier, the granular solid form of anhydrous $NaNO_2$ has the advantage that it would not wet the interior surface of the tank car, and would therefore be easy to purge. This could be a nickel plated tank that is super-hydrophobic with respect to molten sodium, suitable for liquefied nitrogen dioxide, and also suitable for transporting granulated $NaNO_2$ on the return trip. But in an alternative embodiment, the molten sodium nitrite generated by the electrochemical discharge reaction $Na + NO_2 \rightarrow NaNO_2$ could be loaded from

the discharged battery into a thermally insulated tanker car (perhaps equipped with heating coils). The $NaNO_2$ payload would then be kept in the molten state (e.g. at 300 °C) for the duration of the return trip. This would avoid the need to convert molten salt to powdered/granular salt, provides a packing factor of 100%, and would retain substantially all of the heat contained in the sodium nitrite if adequate thermal insulation can be provided.

The two fundamental questions that must be addressed are:

1) If we use uninsulated tank cars and simply allow the contents to cool down to ambient temperature (e.g. 25 °C) during transport, how much of an efficiency penalty will be incurred because we'll eventually have to reheat the contents of the tank car?

2) If we attempt to thermally insulate the tank cars so as to maintain their contents at elevated temperature, how much of an efficiency penalty will be incurred as a result of thermal leakage for a tank car of practical design?

To address question 1, in Figure 48 we have calculated the amount of heat required to raise the temperature of 1 mole of Na, NO_2, and $NaNO_2$ from T = 25 °C to T = T_{final}, where T_{final} is likely of order 300 °C. The molar heat capacity for solid Na (28.2 J mol^{-1} K^{-1}) was obtained from Wikipedia, as was the heat of fusion for sodium metal (2.60 kJ mol^{-1}). Data for the molar heat capacity of molten Na (30.8 J mol^{-1} K^{-1}) was extracted from Argonne National Lab report ANL/RE-95/2.[49] Heat capacity and heat of fusion data for $NaNO_2$ was extracted from the experimental results of Kourkova et al.[50] As shown in Figure 48, $NaNO_2$ exhibits a solid-to-solid phase transition behavior in the vicinity of 165 °C, followed by melting at 271 °C. The less-than-vertical step-like features for the green trace in Figure 48 reflect the limited time resolution of the differential scanning calorimetry measurements made by Kourkova et al. The temperature dependent equation for the heat capacity of NO_2 (g) was obtained from the NIST website,[51] and the data for the heat of vaporization of liquefied NO_2 (38.1 kJ mol^{-1}) was obtained from the Air Liquide Gas Encyclopedia.[52]

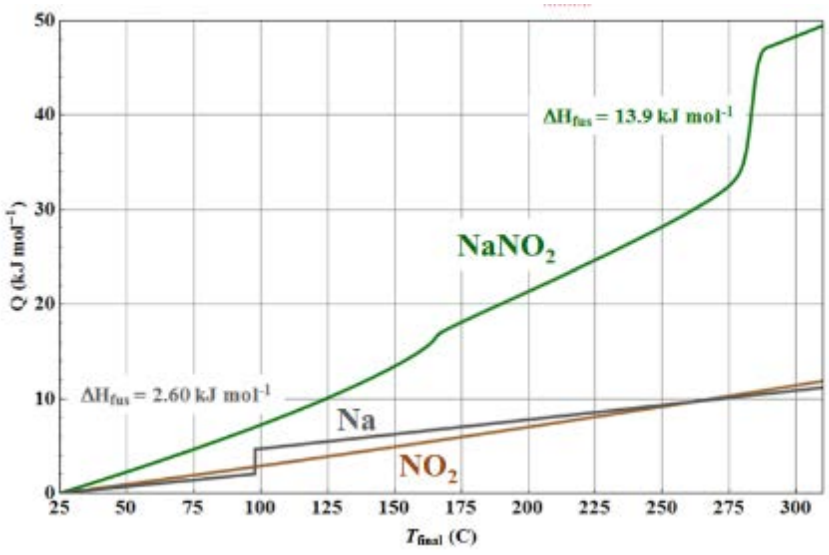

Figure 48: Enthalpy required to heat one mole of $Na/NO_2/NaNO_2$ from 25 C to T_{final}.

Figure 48 indicates that the enthalpy required to heat $NaNO_2$ from 25 °C to 300 °C is 48 kJ mol^{-1}. When compared to the free energy of the reaction Na + NO_2 → $NaNO_2$ (290.4 kJ mol^{-1} at 300 °C) this represents a 17% efficiency penalty. Apparently, allowing the $NaNO_2$ payload to cool to ambient temperature during transport should be avoided if at all possible. Figure 48 indicates that the enthalpy required to heat Na from 25 °C to 300 °C is 11 kJ mol^{-1}, an efficiency penalty of 3.8%. Finally, in the case of NO_2, we find that the enthalpy required to heat NO_2 from 25 °C to 300 °C is 12 kJ mol^{-1}, an efficiency penalty of 4.1%.

The heat of vaporization of NO_2 is 38.1 kJ, but the boiling point of NO_2 is 21 °C. Referring now to Figure 49, for the discharging cycle, vaporization of NO_2 at 21°C can be carried out using extremely low-quality heat, which for all intents and purposes has very low energy cost. Waste process heat and electrical power extracted from the grid during periods of excess electricity production are among numerous options for providing ΔH_{vap} for NO_2 (l). Charging and discharging of the battery is also potentially a significant a source of waste heat, depending on the resistance of the electrolyte and overvoltages present at the two electrodes. The NO_2 (l) → NO_2 (g) conversion process could also be used for thermal management of the inverter circuitry required to convert the dc output of the radical-ion battery to three-phase ac power, thereby also keeping inverter losses to a minimum. On the other hand, it may turn out that in some application settings the simplest and most effective source for supplying any required process heat would be some form of solar thermal power. This is driven in part by (1) the efficiency with which incoming solar radiation may be converted to heat, which is of order 5X the efficiency photovoltaic conversion of sunlight to electricity, and (2) the fact that generation of relatively low quality heat by concentrated solar power (CSP) is inexpensive (because of the relatively modest concentration ratios required to generate temperatures of order 300 °C, and the lack of requirement for refractory materials used in conventional CSP power plants).

During the charging process, heat must be removed from NO_2 (g) evolved at the anionic electrode to allow NO_2 (g) to be condensed to NO_2 (l) for storage. In one embodiment this heat is simply discharged through a heat exchanger to ambient air, water, or soil. In another embodiment, a heat pump may be used to cool the NO_2 (g) while pumping heat back into the electrolyte and/or sodium reservoir to counteract thermal losses to ambient. A bottoming cycle may also be used to recover useful work from hot NO_2 (g) evolved at the anionic electrode as well.

In the case of NO_2, temperature cycling is unavoidable if we desire to store NO_2 in liquid form. But in absolute terms, the 4.1% efficiency penalty calculated earlier is not large. Moreover, the prospects for (1) converting some of this waste heat to useful energy during the charging cycle, (2) harvesting waste heat from charging and discharging of the battery, and (3) the opportunity to mitigate the problem of inverter thermal management and it its associated efficiency penalties during the discharging cycle, are noteworthy.

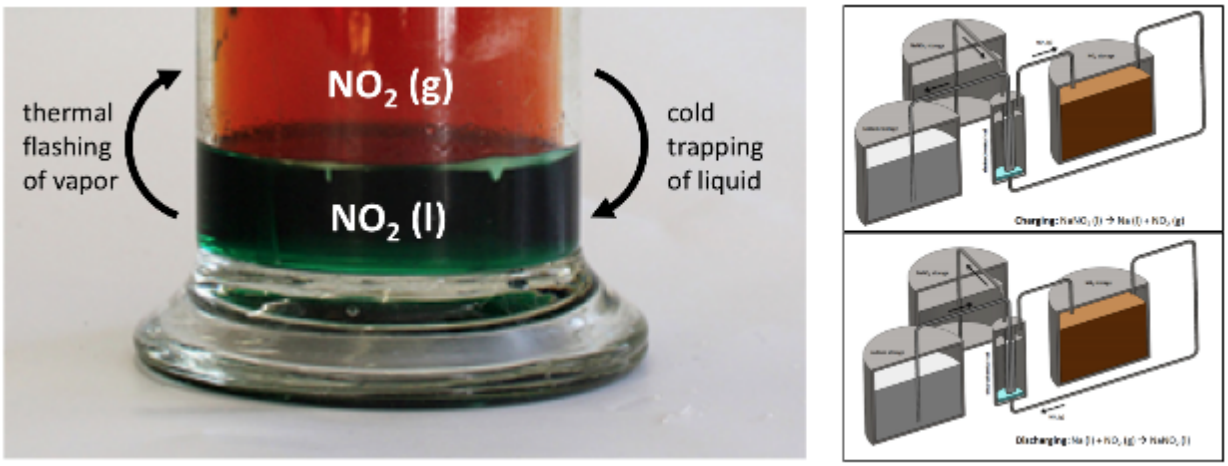

Figure 49: Considerations related to the interconversion of NO_2 liquid and vapor.

A further opportunity for harvesting substantial quantities of waste heat arises during rail transport. Conventional diesel electric locomotives make extensive use of dynamic braking. By rerouting some or all of the electrical connections to the dynamic braking load resistors to resistive heating coils located within each tank car, the very large heat capacity of the molten payload may be used to collect large quantities of heat during the course of transit. High temperature diesel exhaust also provides a potential source of useful waste heat. For example, it might be possible to have the train depart with its molten contents at 280 °C (the melting point of $NaNO_2$ is 271 °C), and arrive at its destination with its molten payload at 310 °C. In a related embodiment, one or more rail cars dedicated to the sole purpose of thermal storage (rather than transporting chemical reagents) may be located directly behind the locomotive(s) to facilitate convenient and efficient collection and storage of waste heat from diesel exhaust and/or dynamic breaking for later use at destination. In light of such opportunities, the relatively small amount of low-grade heat associated with temperature cycling of NO_2 may amount to an efficiency penalty that is effectively zero. But a detailed quantitative analysis of such embodiments is beyond the scope of this discussion.

3.7. To insulate or not to insulate

In the case of $NaNO_2$ and Na, however, the above calculations indicate that a combined efficiency penalty of 21% can be avoided by maintaining both reagents at operating temperature (e.g. 300 °C) at all times. This requires that the proposed thermally insulated tank cars exhibit

very little heat loss. Therefore, our next task is to calculate whether or not this is a realistic expectation. Let us begin by estimating the amount of heat loss expected for each daily trainload of molten $NaNO_2$ and compare it to the amount of electrochemical energy stored in each daily trainload of Na/NO_2 traveling the opposite direction.

Once again, we turn to existing precedents in rail transport in an attempt to ensure realistic calculations. There are, for example, vacuum insulated tank cars used to transport cryogenic materials (Figure 50) such as liquid hydrogen (LH2) at -253 °C that are specifically designed to keep heat transfer from ambient to an absolute minimum (e.g. DOT-113, AAR-204W). For a standard 7,711 kg capacity LH2 tank car, typical boil-off rates are 0.3 to 0.6 % per day.[53] The heat of vaporization of hydrogen is 0.904 kJ mol^{-1} and the density of LH2 is 0.071 g cm^{-3}. The above numbers translate to 110,000 liters of LH2 per tank car with a heat loss rate of 10-20 MJ/day. Earlier we calculated that the volume of the Na/NO_2 payload for a 120-car train was 1.10×10^7 liters, and that the molar volume of $NaNO_2$ is 77% that of $Na + NO_2$ stored separately. Accordingly, we would need of order 80 DOT113 tanker cars to transport the molten $NaNO_2$ on the return trip. This corresponds to 0.8-1.6 GJ day^{-1} of heat loss for the entire 80 car train load of LH2, and represents the combined effects of heat transfer by radiation and conduction.

Figure 50: Cryogenic tank car used to carry liquefied natural gas (LNG) at a temperature of -162 C.

However, we are interested in the amount of heat transfer that would be observed in the case of molten $NaNO_2$, rather than cryogenic LH2. To infer this information on the basis existing LH2 tank cars, we must briefly consider the details of their construction. Referring to Figure 51, super-insulated tank cars such as those used to transport cryogenic fluids use a double-walled hull containing what is referred to as “multi-layered insulation” (MLI). A typical MLI blanket employs 10 to 100 metallized polymer films separated by polyester mesh. For an insulation cavity of a given thickness, optimization of the number of layers (N) represents a balance between radiative losses, which dominate if N is too small, and conduction losses, which dominate if N is too large. Accordingly, in a roughly optimized MLI vessel, conduction and radiation losses are comparable. Thus, we have:

$Q_{(LH2)} = Q_{C(LH2)} + Q_{R(LH2)}$

and:

$Q_{C(LH2)} = Q_{R(LH2)}$

Assuming the thermal conductivity and emissivity of the MLI composite structure is not a strong function of temperature, the ratio of Q_C for molten $NaNO_2$ and LH2 must be of order:

$$\frac{Q_{C(NaNO2)}}{Q_{C(LH2)}} = \frac{T_{NaNO2} - T_{amb}}{T_{amb} - T_{LH2}}$$

and the ratio of Q_R for molten $NaNO_2$ and LH2 must be of order:

$$\frac{Q_{R(NaNO2)}}{Q_{R(LH2)}} = \frac{T^4{}_{NaNO2} - T^4{}_{amb}}{T^4{}_{amb} - T^4{}_{LH2}}$$

The above implies:

$$Q_{NaNO2} = Q_{C(LH2)}\left[\frac{Q_{C(NaNO2)}}{Q_{C(LH2)}}\right] + Q_{R(LH2)}\left[\frac{Q_{R(NaNO2)}}{Q_{C(LH2)}}\right] = \frac{Q_{LH2}}{2}\left[\frac{Q_{C(NaNO2)}}{Q_{C(LH2)}} + \frac{Q_{R(NaNO2)}}{Q_{C(LH2)}}\right]$$

$$Q_{NaNO2} = \frac{Q_{LH2}}{2}\left[\frac{T_{NaNO2} - T_{amb}}{T_{amb} - T_{LH2}} + \frac{T^4{}_{NaNO2} - T^4{}_{amb}}{T^4{}_{amb} - T^4{}_{LH2}}\right]$$

$$Q_{NaNO2} = \frac{Q_{LH2}}{2}\left[\frac{573\ K - 298\ K}{298\ K - 20\ K} + \frac{(573\ K)^4 - (298\ K)^4}{(298\ K)^4 - (20\ K)^4}\right]$$

$$Q_{NaNO2} = \frac{Q_{LH2}}{2}[0.99 + 12.7] = 6.8\ Q_{LH2} = 5.5\ to\ 11\ GJ\ day^{-1}$$

In reality, the thermal leakage would likely be considerably less than this because:

$Q_{R(NaNO2)} \approx 13\ Q_{C(NaNO2)}$

indicates that the optimum MLI layer density for storage of liquid hydrogen is considerably different that for storage of a 300 °C fluid. Moreover, it is unlikely that each shipment of molten $NaNO_2$ would be exposed to ambient temperature for a full 24 hours. Nonetheless, for the purpose of these calculations, let us use the more pessimistic of the above heat loss figures and double it to account for heat loss from molten sodium metal transported in the opposite direction. The resulting figure amounts to roughly 20 GJ day^{-1}. For comparison, the amount of energy stored in the daily shipment of Na/NO_2 was earlier calculated to be 16 GW-hr, which corresponds to 57600 GJ. Thus, we can safely conclude that in a properly insulated tanker car, the energy efficiency penalty for heat loss during transport would be negligible. The same argument should apply to super-insulated containers formatted for trucks, intermodal shipping containers, barges, etc. as well as the large tanks used as reservoirs of molten Na and molten $NaNO_2$ in Figures 27 and 28. Battery modules formatted for tractor trailers or shipping containers could be used to provide highly agile interim deployment capability. This would allow the optimal geographic distribution of grid storage resources to naturally evolve over time to meet changing customer needs.

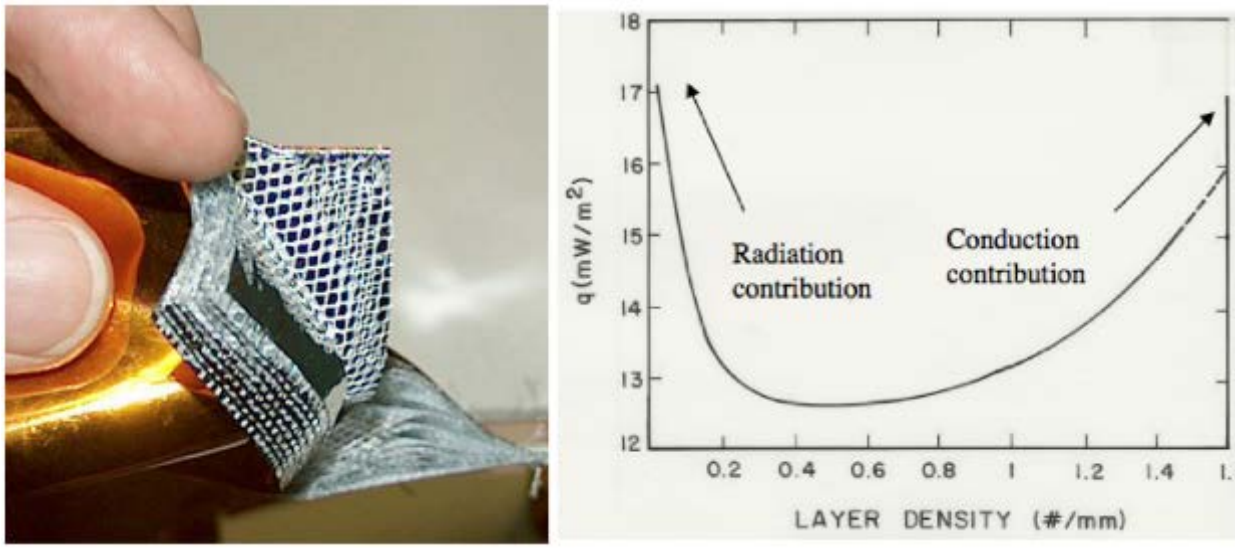

Figure 51: At left, multilayer insulation (MLI) construction showing metal coated plastic layers and scrim separator. https://en.wikipedia.org/wiki/Multi-layer_insulation#/media/File:MultiLayerInsulationCloseup.jpg Original photo by John Rossie of AerospaceEd.org. At right, optimization of layer density to minimize combined heat transfer via conduction and radiation. See for example R. Barron, *Cryogenic Systems*, Oxford University Press, (1985).

Although the above calculations are very rough, they are of significant interest because of existing rail freight corridors that pass through numerous strategically important remote locations (see Figures 52, 53, and 54). For example, the rural/desert southwest is ideally suited to siting utility-scale solar installations. In addition to the specialized application of connecting remotely sited solar, wind, etc. installations to population centers and existing backbones of the electrical grid, such a rolling pipeline transmission model, if it proves to be economically viable, might also be used more generally as an alternative to constructing new high capacity electrical transmission lines. For example, a cost effective and easily deployed grid storage technology could be used to ensure that an existing transmission line is always operated at 100% of its rated current carrying capacity (despite local and regional variations in electricity demand). Grid storage could also be used to eliminate load spikes, thereby extending the lifetime of aging components such as transformers, and allowing some equipment upgrades to be deferred. These benefits of grid storage are in addition to that of eliminating solar and wind over-production scenarios in which power generation capacity is sometimes "thrown away" because it can't be absorbed by the grid.[54]

Thus, in summary, radical-ion battery technology may be capable of addressing both the grid storage and transmission problems that hamper large-scale adoption of intermittent renewables. Progress up the learning curve of this new technology would likely pace its adoption in different applications, however. For example, early stage adoption might emphasize its application to grid storage alone. But if the radical-ion battery technology proves itself to be cost effective and reliable for grid storage, justification for investment in the rail-based approach to addressing the transmission problem described above might eventually become self-evident. For example, if detailed analysis indicates construction of new tank cars specifically adapted to transport of molten Na, molten $NaNO_2$, and/or liquefied NO_2 is advisable, financing of such an undertaking

is far easier if the return on investment can be calculated with relatively low uncertainty based on precedents established in the grid storage industry.

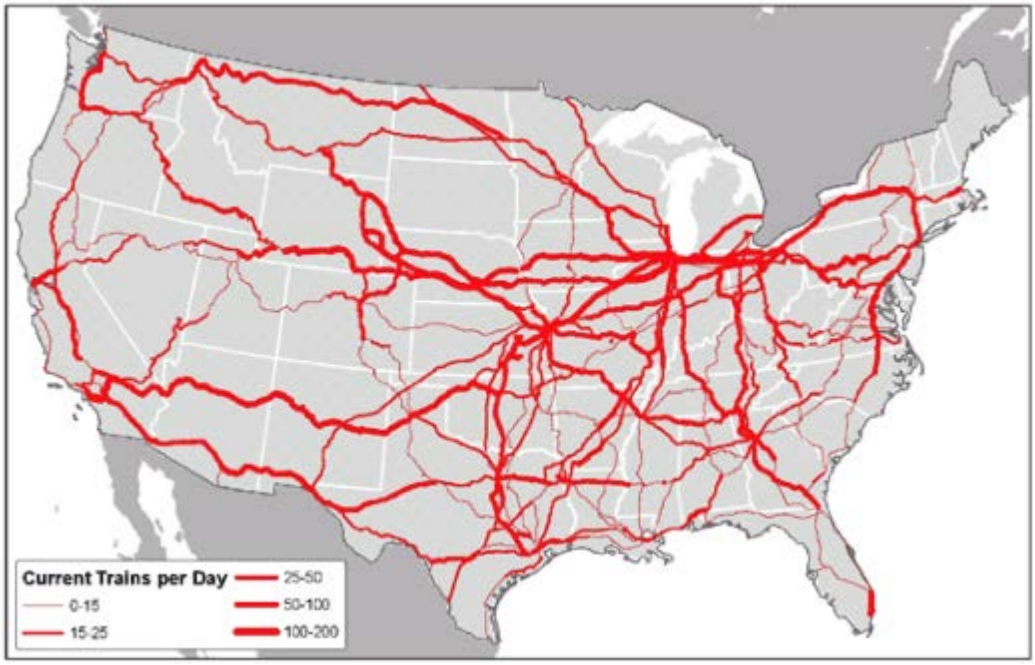

Figure 52: Major rail freight routes in the continental United States. Note the extensive coverage of the desert southwest and great plains regions. Report of the National Surface Transportation Policy and Revenue Study Commission: "Transportation for Tomorrow", http://transportationfortomorrow.com/final_report/chapter_3.htm

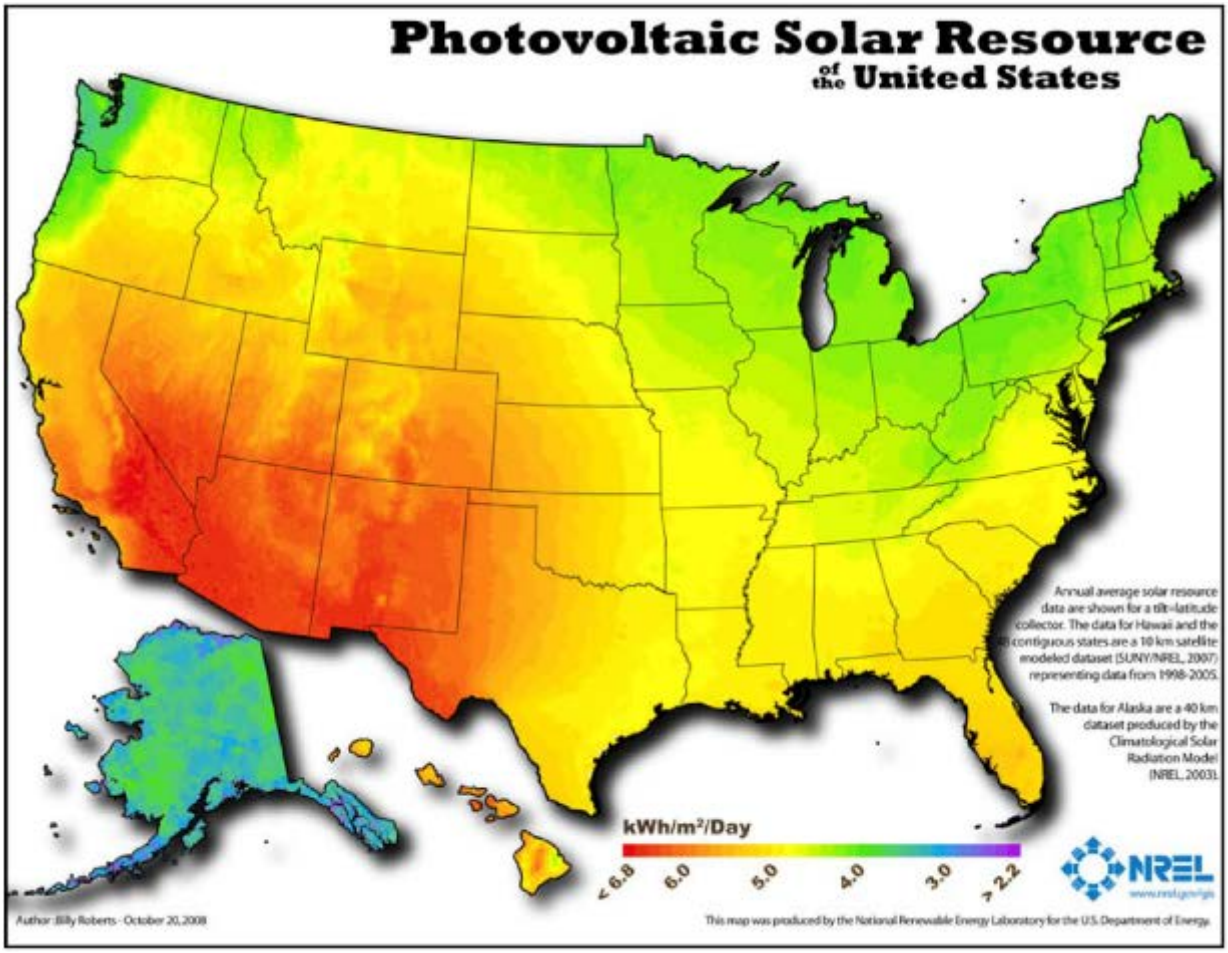

Figure 53: Map of photovoltaic solar resources of the United States. Data obtained from http://greencredential.com/wp-content/uploads/2009/11/map_pv_national_lo-res.jpg, originally compiled by National Renewable Energy Laboratory.

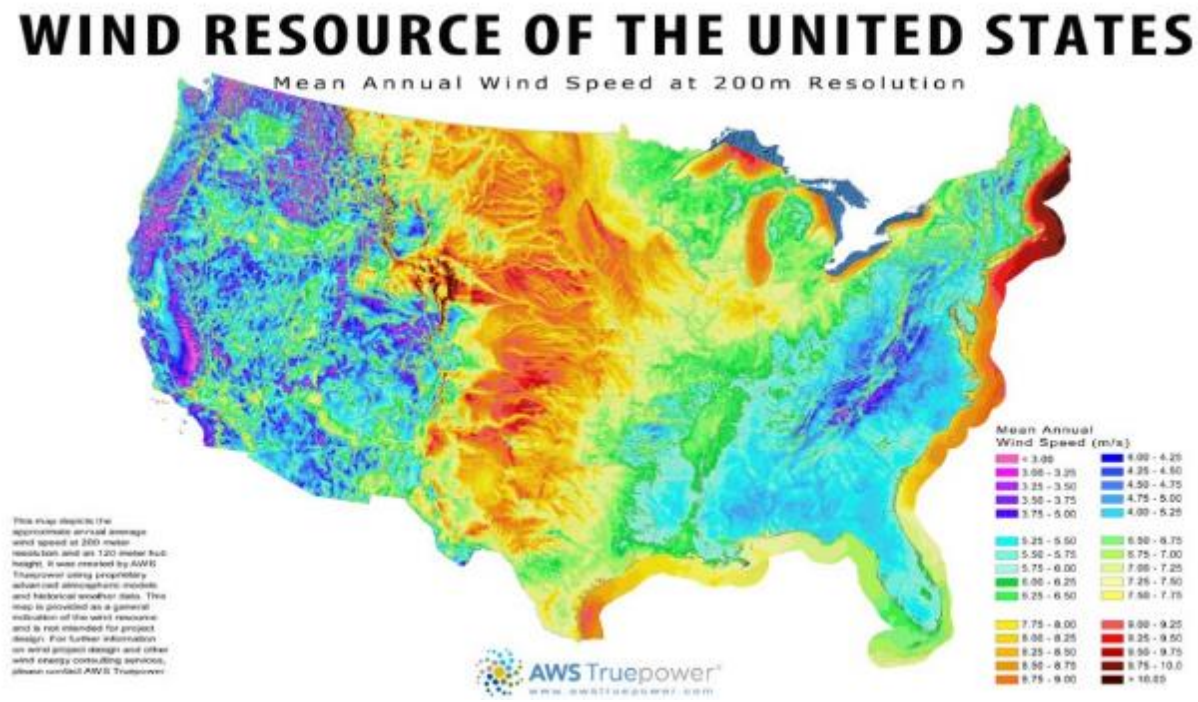

Figure 54: Map of wind power resources of the United States. Data obtained from http://www.tindallcorp.com/120m-map/.

3.8. Electric vehicle applications

Diversifying the energy portfolio of the transportation sector is another fundamentally important objective. This requires that renewable energy achieves much higher penetration in electricity production, and that we develop cost effective batteries for electric vehicles that can be manufactured on a massive scale. Current generation electric vehicles rely primarily on Li-ion battery technology, which results in a very heavy and very expensive vehicle power plant with limited range. For example, consider the Tesla Model S sedan, which achieves an EPA rated driving range of 265 miles with an 85 kW-hr lithium ion battery.[55] The battery pack weighs 540 kg (1200 lb)[56] and accounts for 21 to 22% of the total vehicle cost.[57] Concerns have also been repeatedly raised about limited supply of materials, initially about lithium, but now with an emphasis on cobalt and nickel.[58]

The radical-ion battery could potentially mitigate such problems if the issue of battery thermal management can be effectively dealt with. Earlier we calculated theoretical energy densities of 1.18 kW-hr kg^{-1} and 1.45 kW-hr $liter^{-1}$ for the $NaNO_2$ version of the radical-ion battery. An 85 kW-hr battery would require a total reactant mass of:

$m = (85.0 \text{ kW-hr})/(1.18 \text{ kW-hr kg}^{-1}) = 72.0 \text{ kg} = 159 \text{ lb}$

occupying a reactant volume of:

$V = (85.0 \text{ kW-hr})/(1.45 \text{ kW-hr liter}^{-1}) = 58.6 \text{ liters} = 15.4 \text{ gallons}$

While it must be remembered that these numbers omit the balance of plant for the radical-ion battery, which at a minimum would also include reactant vessels, electrodes, ion-selective membranes, thermal insulation, and thermal management subsystems, the above numbers are

fairly encouraging (especially in light of the low cost and effectively unlimited abundance of sodium, nitrogen, and oxygen).

However, there are least two issues that would have to be critically evaluated for light-duty vehicle applications. The first of these is thermal management. A battery that must be kept at ~300 °C at all times (i.e. during use and during standby) is not a major burden in applications such as stationary power generation because the batteries in question are so large in size, and because they are constantly in use. But the relatively high surface-area-to-volume ratio of an 85 kW-hr battery makes the energy penalty associated with thermal leakage to the environment a potential disqualification.

For example, sodium polysulfide batteries were originally developed by the Ford Motor Company in the 1960s for potential use in light-duty electric vehicles.[59] Sodium polysulfide was also subsequently evaluated for grid storage as well, but the highly corrosive nature of sodium polysulfides has proven to be a very difficult obstacle. Nonetheless, the results of such studies are helpful from the standpoint of evaluating thermal management challenges because the sodium polysulfide battery must be maintained at a temperature of 350 °C. The same is true of many of the original sodium sulfur battery's descendants, such as the ZEBRA battery, which is based on a $Na/NiCl_2$ redox system. On the basis of work conducted on $Na/NiCl_2$ batteries for electric vehicle (EV) applications:[60]

The Think City EV had a choice of ZEBRA and Li-ion. ZEBRA has advantages when operating at extreme temperatures and when the battery is in continuous use, such as in taxis and delivery vans. The ZEBRA battery must be heated to 270–350°C (518–662°F), a temperature that is lower than the original sodium-sulfur battery. Even though special insulation minimizes heat loss, heating consumes 14 percent of the battery's energy per day. Since the energy to keep the battery hot is taken from the battery, the resulting parasitic load, or self-discharge, is 18 percent. An active ZEBRA battery should be either plugged in and on charge or in use. It takes 3–4 days to cool down, and reheating takes about two days depending on the SoC at time of shutdown.

We can take 14% as preliminary estimate of the efficiency penalty that would be incurred in the application of a $NaNO_2$ radical-ion battery in a light-duty electric vehicle application. As discussed later, it should be possible to use a $LiNO_2$ instantiation of the radical-ion battery to bring operating temperatures down to ~225 °C, which would likely reduce the efficiency penalty to ~10%, wherein the use of lithium is acceptable from a materials supply chain standpoint because cobalt and nickel would not be required. It would further need to be determined whether such a 10% penalty is acceptable for light duty electric vehicles. On the other hand, thermal efficiency penalties would be expected to be far smaller for transportation applications involving much larger motors, such as railroad locomotives, buses, trucks, and ships.

The other issue that must be negotiated is vehicle safety. In conventional vehicles, it is recognized that a 10-gallon tank of gasoline represents a non-negligible safety risk, and that the presence of extremely flammable liquid contributes in some measure to injuries and fatalities resulting from automobile accidents. The question that must be answered is whether the engineered safety systems required to render a system such as a $NaNO_2$ battery comparably safe would be economically viable. Alternatively, the lower reactivity of lithium compared to sodium might provide a more cost-effective route to attaining such safety objectives. But in either case, the liquefied NO_2 reagent would need to be appropriately secured as well. In the event that radical-ion battery technology proves successful for applications such as grid storage, progress up the learning curve of this new technology, and further insights regarding improved system

architectures would likely inform such evaluations. It is beyond the scope of this discussion to analyze these issues in greater depth, however.

3.9. Alternative chemistries, chemical additives, and further compositional variants

NO_2^-/NO_2 has thus far emerged as the most promising radical-ion candidate for the anionic electrode. There are, however, a number of options that are clearly worth investigating for the cationic electrode. In principle any cation whose neutral species comprises a free radical and that forms an ionic nitrite salt which is stable above its melting point may be among those considered. One of the most important examples is the $Li/LiNO_2/NO_2$ system, which offers a comparable cell voltage to $Na/NaNO_2/NO_2$, but features lower operating temperature, fewer safety concerns for applications such as electric vehicles, and higher gravimetric energy density.

Using tabulated thermodynamic data for the standard free energy of formation for each of the reagents:[61] [62]

$\Delta G_f°(Li) = 0$ kJ mol^{-1}

$\Delta G_f°(NO_2) = +51.9$ kJ mol-1

$\Delta G_f°(LiNO_2) = -302$ kJ mol^{-1}

we calculate the change in free energy for the $Li + NO_2 \rightarrow LiNO_2$ reaction under standard state conditions to be:

$\Delta G° = -353.9$ kJ mol^{-1}

from which we calculate a standard state electrochemical potential of:

$$E° = \frac{\Delta G_f°}{n\,F} = \frac{353900\ J\ mol^{-1}}{96485\ C\ mol^{-1}} = 3.67\ V$$

This is 5% higher than E° for the $Na/NaNO_2/NO_2$ system (3.49 V). The melting point of $LiNO_2$ is 222 °C, and the melting point of lithium metal is 181 °C. Accordingly, we might contemplate operating such a battery at temperatures as low as ~225 °C. There are already mature Li-ion-selective membrane materials such as LISICON; in the future it may be possible to leverage work that is currently underway to identify Li-ion-selective membranes for use in conventional Li-ion battery applications.[63] The anomalously small ionic radius of Li^+ may greatly facilitate the identification ultra-high-performance Li^+ membrane materials as well.

In the case of potassium, using tabulated thermodynamic data for the standard free energy of formation for each of the reagents:[64] [65]

$\Delta G_f°(K) = 0$ kJ mol^{-1}

$\Delta G_f°(NO_2) = +51.9$ kJ mol-1

$\Delta G_f°(KNO_2) = -335$ kJ mol^{-1}

we calculate the change in free energy for the $K + NO_2 \rightarrow KNO_2$ reaction under standard state conditions to be:

$\Delta G° = -353.9$ kJ mol^{-1}

from which we calculate a standard state electrochemical potential of:

$$E° = \frac{\Delta G_f°}{n\,F} = \frac{386900\ J\ mol^{-1}}{96485\ C\ mol^{-1}} = 4.01\ V$$

This is 15% higher than E° for the $Na/NaNO_2/NO_2$ system (3.49 V). High performance potassium-ion-selective membranes based on beta-alumina are commercially available as well.[66] The main obstacle to direct exploitation of the $K/KNO_2/NO_2$ system is that heating KNO_2 to its melting point (438 °C) results in gradual thermal decomposition, starting at ~410 °C.[67] Moreover, in absolute terms, the melting point of KNO_2 is inconveniently high. We will discuss a potential solution to these problems shortly.

Other nitrites that are known to exist include Rb, Cs, Ca, Sr, Ba, La, Ni, Ag, Hg, Tl, Pb, Pr, Nd, Sm, Tb, Dy, and Yb. There are also elements for which the existence of stable nitrites is suspected but uncertain (Co, Pd, Cu, Cd)[68]. Some of the nitrite species having less electropositive cations are thought to be covalent rather than ionic. The elements that are known not to form nitrite compounds (most of the transition metals for example) are also of interest from the standpoint of selecting electrode materials that will not be subject to corrosion. Within this group of non-nitrite-forming elements, a further category are those that do not form an electrically insulating oxide layer in the presence of molten nitrite salt, or catalyze thermal decomposition of the NO_2^- ion.

Among the various elements other than Li, Na, and K known to form nitrites, many are immediately disqualified from practical applications due to cost or toxicity. In addition, many of these nitrite compounds undergo thermal decomposition prior to melting as was noted earlier for potassium. For example, calcium nitrite is potentially interesting from the standpoint of low cost and low toxicity. And even though elemental Ca does not actually have an odd number of electrons as is the case with alkali metals, it is still very chemically reactive. We would therefore expect a low overvoltage at a Ca/Ca^{2+} cationic electrode. Calcium metal's chemical reactivity is on par with lithium, in accordance with the diagonal rule of the periodic table,[69] and might therefore be of interest for electric vehicle applications. But the onset of thermal decomposition to N_2O (g) is observed at 220 °C, while the melting point of $Ca(NO_2)_2$ is 390 °C.[70]

In the case of KNO_2, it may be possible to address the thermal decomposition problem by blending KNO_2 with other species that effect freezing point depression. Such additional species may exhibit no electrochemical reactivity, may or may not have cations and/or anions in common with the electrochemically active species, and/or may comprise nitrite salts that may be electrochemically active or inactive.

In the case of KNO_2, we contemplate various binary, ternary, quaternary, quinary, etc. salt mixtures to affect lower temperature operation, so as to achieve the higher operating voltage provided by the $K/KNO_2/NO_2$ system while avoiding thermal decomposition of KNO_2, or for the purpose of using KNO_2 as a freezing point depressant, or both. For example, referring to Figure 55, $NaNO_2$ and KNO_2 form a binary eutectic with a melting point of ~225 °C, as well as a wide range of $NaNO_2/KNO_2$ mole fraction mixtures with melting points well below the thermal decomposition temperatures of both KNO_2 and $NaNO_2$. In one embodiment, KNO_2 is used simply to depress the freezing point of a majority $NaNO_2$ electrolyte from 271 °C to <250 °C.

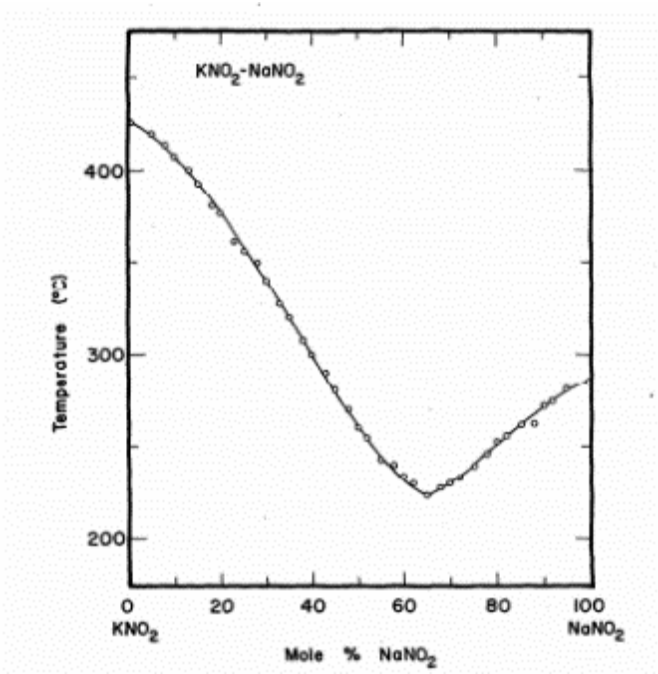

Figure 55: Temperature-composition phase diagram for KNO_2-$NaNO_2$. G. Janz, U. Krebs, H. Siegenthaler, and R. Thompkins, "Molten Salts: Volume 3, Nitrates, Nitrites, and Mixtures, Electrical Conductance, Density, Viscosity, and Surface Tension Data", J. Phys. Chem. Ref. Data, Vol. 1, No. 3 (1972).

This might be done for purpose of allowing Kalrez fluoroelastomer O-rings having a maximum continuous service temperature of 260 °C to be used, for example.[71] As $NaNO_2$ is added/withdrawn to the electrolyte during charging and discharging, the freezing point of the electrolyte may vary between 225 °C ≤ T ≤ 250 °C as the mole fraction of $NaNO_2$ is varied over the approximate range of 50 to 80%. Alternatively, we might use a K-ion-selective electrode and operate only the $K/KNO_2/NO_2$ redox cycle (between 20 and 50% mole fraction of KNO_2).

In another embodiment, $NaNO_2$ could be replenished during the charging process to keep the melting point of the electrolyte constant (e.g. to hold the electrolyte at the eutectic mole fraction having a melting point of ~225 °C). Such a strategy might be useful for a facility that is used to convert $NaNO_2$ to Na and NO_2 using renewable energy at a remote location, wherein the Na/NO_2 reagents are then shipped by rail to be converted into electrical power elsewhere.

To make a system based on the 65/35 $KNO_2/NaNO_2$ eutectic having a melting point of 225 °C that would maintain the correct mole fraction of $NaNO_2/KNO_2$ during both charging and discharging, we could implement two separate ion-selective cationic electrodes for Na and K (electrically in parallel), in conjunction with control circuitry that restricts the Na and K charging/discharging currents to a predetermined ratio (e.g. by operating only one electrode at a time and varying the duty cycle between the two electrodes). Such a cell design might allow operation at 230 °C, such that silicone O-rings, gaskets, etc. may be used. The molten Na and K metal collected could be either kept separately or allowed to mix to form a NaK alloy. Referring to Figure 56, we see that that the 65/35 $KNO_2/NaNO_2$ eutectic would form a 65/35 Na/K alloy with a melting point of order 0 °C. This sub-room-temperature melting point might prove useful for one or more practical/logistical reasons.

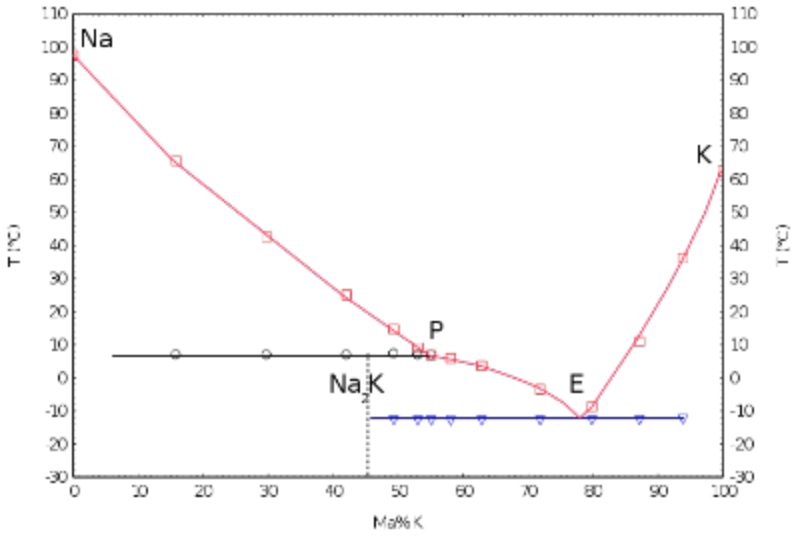

Figure 56: Temperature-composition phase diagram for Na-K alloy. G.L.C.M. van Rossen, H. van Bleiswijk: Über das Zustandsdiagramm der Kalium-Natriumlegierungen, in: Z. Anorg. Chem., 1912, 74, S. 152–156.

Referring now to the $LiNO_2/NaNO_2$ phase diagram of Figure 57, we may contemplate analogous cell designs having electrolyte temperatures as low as ~150 °C. The melting point of lithium metal is 181 °C, however, which would set the minimum electrolyte temperature if $LiNO_2$ is to be an electrochemically active constituent of such a cell. On the other hand, it is clear that $LiNO_2$ could play an important role as an electrolyte freezing point depression additive in a $Na/NaNO_2/NO_2$ cell.

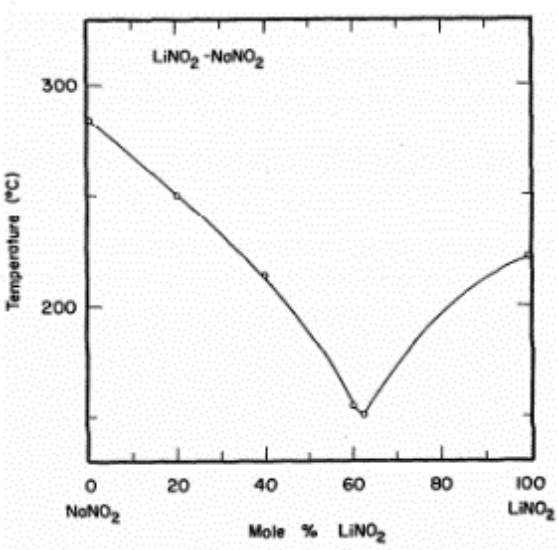

Figure 57: Temperature-composition phase diagram for $LiNO_2$-$NaNO_2$. G. Janz, U. Krebs, H. Siegenthaler, and R. Thompkins, "Molten Salts: Volume 3, Nitrates, Nitrites, and Mixtures, Electrical Conductance, Density, Viscosity, and Surface Tension Data", J. Phys. Chem. Ref. Data, Vol. 1, No. 3 (1972).

Referring next to Figures 58 and 59, we observe that $Ca(NO_2)_2$ may have utility as a freezing point depressant as well. Both the $NaNO_2/Ca(NO_2)_2$ and $KNO_2/Ca(NO_2)_2$ binary eutectics have melting points in the vicinity of 200 °C. More generally, through the use of ternary and higher salt mixtures, melting points may be manipulated further, albeit at the expense of increased complexity. Although ternary mixtures of $LiNO_2/NaNO_2/KNO_2$ have yet to be extensively explored, the literature does contain one characterization of the Li/Na/K system in which nitrite and nitrate ions are present in a 1:1 ratio that illustrates the extensive latitude provided by ternary systems (Figure 60).

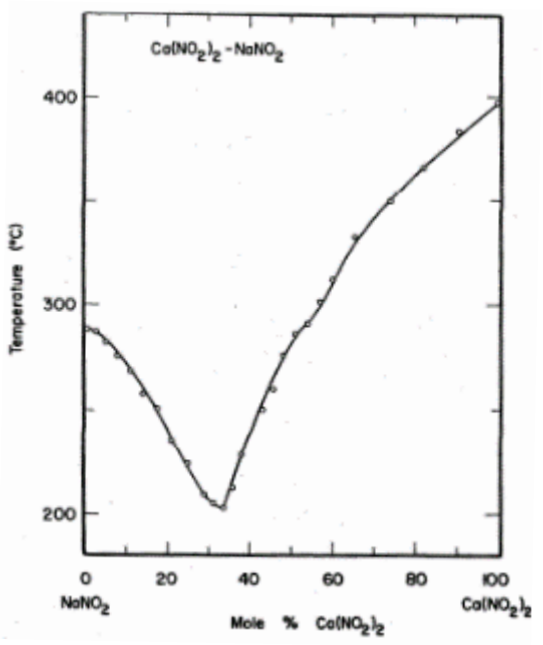

Figure 58: Temperature-composition phase diagram for $NaNO_2$-$Ca(NO_2)_2$. P. Protsenko, B. Medvedev, The K, Li // NO2, NO3 System, Russian Journal of Inorganic Chemistry, 8(12) pp. 1434-1436 (1963).

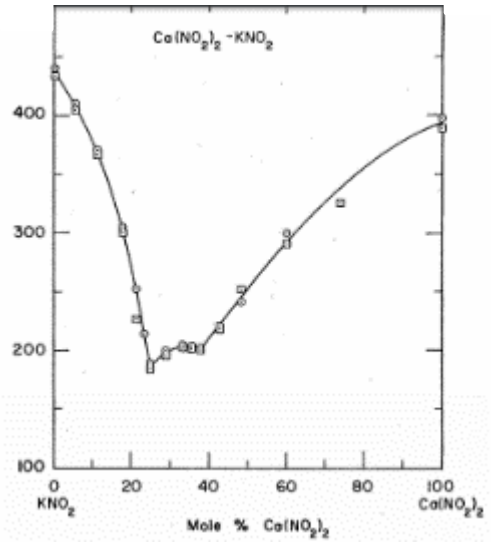

Figure 59: Temperature-composition phase diagram for KNO_2-$Ca(NO_2)_2$. Protsenko, P.I., Medvedev, B.S. (1966) Phase diagrams of binary systems formed by the nitrites of the alkali metals and calcium (translated), Ukrainskii Khimicheksii Zhurnal 32(7) pp. 690-694.

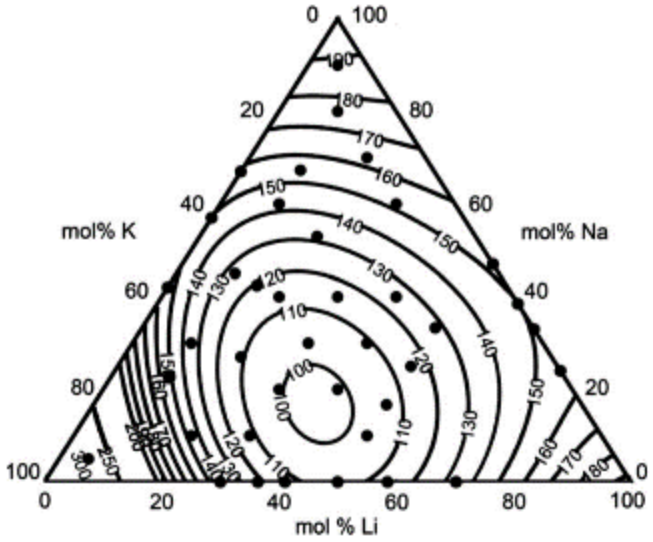

Figure 60: Li/Na/K system in which nitrite and nitrate ions are present in a 1:1 ratio. L. Andrej, Y. Nam, and E. Wang. "(Solar Thermal) Heat Transfer Fluids." Annual Review of Heat Transfer 15, 2012.

The $LiNO_2/KNO_2$ binary salt system is potentially very interesting. Although Li and K metal do not appear to form a binary alloy in any known stoichiometry,[72] the $LiNO_2/KNO_2$ binary salt system is remarkable in its ability to form low-melting mixtures. For example, the $LiNO_2/KNO_2$ binary eutectic has a melting point of 98 °C.[73] Therefore, we might contemplate a radical-ion battery in which $K/KNO_2/NO_2$ is the electrochemically active constituent, and $LiNO_2$ is used as

a freezing point depressant, wherein the chemical composition of the mixed electrolyte may vary over some range suitably close to the eutectic mole fraction.

For example, referring to Figure 61, the melting point of the $LiNO_2/KNO_2$ binary salt system is restricted to the range 98 °C ≤ T ≤ 150 °C if the mole fraction of KNO_2 (X) is kept between a lower limit of X_{min} = 30% and an upper limit of X_{max} = 50%. In the fully discharged state (X = X_{max}), the mass of the electrolyte is at a maximum, and the mass fraction (F) of the electrolyte that comprises KNO_2 is given by:

$$F = \frac{M_{KNO2}\, X_{max}}{M_{LiNO2}(1-X_{max}) + M_{KNO2}\, X_{max}} = \frac{(85.10\ gm\ mol^{-1})\ (0.50)}{(52.95\ gm\ mol^{-1})\ (0.50) + (85.10\ gm\ mol^{-1})\ (0.50)} = 61\%$$

The fraction of the electrochemically active reagent (KNO_2) that is available for use (f) is given by:

$$f = \frac{X_{max} - X_{min}}{X_{max}(1 - X_{min})} = \frac{0.50 - 0.30}{0.50\ (1 - 0.30)} = 57\%$$

Thus, the mass fraction of the electrolyte as a whole that is electrochemically active is:

$$Ff = \frac{M_{KNO2}\ (X_{max} - X_{min})}{(1 - X_{min})[M_{LiNO2}(1 - X_{max})\ +\ M_{KNO2}\, X_{max}]} = 35\%$$

The gravimetric energy density of the electrolyte is only 35% of a theoretical all-KNO_2 radical-ion battery, because 65% of the electrolyte is dead weight from an electrochemical standpoint.

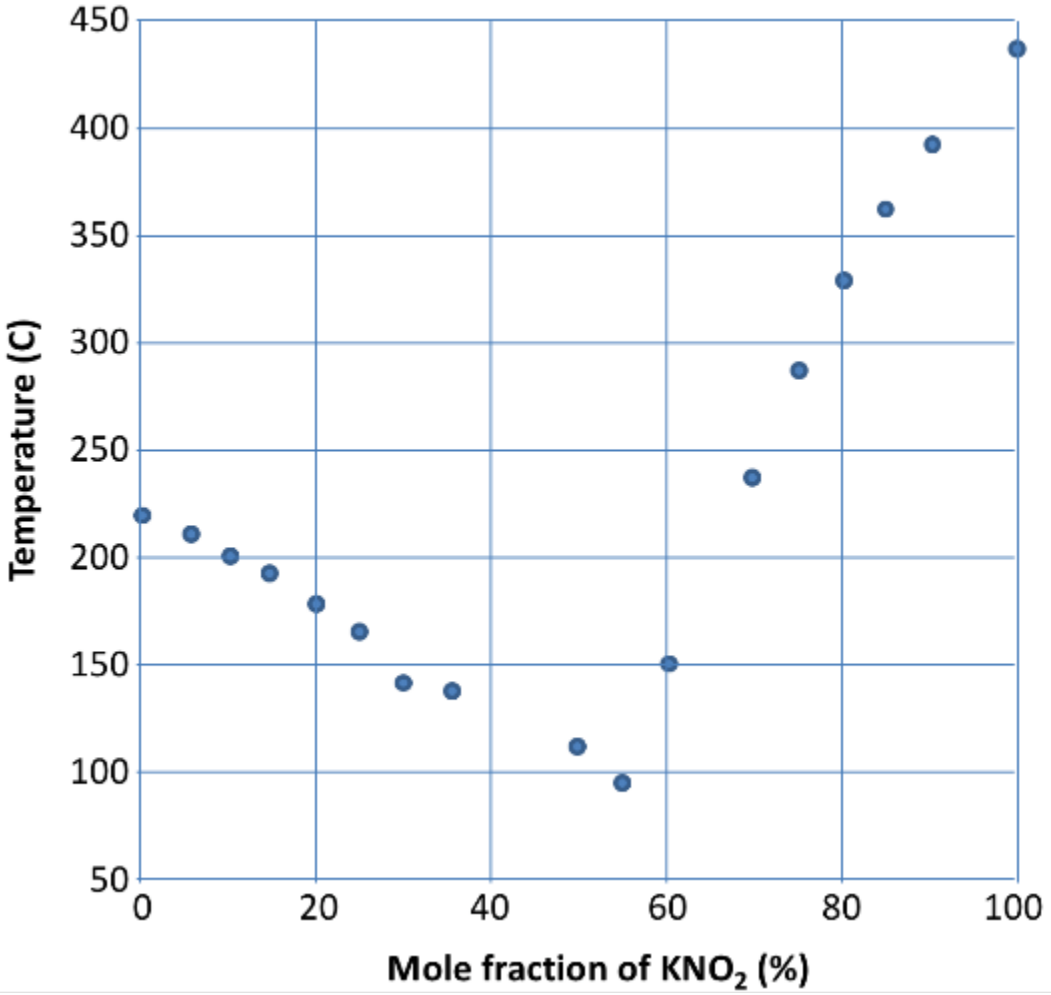

Figure 61: Temperature-composition phase diagram for $LiNO_2$-KNO_2. Reproduced from P. Protsenko, B. Medvedev, The K, Li // NO_2, NO_3 System, Russian Journal of Inorganic Chemistry, 8(12) pp. 1438-1436 (1963).

Earlier we calculated that the mass of the electrolyte for an 85 kW-hr light-duty electric vehicle (Tesla Model S Sedan) battery was 72 kg for a $Na/NaNO_2/NO_2$ radical-ion battery. If we apply a 65% dead-weight penalty to the electrolyte of such a battery, we incur a mass penalty of 134 kg. Considering that the existing 85-kW-hr Li-ion battery used in the Tesla Model S Sedan weighs 540 kg, and that a typical Sedan might weigh 1500 kg, incurring a 134 kg weight penalty to allow operation at a temperature of 150 °C may be worthwhile. Moreover, it is likely that a ternary or quaternary salt mixture using $NaNO_2$ and/or $Ca(NO_2)_2$ additives could expand the KNO_2 mole fraction range over which low temperature operation can be realized, therefore reducing the weight penalty relative to that calculated above. Accordingly, further investigation into the details of such ternary and quaternary salt systems appears to be warranted. In conducting such an investigation, it is useful to point out an important property of the algebraic expression for F f. We calculated above that for the case X = 0.40±0.10, the mass fraction of usable electrolyte was F f = 35%. If instead the same ±0.10 composition range is applied to the case 0.80±0.10, we find F f = 69%. This emphasizes the importance of searching for highly

potent freezing point depression additives that allow us to operate on the far right-hand side of the additive/electrolyte phase diagram.

On the other hand, such an investigation may reveal that a simple $Li/LiNO_2/NO_2$ radical-ion battery operating just above the melting point of $LiNO_2$ (222 °C), or a simple $Na/NaNO_2/NO_2$ radical-ion battery operating just above the melting point of $NaNO_2$ (271 °C), is the best option for light-duty vehicle applications. The correct answer depends in part on available materials/techniques for reliable seals and low-loss thermal insulation. In addition, many ion-selective membrane materials exhibit higher resistivity at lower temperatures, such that resistive losses may curtail prospects for reduced operating temperature. At present we are relegated to outlining the handful of representative examples described above rather than making fully definitive recommendations.

In further embodiments, one or more electrolyte additives directed towards increasing the solubility of NO_2 in the electrolyte may be employed, and/or one or more electrolyte additives may be included to suppress unwanted side reactions such as $NO_2^- + NO_2 \rightarrow NO_3^- + NO$ discussed earlier (either by lowering the operating temperature of the electrolyte, chemically inhibiting the forward reaction, accelerating the reverse reaction, or some combination thereof). In addition to the use of additives in the molten electrolyte, we also contemplate the use of additives to lower the melting point and/or improve the wetting behavior of the various molten metal species in question. For example, earlier we noted $LiNO_2/NaNO_2$ could allow electrolyte temperatures as low ~150 °C, but that the melting point of lithium metal is 181 °C. Figure 62 indicates that we could consider alloying lithium metal with calcium metal to alleviate this difficulty. In such an embodiment, the calcium metal would merely serve as a freezing point depressant and would be sequestered from the electrolyte compartment by the ion-selective membrane. The 92/8 mole fraction Li/Ca alloy forms a eutectic that melts at only 141 °C, but the melting point is relatively sensitive to composition. Accordingly, we contemplate using a ternary electrolyte such as $LiNO_2/NaNO_2/Ca(NO_2)_2$ in which the Li and Ca are maintained at a 92/8 mole fraction ratio on both sides of the ion-selective membrane, wherein separate lithium and calcium ion-selective electrodes deliver Li and Ca ions to a common molten Li/Ca metal alloy reservoir.

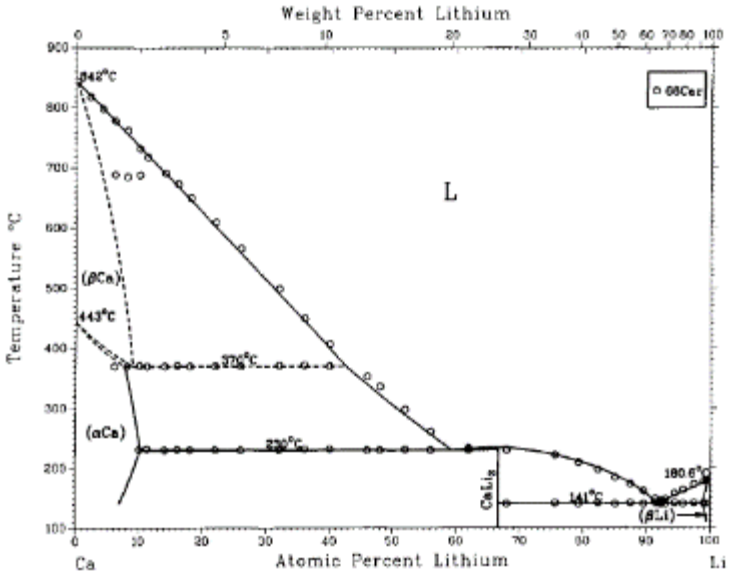

Figure 62: Phase diagram for binary calcium–lithium alloy. C. Bale, A. Pelton, "The Ca-Li (Calcium-Lithium) System", Bulletin of Alloy Phase Diagrams, Vol. 8, No. 2 (1987).

One type of electrolyte additive that deserves special attention is the nitrate ion. Consider, for example, sodium nitrate. Electrolysis of molten sodium nitrate occurs at a higher voltage than electrolysis of molten sodium nitrite:

$NaNO_3 \rightarrow Na + NO_2 + ½\ O_2$

$\Delta G_f°(Na) = 0\ kJ\ mol^{-1}$

$\Delta G_f°(NO_2) = +51.9\ kJ\ mol\text{-}1$

$\Delta G_f°(O_2) = 0\ kJ\ mol^{-1}$

$\Delta G_f°(NaNO_3) = -365.9\ kJ/mol$

$\Delta G° = -417.2\ kJ\ mol^{-1}$

$$E° = \frac{\Delta G_f°}{n\ F} = \frac{417200\ J\ mol^{-1}}{96485\ C\ mol^{-1}} = 4.32\ V$$

This is 830 mV greater than E° for $NaNO_2$, which implies that there should be a "voltage window" within which nitrite ions are electrochemically active and nitrate ions are not. One of the reasons that this is potentially important is that there are numerous documented nitrite/nitrate salt mixtures exhibiting strong freezing point depression effects that may be of interest. In addition, the presence of nitrate ion may be useful from the standpoint of enhancing the solubility of NO_2 in the electrolyte. The addition of nitrate ion to the electrolyte does not violate the "like dissolves like" solubility rule, and a mixture of NO_2^- and NO_3^- ions presents numerous geometric permutations for formation of a solvent sphere around NO_2 molecules. This may result in a synergistic solubility enhancement effect. Finally, the presence of substantial quantities of nitrate ion could potentially help push the equilibrium $NO_2^- + NO_2 \rightarrow NO_3^- + NO$ reaction to the left, thereby reducing the mole fraction of NO in the system.

During the past several decades, extensive research of binary, ternary, quaternary, etc. nitrite/nitrate salt mixtures has been undertaken for the purpose of assessing candidate fluids for high temperature storage of solar thermal power. One relatively recent publication that is representative of such work is "Recent Progress in Alkali Nitrate/Nitrite Developments for Solar Thermal Power Applications" by T. Bauer, D. Laing, and R. Tamme.[74] This and related publications on solar thermal storage media catalog numerous nitrate/nitrite salt compositions having widely varying properties. Figure 63, for example, which is reproduced from Bauer, Laing, and Tamme, shows a ternary phase diagram for Li/Na/K in which the NO_3^-/NO_2^- molar ratio is constrained to be 0.56. The phase diagram shows a low melting ternary Li33/Na19/K48 composition with a melting point of less than 80 °C, and also provides broad guidance regarding regions of the phase diagram in which melting point is relatively insensitive to changes in composition.

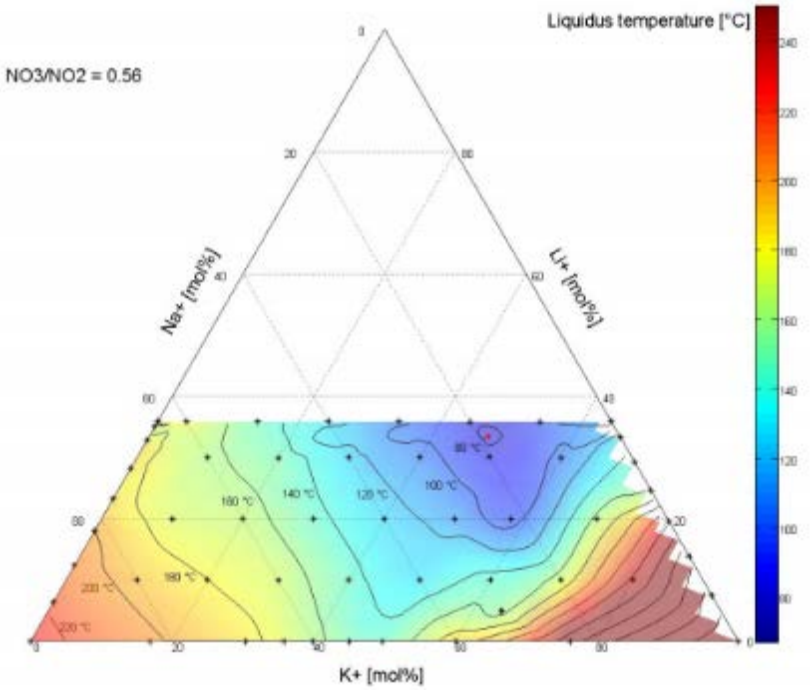

Figure 63: Ternary phase diagram for Li/Na/K in which the NO_3^-/NO_2^- molar ratio is constrained to be 0.56. T.Bauer, D.Laing, and R.Tamme, "Recent Progress in Alkali Nitrate/Nitrite Developments for Solar Thermal Power Applications", Molten Salts Chemistry and Technology Conference, MS9, Trondheim, Norway, 5 - 9 June 2011, Page 1/10.

In further embodiments, the nitrate ion may be used as the electrochemically active constituent, in addition to, or rather than nitrite. In one all-nitrate embodiment for example, the electrolyte comprises substantially pure $NaNO_3$, and NO_3^- ions are oxidized at the anionic electrode. This process may occur via the electrode reaction:

$$NO_3^- \rightarrow NO_3\,(g) + e^-$$

followed by thermal dissociation of NO_3 (g):

$2\ NO_3\ (g) \rightarrow 2\ NO_2\ (g) + O_2\ (g)$

via a number of possible mechanisms involving NO or NO_2, such as:

$2\ NO_3\ (g) \rightarrow 2\ NO\ (g) + 2\ O_2\ (g)$
$2\ NO\ (g) + 2\ O_2\ (g) \rightarrow 2\ NO_2\ (g) + O_2\ (g)$

or:

$2\ [NO_3\ (g) \rightarrow 2\ NO_2\ (g) + 2\ O\ (g)]$
$O\ (g) + O\ (g) \rightarrow O_2\ (g)$

Alternatively, NO_3 fragmentation may occur during the electrochemical oxidation step via:

$NO_3^- \rightarrow NO_2\ (g) + O\ (g) + e^-$

or:

$NO_3^- \rightarrow NO\ (g) + O_2\ (g) + e^-$

In the final analysis, however, regardless of the exact mechanism we expect Na to be deposited at the cationic electrode, with NO_2 and O_2 gas collected above the anionic electrode.

It may then prove possible to operate a discharging process, wherein NO_2 (g) and O_2 (g) are bubbled into (or otherwise delivered to) the electrolyte to run the above reaction in the backward direction. For example, this process could occur via the electrode reaction:

$NO_2\ (g) + e^- \rightarrow NO_2^-$

followed by oxidation of NO_2^- to NO_3^- by the O_2 (g) present. Although sodium nitrate has been used to illustrate the above example, it will be understood that any appropriate nitrate salt may be employed in a similar manner.

4. OTHER ASPECTS OF CELL CONSTRUCTION

Moving on to other aspects of cell construction, in some embodiments, physical contact between the molten metal and its respective ion-selective electrode is maintained by hydrostatic pressure (e.g. a column of molten sodium contained in a vertically oriented sodium-beta-alumina tube that is closed at the bottom). In other embodiments, additives are used to improve wetting of the ion-selective electrode surface by the molten metal. For example, small quantities of cesium metal added to molten sodium have been shown to improve wetting of sodium-beta-alumina at low temperatures.[75] In our laboratory we are currently experimenting with materials that can applied to the molten-metal side of the ion-selective electrode that have a very high affinity for the ion-selective electrode material, remain in place as a thin layer of highly adherent liquid, and also allow the passage of molten sodium. Early experiments involve the application of gallium metal to soda lime glass, but the same principle could be generalized to a variety of other molten metals, coating materials, and electrode compositions. In other embodiments physical and

electrical contact of the molten metal with the ion-selective electrode surface may be facilitated by the use a sponge-like material such as, but not limited to, metal wool, carbon felt, or glass wool. In further embodiments, the molten-metal side of the ion-selective electrode is partially coated with a material that improves the wetting of molten metal but does not cover the surface of the ion-selective electrode entirely. For example, sputtering or evaporation could be used to deposit a fraction of a monolayer of material having high affinity for wetting of the molten metal in question.

Finally, it will be understood that there is a potentially a wide range of materials that may be used for ion-selective electrodes. For example, alternatives to beta-alumina such as NASICON[76] are currently under investigation. Nano-porous films including engineered structures fabricated by multistage "stack-and-draw" techniques[77] may be used as well. Mechanical reinforcement of brittle ion-selective membrane materials such as ceramics and glass may be affected by deposition of thin layers of such materials on porous (e.g. sintered) support structures or via incorporation of reinforcing fibers, wire, mesh, etc. on the surface and/or interior of such membrane materials. Two or more redundant membranes in series may also be used to lower the probability of a membrane breach. In one such embodiment, a plurality of membrane layers which are made thin enough that individual layers exhibit a high degree of mechanical flexibility (and therefore resistance to breakage) are partially sintered together to create a structure that resists crack propagation in the direction normal to the surface of the membrane. In a related embodiment, rather than being sintered, adjacent layers are bonded together with a thin layer of material that permits passage of the desired cation (e.g. Na^+), such as a metal that is liquid at the operating temperature of the cell, and that exhibits good wetting and adhesion to the membrane material. More generally it will be noted that in the event that radical-ion battery technology proves itself well suited to important applications such as grid storage, development of successive generations of high performance ion-selective electrode materials may intensify significantly.

4.1. Electrical configuration of cells

In many applications it is highly desirable to operate a large number of cells in series to minimize the overall resistive losses of system as a whole, enable the use of smaller gauge wire for routing of electrical power, minimize diode forward voltage drop efficiency penalties associated with some types of dc-dc converter and inverter architectures, etc. For example, in one variant of the battery pack used in the Tesla Model S Sedan, a total of 6912 Li-ion cells are configured as 16 modules placed electrically in series. The module voltage is 21.6 V, resulting in a bus voltage of order 350 V. Each 21.6 V module in turn contains 432 Li-ion cells comprising 72 submodules wired in parallel, wherein each submodule comprises 6 Li-ion cells in series. Likewise, in the case of solar PV systems, each photovoltaic cell has an output voltage of order 0.6 V, but the typical dc bus voltage for a PV installation as a whole might be 600 V.

A battery technology such as that proposed here must therefore be well adapted to the construction of compact series-connected multi-cell modules whose internal series connections add negligible electrical resistance. Figure 64 shows such a series-connected stack in schematic form. In this particular example, the electrolyte is $NaNO_2$, the ion-selective membrane is Na-β-Al_2O_3, the cationic electrode is sodium metal, and the anionic electrode is 304 stainless steel (304 SS). It will be understood that this representative example is but one of many different materials combinations that could be used for the electrolyte, ion-selective membrane, and/or

electrodes. The seals (shown in orange) may comprise O-rings, elastomer gaskets, etc. It will be noted that the 304 SS electrode serves not only as the anionic electrode, but also forms part of the molten sodium metal containment vessel, and functions as a low resistance electrical connection between successive unit cells.

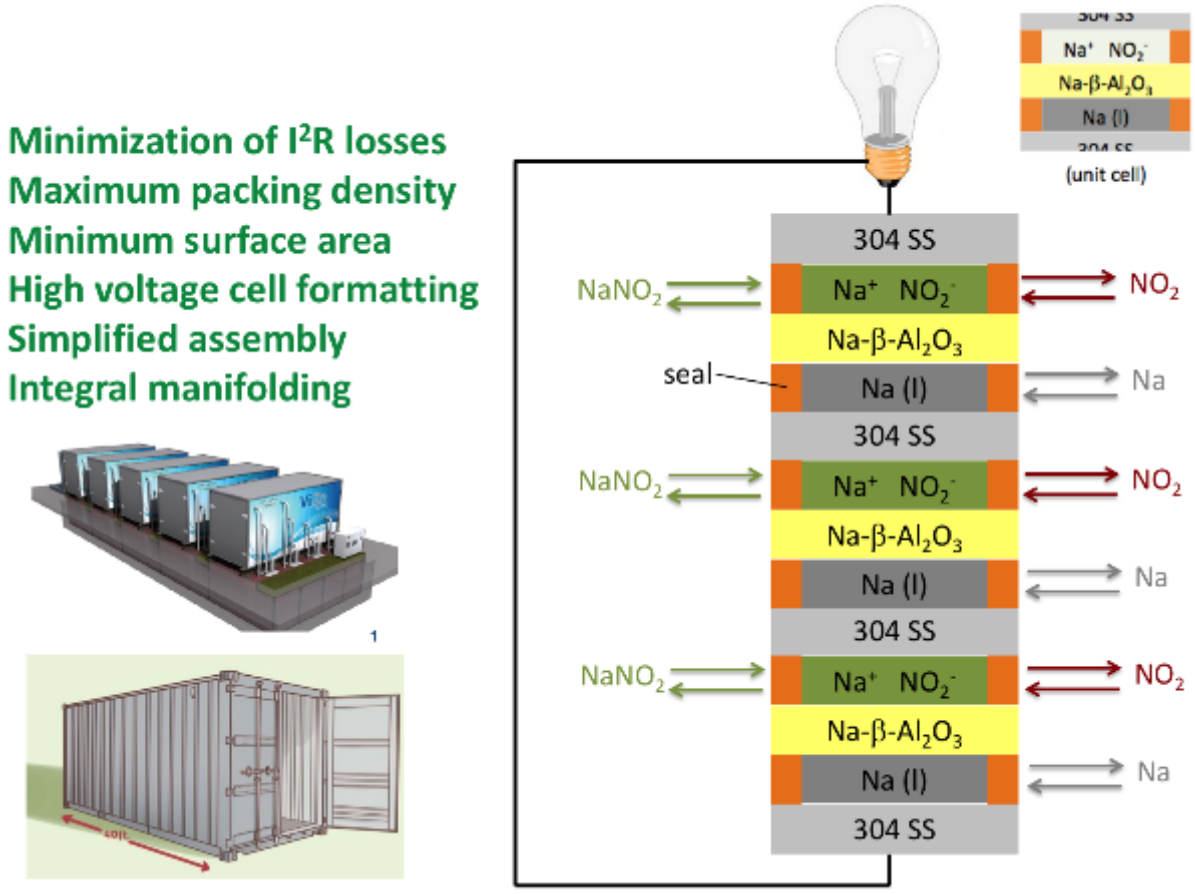

Figure 64: The ultimate objective is a modular, stacked, planar device architecture well suited to low-cost, highly automated mass production

Referring now to Figure 65, in various embodiments, the stack is constructed in a manner that all mechanical design features required to accommodate seals, inlet/outlet manifolds, NO_2 (g) spargers (not shown), etc. may be incorporated into the 304 SS plates. Such a design is directed towards making the Na-β-Al_2O_3 membranes assume the form of featureless ceramic plates requiring no machining or other post processing steps. When assembled, the stack could be configured such that sealing at the electrode/O-ring/ceramic interface occurs without any form of electrical contact between the electrode and the ceramic plate (e.g. O-rings not fully compressed). Such an arrangement would also allow for thermal expansion/contraction in the axial direction without subjecting the Na-β-Al_2O_3 ceramic plates to excessive mechanical stress.

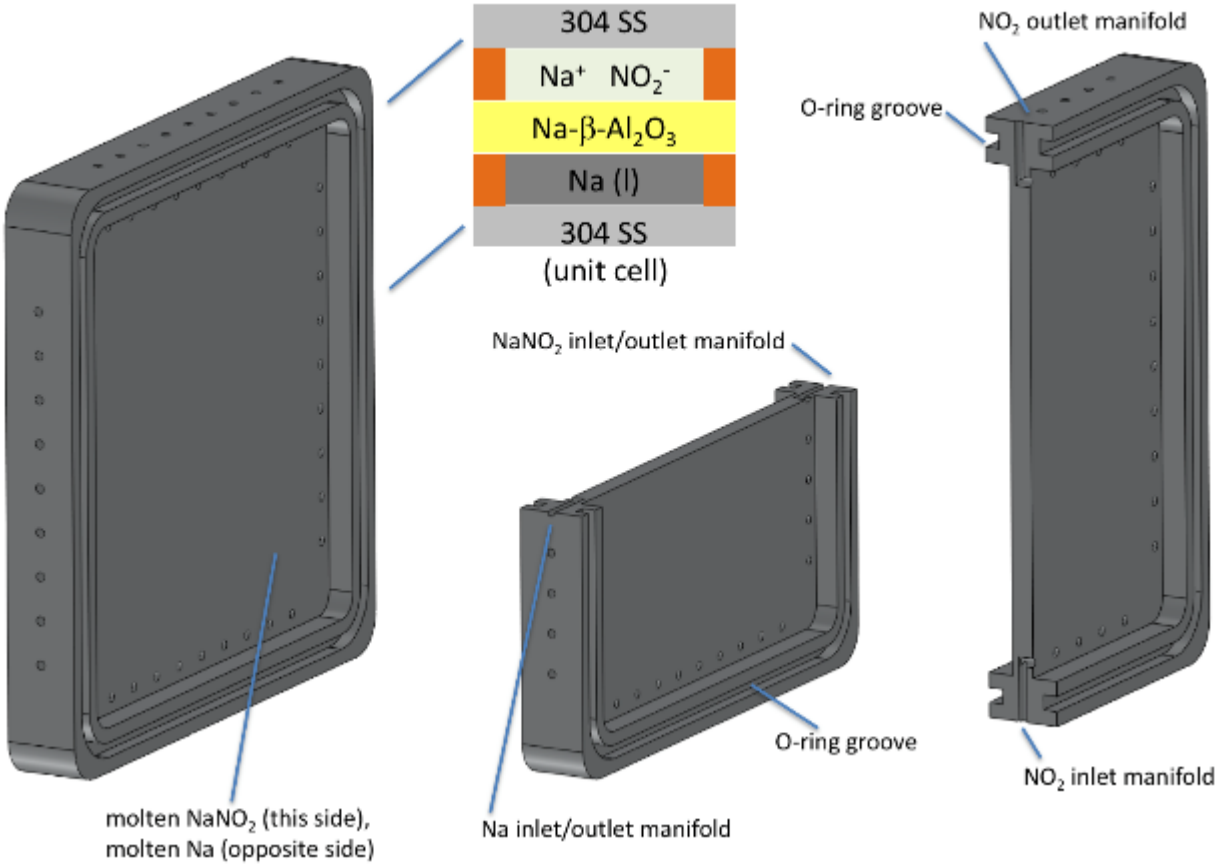

Figure 65: Seals, inlet/outlet manifolds, NO_2 (g) spargers (not shown), etc. may be incorporated into 304 SS plates.

The active portion of the 304 SS anionic electrode may be porous, textured, or otherwise adapted to providing maximum available surface area. The active portion of the 304 SS anionic electrode may further comprise a structure that functions as both an electrode and a sparger for NO_2 gas (e.g. a sintered 304 stainless steel plate with an internal cavity that functions as a gas manifold for NO_2 gas distribution). Portions of such an electrode may be coated with a thin layer of catalytically active material or otherwise chemically treated to improve electrode reaction kinetics. The physical orientation of the stack may be chosen so that NO_2 gas is introduced at the bottom of the electrolyte compartment and/or withdrawn at the top of the electrolyte compartment so as to prevent formation of trapped gas bubbles. Manifolds for reagent introduction and withdrawal are depicted as a plurality of simple holes in Figure 65, but it will be understood that additional features adapted to routing of reagents between unit cells and multiple series stacks may be included as well.

4.2. Preliminary reduction to practice

Preliminary data was collected with a laboratory prototype of a $NaNO_2$ radical-ion battery constructed using a sodium silicate glass ion exchange membrane. The molten salt bath, the wall of which functioned as the anionic electrode, comprised a thick-walled, closed-bottom cylinder made of 304 stainless steel. The heated bath included a vented cover, such that the partial pressure of NO_2 above the molten $NaNO_2$ bath was presumably 1 atm under steady state

operation. The shape of the soda-lime glass membrane was similar to the Na-ion-selective membrane depicted in Figure 26, a thin-walled cylindrical tube closed off at the bottom. The outer diameter of the tube was 20.0 mm, and the wall thickness was 0.60 mm. The bottom ~80 mm of the closed-bottom tube was inserted into the molten electrolyte. The nominal composition of the soda-lime glass membrane used for this experiment was 72% SiO_2, 16% Na_2O, 4% MgO, 3% CaO, 2% Al_2O_3, and 1% K_2O.

A plot of the ionic conductivity of sodium silicate glass at 300 °C as a function of mole fraction of sodium oxide is shown in Figure 66. At elevated temperature and sufficiently high concentration of Na_2O, the silicate glass matrix may exhibit sodium ion conductivities upwards of 10^{-3} Ω^{-1} cm^{-1}, although the mole fraction of sodium oxide is limited by practical considerations such chemical resistance, devitrification, etc. Na-β-Al_2O_3 can be thought of as an alumina analog of such sodium silicate glasses. Although the ionic resistance of the soda-lime glass ion exchange membrane used in these proof of concept experiments was of order 100 Ω (several orders of magnitude higher than an ion exchange membrane would be in a practical battery), this early prototype device facilitated the construction of a functioning electrochemical cell based on the principles described herein. Open circuit output voltages, their temperature dependence, and confirmation of the identity of the products generated by the charging reaction were all verified and found to be fully in agreement with theory. Construction of a fully functional $NaNO_2$ radical-ion single-cell battery based on a sodium-beta-alumina membrane is now underway.

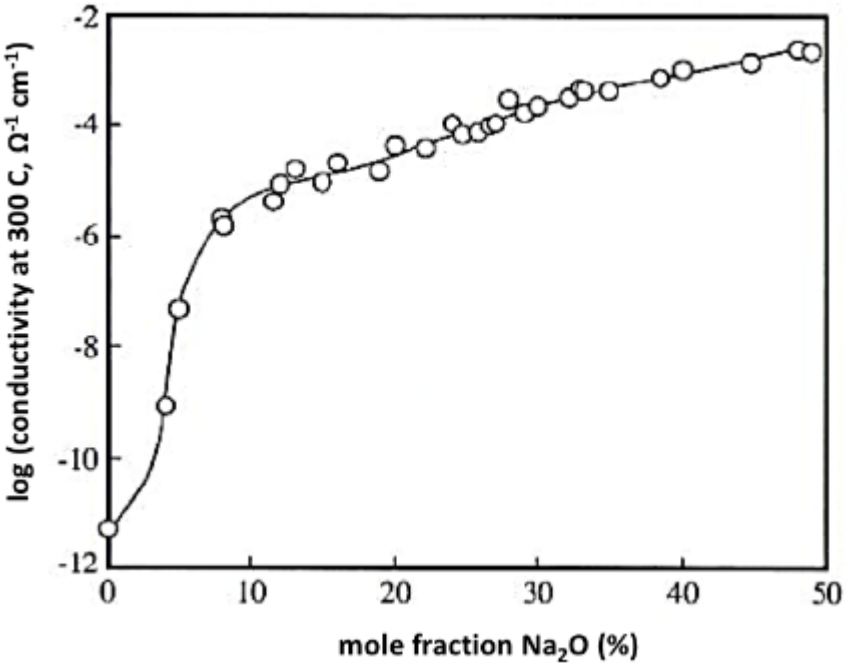

Figure 66: Ionic conductivity of sodium silicate glass at 300 C as a function of mole fraction of sodium oxide. J. Shelby, *Introduction to Glass Science and Technology*, 2nd edition, Royal Society of Chemistry (2005).

5. INTERIM SUMMARY

We have used the term "battery" to describe the proposed technology, whose purpose is to provide a practical means to store electrical power in a manner that is efficient, cheap, and highly scalable. Strictly speaking, the terms "battery", "fuel cell", and "flow battery" are intended to have distinct meanings, but in practice we often encounter the term "battery" as a broad and generic descriptor. To avoid any potential confusion, let us take this opportunity to summarize what is being proposed.

A good analogy can be drawn from longstanding proposals for a "hydrogen economy". In one instantiation, part of the hydrogen economy model entails storing electrical power generated by intermittent sources such as solar and wind in the form of hydrogen and oxygen; H_2 and O_2 are generated by electrolysis of water, put into storage, and then later "burned" in a fuel cell to generate electricity during a different portion of the diurnal cycle. In qualitative terms, such a "regenerative hydrogen fuel cell" approach is a sensible idea. But in quantitative terms the numbers do not work out. Referring back to Figure 7, the substantial irreversibility of the H_2/O_2 electrochemical cell (as manifested by high overvoltage) results in a roundtrip electrical storage efficiency of order 30%.[78] Moreover, the economics of storage for hydrogen and oxygen is very unfavorable because neither can be readily liquefied. Part of this problem can be circumvented by using air instead of oxygen in such a regenerative fuel cell. But dilution of oxygen to 21% interferes with fuel cell kinetics, and making such a regenerative fuel cell an open system renders it vulnerable to chemical contaminants present in the atmosphere.

Using $NaNO_2$ as the representative example, in the radical-ion battery, $NaNO_2$ takes the place of water, Na takes the place of hydrogen, NO_2 takes the place of oxygen, and our design intent can be summarized as follows:

1) Seek out electrochemical systems that feature high output voltage, so as the minimize I^2R losses.
2) Consider only chemical reagents that can easily and safely be stored in the condensed phase, in a failsafe manner.
3) Disqualify candidate electrochemical systems that require exotic electrode structures, and/or electrode structures that are sensitive to changes in micromorphology, vulnerable to chemical passivation, or capable of dendritic growth.
4) Keep operating temperatures low enough to avoid high thermal losses and enable the use of elastomeric seals.
5) Consider only earth-abundant raw materials for which the existing infrastructure of the chemical industry can meet scaling requirements in the immediate future.
6) Avoid the use of any chemical reagents having persistent toxicity.
7) Keep the chemistry as simple as possible to minimize the number of permutations for unwanted side reactions and other forms of chemical incompatibility.
8) Include a strategy for facile delivery of reactants to the electrochemical reaction zone, and facile removal of products (e.g. exploitation of NO_2 bubble buoyancy during charging).

9) Search for electrochemical systems that may permit the use of two-phase electrochemistry to circumvent the kinetic penalty of triple-phase boundary electrochemistry commonly encountered in fuel cells.
10) Use the stubborn problem of sluggish electrochemical reaction kinetics such as that encountered in the H_2/O_2 electrochemical system as a powerful down select tool for screening candidate electrochemical reactions/reagents.
11) Attempt to identify simple electron transfer reactions that involve no making or breaking of bonds, no substantial motion of nuclei, no requirement for multi-molecule transition state reaction complexes, and exploit the resulting low activation energy to obviate the need for catalysts such as platinum.
12) Exploit the anomalous properties of NO_2, which is one of just a few examples of molecules that form a stable free radical and a stable companion anion, and whose dimerization to N_2O_4 and relatively high intermolecular forces result in a surprisingly high boiling point.
13) Use an ion selective membrane to enforce the outcome of the energetic "combustion" reaction $Na + NO_2 \rightarrow NaNO_2$, which would not occur if Na and NO_2 were combined directly.
14) Attempt to identify a candidate electrochemical system having an energy density high enough to make it practical to replicate the "rolling pipeline" transmission model used in the coal industry.
15) Attempt to identify an electrochemical system that also has potential to address the needs of the transportation sector.

Ultimately, we found it worthwhile to prepare a list of frequently asked questions and misconceptions concerning the proposed battery chemistry. In the interest of clarity, we have this FAQ sheet in Figure 67.

Is the proposed technology some type of sodium-sulfur battery? No, the RIFB uses the half-reaction pair $Na - e^- \rightleftharpoons Na^+$ $NO_2^- \rightleftharpoons NO_2 + e^-$. It contains no sulfur and functions very differently than a sodium-sulfur (or Na-$NiCl_2$) battery. But the RIFB does exploit sodium-doped beta alumina ($Na\text{-}\beta\text{-}Al_2O_3$), an ionic conductor originally developed for sodium-sulfur batteries. This alumina barrier allows passage of sodium ions (but not electrons) under an applied electric field, while preventing molten Na from coming into contact with NO_2 and molten $NaNO_3$.

One of the active reagents is NO_2, so this system must involve storage of compressed gas, which is unattractive. This system does not use any compressed gas. NO_2, which has a boiling point of 21 C, is stored as a liquid in a steel tank at ambient pressure. Underground storage of the NO_2 tank may be used to ensure that its temperature is passively maintained below 21 C.

Why didn't you collaborate with traditional subject matter experts (e.g. career electrochemists) during invention of RIFB technology? We were explicitly told by our DOE program manager to avoid consulting with traditional subject matter experts. The SunShot Innovator in Residence (SSIR) program entails the intentional use of "outsiders" in an effort to come up with outside-the-box ideas.

Has RIFB technology been peer reviewed by traditional subject matter experts? Yes. Our DOE sponsor did recently subject this work to an independent third party peer review by an expert in electrochemistry and battery design. The reviewer verified the novelty of RIFB technology and was unable to identify any show stoppers in the proposed device architecture. A complete record of written reviewer/reviewee correspondence is available upon request.

I'm still skeptical. We have been unable to identify any showstoppers to date. But if you can, we would be grateful for any such insights.

Do you have data from a laboratory prototype device? Yes, and we are observing excellent agreement between experiment and theory. At present we are focusing on detailed kinetic studies that will inform the design of version 2 cell.

This is extremely exciting work and the potential implications are very far reaching. How much funding does the team have to work on it? We only have the 1.0 FTE/year of funding associated with the SSIR program. We need a significant increase in funding to execute the list of tasks required for technology maturation. We are now attempting to alert relevant points of contact at DOE that a technical breakthrough has occurred and more funding is urgently needed.

Storing large quantities of molten Na and liquid NO_2 must be dangerous. Molten Na and liquid NO_2 are important precursors for industrial chemical synthesis. Both materials are routinely shipped by the train load in steel tanker cars (DOT 105J300W and DOT 105A500W, respectively). In the Radical Ion Flow Battery, molten Na and liquid NO_2 are stored in separately located, unpressurized, steel vessels.

It's hard to believe that at an operating temperature of 280 C the amount of heat lost to ambient is negligible. To be more specific, it's negligible compared to internal ohmic heating (even for the case of a hypothetical 99%-efficient battery). It is also very counterintuitive how slowly large objects cool due to the L^2 dependence described in slide 5. For example, the steel reinforced concrete of the Hoover Dam contains a massive network of cooling pipes, because otherwise it was estimated that the concrete would have taken 125 years to cool once poured (despite the fact that concrete is a relatively poor thermal insulator).

This is a flow battery, so presumably the active medium ($NaNO_2$) must be dissolved in water or some other solvent. No, there are no solvents or other diluents. The flow battery's active medium is pure molten $NaNO_2$, which has a melting point of 271 C. Molten $NaNO_2$ also serves as the electrolyte and has extremely high ionic conductivity (κ ~ 1.40 Ω^{-1} cm^{-1}). The lack of diluents and the very high volumetric energy density of dissociated $NaNO_2$ (1.95 kW-hr $liter^{-1}$) minimizes the size of the electrochemical cell and storage tanks, thereby minimizing the cost of construction materials.

It looks like 304 stainless steel is the most expensive material used to construct this device. Are you going to need a lot of it? What portion of the system requires the use of 304 stainless steel, rather than mild steel? 304 stainless steel, commonly used for kitchen utensils, is not a particularly expensive engineering material. In the RIFB, only the electrochemical cell portion of the flow battery, which is relatively small in size, uses 304 stainless steel. We will eventually investigate whether an incremental cost reduction can be realized by using mild steel for the electrochemical cell as well.

Hermetic seals have been a big problem for sodium-sulfur batteries. Have you addressed the issue of seals? Yes. The seal technology we use can't stand up to the highly corrosive sodium polysulfides used sodium-sulfur batteries either. But it is unaffected by exposure to molten Na, molten $NaNO_3$, and NO_2.

The only chemical ingredient that must be supplied to the RIFB is $NaNO_3$. But the synthesis of sodium nitrite from sodium chloride and air generates chlorine. Is this a problem? No, chlorine is among the top ten chemicals produced worldwide and typically sells for $200 per metric ton. Even if RIFB were implemented worldwide by 2030 under a 100% renewables scenario, it would not perturb the existing Cl_2 supply chain significantly.

Lithium ion batteries are starting to be used in some grid storage applications. How can RIFB technology compete? RIFB technology covers a different grid storage application space that requires massively scalable electrochemical storage at extremely low per-unit cost. This class of grid storage battery also needs to withstand ~10,000 charge/discharge cycles without capacity fade; Li-ion batteries cannot meet this requirement. The relative scarcity of cobalt is also an impediment to manufacturing very large Li-ion batteries in very large volume.

Figure 67: Questions and misconceptions encountered in early discussions of RIFB technology.

5.1. The version 1 RIFB cell

Next, we explored risk reduction of the proposed radical-ion battery. The first data set recorded for the version 1 (v1) electrochemical cell is shown in Figure 68. Details of apparatus construction is documented in Figures 69 – 73. While this v1 prototype cell is not particularly well suited for quantitative chemical kinetic studies, such an electrochemical kinetic test bed is currently under construction in Sandia, NM and will be utilized in future work. Having said that, the v1 cell demonstrated both the open circuit cell potential, and low internal cell resistance (30 mΩ) predicted for the proposed battery, as intended. The most important return on investment for construction of the v1 was moving up the learning curve of RIFB implementation. For example, construction of the v1 cell required all issues associated with materials compatibility to be carefully examined and resolved. Some of the most important findings are as follows:

1) There are no polymeric or elastomeric materials that can be used for hermetic seals that can withstand both the thermal and chemical environment internal to the RIFB cell. At an operating temperature of ~300 °C, molten sodium nitrite is a powerful oxidizer, as is nitrogen dioxide. Moreover, molten sodium is an extremely powerful reducing agent, rendering incompatible what are normally considered chemically inert perfluoropolymers. The inability to employ mechanically compliant gasket/seal materials presents a major challenge.

2) Some of the required seals must also be neither electronically nor ionically conductive. This rules out all metals and many glass compositions.

3) In the absence of mechanical compliance, whatever rigid material is used for seals and joints must be closely compatible with its adjoining materials from the standpoint of thermal coefficient of expansion.

4) Ingress of moisture over an extended period of time is expected to lead to corrosion via formation of nitric acid. Whatever seal material is chosen must have an H_2O permeation rate that for all intents and purposes is zero. A seal/substrate material interaction that relies on Van der Waals forces as opposed to true chemical bonding to create such a long-service-life hermetic seal is a potential liability.

5) The only class of material that was found to be compatible with all of the above requirements are certain classes of vitreous enamel coatings. Referring now to Figure 74, such vitreous enamel coatings typically comprise a mixture of sodium-aluminosilicate glass and an insoluble matrix of finely powdered fused silica. As discussed later, the addition of 0.5% cobalt (II) oxide ensures the formation of oxygen bridging bonds between the vitreous phase and steel during firing. Figure 75 shows a 304 stainless steel coupon coated with A. O. Smith's composition VS-206 enamel, and a pair of 304 stainless steel flanges bonded together using the same vitreous enamel composition. A mixture of 42 parts water to 100 parts powdered enamel by mass was used to prepare the enamel slip. The resulting suspension is highly thixotropic, but when agitated thoroughly has a viscosity comparable to pancake syrup. Surface preparation of the 304 steel parts comprised grit blasting with 80-grit alumina, followed by solvent cleaning to remove any hydrocarbon residue. After drying at 80 °C, the enamel coatings were fired at 860 °C in air. Referring to Figures 75 and 76, it is easy to underappreciate the remarkable properties of enamel coated steel, perhaps because it's an old technology that we encounter in our everyday lives.

6) 304 stainless steel did not exhibit problems with corrosion during extensive operation of the v1 cell. The TIG welded 304 stainless steel joints used in the v1 cell also did not experience any corrosion.

7) Any laboratory apparatus constructed for the purpose of conducting analytical measurement or proof-of-concept testing that is subject to exposure to $NaNO_2$ and NO_2 at temperatures of ~300 °C may be constructed from conventional borosilicate glassware, and can employ 304 stainless steel for plumbing and porous electrodes. The only material that was found to be satisfactory for sealing of tapered ground glass joints for these operating conditions was Krytox XHT-BDX perfluorinated grease. Early attempts to use other seal materials was time consuming, and in some instances exhibited far worse compatibility with NO_2 than claimed by the manufacturer.

8) Attempts to use peristaltic pumps for circulation of NO_2 were unsuccessful. Even for room temperature operation, there was no tubing material available having both the

elastomeric properties required for a peristaltic pump and the requisite chemical resistance to stand up to NO_2. Ultimately, we were able to find a mechanical diaphragm pump whose only wetted surfaces comprised Teflon and stainless steel (Cole-Parmer model L-79200-30).

9) For handling of NO_2 gas, laboratory glassware employing PTFE stopcocks proved reliable subject to the obvious temperature limitations of PTFE. For long runs of flexible tubing, PTFE tubing was found to be the most satisfactory material for flexible NO_2 plumbing. Referring to Figure 77, it is also possible to form a reliable hermetic seal between a borosilicate glassware hose barb and slightly undersized thick-walled PTFE tubing (e.g. 3/8" OD, ¼" ID) by preheating both the tubing and the hose barb and forcing the tubing over the hose barb. Refractive index matching at the PTFE/glass interface makes it possible to inspect wetting of the two surfaces by eye under suitable illumination. Mechanical creep of the PTFE material under the resulting tensile loading, leading to loosening of the joint, was not observed over many months of service.

10) As expected, there were no chemical compatibility problems encountered between the sodium-beta-alumina separator (Ionotec, part number B2-220-LNZ) used in the v1 device and $NaNO_2$ + NO_2 at ~300 °C.

11) Joining of porous sintered stainless steel components to surrounding stainless steel fixtures is not easily carried out by welding or brazing. Press fitting can be used in applications where small leaks at the edges of the sintered stainless steel part can be tolerated. This was the case of the 2-inch-diameter, 2-micron-pore-size sintered stainless steel disc used for the sparger in the NO_2 electrode of the v1 cell. The best practice is conduct the stainless steel sintering operation with the surrounding stainless component (e.g flange) present to ensure proper fusing at the interface.

12) NO_2 is available as a liquid in steel gas cylinders but requires in situ purification prior to use. The main impurity is nitric acid resulting from the presence of H_2O. Drying of NO_2 gas with P_2O_5 desiccant is very effective, and this system can be plumbed to allow regeneration of the P_2O_5 desiccant by baking out under vacuum. A series of freeze-pump-thaw cycles is then used to remove the other major impurity, nitric oxide. Once purified and confined to laboratory glassware having wetted surfaces of only borosilicate glass, stainless steel, PTFE (tubing, stopcocks), and Krytox XHT-BDX perfluorinated grease, no degradation of the purified NO_2 sample was observed over time. It should be understood, however, that an actual RIFB would be commissioned in the field starting with only $NaNO_2$; Na and NO_2 are generated in situ during the charging process.

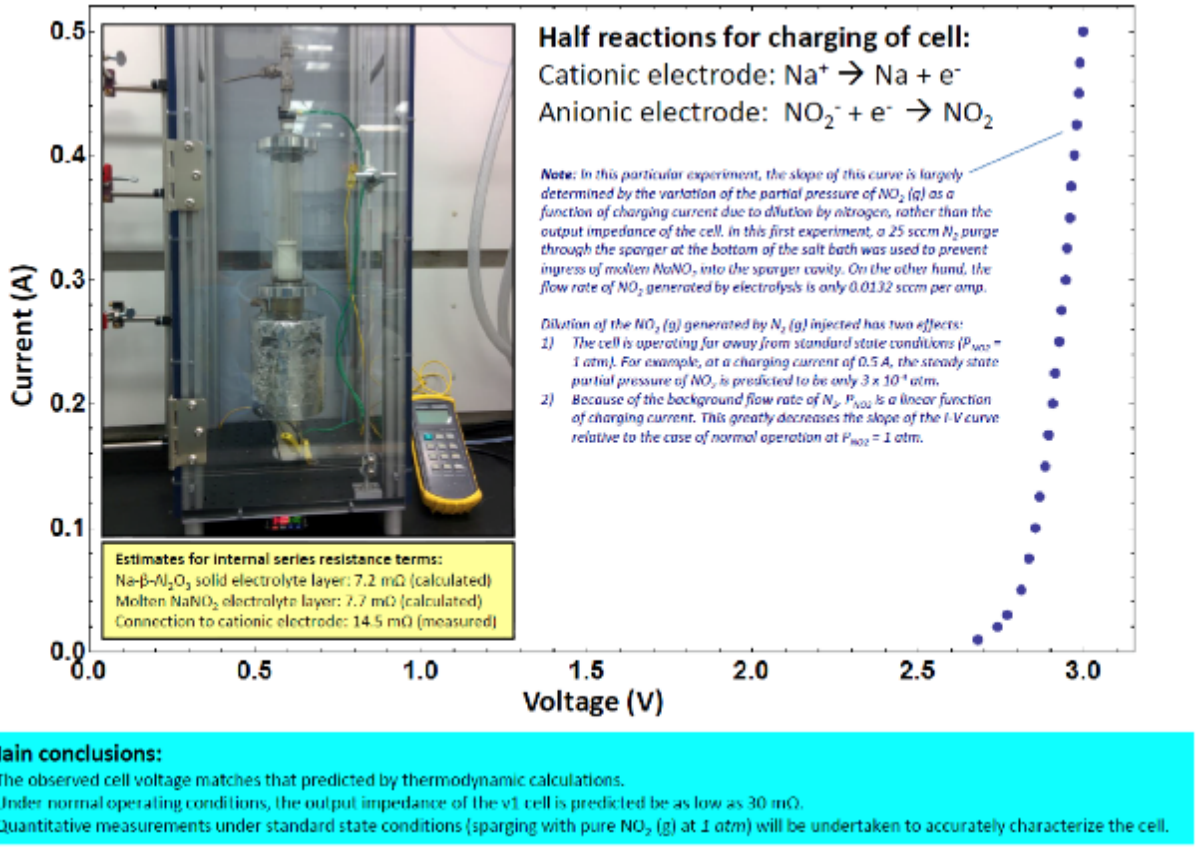

Figure 68: First laboratory data recently recorded with v1 cell. The I/V curve shows excellent agreement with theory.

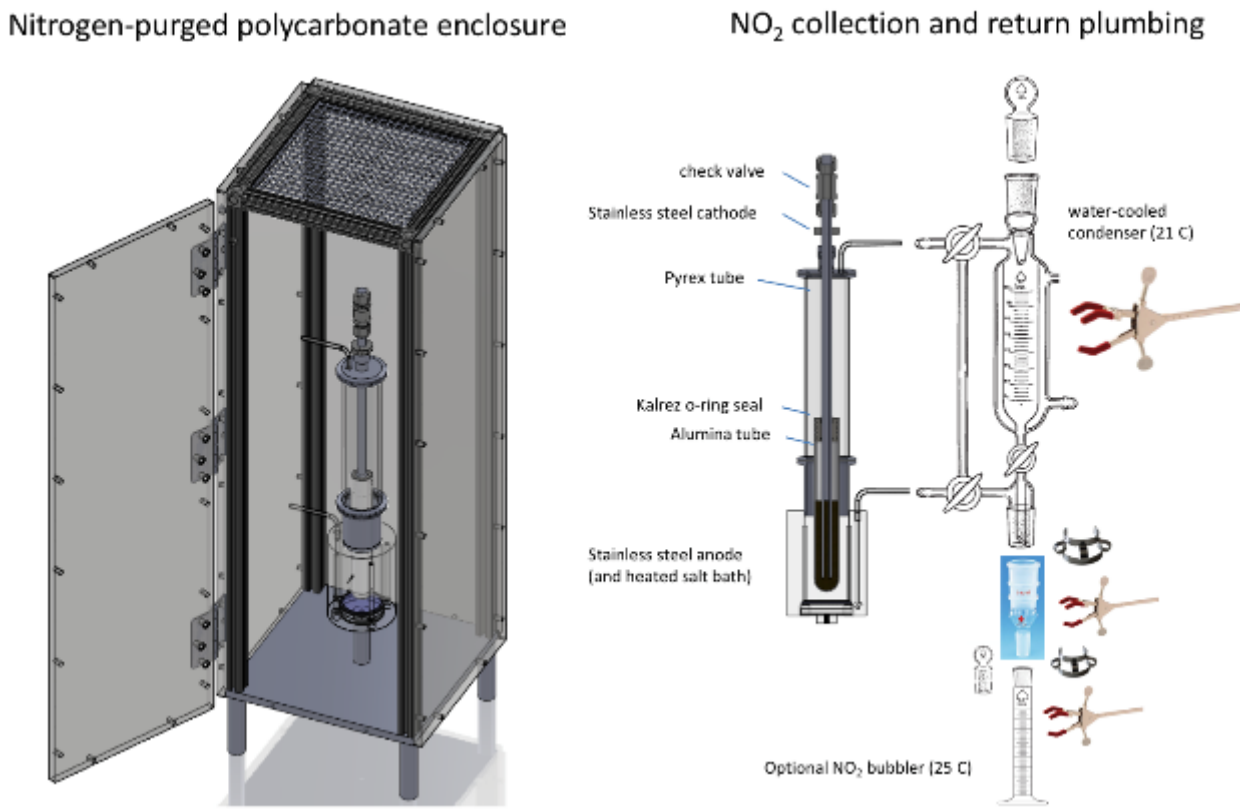

Figure 69: Additional detail concerning the construction of the v1 cell apparatus.

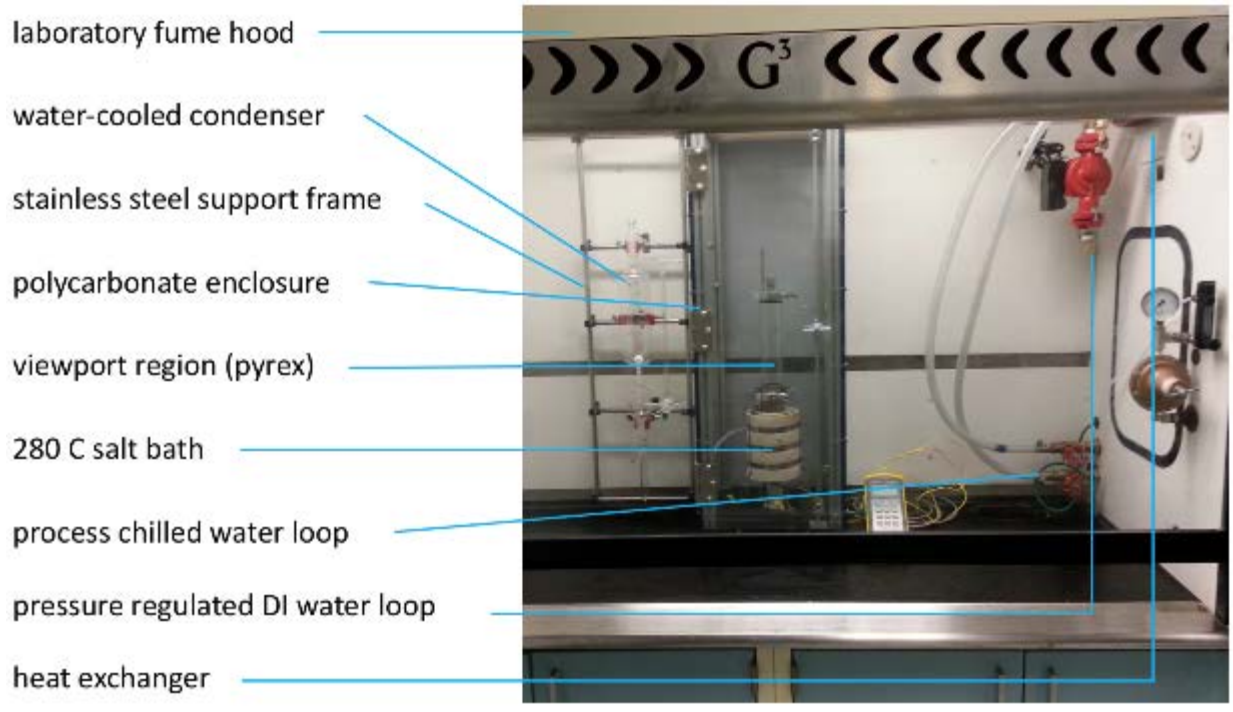

Figure 70: Additional detail concerning the construction of the v1 cell apparatus.

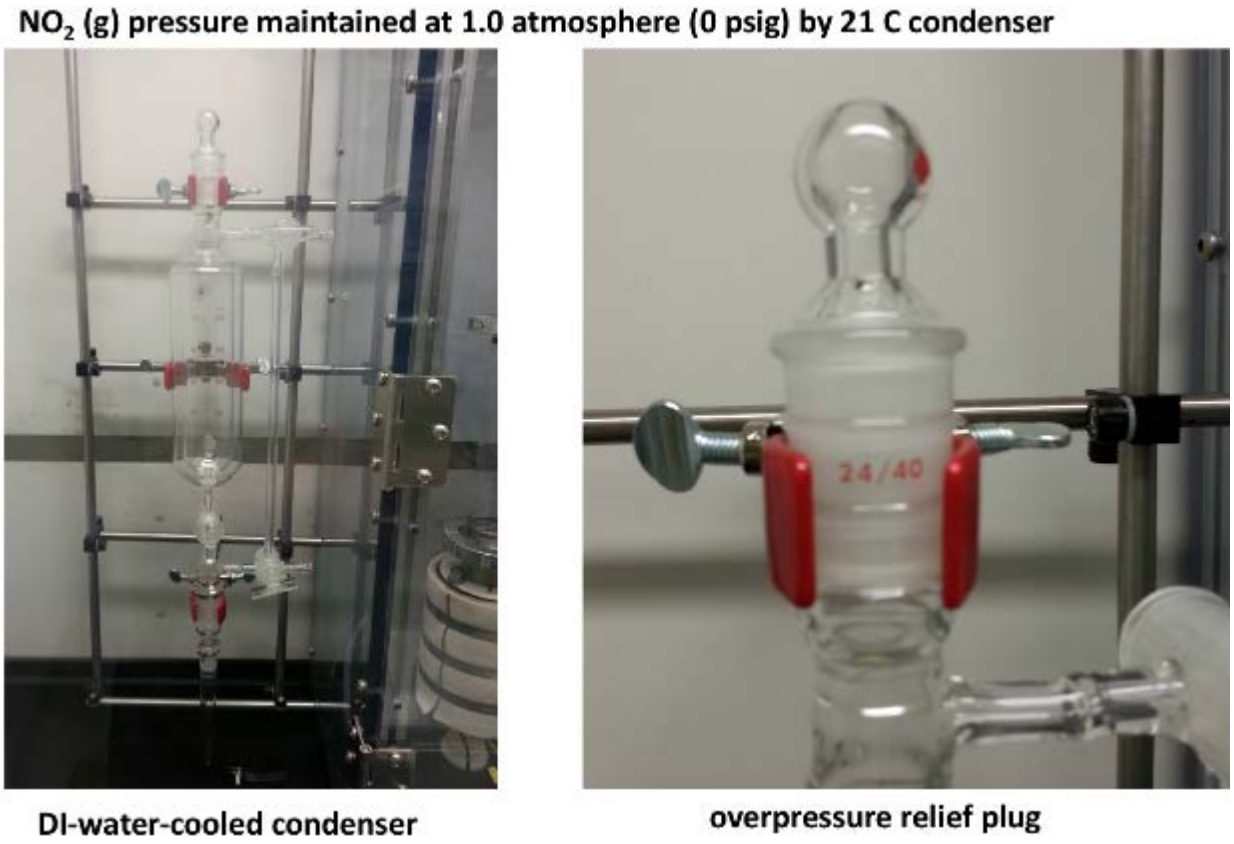

Figure 71: Additional detail concerning the construction of the v1 cell apparatus.

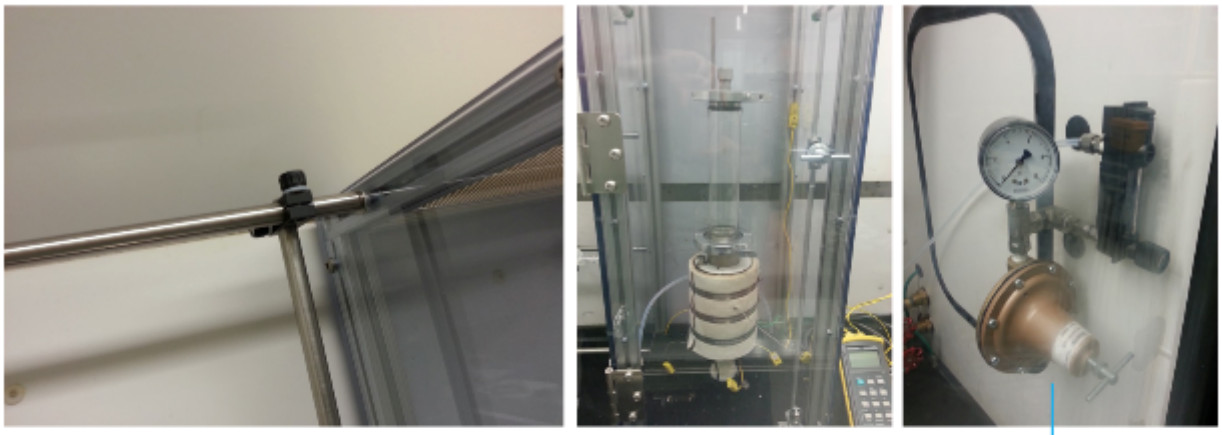

Construction protocol:
1”-square extruded aluminum 80/20 structural framing
½-thick laser cut polycarbonate panels
½” diameter 316 stainless steel solid rod frame work
Right-angle post connectors based on yoke rather than screw engagement
¼-20 threaded fasteners
Plumbing components: Kwik-flange, Ultratorr, and Swagelok
EPDM rubber tubing (for chemical compatibility with NO_2)
monolithic 304 stainless steel salt bath
4 x 100 W cartridge heaters
Digital PID temperature controller
Actively N_2 purged polycarbonate enclosure
Nomex aramid fiber thermal insulation (rated to 315 C)

Figure 72: Additional detail concerning the construction of the v1 cell apparatus.

Heat exchanger used to isolate condenser from process chilled process water loop
3-way valves allow connection to constant temperature bath or chilled process water.
DI-water loop uses centrifugal pump incapable of exceeding 10 psig pressure*
* maximum operating pressure of 15 psig recommended by Ace glassware includes large safety factor.

Figure 73: Additional detail concerning the construction of the v1 cell apparatus.

Dirt cheap, refractory, mechanically shock resistant, chemically resistant, excellent adhesion

Figure 74: Glass enamel coated steel is a remarkable technology.

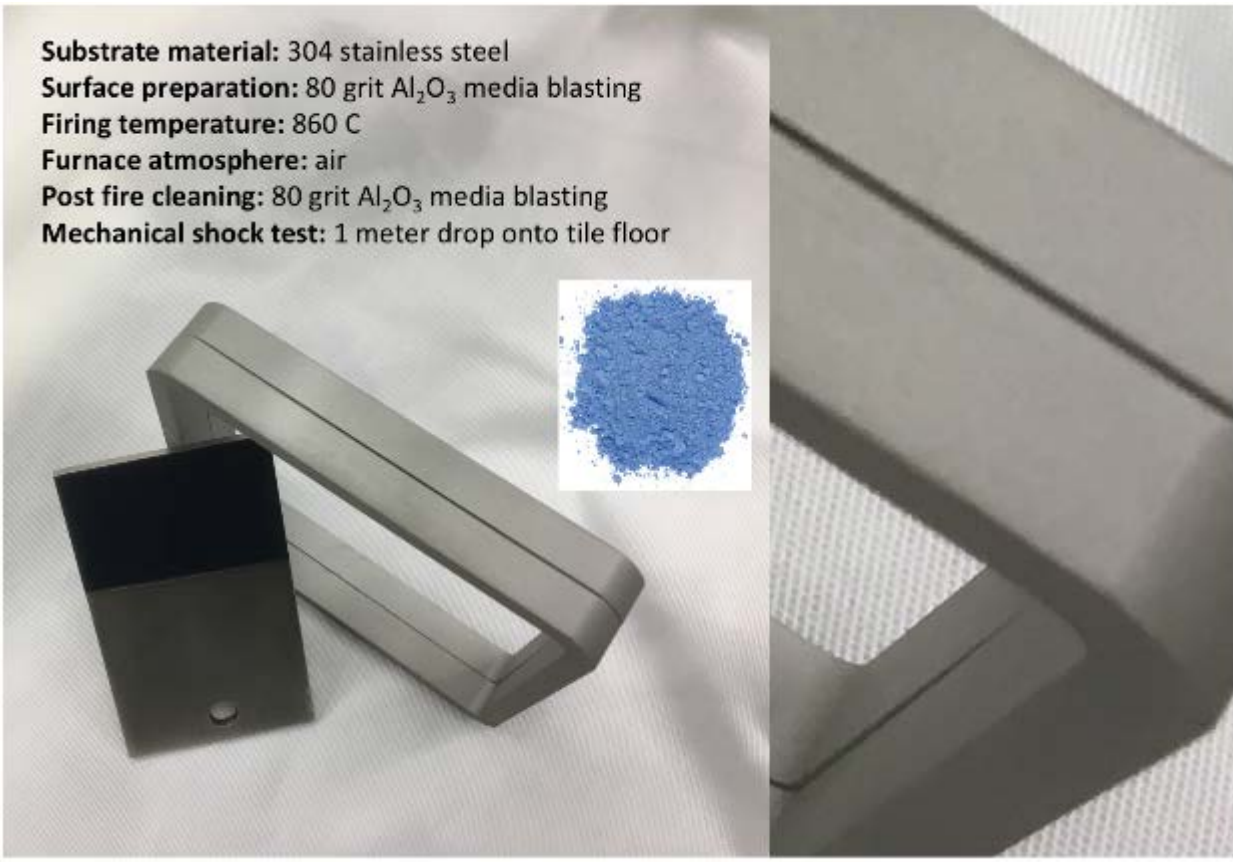

Figure 75: Porcelain enamel frit. Dip coated 304 SS coupon & hermetically joined 10-cm-diameter 304 SS flanges.

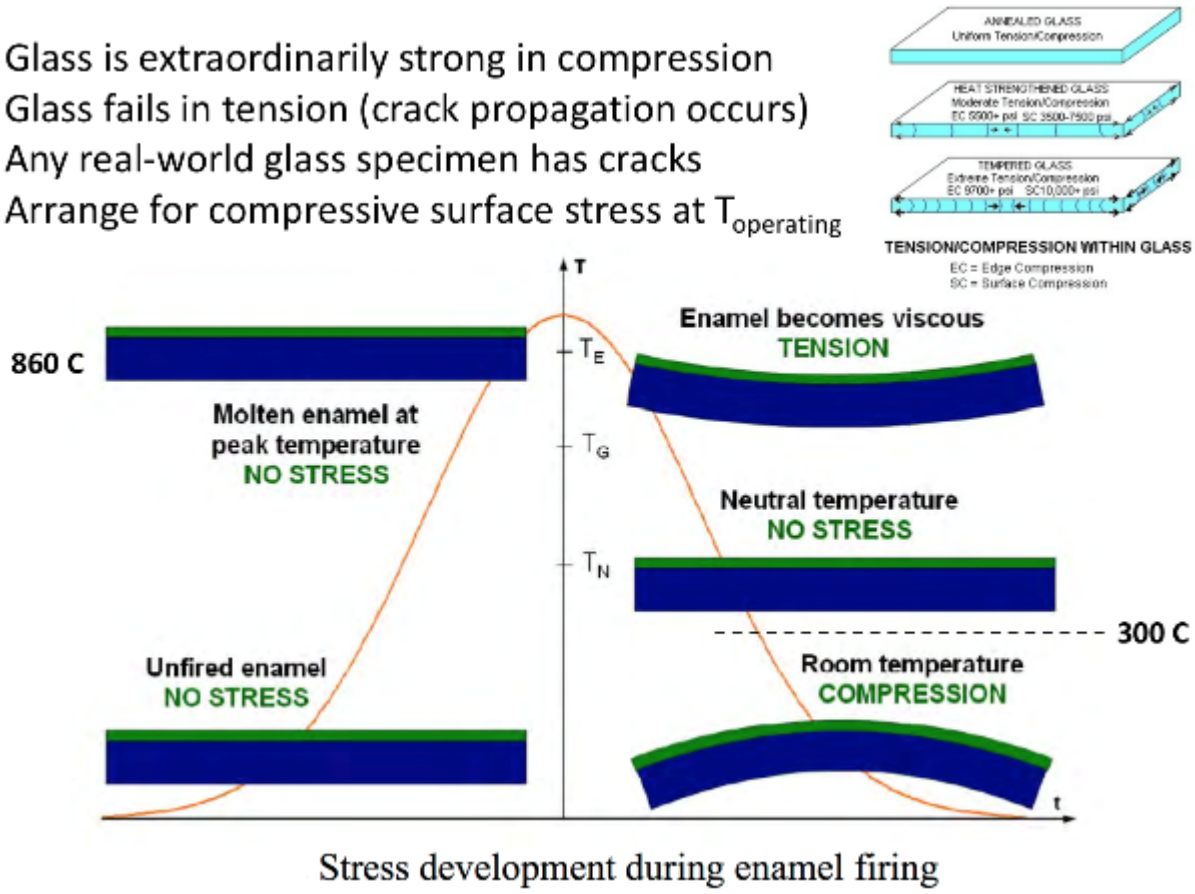

Figure 76: The extreme durability of glass enamel coated steel is attributable to the same thermo-elastic stress phenomenon exploited in tempered glass.

Figure 77: A reliable hermetic seal between a borosilicate glassware hose barb and slightly undersized thick-walled PTFE tubing (e.g. 3/8" OD, ¼" ID) suitable for NO_2 service can be formed by preheating both the tubing and the hose barb and forcing the tubing over the hose barb.

The work conducted on the v1 device prompted a great deal of discussion about how a production device might be designed and manufactured at low cost. Figure 78 shows a modular planar stack design based on a Na-β-Al_2O_3 separator, and vitreous glass ceramic seals. The v1 device attempted to use a Kalrez fluoropolymer o-ring located at a remote location that never exceeded ~200 °C. This proved to be unworkable. NO_2 bubbles generated at the anionic electrode would burst upon floating up to the surface of the molten $NaNO_2$ electrolyte, lofting fine droplets of molten $NaNO_2$ upward, carried by the flow of NO_2 gas. These droplets would then condense in the cooler region adjacent to the Kalrez o-ring. Eventually most of the $NaNO_2$ would be extracted from the electrochemically active region of the cell and deposited in the form of a solid mass. Operation of the v1 device made it clear that all regions of a v2 cell must operate above the melting point of $NaNO_2$ so as to allow droplets of $NaNO_2$ entrained in the NO_2 flow to drain back into the electrolyte reservoir as a liquid.

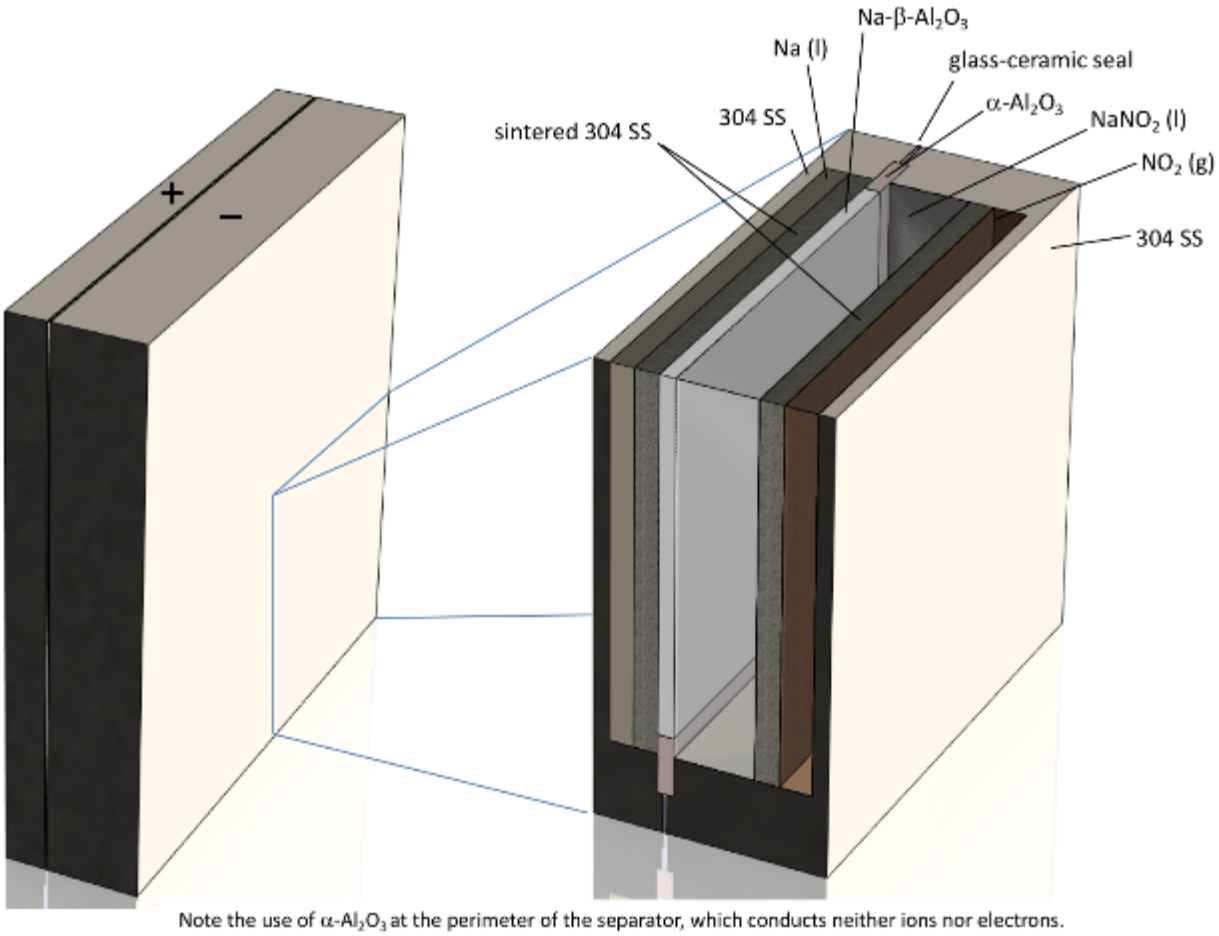

Figure 78: Planar-stack version of RIFB electrochemical cell.

5.2. Cell stacking considerations and the rethinking of sodium electrode design

The question of how successive cells should be stacked in series is also an important one. One school of thought is that each individual cell should be fabricated in manner like the cell shown in Figure 78, wherein each cell is a hermetically sealed unit, with no hermetic seals shared between adjacent stacked cells. Rather, each cell would simply comprise a two-piece rectangular enclosure, with the pieces joined together by a vitreous ceramic seal. Adjacent cells would then be placed front-to-back in ohmic contact, perhaps soldered together or wetted with molten solder to minimize electrical contact resistance. Such a scheme has the advantage that quality control of hermetic seals during manufacturing would be confined to individual cells, rather than spanning a large number of adjacent cells. Alternatively, as shown in Figure 79, adjoining cells could be laser seam welded together, sharing a common stainless steel partition that is wetted on one side with molten sodium and the other side with NO_2 gas. Electrically conductive “gas manifold pillars” would allow ample clearance for gas flow but provide a short electrical path between the shared partition and the sintered stainless steel electrode structure. Because the electrical conductivity of stainless steel is relatively low, minimization of the conduction path length must be given due consideration.

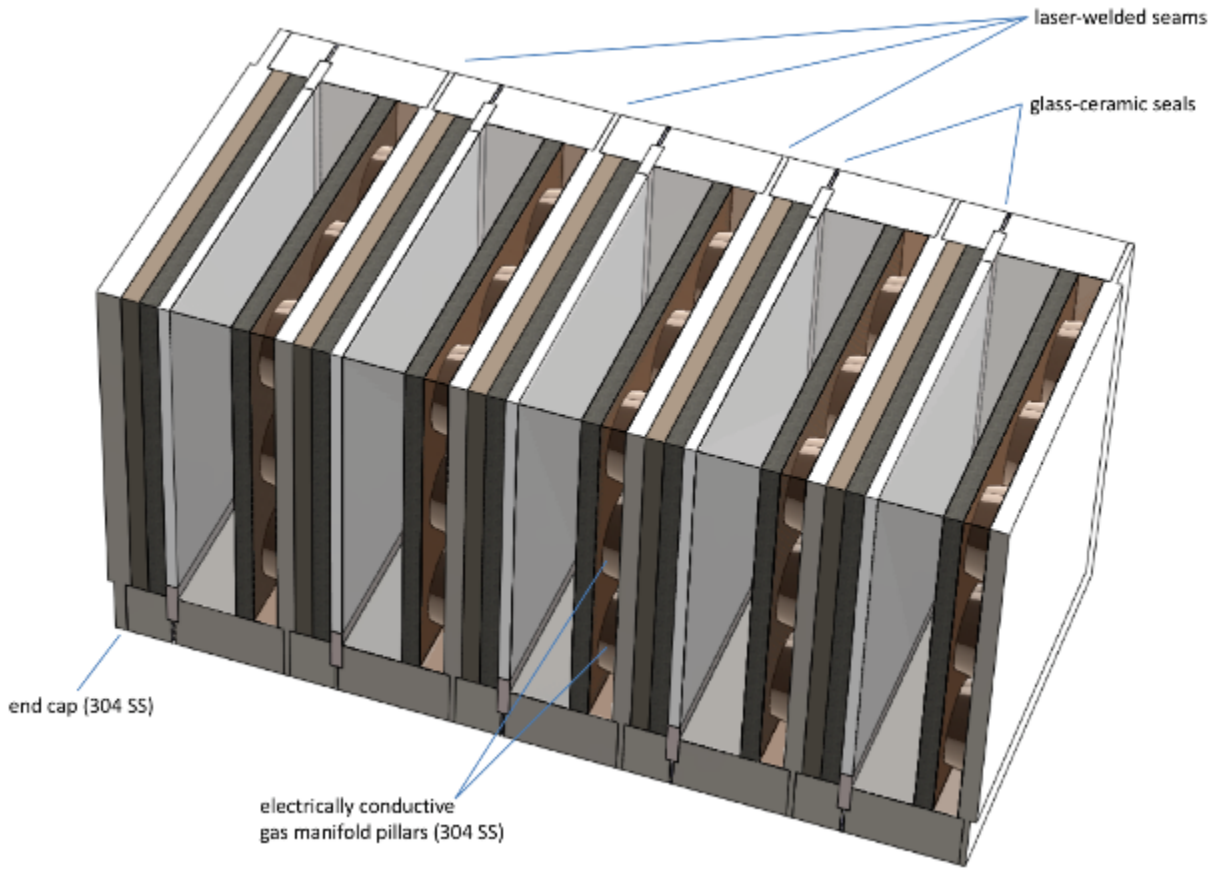

Figure 79: One example of a proposed planar stack assembly scheme.

Figure 80 depicts how such a system might be assembled from low-cost sub-components. For example, the vitreous ceramic seal might best be placed as a solid preform that is subsequently laser welded, and for components containing sintered stainless steel, the sintering process would be carried out inside a surrounding stainless steel frame prior to assembly; as mentioned above, welding, brazing, or press fitting sintered stain steel parts subsequent to their manufacture is fraught with difficulty. Both the “end cap” and “end cap with electrically conductive manifold pillars” would be low-cost forged stainless steel parts. The α/β-alumina plate is intended to function as a conventional sodium-beta-alumina Na^+ ion conducting separator, surrounded by an undoped α-alumina frame that is CTE-matched to the β-alumina structure, but non-conductive with respect to both electrons and ions. The second framed sintered insert was contemplated as a structural support for the α/β-alumina panel, which as we explain below, led to a rethinking of the entire electrode structure. This is an excellent example of a derisking activity. What good is an extremely facile NO_2/NO_2^- half-reaction if the sodium electrode on the opposite side of the electrochemical cell remains a major liability?

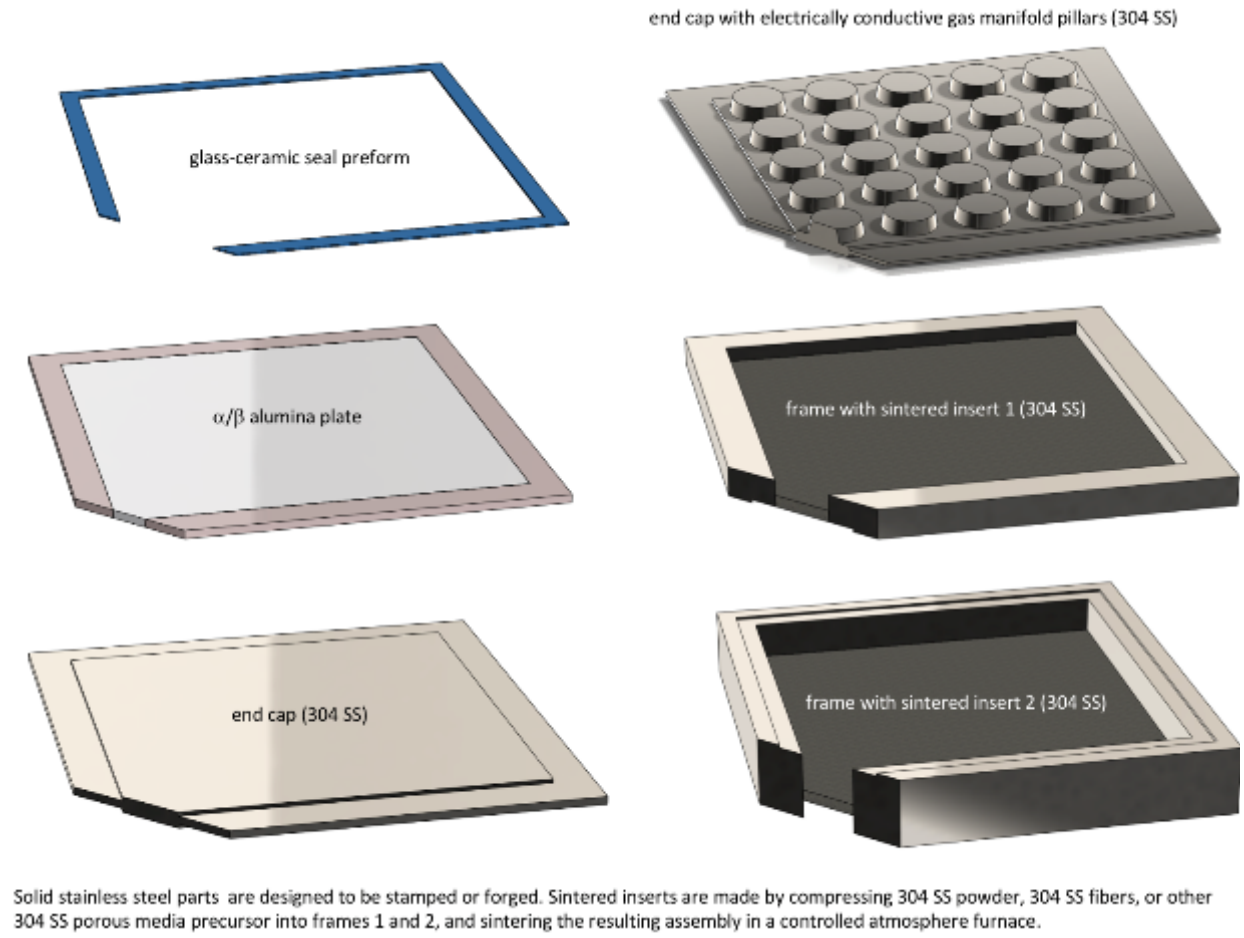

Figure 80: Mass-produced stack components.

The notion of depositing the ceramic separator on a sintered metal substrate is very attractive, because we would like to make the ceramic separator as thin as possible to minimize ohmic losses, but we also don't want it to be mechanically delicate. Needless to say, the separator cannot be allowed to catastrophically fail, thereby allowing molten sodium and molten sodium nitrite to mix together. The separator must be designed as a composite structure that can't mechanically fail, but at worst, develop a hairline fracture across the ceramic separator that would scab over with a seam of chemically inert Na_2O. But attempts to design and test such a composite structure met with a fundamental problem. If the substrate material is a metal or other material that conducts electrons, consider what will happen if it is bonded directly to the sodium-ion-conducting separator material. This creates a situation in which Na^+ ions and electrons can unite at the interface during the battery charging cycle, thereby generating an "embolism" of molten sodium metal that acts to pry the two surfaces apart. This is in fact what was observed in lab: spallation of the sodium-ion-conductive coating from the metallic substrate upon the application of current. For this reason, it is not viable to simply apply an ionically conductive coating over a hollow, porous, sintered metal electrode such as that shown in Figure 81.

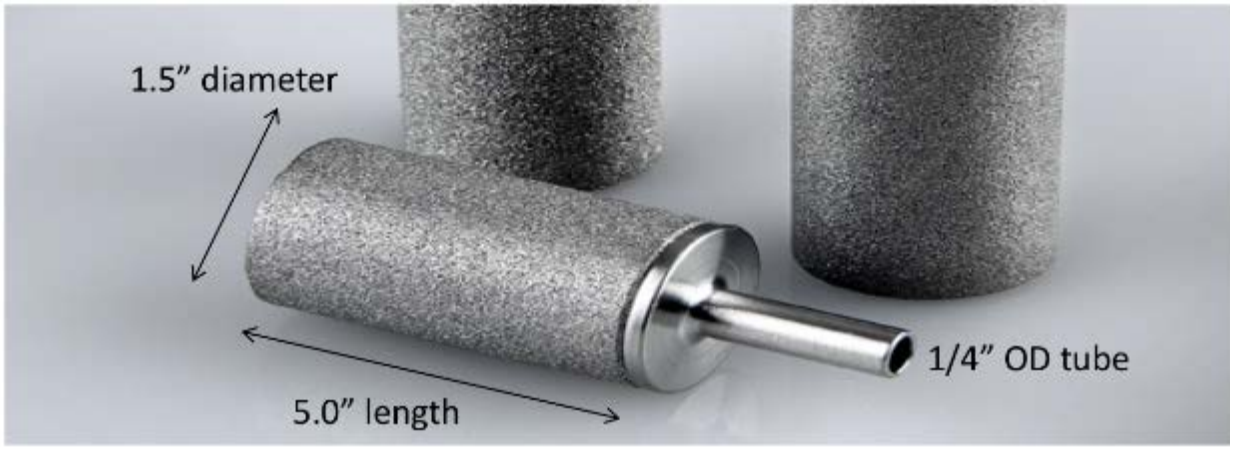

Figure 81: Commercially available sintered stainless steel sparger.

This "sodium embolism" problem, along with need to employ a benign-failure-mode sodium electrode in a practical cell compelled us to initiate a study in Year 2 to explore an alternative Na electrode structure. As shown in Figure 82, the objective of devising such structure is complicated by numerous engineering and materials compatibility requirements (such as the presence of a high-current metallic electrical feedthrough) *all of which must be met simultaneously*. Moreover, any proposed design must be fully compatible with low-cost, high-volume manufacturing.

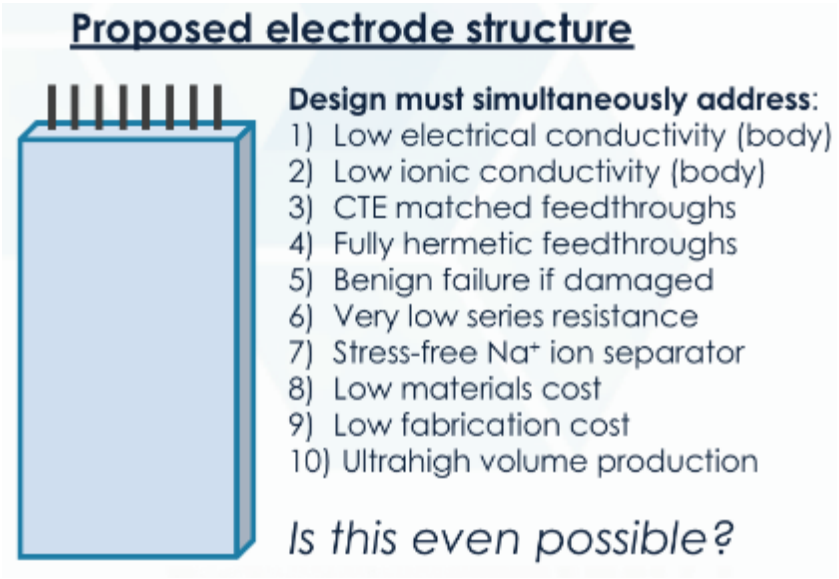

Figure 82: Rough schematic diagram of proposed sodium electrode structure.

Let us take a moment to review, to ensure that we fully understand all of the problem-solving constraints we are working under. As discussed above, in principle, the most rudimentary architecture for a sodium electrode is a closed envelope of super ionically conducting material containing molten sodium metal, immersed in a surrounding electrolyte, equipped with some

form of hermetically sealed electrical feedthrough that does not make galvanic contact with the liquid electrolyte. Note that in contrast to the planar-stack cells depicted in Figures 78 and 79, such an isolated, closed-envelop sodium electrode would make it possible to construct a series RIFB stack in a manner analogous to a lead acid battery. Referring to Figure 83, such a series cell could comprise a common housing divided into individual cells by electrically insulating partitions, wherein each cell has a sodium electrode and an NO_2 electrode, both immersed in a local reservoir of $NaNO_2$ electrolyte. Electrical connections between successive cells would be made through metallic bus bars (e.g. stainless-steel-clad copper) located above the electrically insulating partitions. The head space would constitute a common manifold for NO_2 gas evolved. This architecture eliminates the need to make inter-cellular hermetic seals. It also eliminates thermomechanical stresses that might otherwise cause problems in a rigidly connected stack. Moreover, it provides a simple solution to the challenge of making high-current electrical interconnects between neighboring cells. Finally, from the standpoint of quality control, we would like to have the fabrication of vitreous hermetic seals be conducted on the assembly line under tight process control, in manner similar to the mass production of spark plugs in the automotive industry. Individual parts that do not pass QC can be discarded, rather than having to discard the entire cell. This is an important consideration, because the optimum number of cells per module at which production cost is minimized may turn out to be a fairly high number.

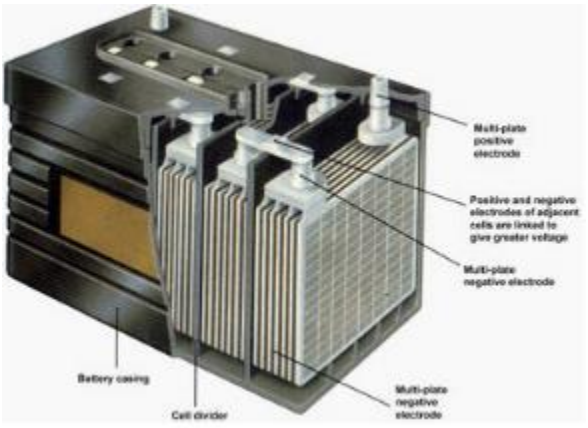

Figure 83: Series cell stacking scheme used in lead acid batteries.
https://www.edgefx.in/wp-content/uploads/2014/07/21.jpg

Returning to the problem at hand, the super-ionically conducting membrane must readily transmit sodium ions but block transmission of electrons. Even a small electron leakage current is prohibitive, because it would allow electrochemical reduction of Na^+ to Na on the electrolyte side of the separator, followed by irreversible reaction of Na + $NaNO_2$. Unfortunately, many materials that are excellent electronic insulators at room temperature become somewhat conductive at elevated temperature (~300 °C), thereby making them unsuitable for this application.

Referring now to Figure 84, the electrical feedthrough must block conduction of sodium ions but allow facile transmission of electrons. During charging, sodium ions migrate from the electrolyte into the electrode where they unite with an electron to form sodium metal. During discharging, sodium metal atoms are split into sodium ions and electrons that travel to the electrolyte and

electrical feedthrough, respectively. The electrical feedthrough establishes galvanic contact via immersion in sodium metal.

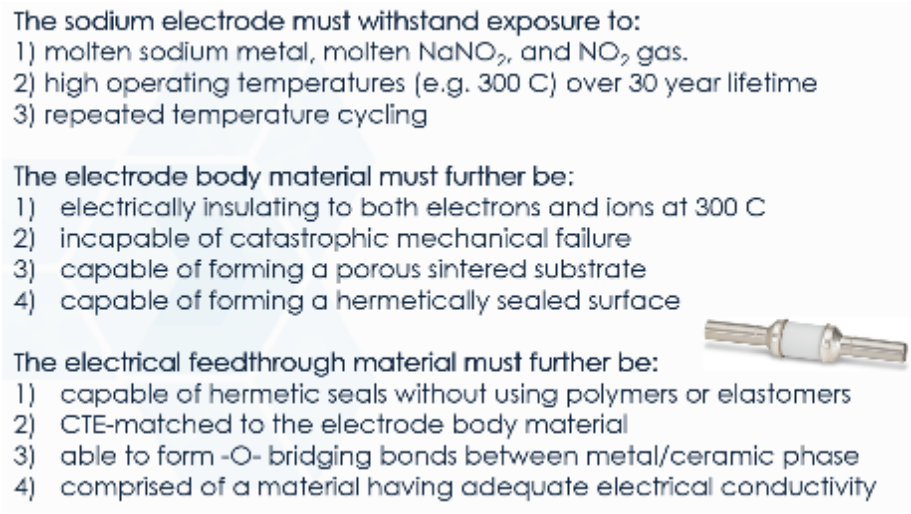

Figure 84: Down-select of the electrode body and feedthrough material.

The desire to keep ohmic losses to a minimum implies that the thickness of the super-ionically conductive separator must be minimized. But this is counterproductive from the standpoint of rugged electrode design, and suggests the use of a thin (a few hundred microns) layer of super-ionic separator material supported by a rigid substrate. This substrate material must in turn meet several requirements. First, the substrate must comprise a mechanically strong/tough structure that is inexpensive and easy to fabricate. Second, the substrate material must not allow conduction of electrons under an applied electric field. For example, while sintered stainless steel is a potentially attractive electrode substrate material, conduction of electrons would allow formation of sodium metal at the substrate/separator interface. Formation of molten sodium at the interface between these two rigid materials would result in a “sodium embolism” that causes spalling of the electrode coating. Third, the substrate material must be porous to allow passage of molten sodium to and from the super-ionically conductive coating. Fourth, the substrate material must not present any problems from the standpoint of CTE mismatch with respect to the adjacent incompressible materials; thermo-elastic stress is significant challenge whenever brittle materials are used over a wide range of temperature (in this case, room temperature to ~300 °C). Delamination and outright structural failure is inevitable if CTE engineering of interfaces is not managed very carefully. Moreover, while fabrication of a composite structure comprising two CTE-matched materials drastically narrows materials selection, maintaining CTE compatibility between three or more different materials increases such constraints exponentially.

Keeping all the above considerations in mind, we must also select a super-ionically conductive coating material that can readily be deposited on a substrate in a simple, high-throughput manufacturing process. This makes materials that are electrically anisotropic, such as Na β-Al_2O_3, extremely problematic. While this is suggestive of using NASICON, applying a uniform layer of NASICON to the substrate (e.g. by sintering at 1150 to 1300 °C)[79] is not an easy process to carry out, and further implies that thermo-elastic stress would have to managed over a much wider temperature range (during cooling from ~1200 °C to room temperature).

Figure 85 is provided for readers unfamiliar with the phenomenon of ionic conductivity. A good ionic conductor is a material that conducts one or more selected ions under the influence of an applied electric field with minimal ohmic resistance, but blocks conduction of electrons. A wide variety of pure materials are known to exhibit ionic conductivity at sufficiently high temperature, and in principle any condensed phase material lacking conduction band electrons and having one or more mobile ionic species can exhibit the effect. Figure 85 shows a photo of an incandescent lightbulb whose inner surface is coated with droplets of sodium metal. The glass portion of the incandescent bulb was immersed in molten sodium nitrate at 400 °C, contained in a heated stainless steel crucible. The stainless steel crucible was positively biased with respect to the power supply used to illuminate the bulb's tungsten filament, from which electrons were sourced by thermionic emission. The space charge deposited on the interior surface of the glass bulb created the electric field necessary to initiate ionic conduction through the 0.6-mm-thick soda-lime glass envelope of the light bulb. This simple experiment illustrates the wide variety of potential materials that are potentially worthy of consideration for ionically conductive coatings.

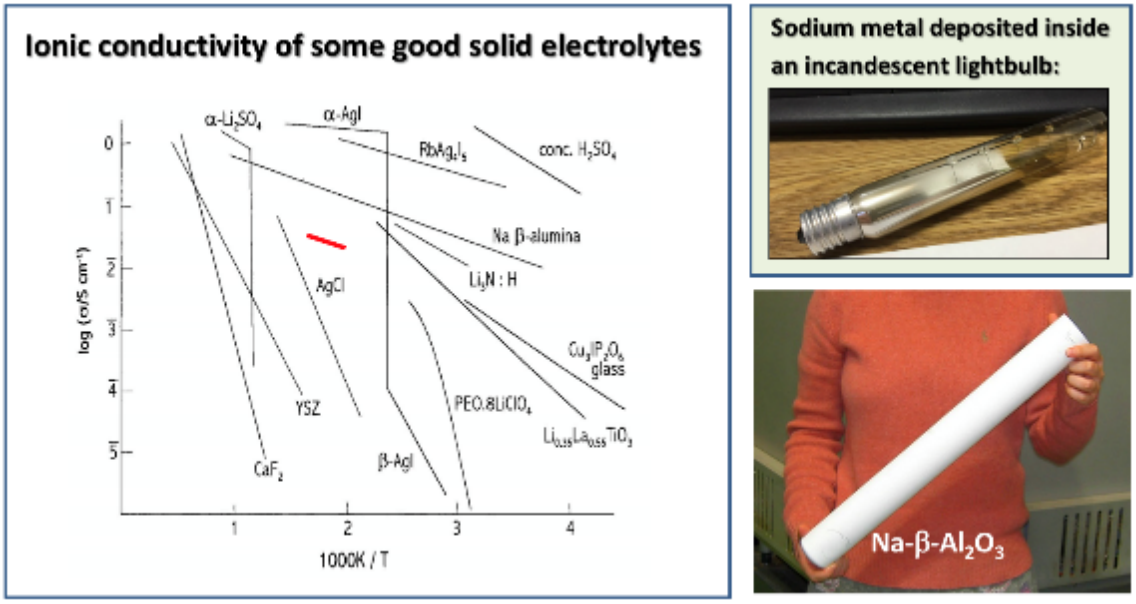

Figure 85: The phenomenon of ionic conductivity is well known.

Referring now to Figure 86, this led us to investigate relatively recent work by Braga et al.[80] on amorphous glassy super-ionically conductive anti-perovskite materials. These "electronically inverted" perovskite materials were conceived of as analogs to perovskites such as $NaMgF_3$, which exhibits super-ionic conductivity with respect to fluoride ions. Selectively doped XOA_3 anti-perovskites (where X = Cl, Br and A = Li, Na) have been shown in recent years to provide higher super-ionic conductivity for Li and Na than prior art materials such as Na-β-Al_2O_3 or NASICON, and at much lower temperature. Moreover, anti-perovskite materials such $BrONa_3$ are easily prepared from inexpensive reagents, and exhibit isotropic ionic conductivity. Another important realization made during this project was that the low melting point (~400 °C) of these materials not only makes it relatively easy to apply them as a thin coating to a substrate, it also solves the problem of CTE mismatch between the substrate and the super-ionically conductive coating. This stems from the very low glass transition temperatures of materials such as $BrONa_3$, which provides for in situ stress relieving of the coating during device operation. This implies

that while CTE matching must still be achieved between the substrate, electrical feedthrough material, and hermetic seal material, we do not have the onerous constraint of also CTE matching the super-ionic coating to the substrate.

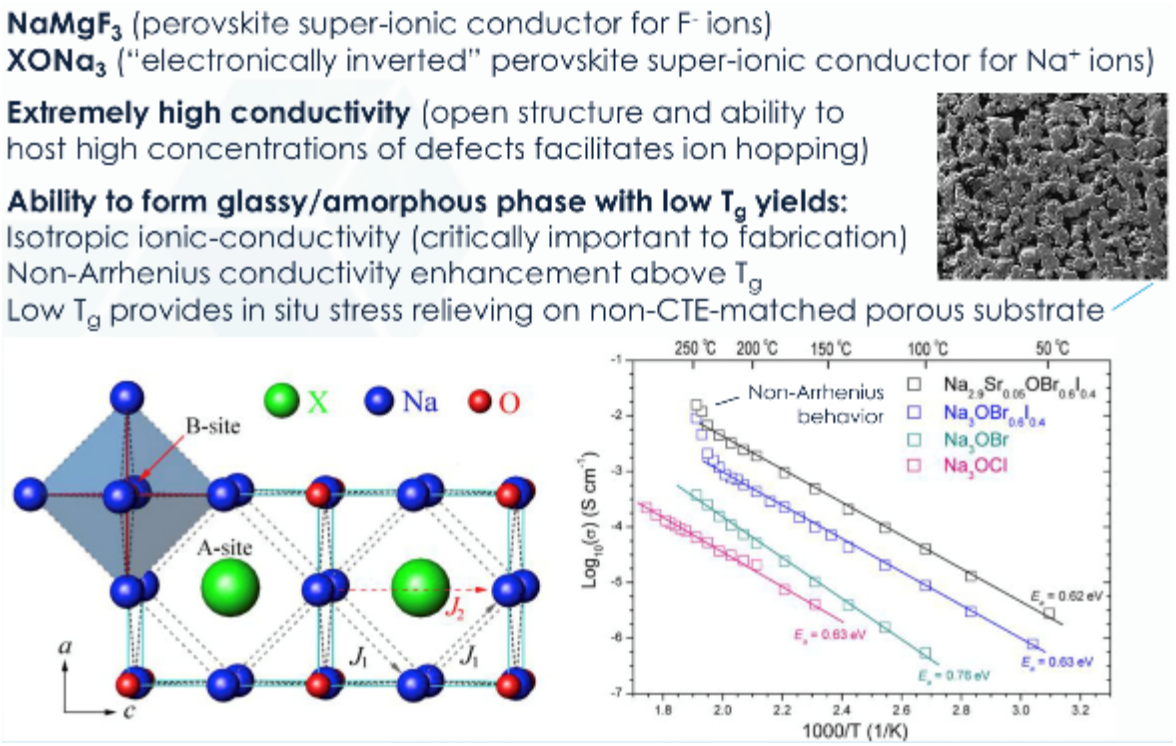

Figure 86: Down-select of super-ionic coating material.

The pursuit of a porous substrate material that is CTE matched to the electrical feedthrough material, and hermetic seal material, while also providing low electronic conductivity at elevated temperature, required us to scour the relevant scientific literature in the hope that such a combination of materials could be found. This work was informed by earlier technical due diligence that the team performed on candidate seal materials, which, among other things, indicated that there are no elastomeric seal materials capable of withstanding molten sodium metal, molten sodium nitrite, and NO_2 gas at a continuous operating temperature 300 °C.

We did find, however, several rigid ceramic/glass materials that can reliably form a CTE-matched seal to various steel alloys that are available at low cost and suitable for mass production. A key milestone in the development of such metal-to-ceramic sealing materials in the prior art was a realization that additives such as cobalt (II) oxide at the 0.5% to 1.0% level, could be added that effect an in situ electrochemical reaction during firing that creates O-O bridging bonds between the metallic and ceramic phases.[81] This is in stark contrast to other types of non-mechanically-compliant sealing materials that rely on weak Van der Waals bonding between the two dissimilar phases, or an interference fit.

Another critically important realization occurred while researching the fabrication process for the porous substrate. At the outset of this project, the porous substrate was envisioned to be a hollow sodium containing vessel fabricated from sintered ceramic powder such as alumina. The original design intent was make the wall thickness of the porous substrate thick enough to provide the

desired mechanical strength. In the event of a hairline fracture, percolation of liquid sodium into molten $NaNO_2$ electrolyte would be too slow to generate the heat required for a runaway reaction. Rather, the immediate formation of a sodium oxide “scab” would preclude further ingress of molten sodium.

But red-teaming of this initial concept revealed several problems. The first problem concerns catastrophic failure. Severe mechanical trauma could result in complete fracture of such a vessel, in which case a violent reaction with the electrolyte would occur, and presumably combustion of all the sodium metal contained inside the vessel. In addition, manufacturing of such a hollow sintered vessel is not particularly straightforward, and would probably entail fabrication of two halves of a clamshell structure that must subsequently be fused together. A further problem concerned the very high sintering temperatures of materials such as alumina (originally selected because of its low cost and excellent insulating properties at elevated temperature).

These series of red teaming sessions, interspersed with extensive literature searches, eventually led to a conceptual breakthrough. Referring to Figure 87, we realized that we could replace the hollow sintered ceramic structure (fused clamshell) with a solid body comprising an open-cell ceramic foam. Such a ceramic foam would likely have an open volume of ~80% and a mean pore size of 100 microns. This provides for efficient volumetric storage of sodium metal, and the resulting porous “bone-like” structure is extremely tough, and naturally adapted to arresting crack propagation. The small pore size would also provide the flow-rate limiting function discussed earlier, in which molten sodium is only able to slowly percolate through such a structure. Recall that such flow restriction renders hairline cracks and other small-scale breaches of the super-ionically conductive coating self-healing.

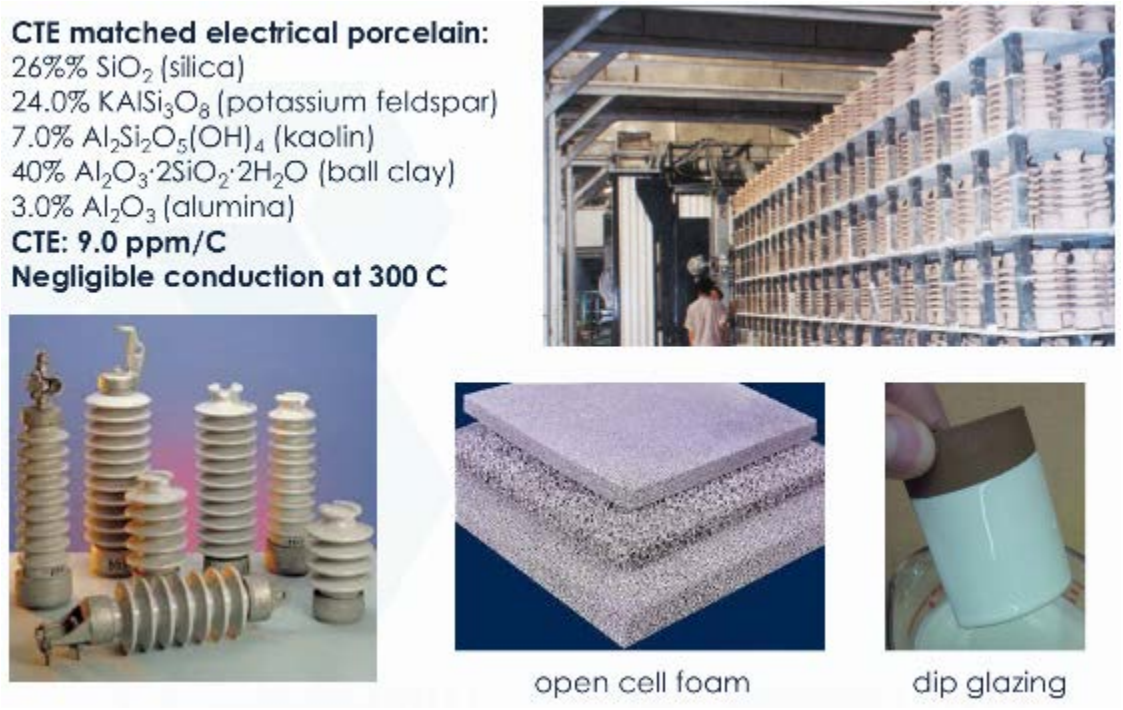

Figure 87: Sodium electrode body material.

Referring now to Figure 88, the foam core electrode concept was also informed by literature review and subsequent laboratory experiments concerning the fabrication of such ceramic foam structures. Open cell structures can be fabricated by immersion of an open cell sponge material (e.g. polyurethane) in an aqueous suspension of ceramic particles (commonly referred to as "slip"), which is then compressed between rollers to achieve a predetermined loading of slip, dried, and then fired. The shape, dimensions, and porosity of the finished part are dictated by those of the original foam template. The dried, ceramic-impregnated sponge is rigid and easy to handle prior to firing, and the template material (e.g. polyurethane) is simply removed by pyrolysis during firing in air. A series of experiments we performed to evaluate different types of foam indicated that a template such as open-cell polyurethane is first converted to a graphitic foam of identical shape and size between 400 – 600 °C, followed by conversion of graphite to CO and CO_2 gas above 750 °C. Pyrolysis of the foam template is known to induce defects in the remaining ceramic structure. In high stress structural applications, re-immersion of the ceramic foam in slip, followed by refiring can be used to repair such defects. But our experiments indicate that the resulting structure has more-than-adequate strength for the present application. We also demonstrated that the drying step could be eliminated by placing the wetted foam in a kiln at room temperature and simply running the firing cycle, during which water is apparently driven off without causing damage to the porous structure or deformation of the part. The result is an extremely inexpensive and straightforward fabrication process. Moreover, a higher viscosity version of the same ceramic slip mixture may be used for dip coating and subsequent firing to create exterior surfaces that are hermetically sealed in predetermined locations.

Figure 88: Fabrication of open-cell porcelain foam electrode cores.

There are, however, other engineering requirements that must be met. We need the ceramic material in question to be capable of engaging in the cobalt (II) oxide redox reaction that results in formation of -O- bridging bonds at the ceramic/metal electrical feedthrough interface, and we need this same ceramic material to be CTE matched to the electrical feedthrough material. The

electrical feedthrough material must be non-reactive to NO_2 gas at 300 °C, and we are prohibited from using ceramic materials whose electrical properties deteriorate at elevated temperature. Finally, we would like the electrical feedthrough material to have high electrical conductivity to minimize ohmic losses.

As described in Figure 89, further research revealed that all the above requirements could be met in the following manner. The metallic material chosen for the electrical feedthrough is 410 stainless steel. Alternatively, 430 stainless steel may also be used. These two alloys are chemically compatible with NO_2 gas at 300 °C, and chemically compatible with the cobalt (II) oxide redox reaction used to form oxygen bridging bonds. The main drawback of 410 stainless steel is low electrical conductivity (3.0% IACS, where copper is 100% IACS).[82] But the problem of low electrical conductivity can be circumvented in two ways. First, 410 stainless steel can be joined to copper by brazing, friction welding, etc. This necessitates only a very short distance over which 410 stainless steel must transmit electrical current. Second, we are free to fabricate the 410-stainless-steel electrical feedthrough pins in the form of thin-walled hollow tubes that are filled with molten sodium metal, which has excellent electrical conductivity (40% IACS). In one instantiation, the thin-walled tubes in question would be closed off at one end to provide a fully hermetic, standalone sodium electrode; the open end of the 410-stainless-steel tubing would terminate inside the ceramic foam core of the electrode. Alternatively, if arranged as a flow battery, the hollow 410 stainless tubing would serve as a fluidic connection between the electrode an external sodium reservoir. One version of the proposed electrode structure is shown in Figure 90.

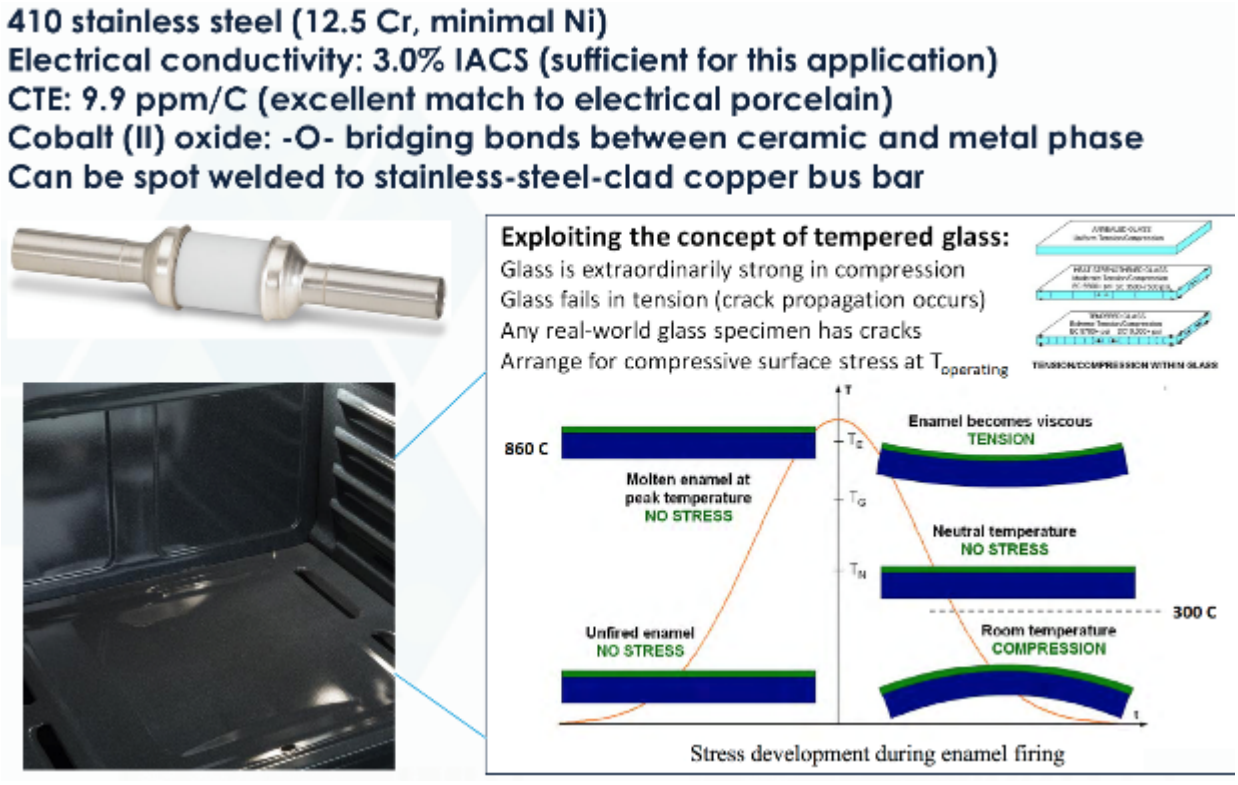

Figure 89: Down-select of electrical feedthrough material.

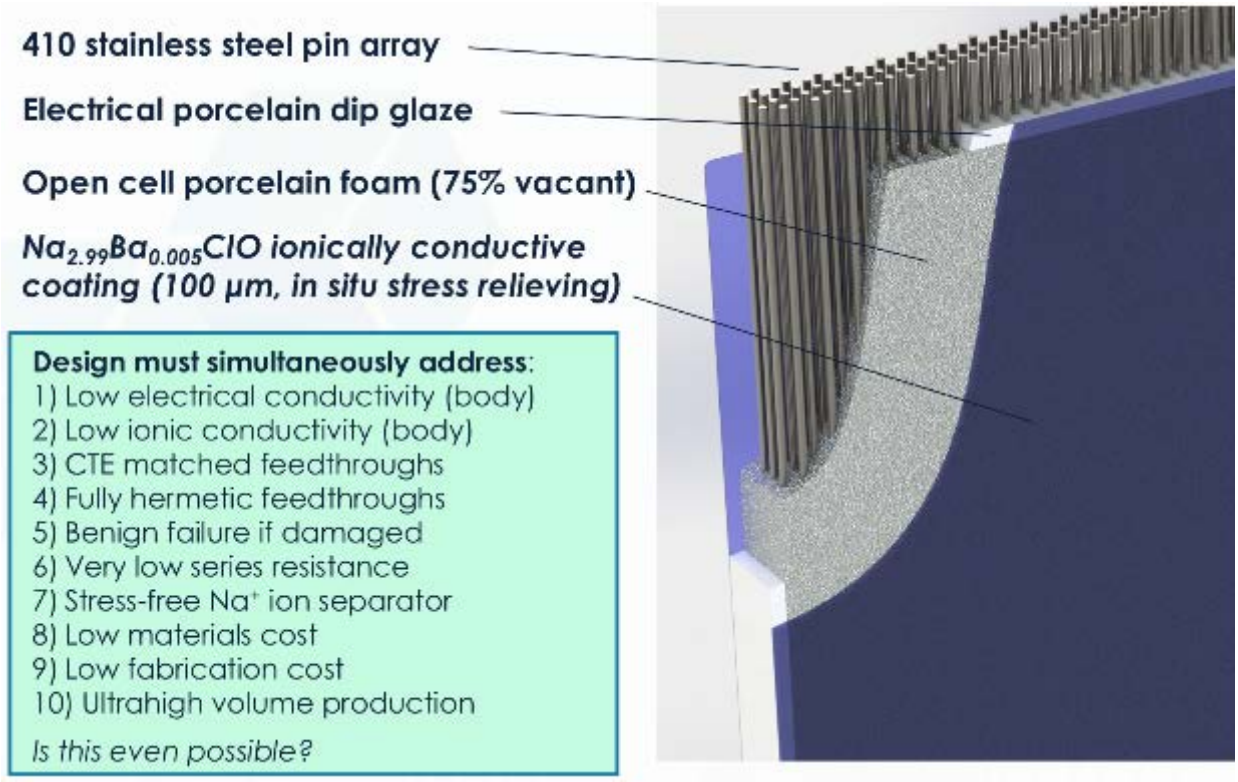

Figure 90: Final concept for proposed sodium electrode.

The above considerations eventually led us to down-select the ceramic material to a 9 ppm/°C CTE "electrical porcelain" composition that is known for low leakage electrical properties, is composed of low-cost ingredients, and that entails the use of firing temperatures that can be routinely achieved in low-cost furnace equipment. The down-selected porcelain composition was 26% SiO_2 (silica), 24.0% $KAlSi_3O_8$ (potassium feldspar), 7.0% $Al_2Si_2O_5(OH)_4$ (kaolin), 40% $Al_2O_3{\cdot}2SiO_2{\cdot}2H_2O$ (ball clay), 3.0% Al_2O_3 (alumina). This porcelain composition can be fired in conventional "Cone 10" 1300 °C furnaces based on alumina refractory brick and sintered Kanthal alloy electrical heating elements. For high-volume production, a natural-gas-fired alumina-lined steel furnace would be used. The five precursor materials were ground together in an alumina ball mill for several hours, and a slip mixture of appropriate viscosity was prepared by blending with 50% de-ionized water by mass.

We also undertook a parallel research thrust that concerned bulk synthesis of the doped anti-perovskite super-ionically conducting material, initially targeting the composition of $Na_{2.99}Ba_{0.005}ClO$ investigated by Braga et al. Review of the literature on anti-perovskite synthesis indicated significant uncertainty about the role of water in the synthesis process, including the final quantity of water remaining in the product. Consider the synthesis reaction for Na_3OCl:

$$NaCl + 2\ NaOH \rightarrow Na_3OCl + H_2O$$

The two precursors, NaCl and NaOH, are high-melting crystalline solids, whereas the product Na_3OCl is a low-melting glassy/amorphous phase. The conventional approach to synthesis entails dissolution of the two ionic precursors in water to form an intimate mixture of precursor ions in the appropriate stoichiometry, after which the sample is reacted for several hours at

elevated temperature (e.g. 250 °C). The resulting material is ground up into fine powder, and x-ray diffraction is used to verify that the crystalline precursors have fully converted to the corresponding glassy/amorphous phase.

One potential concern with this synthesis route is that it may entail significant uncertainty regarding the amount of water that remains in the sample. To circumvent this issue, we constructed a solid-state reactor comprising an all-alumina ball mill (to avoid contamination) that operates in temperature controlled oven capable of operating up to 325 °C (Figure 91). The precursor ingredients are added to the ball mill in powder form, and the grinding action of the alumina media serves break up any large particles and thoroughly mix the precursor materials. For example, to synthesize of one mole of $Na_{2.99}Ba_{0.005}OCl$:

$$NaCl + 1.99\ NaOH + 0.005\ Ba(OH)_2 \cdot 8\ H_2O \rightarrow Na_3OCl + 1.04\ H_2O$$

we combine:

58.440 gm NaCl + 79.594 gm NaOH + 1.577 gm $Ba(OH)_2 \cdot 8\ H_2O$

to form:

120.42 gm Na_3OCl + 18.741 gm H_2O

at a reaction temperature of 240 °C. A further advantage of the ball mill reactor is that we can explore reaction conditions at further elevated temperatures without concern that the powder will consolidate into a molten mass of sticky material, thereby arresting grain refinement. If this happens, we can simply reduce the temperature and regrind the material into powdered form. This $Na_{2.99}Ba_{0.005}OCl$ material synthesized in the above reactor will be characterized by coin cell impedance spectrum analysis and x-ray diffraction with the assistance of Vitale Stavila of Org. 8341 as part of a follow-on R&D effort.

Temperature controlled ball mill (25 – 325 C)
All Al_2O_3 construction avoids contamination
Continuous grain refinement during synthesis
Ability to cycle between melting and grinding
Reproducible dehydration of reagent mixture
Fully deterministic solid state synthesis
Highly scalable for mass production

Verification of Na^+ ionic conductivity: coin cell impedance analyzer (8341)

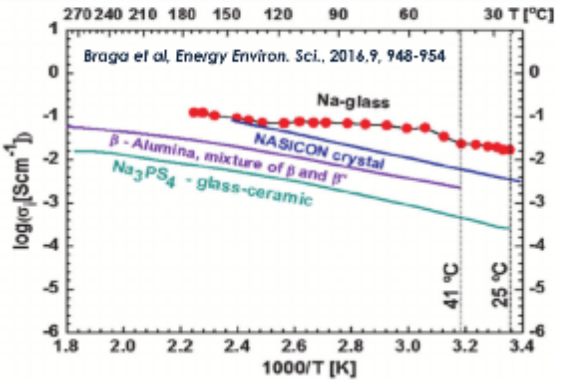

Verification of amorphous structure: powder x-ray diffraction (8341)

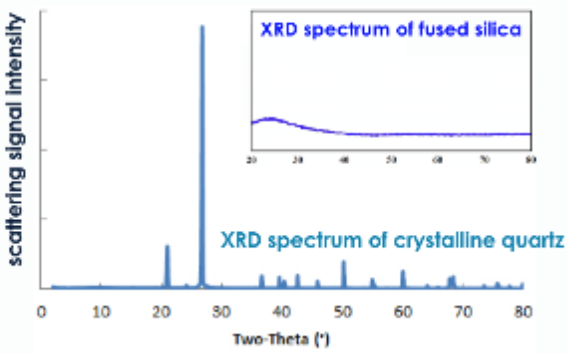

Figure 91: Solid-state synthesis of $Na_{2.99}Ba_{0.005}ClO$.

Implementation of the rotary ball mill apparatus was not without its difficulties. In a traditional bill mill, the cylindrical jar rests on two rollers, one of which is driven by an electric motor, and one of which is an idler roller. The weight of the fully loaded cylindrical jar provides adequate roller traction, and the roughly 10:1 gear reduction provided by the roller-to-cylinder diameter ratio is used to match the electrical motor to the speed/torque requirements of the ball mill. This arrangement works well if (1) there is adequate traction between the roller and cylindrical tumbler, and (2) the cylindrical tumbler is sufficiently uniform in diameter.

In the present application, it was necessary to use an all-alumina ball mill jar and tumbling media to prevent contamination of the super-ionically conductive coating material. A second, larger ball mill was procured for formulation of the electrical porcelain composition. Both the small (1 liter) and large (5 liter) ball mill jars were badly out of round and irregularly tapered along their length. Ordinarily, such a problem would be solved using rubber rollers or other such mechanically compliant surfaces. This approach was precluded by the 325 °C operating temperature requirement, however. The alumina cylinders could not be drilled and/or tapped to permit the use of traditional mechanical fasteners, and adhesive bonding to the alumina cylinders was out of the question because of the 325 °C operating temperature. Ultimately, we determined that the traditional traction drive was not viable and would have to be replaced by a direct drive mechanism.

The version 2 rotary ball mill furnace (Figure 92) suspends the ball mill jar in a rigid mechanical yoke that is welded to a 2” diameter hollow steel shaft supported by two roller bearing assemblies external to the oven. The hollow steel shaft has a thin wall (0.125”) and is loosely filled with fiberglass insulation, both of which inhibit conduction of heat from the oven to the mechanical drive system. The system is driven by a variable speed 0 to 500 rpm, ¼ horsepower permanent magnet dc gear motor. The motor is mechanically coupled to the drive shaft via #35 steel roller chain. The motor-shaft sprocket has 10 teeth, and the drive-shaft sprocket has 72 teeth. The resulting 7.2:1 gear reduction provides an operating speed range of 0 to 70 rpm, which is ideally suited to this application. The bearing assembly closest to the oven is rated for continuous operation at 225 °C, whereas the bearing assembly adjacent to the 72-tooth sprocket is a less expensive component only rated to 110 °C. The principal challenge in the implementation of such a direct drive system is the extreme stiffness required of both the drive shaft and surrounding frame to support the heavy overhanging load of the alumina ball mill jars.

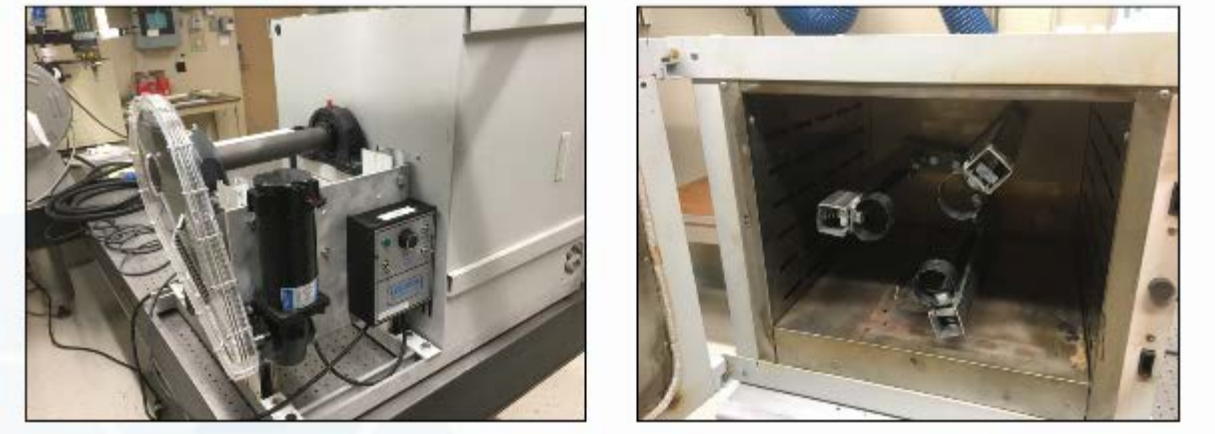

Figure 92: Version 2 rotary ball mill furnace apparatus.

In summary, through careful study of the literature and lengthy design iteration, we were able to devise an electrode structure that **simultaneously meets all ten** of the sodium electrode application requirements: 1) low electrical conductivity of the electrode/substrate material at elevated temperature (300 °C), (2) low ionic conductivity of the electrode/substrate material at elevated temperature, (3) CTE-matched metallic electrical feedthrough functionality, (4) fully hermetic electrical feedthrough ceramic/metal seals based on -O- bridging bonds at the phase interface, (5) an open cell porous internal structure that resists catastrophic mechanical failure and restricts flow of molten Na in the event of a breach, (6) very low series resistance for both the ionically conductive coating and electrical feedthroughs, (7) in situ stress relieving of the superionic glass electrode coating to eliminate substrate CTE mismatch, (8) low materials cost for all components, (9) low fabrication costs, and 10) scalability to ultra-high-volume mass production. The electrode core material was down selected to a 9.0 ppm/°C electrical porcelain composition that is CTE matched to the 410 stainless steel feedthrough material. We demonstrated fabrication of the electrode core in the form of an open-cell rigid ceramic porcelain foam by immersion of an open-cell polyurethane foam template in a 50% aqueous suspension of powdered porcelain, followed by direct firing at 1300 °C. We also developed a novel solid-state reactor for synthesis of $Na_{2.99}Ba_{0.005}ClO$ and its analogs at elevated temperature in an all-alumina ball mill apparatus that provides continuous grain refinement during synthesis. This approach is intended to eliminate the potential for irreproducible results, and allows the synthesis reaction to be carried out under molten conditions if desired, with subsequent recovery of the product in powder form.

6. CONCLUDING REMARKS

6.1. Point of reckoning, mid-stage RIFB R&D strategy

Based on the lessons learned during construction and operation of the v1 device, and subsequent analysis of manufacturability and sodium electrode safety, a four-pronged strategy was devised to continue moving RIFB forward on all fronts. First, planning and construction of a test bed for quantitative electrochemical kinetic measurements of the

$$NO_2 + e^- \rightleftarrows NO_2$$

reaction couple at the interface of the molten $NaNO_2$ electrolyte and the porous stainless steel electrode was undertaken. In parallel, we initiated design and planning of experiments for various aspects of derisking. As alluded to earlier, derisking means answering questions like, "even if the $NO_2 + e^- \rightleftarrows NO_2$ redox chemistry exhibits ideal properties, how are you going to devise a practical, reliable, and cost-effective means of circulating the reagents (molten sodium metal, molten $NaNO_2$ salt, and NO_2) through the flow battery during operation over the 30-year service lifetime of the battery?" Third, with the design of the real-world cell beginning to crystallize, it seemed prudent to undertake a preliminary techno-economic analysis to ensure that RIFB technology was on a path that could ultimately prove economically competitive. Such techno-economic analysis would also presumably result in further refinement of a designed-for-manufacturability device. Fourth, given that the ideation phase of the SSIR program was complete, we vetted the RIFB concept and R&D strategic roadmap over the course of 10

briefings (and subsequent correspondence) with a wide variety of subject matter experts, asking them to identify conceptual flaws, technical weaknesses, or possible show-stoppers. The purpose of these briefings was to determine if something important had been overlooked (and to establish teaming relationships for future work). No showstoppers or significant oversights were identified. The primary concern of these reviewers was that the molten salt $NO_2^- \rightleftarrows NO_2 + e^-$ redox couple has been the subject of only cursory scientific investigation to date because it was presumably only of academic interest.

To put all of this on a more concrete footing, we also decided to seek feedback for our future research and development plan. Here is an overview of the briefing that was prepared:

> This next R&D phase will test the hypothesis that the $NO_2^- \rightleftarrows NO_2 + e^-$ redox couple is a fully reversible electrochemical half reaction that is free of the electrolyte side reactions that lead to capacity fade in prior art battery chemistries, and that can be paired with a transition metal electrode having an NO_2 adsorption isotherm suitable for high-current-density operation. If this hypothesis is proven to be correct, the $NO_2^- \rightleftarrows NO_2 + e^-$ redox couple can be used in conjunction with recent advances in amorphous-glass alkali-ion solid electrolytes (e.g. $A_{2.99}Ba_{0.005}O_{1+x}Cl_{1-2x}$, A = Li, Na)[83] to create a new class of flow battery based on the electrolysis of ANO_2 ($A \rightleftarrows A^+ + NO_2^- \rightleftarrows NO_2$) called a Radical-Ion Flow battery (RIFB).[84] The RIFB is uniquely suited to the most challenging grid storage application: 8-hour grid storage required to address the intermittency of renewable energy sources such as solar and wind.[85] The RIFB was invented in Year 1 of DOE's Inaugural SunShot Innovator in Residence Program after a five-month-long literature search to compile an exhaustive list of the pitfalls (18 total) that have prevented prior art batteries from succeeding in this demanding application. The top five pitfalls include: (1) use of prohibitively expensive materials, (2) lack of scalability due to limited material abundance, (3) sluggish electrochemistry at one or both electrodes, (4) unwanted side reactions leading to capacity fade and/or internal corrosion, and (5) comingling of highly reactive chemical reagents (making fire suppression extremely difficult in the event of an accident).
>
> As described below, RIFB technology was designed from first principles to solve the problem of grid storage in its entirety. But the electrochemistry of the molten salt NO_2^-/NO_2 redox couple that forms the heart of this novel battery is largely unexplored. Risk reduction of this potentially game changing technology hinges on verifying the above NO_2^-/NO_2 redox couple hypothesis.
>
> The Radical-Ion Flow Battery has a number of uniquely advantageous properties, most of which stem from introduction of the $NO_2^- \rightleftarrows NO_2 + e^-$ redox couple. NO_2 is one of the only chemical species that exists as a stable free radical. The radical-ion reaction $NO_2^- \rightleftarrows NO_2 + e^-$ is hypothesized to have very low activation energy because, in contrast to many prior art energetic electrochemical reactions, it does not involve breaking of chemical bonds, only electron transfer. Although NO_2 is evolved as a gas at the anode during charging, its anomalously high boiling point (21 °C) means that it can be conveniently stored in the condensed phase at room temperature without pressurization. In the RIFB, the molten electrolyte and electrochemically active species (hereafter assumed to be $NaNO_2$, although $LiNO_2$ is potentially attractive for some applications)

are one and the same; there is no kinetic penalty associated with dilution of the electrochemically active constituents in the electrolyte. The cell potential is large (3.0 V), the ionic conductivity of the molten electrolyte is extraordinarily high (1.40 Ω^{-1} cm^{-1}),[86] and as explained shortly, there is no reason to expect a need for exotic catalytic materials (e.g. Pt, Pd) at the NO_2^-/NO_2 electrode; operation in the 230 °C to 280 °C temperature range provides very facile kinetics.

The only chemical reagent required to construct a RIFB in its fully discharged state is sodium nitrite salt. Bulk $NaNO_2$ costs only \$0.40/kg[87] because it is derived from NaCl, N_2, and O_2. The RIFB is implemented as a flow battery, thereby decoupling design requirements for energy storage and peak power handling capability, and allowing the reactive constituents (Na metal and liquefied NO_2) to be safely stored in separate locations. While both molten Na and liquefied NO_2 are hazardous materials, they are both routinely shipped in rail tanker cars,[88] and neither exhibits persistent toxicity in the environment or human body. Unlike a traditional flow battery, the RIFB has no requirement for pumps; reagent transport is completely passive (gravity fed in one direction and caused by volumetric displacement of electrochemically generated fluid in the opposite direction). The extremely high energy density of Na + NO_2 (1.45 kW-hr/liter) also minimizes the size and cost of tanks required for the flow battery. It should be further noted that at a size ≥1 m^3, the estimated 5% round-trip loss for the RIFB charge/discharge cycle maintains elevated operating temperature without additional input of heat.

Referring now to Figure 93, we describe how the next phase of RIFB R&D was to be broken down into well-defined tasks:

Task 1) thermodynamic reversibility of the $NO_2^- \rightleftarrows NO_2 + e^-$ redox couple: We propose to make a series of electrochemical measurements on an NO_2^-/NO_2 molten salt concentration cell. As shown in Figure 93, the cell comprises three sintered porous metal electrodes of identical construction, sparged with NO_2 gas at atmospheric pressure, immersed in a molten electrolyte comprising pure $NaNO_2$, all of which is enclosed in an isothermal chamber. The left and right working electrodes allow both the forward and reverse rates of the $NO_2^- \rightleftarrows NO_2 + e^-$ redox couple to be measured simultaneously as a function overpotential (relative to a center reference electrode). Operation of the NO_2^-/NO_2 concentration cell does not entail activation of any $Na \rightleftarrows Na^+$ electrochemical processes and leaves the composition of the electrolyte nominally unaltered. It will also be understood that the design of the concentration cell shown in Figure 93 is in no way meant to suggest how a practical NO_2 electrode would be implemented in a fully engineered RIFB device.

At a superficial level, quantification of reversibility entails measurement of the overpotential at each electrode at a target current density, such as 100 mA/cm^2, as a function of temperature, NO_2 mass flow rate, and electrode composition. Referring to Figure 94, from the standpoint of thoroughly understanding questions surrounding reversibility, the workhorse analytical techniques we will employ are (1) cyclic voltammetry and (2) impedance spectrum analysis. Cyclic voltammetry is particularly useful for preliminary qualitative analysis. It quickly provides insight regarding electrochemical reversibility, the presence of intermediates in redox reactions, and the onset of mass transport limitations to current density. Impedance spectrum analysis is

more time intensive, but far better suited to quantitative analysis. It typically provides accurate and cleanly separated measurements of charge transfer resistance, electrolyte resistance, and the additional impedance contribution of mass transport effects. As outlined in Figure 95, our decision not to employ quantum chemistry modeling in the proposed R&D reflects the fact that the thermodynamics are already known and the kinetics can be measured accurately in the laboratory.

Task 2) mechanism of rate limiting step at the electrode: The question of whether or not the $NO_2^- \rightleftarrows NO_2 + e^-$ redox couple can be made to behave as a highly reversible half reaction depends a great deal on the mechanism of the rate limiting step for the forward and backward reactions at the electrode surface. The first step of the $NO_2^- \rightarrow NO_2$ half reaction is abstraction of an electron at the metallic electrode surface, M, wherein NO_2 is adsorbed on the surface of the electrode:

$NO_2^- + M \rightarrow (NO_2)\text{─}M + e^-$ (electron transfer with NO_2 adsorption)

At low adsorption coverage ($\theta \approx 0$), the simplest desorption mechanism to release NO_2 (thereby completing the $NO_2^- \rightarrow NO_2$ half reaction) is presumably:

$(NO_2)\text{─}M \rightarrow NO_2 + M$ (unimolecular NO_2 desorption)

Alternatively, an electrolyte NO_2^- ion may form a reaction complex with the adsorbate $(NO_2)\text{─}M$:

$NO_2^- + (NO_2)\text{─}M \rightarrow N_2O_4 + M + e^-$ (electrochemical bimolecular NO_2 desorption)

$N_2O_4 \rightarrow 2\ NO_2$ (thermal dissociation)

At higher surface coverage (i.e. higher charging current densities), the bimolecular surface reaction to form the NO_2 dimer may be important as well.

$(NO_2)\text{─}M + (NO_2)\text{─}M \rightarrow N_2O_4 + 2\ M$ (surface bimolecular NO_2 desorption)

$N_2O_4 \rightarrow 2\ NO_2$ (thermal dissociation)

Given that there is no breaking of covalent bonds in the $NO_2^- \rightleftarrows NO_2 + e^-$ electron transfer process, it is very unlikely that the electron transfer step will be non-rate-limiting. For the kinetics of the charging process to be facile, the $(NO_2)\text{─}M$ bond must not be too strong; otherwise desorption of NO_2 after completion of the electron transfer step could constitute a kinetic bottleneck. On the other hand, for the kinetics of the $NO_2^- \leftarrow NO_2$ discharging process to be facile, we need the $(NO_2)\text{─}M$ to be strong enough that the equilibrium coverage of adsorbed NO_2 is high enough to support the electron transfer reaction in which NO_2 and an electron are united to form a nitrite ion at an appreciable rate. Although this is very reminiscent of the classic “volcano plot” for H_2 evolution during electrolysis of H_2O (Figure 96), there is a critically important distinction. In the unusual case of the $NO_2^- \rightleftarrows NO_2 + e^-$ redox couple, because there is no requirement for breaking of chemical bonds, we hypothesize that we should be free to use electrode materials having relatively weak $(NO_2)\text{─}M$ adsorption, thereby facilitating the goal of achieving very high exchange current density. Accordingly, Task

2 will focus on candidate electrode materials having moderate (NO_2)─M bond enthalpy, electrode materials that naturally passivate in the molten salt electrolyte to achieve the same result, or electrolyte trace additives that could be used provide the desired degree of surface passivation.

1) Quantify degree of thermodynamic **reversibility** for $NO_2^- \rightleftarrows NO_2 + e^-$ redox couple
2) Identify mechanisms of **rate limiting steps** at the electrode/electrolyte interface
3) Analyze potential **electrolyte side reactions** on the NO_2^-/NO_2 side of the cell
4) Analyze potential **electrode corrosion** reactions on the NO_2^-/NO_2 side of the cell
5) Quantitatively prove viability of the required NO_2 **gas diffusion electrode** (GDE)

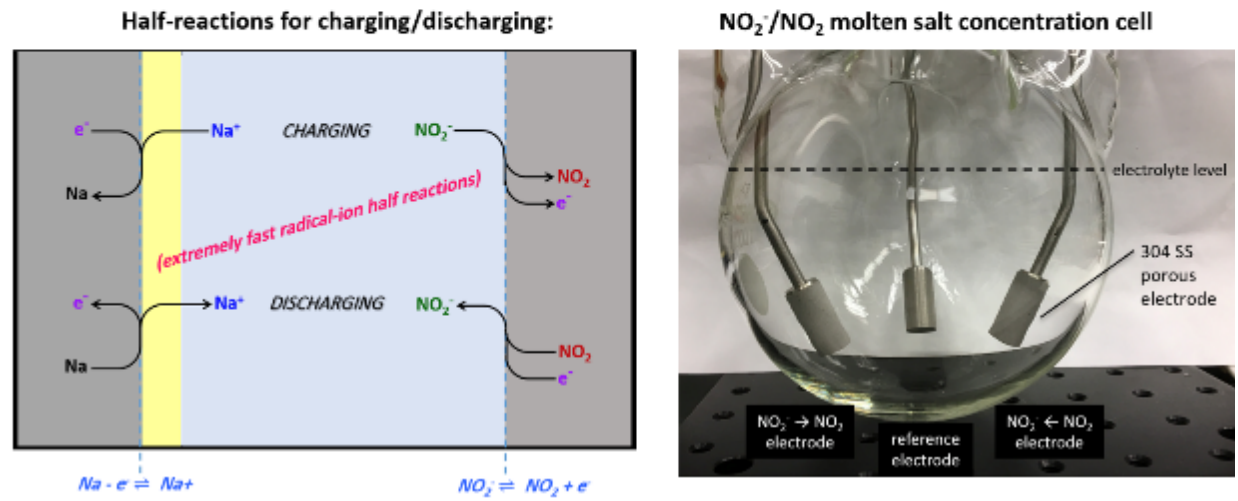

Figure 93: Testing the NO_2^-/NO_2 redox hypothesis can be broken down into five tasks.

- **Cyclic voltammetry signature: temperature, composition or time dependent?**
- **Impedance spectroscopy: Do we have a rigorous system model that makes sense?**
- **Impedance spectroscopy: What needs to be improved to reach 100 mA/cm^2?**
- **Both techniques: Under what conditions is transport rate limiting?**

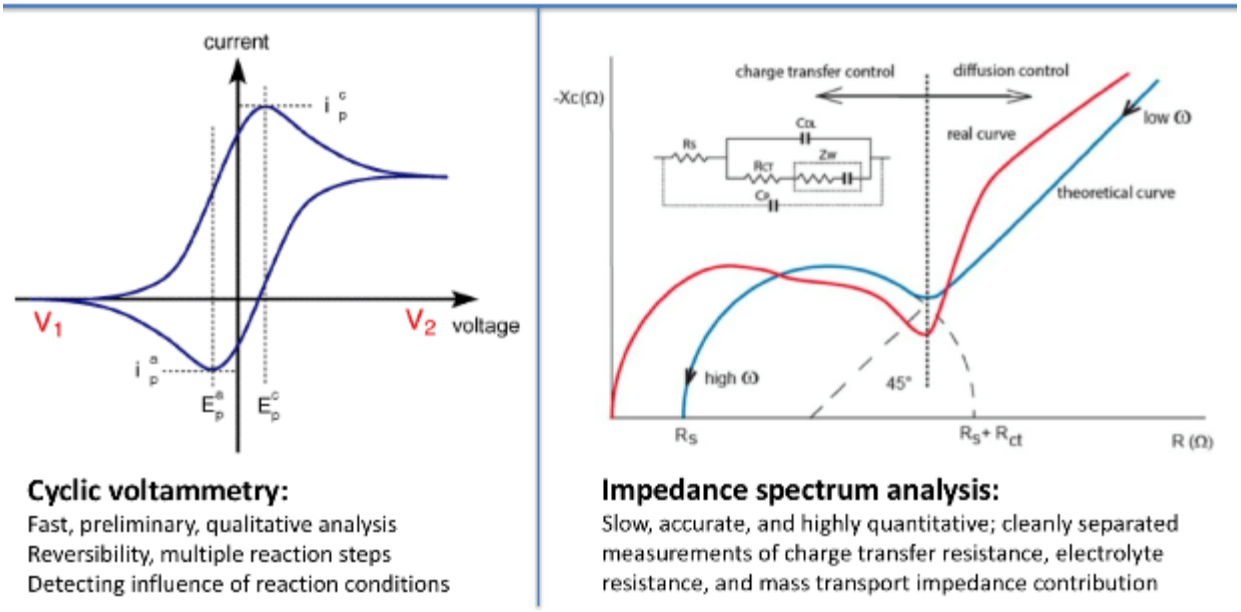

Cyclic voltammetry:
Fast, preliminary, qualitative analysis
Reversibility, multiple reaction steps
Detecting influence of reaction conditions

Impedance spectrum analysis:
Slow, accurate, and highly quantitative; cleanly separated measurements of charge transfer resistance, electrolyte resistance, and mass transport impedance contribution

Figure 94: Workhorse analytical techniques for investigation of the NO_2^-/NO_2 redox hypothesis.

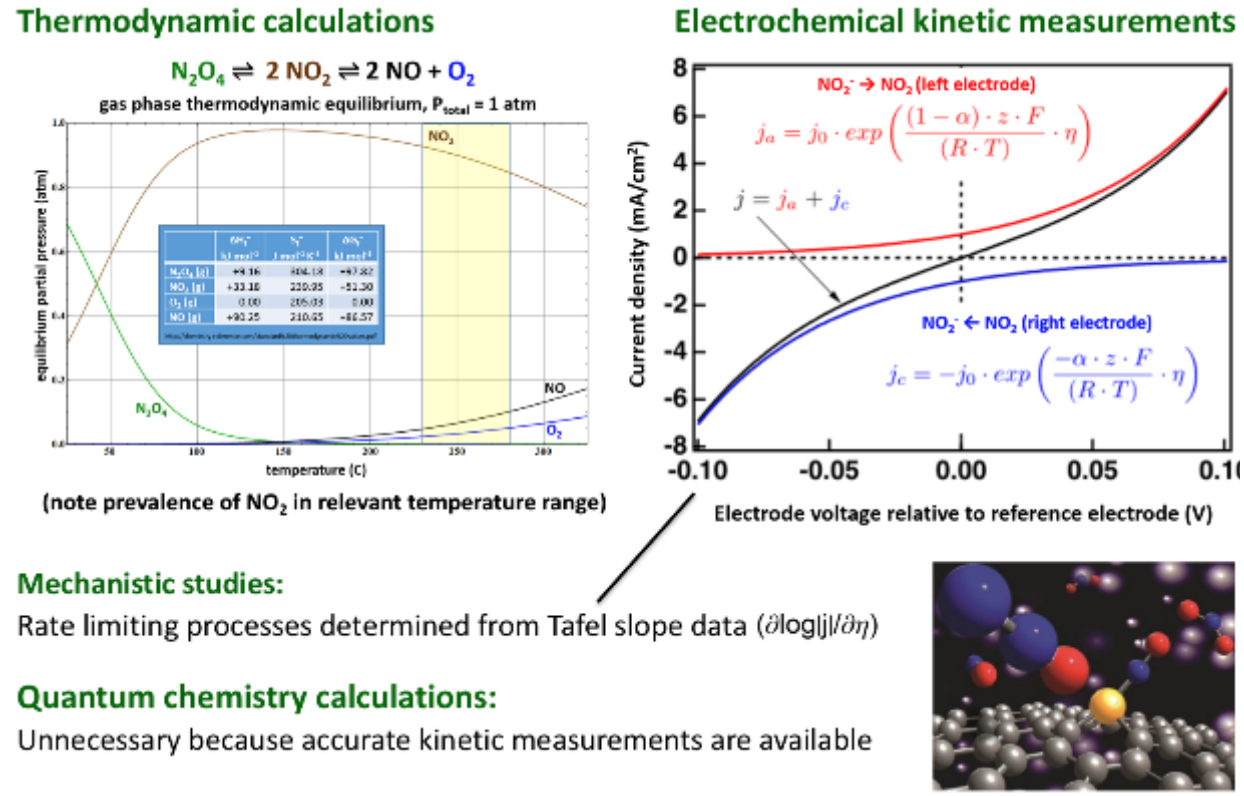

Figure 95: Thermodynamic calculations based on tabulated data and experimental electrochemical kinetic measurements can provide the mechanistic insight required.

Butler-Volmer equation is not valid (electron transfer is not the rate limiting step)

$NO_2^- + M \rightarrow (NO_2){-}M + e^-$	(electron transfer with NO_2 adsorption)
$(NO_2){-}M \rightarrow NO_2 + M$	(simplest desorption mechanism at low coverage)
$NO_2^- + (NO_2){-}M \rightarrow N_2O_4 + M + e^-$	(electrochemical bimolecular NO_2 desorption)
$N_2O_4 \rightarrow 2\ NO_2$	(thermal dissociation)
$(NO_2){-}M + (NO_2){-}M \rightarrow N_2O_4 + 2\ M$	(surface bimolecular NO_2 desorption)
$N_2O_4 \rightarrow 2\ NO_2$	(thermal dissociation)

Surface chemistry of the electrode:

- No breaking of chemical bonds
- Implies weak NO_2 adsorption desirable
- Electrode material down select
- Passivation additives
- bifunctional electrode materials

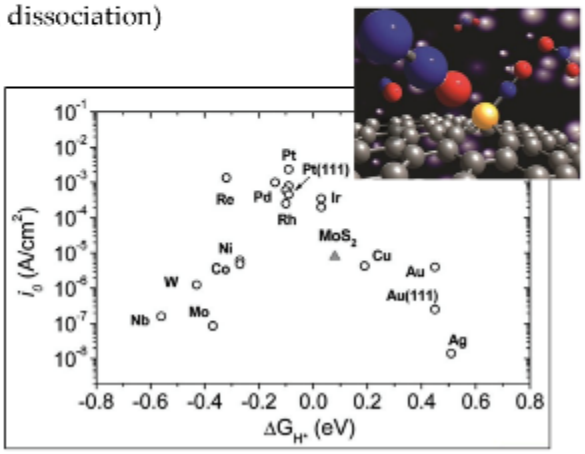

Figure 96: What is the rate limiting step as a function of NO_2 adsorption coverage?

Referring now to Figure 97, the methodology we will use for mechanistic studies of the NO_2^-/NO_2 side redox couple entails analysis of the Tafel slope ($\partial \ln|j|/\partial\eta$) for the forward and reverse $NO_2^- \rightleftarrows NO_2 + e^-$ processes as a function of overpotential. This methodology is succinctly illustrated by the simple example, $Cu^{2+} + 2\ e^- \rightarrow Cu$.

Mechanism	Cathodic Tafel slope	Anodic Tafel slope
Simultaneous $2e^-$ transfer	$(60\ mV)^{-1}$	$(60\ mV)^{-1}$
Sequential $1e^-$ transfer, $Cu^{2+} \rightleftarrows Cu^+$ rate limiting	$(120\ mV)^{-1}$	$(40\ mV)^{-1}$
Sequential $1e^-$ transfer, $Cu^+ \rightleftarrows Cu$ rate limiting	$(40\ mV)^{-1}$	$(120\ mV)^{-1}$

Experimental Tafel slopes for aqueous redox processes at room temperature routinely vary between $(30\ mV)^{-1}$ and $(240\ mV)^{-1}$ and are typically overvoltage dependent, with different mechanisms becoming more or less dominant as adsorption coverage varies. A very small Tafel slope such as $(240\ mV)^{-1}$ implies operation at relatively high overvoltage, which is undesirable. Moreover, such mechanistic studies may suggest the use of two intermingled electrode materials, one of which provides better performance at low current density, and one that provides better performance at high current density.

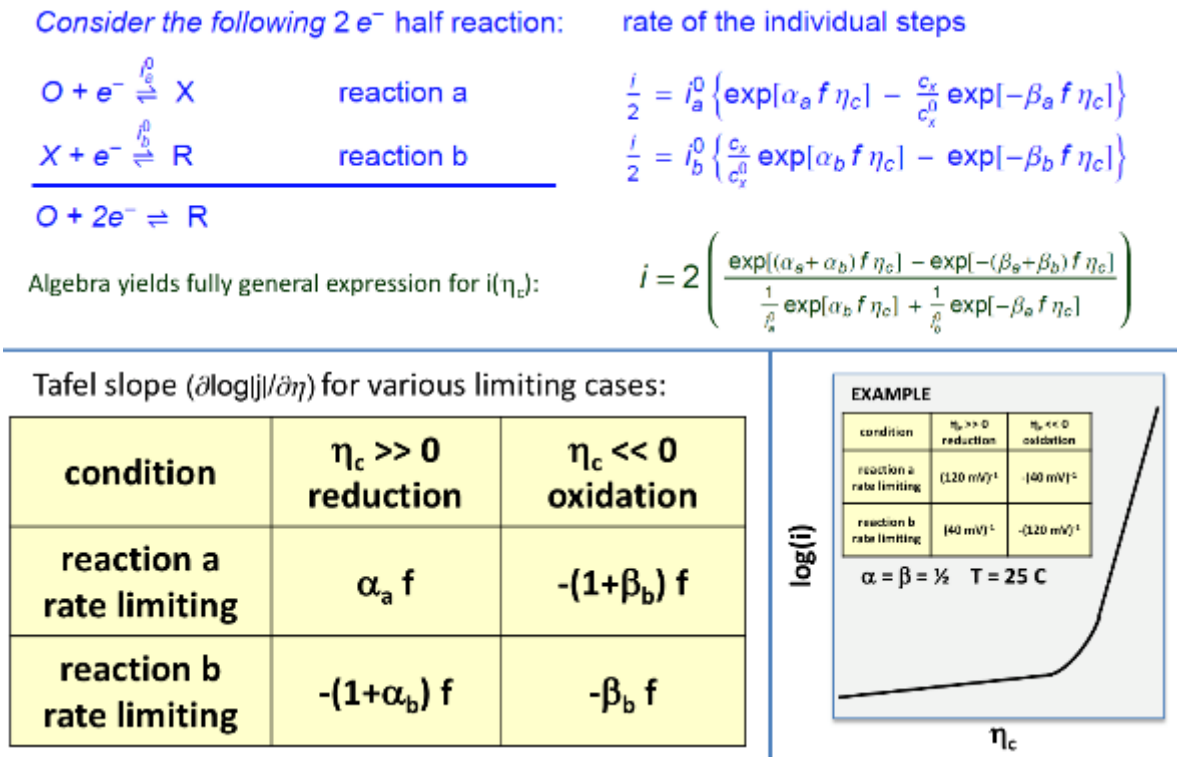

Figure 97: Inferring rate limiting processes from Tafel slope analysis.

Task 3) potential electrolyte side reactions on the NO_2^-/NO_2 side the RIFB electrochemical cell: An outstanding feature of the proposed electrochemical cell is the very small number of permutations for chemical side reactions. Within the electrolyte, only three species are present: Na^+, NO_2^-, and NO_2. Review of relevant available literature suggests only one side reaction of potential significance:[89]

$$NO_2 + NO_2^- \rightleftarrows NO + NO_3^-$$

Depending on the forward and backward rate constants of the above reaction and their temperature dependence, the implications of this redox reaction could be negligible, manageable, or deeply problematic. In addition to the chemical equilibrium condition,

$$k_f [NO_2] [NO_2^-] = k_b [NO] [NO_3^-],$$

we have the design requirement of non-pressurized operation; the sum of all partial pressures must be maintained at 1 atm. If we adjust the temperature controlled NO_2 reservoir accordingly, the mole fraction of NO_2^- ion will remain constant, even as the cell is charged/discharged. Provided the ratio k_b/k_f is not too extreme, the background equilibrium process $NO_2 + NO_2^- \rightleftarrows NO + NO_3^-$ will not interfere with cell operation. In fact, we may even be able to exploit this background equilibrium process to achieve freezing point depression. In the case of $NaNO_2$, for example, pure $NaNO_2$ has a melting point of 271 °C, whereas a 60/40 mole fraction mixture of $NaNO_2/NaNO_3$ forms a eutectic with a melting point of only 225 °C. Use of the $NaNO_2/NaNO_3$ eutectic is potentially highly advantageous from the standpoint of engineering reliable hermetic seals; closed-cell PTFE foam is an excellent candidate gasket material, but it is

only rated for operation to 260 °C. At a given operating temperature (k_f and k_b are both temperature dependent), we are free to adjust the partial pressure of NO_2 to maintain the 3:2 eutectic ratio:

$$P_{NO2}(T) = \frac{1}{1 + \frac{k_f(T)}{k_b(T)} \frac{[NO_2^-]}{[NO_3^-]}} = \frac{1}{1 + \frac{3}{2} \frac{k_f(T)}{k_b(T)}}$$

Provided the ratio $k_f(T)/k_b(T)$ is not too large, the partial pressure of NO_2 will be large enough to avoid incurring a significant kinetic penalty for the discharging reaction. In the unlikely event that $k_f(T)/k_b(T) >> 1$ at all operating temperatures open to consideration, we will need to evaluate alternative strategies, such as allowing the mole fraction of NO_3^- to be increased further. This could negate, or even reverse to some extent, the freezing point depression advantage of the binary salt mixture (pure $NaNO_3$ melts at 308 °C), but it would not prevent the RIFB cell from being viable because the cell voltage is too low (by 800 mV) to electrochemically dissociate NO_3^- into NO_2 + ½ O_2. In any of the above cases, it should be understood that the presence of a significant mole fraction of NO_3^- ion does not mean that only a portion of the molten electrolyte is usable. Rather, at any given time a portion of the NO_2^- available for reaction is temporarily stored in a coexisting NO_3^- reservoir. Figures 98 and 99 provide an overview of the potential chemical interactions that are in play.

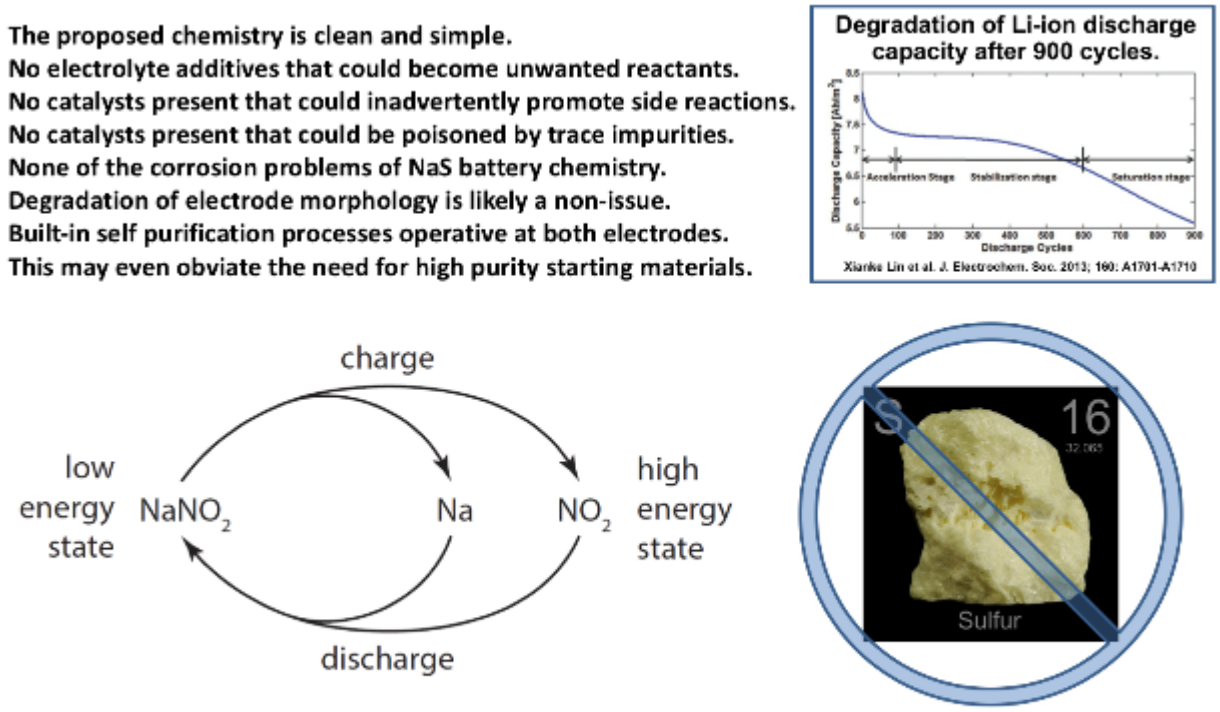

Figure 98: The quest to remain chemically pure and prevent capacity fade.

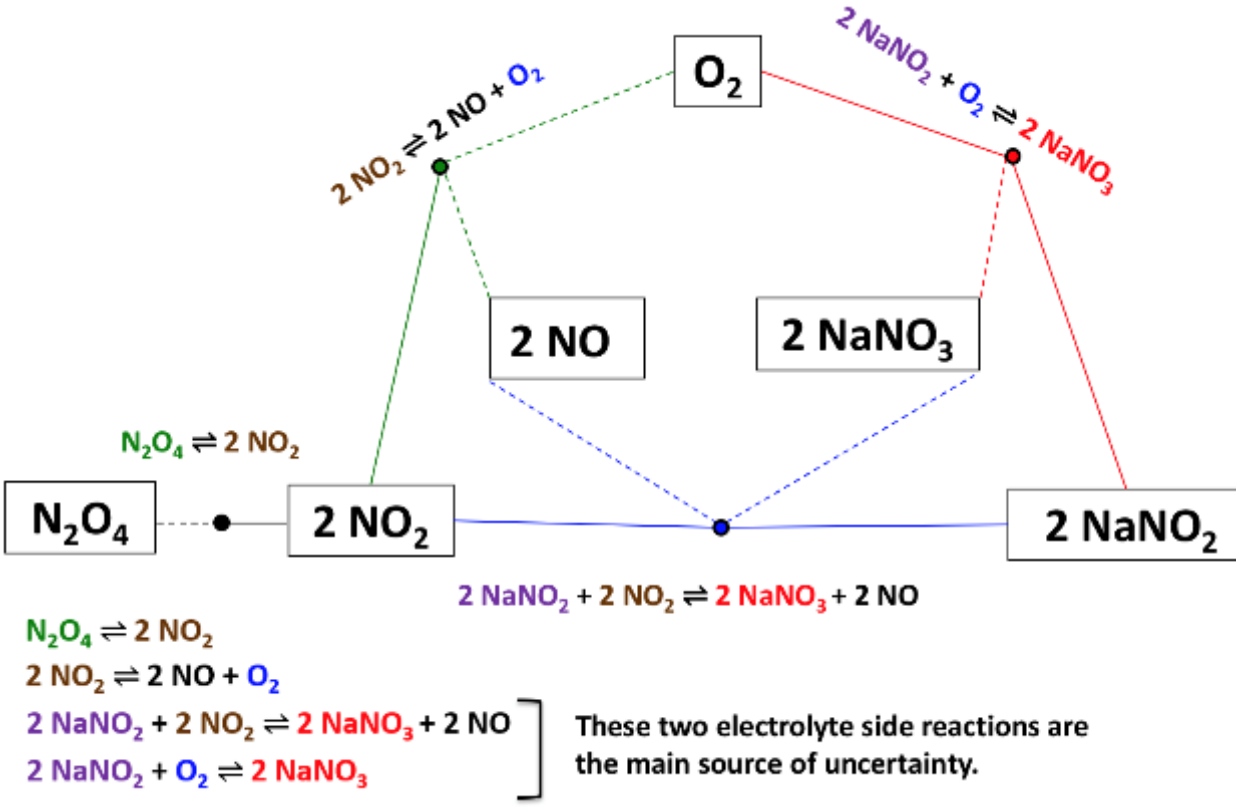

Figure 99: Study of possible electrolyte side reactions.

Task 4) potential corrosion reactions: When a RIFB cell is first commissioned, it contains $NaNO_2$ (but no Na or NO_2), which is extremely hygroscopic. Any water present raises serious concerns about internal corrosion by HNO_3. Maintaining anhydrous conditions is therefore likely to very be important. There is surprisingly little information in the primary literature pertaining to rigorous desiccation of NO_2, although desiccants such as P_2O_5 have been used for the preparation of nitric acid anhydride (N_2O_5). An important part of the proposed research is to fully understand to what extent water can be excluded from the system, and to the extent that traces of H_2O remain present, what countermeasures are most effective and practical and what candidate electrode materials may be rendered impractical.

The presence of H_2O and other gas phase contaminants will be monitored by room temperature FTIR absorption spectroscopy upstream of the NO_2 reservoir. Atomic Emission Spectroscopy (AES) and/or Atomic Absorption Spectroscopy (AAS) will be used to test for the presence of electrode degradation products in the molten electrolyte. We will also construct an NO_2^-/NO_2 concentration cell test bed for coupon-level testing of electrode materials that can subsequently be analyzed by Scanning Electron Microscopy / Energy Dispersive X-Ray Spectroscopy (SEM/EDS), and Auger Electron Spectroscopy (AES). It is critically important to understand which candidate electrode materials have the potential for continuous operation with no signs of degradation given the requirement for a 30-year, 10,000 charge/discharge cycle lifetime. The sensitivity of the above analytical techniques is required to detect slow corrosion reactions after only

~10^2 charge/discharge cycles. Such analytical techniques will also be used to examine the potential role of passivating agents introduced for the purpose of tuning the (NO_2)─M adsorption enthalpy and/or inhibition of electrode corrosion.

Task 5) NO_2 gas diffusion electrode (GDE): In conventional fuel cells, the very low solubility of species such as H_2 and O_2 in the electrolyte necessitate the use of the gas diffusion electrodes. Based on very limited information in the literature, the solubility of NO_2 in molten $NaNO_2$ is estimated to be only 5 ±3 mM.[90] Accordingly, we anticipate the use of a porous electrode structure that can be simultaneously infused with molten $NaNO_2$ electrolyte and NO_2 gas. Referring to Figures 100 and 101, ideally such a GDE allows a surface layer of molten electrolyte to wick deep into the porous structure while allowing deep penetration of NO_2 gas from the opposing direction.[91] Early work will likely emphasize GDEs fabricated from compressed stainless steel fibers. The addition of non-wetting fibers (e.g. PTFE could be considered for a certain range of operating temperatures) may also be explored as a strategy for ensuring that bridging of internal channels by molten salt electrolyte does not occur. Despite the high likelihood of using porous electrode structures to reach our target current density of ~100 mA/cm^2, early experiments with simple planar or quasi-planar electrode surfaces are critically important to accurately characterize the effect of electrode material properties on electrochemical kinetics prior to undertaking construction and testing of more complex electrode designs.

Figure 100: Techniques for mathematical modeling of the sintered stainless steel gaseous diffusion electrode are already well known.
https://www.geodict.com/Solutions/Electrochemistry/fuelcells.php

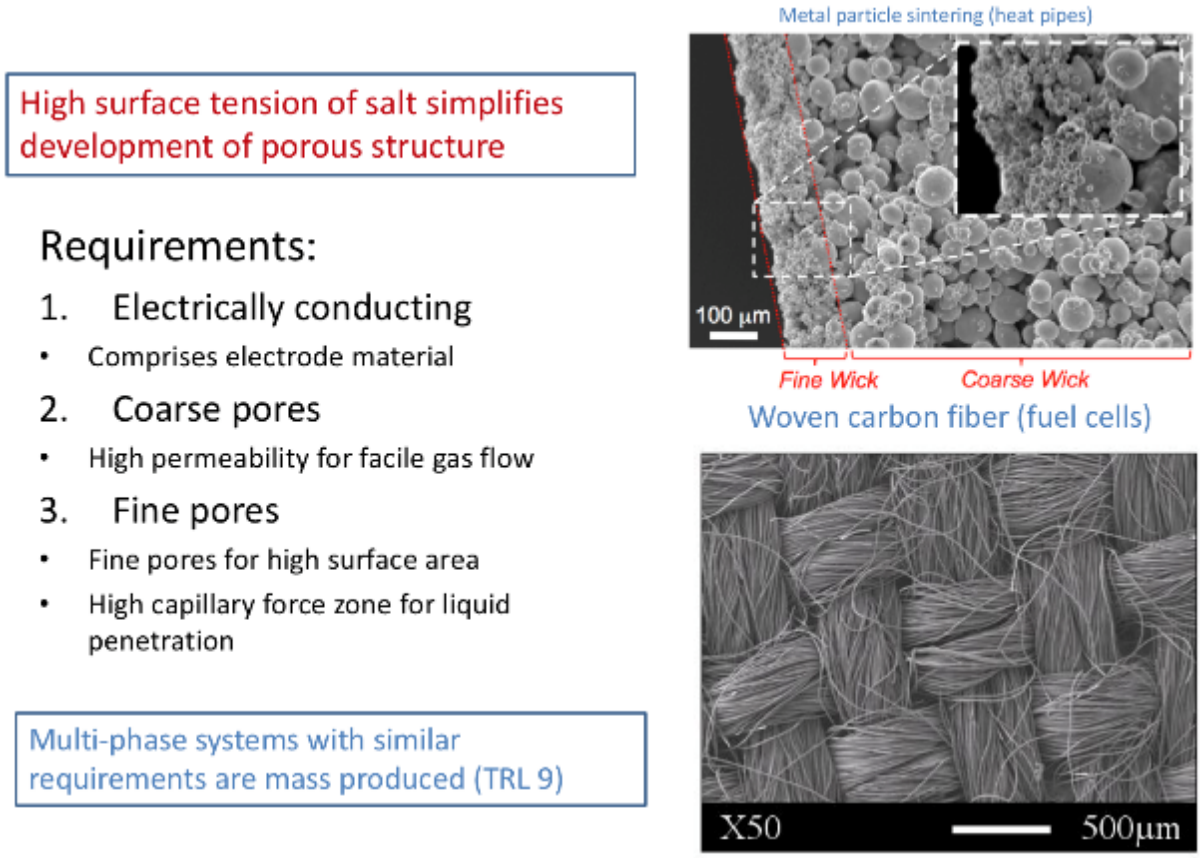

Figure 101: The design objective is 100 mA/cm^2 at η < 50 mV.

Subjecting the above proposed R&D roadmap to the scrutiny of various subject matter experts was very time consuming, but ultimately reassuring.

Shortly thereafter, we discovered a patent application from a German battery company, Battery Consult Gmbh, with a priority date of December 23, 2014, whose abstract is reproduced below:

Molten salt electrochemical flow cell (WO2016102373A1)
Abstract: A rechargeable molten salt electrochemical flow cell according to the present invention comprises a cathode compartment containing a cathode material comprising a liquid metal nitrite salt and nitrogen dioxide, an anode compartment containing an anode material comprising an liquid elemental metal, and a solid membrane separating the cathode and anode compartment and being in contact on one side with the cathode material and on the other side the anode material, said membrane being capable of selectively allowing the exchange of metal ions between the cathode and anode material, whereby the underlying redox reaction is according to the equation: $MeNO_2$ (liq.) <-> Me (liq.) + NO_2 (gas. or liq.).

Inventors: Mihai Stefan Viciu, Cord-Henrich Dustmann, Akane Elisabeth Hartnebach, Michael Harald Bayer

The RIFB patent application filed under the SSIR program had a priority date of February 18, 2016; the Battery Consult Gmbh patent application emerged from its publication blackout period on June 23, 2016. For this reason, there was no way to know that parallel work on the proposed battery chemistry had recently been initiated elsewhere. We became aware of the Battery Consult Gmbh patent application in November 2016. As one might expect, since RIFB was independently invented, there are many embodiments and concepts in the RIFB patent application that are distinct from the Battery Consult patent application.

At a minimum, the Battery Consult Gmbh patent application demonstrates that there are career battery experts concerned with developing products for real-world applications who very recently had many of the same technical insights discussed in this document. This is also reassuring, and moving forward it will be interesting to see how the proposed battery chemistry pans out for grid storage applications.

6.2. First-order techno-economic analysis

Remember, none of the above technical work on RIFB is particularly interesting if we do not have a credible path to a cost-competitive grid storage solution. Extreme cost sensitivity, along with astronomically large scalability requirements, are much of what makes bulk grid storage such a formidable technological challenge. Thus, to close out this report, I would like to share results of the preliminary techno-economic analysis we undertook for RIFB grid storage technology. It is by no means complete, but the results are quite encouraging.

As depicted the schematic diagrams of Figures 102 and 103, we envision that unlike conventional flow batteries, the transport of reagents through a RIFB device would be entirely passive, requiring no pumps. During discharging, molten Na is gravity fed to the electrochemical cell on an as needed basis as shown in Figure 102, while electrochemical displacement moves the flow molten $NaNO_2$ upward against the force of gravity. The hydrostatic head of NO_2 liquid is used to deliver it to a recuperator/evaporator that supplies gas to the NO_2 electrode. As illustrated in Figure 103, during charging, electrochemical displacement moves the flow of molten Na upward against the force of gravity, and molten $NaNO_2$ is gravity fed. NO_2 gas evolved during electrolysis of molten $NaNO_2$ is cold trapped at the liquid NO_2 reservoir which is cooled by a heat pump. The energy efficiency penalty for the charge/discharge cycle incurred by use of such a heat pump is estimated to be only 1%; a seasonally averaged heat pump COP of ~4 can be realized because the phase transition temperature for NO_2 is 21 °C. In addition to having no requirement for pumps, the cost of plumbing for a RIFB is very low compared to conventional flow batteries because the volumetric flow rates are so small; recall that unlike other flow battery technologies, RIFB has the advantage of no diluents.

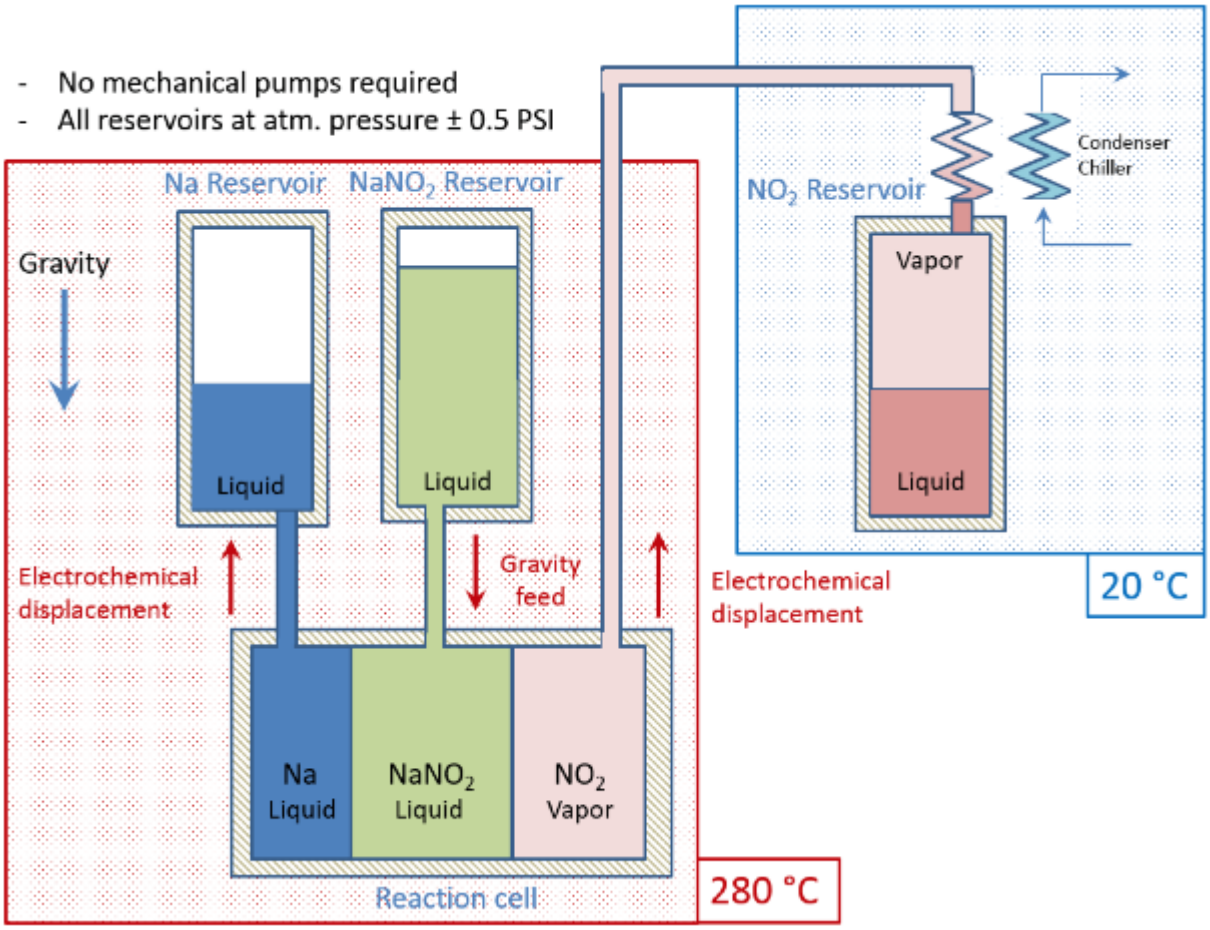

Figure 102: Charging process for Radical Ion Flow Battery.

- No mechanical pumps required
- All reservoirs at atm. pressure ± 0.5 PSI

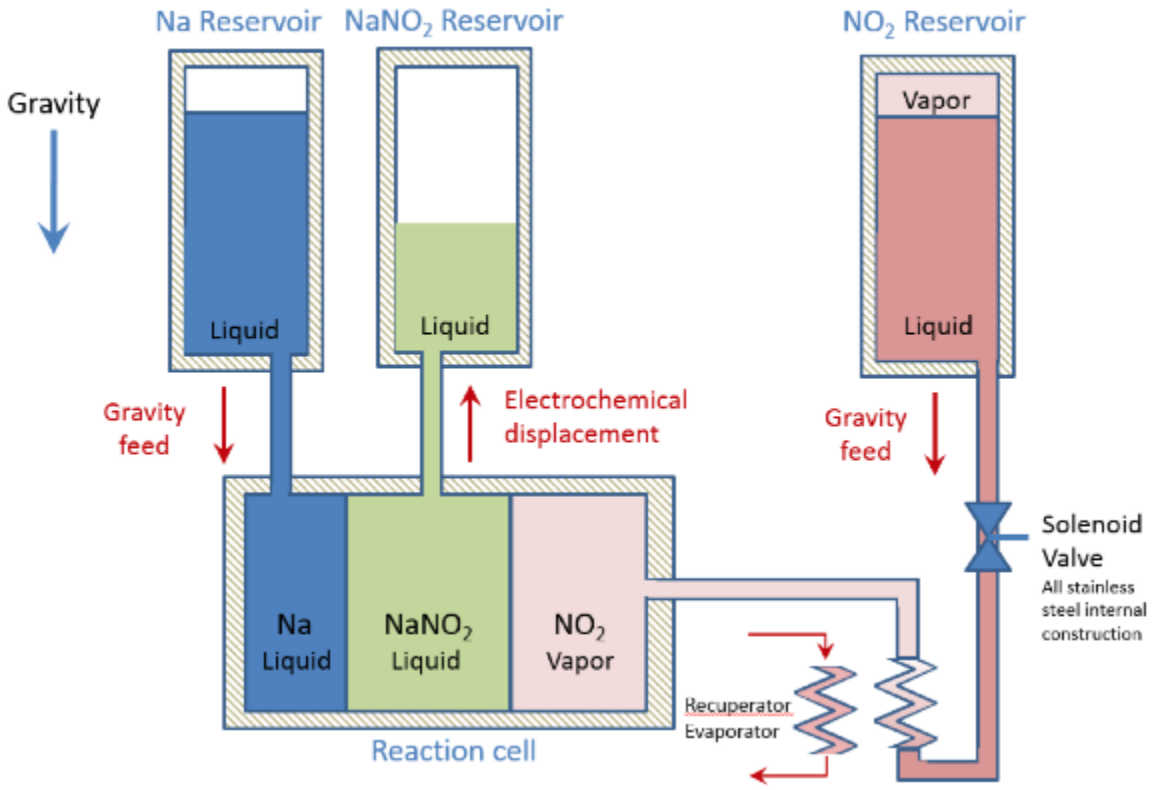

Figure 103: Discharging process for Radical Ion Flow Battery.

Referring now to Figure 104, to conduct this preliminary techno-economic analysis, we assumed that the end-use application would be 8-hour grid storage to buffer the diurnal variability of intermittent renewables. The system was sized at 100 MW power and 800 MW-hr storage capacity per the guidelines provided by Lazard in Figure 104. We also compared the footprint of an 80 MW-hr capacity RIFB installation to that of the recently constructed 80 MW-hr Mira Loma substation (Figure 105), which is based on Li-ion batteries from Tesla, Inc. As indicated in Figure 106, the RIFB installation is quite compact. This includes the inverter hardware, an appropriately sized heat pump, and appropriately sized tanks for reagents.

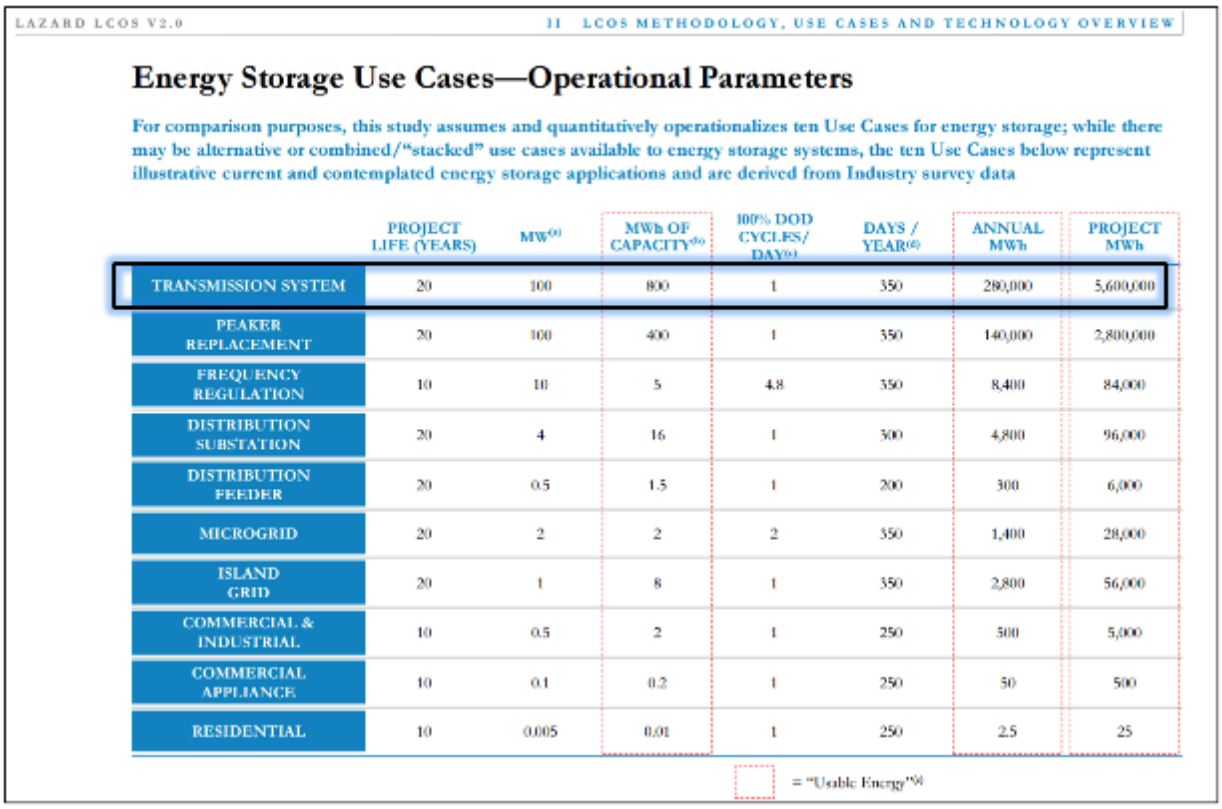

Figure 104: The RIFB target application space is 8-hour energy storage to address the intermittency problem of renewable energy. Seasonal energy storage is also likely to emerge as an important application space in some geographical regions.

Figure 105: The most recent deployment of a large-scale grid storage battery in the U.S.

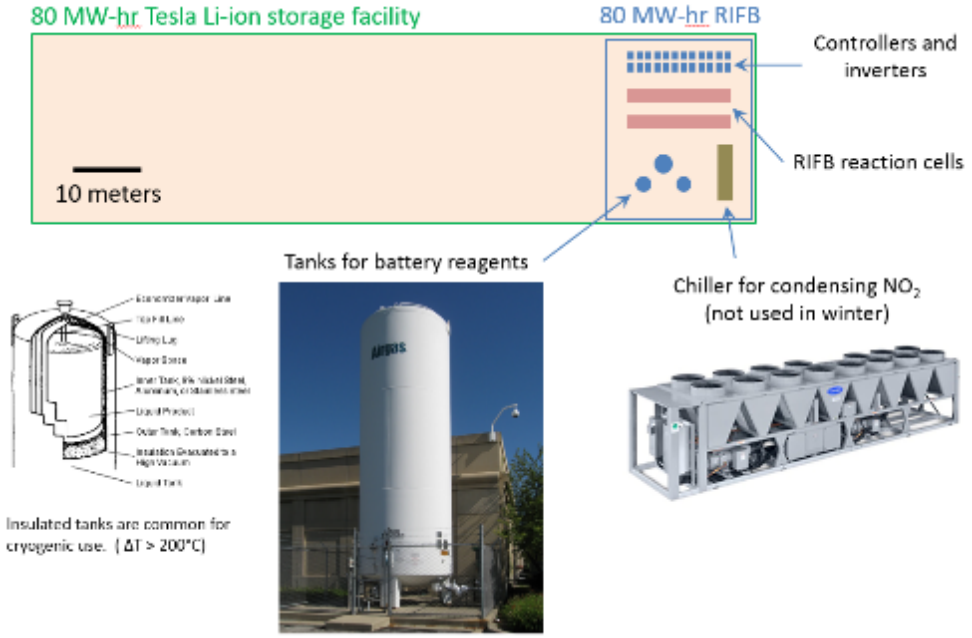

Figure 106: Comparing the calculated physical size of an 80 MW-hr RIFB installation an 80 MW-hr Li-ion installation.

The pie chart of Figure 107 shows the estimated CAPEX of RIFB sub-systems relative to DOE's aspirational goal of $100/kW-hr LCOE. The bidirectional dc-to-three-phase-ac inverter and its associated control system amounts to $26 per kW-hr of installed capacity. This number is based on inverter hardware commercially available from Tesla, and was verified by other industry stakeholders as a good conservative estimate. To obtain a conservative estimate for the cost of the storage tanks, we priced cryogenic storage tanks of comparable volume used to store liquid nitrogen. This is likely a conservative estimate because such tanks are constructed to operate at 400 psi for applications in which pressurized LN_2 blow off is the desired output. What the molten Na, molten $NaNO_2$, and liquefied NO_2 tanks do have in common with an LN_2 tank is steel construction and substantial thermal insulation. But there is no requirement for pressurized operation, so presumably construction would be significantly lighter than a tank rated for 400 psi. On the other hand, recalling Figure 83, earlier we advocated for a series cell configuration analogous to that used in a lead acid battery, comprising a common housing divided into individual cells by electrically insulating partitions, wherein each cell has a sodium electrode and an NO_2 electrode, both immersed in a local reservoir of $NaNO_2$ electrolyte. Such a system containing n cells would require n independent 3/8"-diameter steel lines to run from the RIFB cell stack to the sodium storage tank. The sodium storage tank would then require n electrically isolated vertical tubes, each containing a column of molten sodium metal that serves as the reservoir for an individual cell. Thus, the aforementioned molten sodium "tank" would actually comprise a thermally insulated hermetic enclosure housing an array of such cylindrical or prismatic tubes. The resulting cost increase would not be large, but it would not be negligible either. For this reason, LN_2 cryrogenic storage tanks rated at 400 psi operating pressure were used as conservative proxy for CAPEX estimation. The final figure was $6 per kW-hr of installed capacity based on cryogenic tanks sold by Linde.

Heat pump CAPEX for the 100-MW/800 MW-hr RIFB facility amounted to $1/kW-hr of installed capacity, and reagent cost amounted to $0.3/kW-hr of installed capacity. The very low cost of $NaNO_2$ ($0.40/kg), which is the only chemical reagent that would be required to commission a RIFB storage battery, is especially important for the application of seasonal grid storage. For seasonal grid storage, LCOE targets would likely be in the $5 to $20 per kW-hr of installed capacity range. In this application the low cost of the chemical reagent, the ability to use steel tanks, and the ability to keep tanks and plumbing very compact (because there is no dilution penalty) are all very important factors.

The remaining budget for the 100-MW/800 MW-hr RIFB facility of $67/kW-hr installed capacity would need to cover the cost of the cell stack, plumbing, siting, installation, and regulatory compliance. As currently planned, construction of the cell stacks requires no use of exotic materials, making the overall goal of $100/kW-hr of installed capacity very plausible. In the case of seasonal storage, the only subsystems that would need to be scaled up are the tanks, plumbing, and reagent. Given that these amount to an estimated $7.30/kW-hr of installed storage capacity, if the remainder of RIFB technology maturation is successful, the long-term goal of seasonal grid storage is potentially viable.

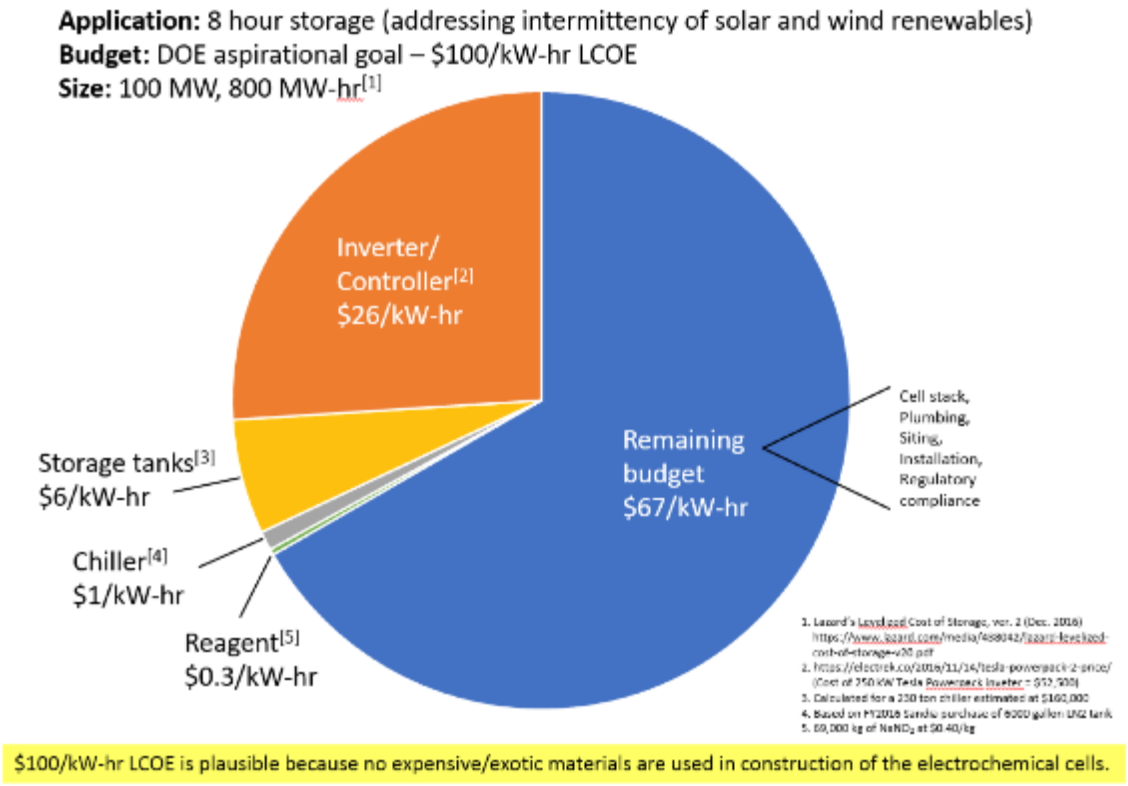

Figure 107: RIFB balance of plant, CAPEX estimates for major components.

Figures 108, 109, 110, and 111 are intended to provide a final summary of device architecture, application space, underlying design strategy, and feature set of Radical-Ion Flow Battery technology. It is our hope that the remaining derisking work can be conducted in the near future.

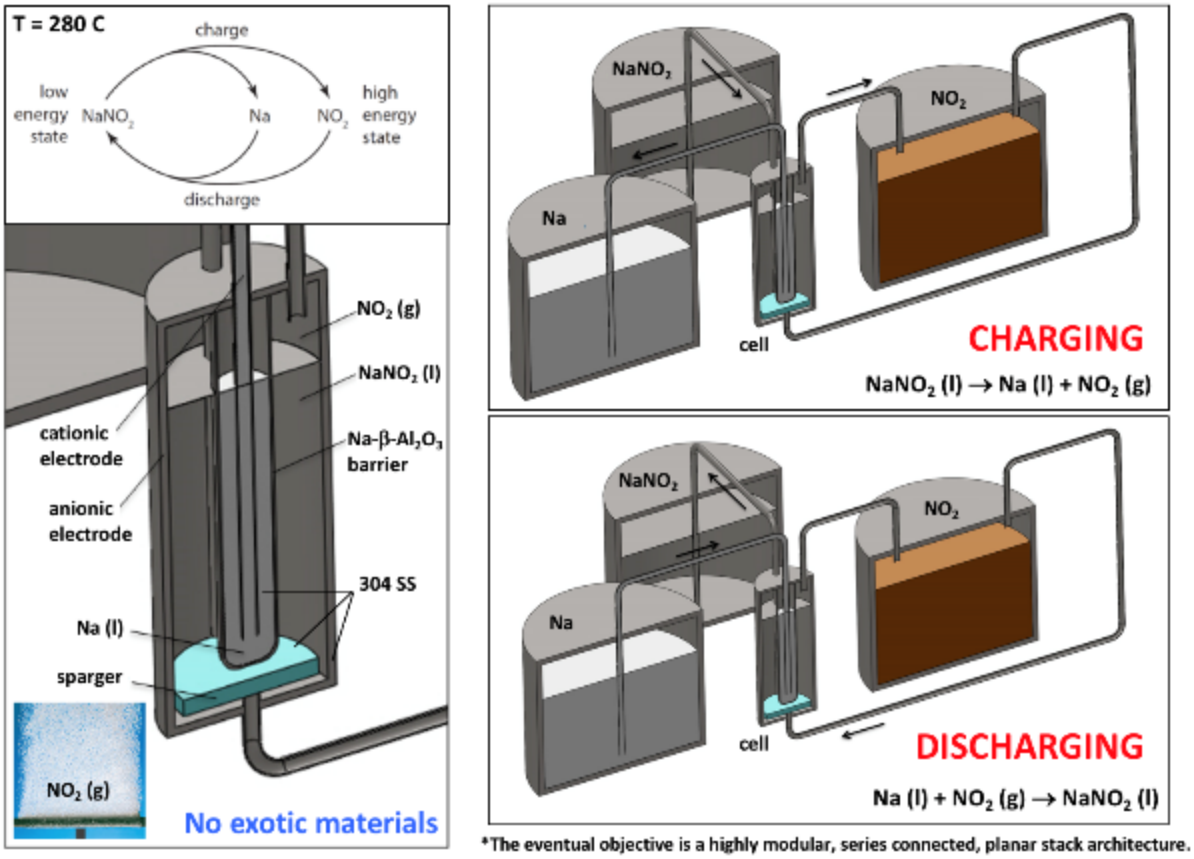

Figure 108: Summarization of the RIFB device architecture (multi-cell stack not shown*).

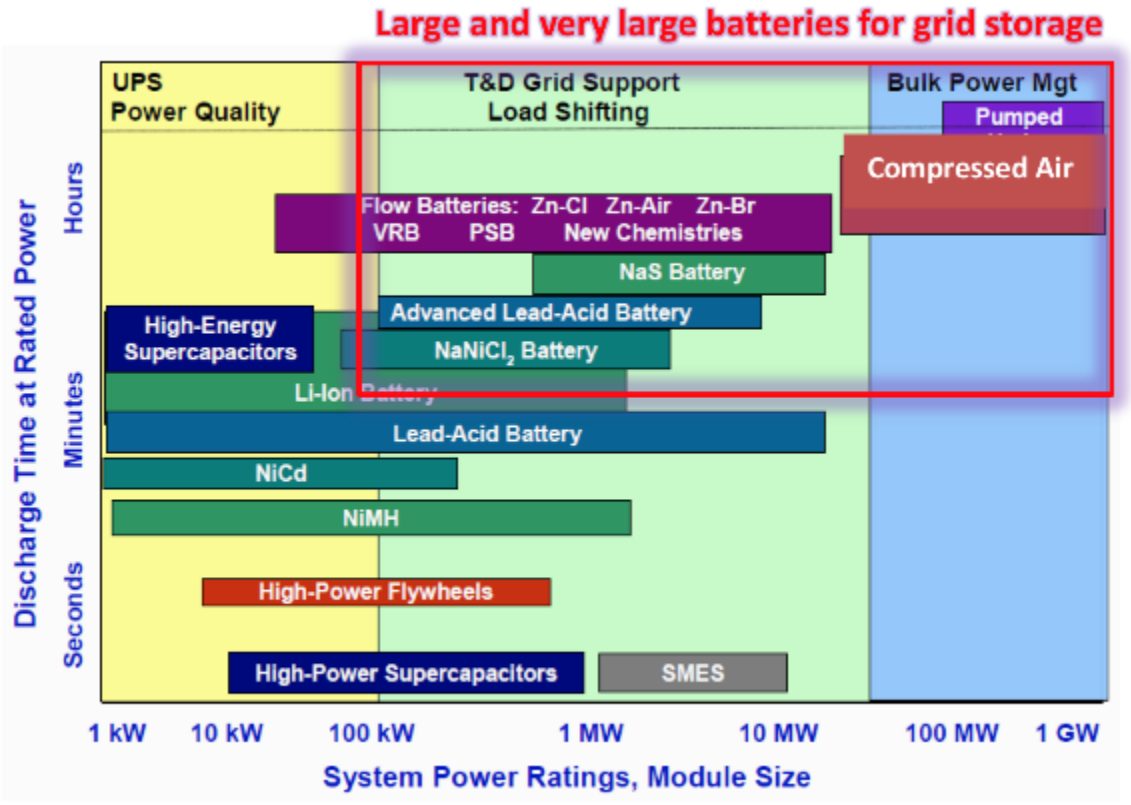

Adapted from *DOE/EPRI 2013 Electricity Storage Handbook*

Figure 109: Target application space for Radical-Ion Flow Battery technology.

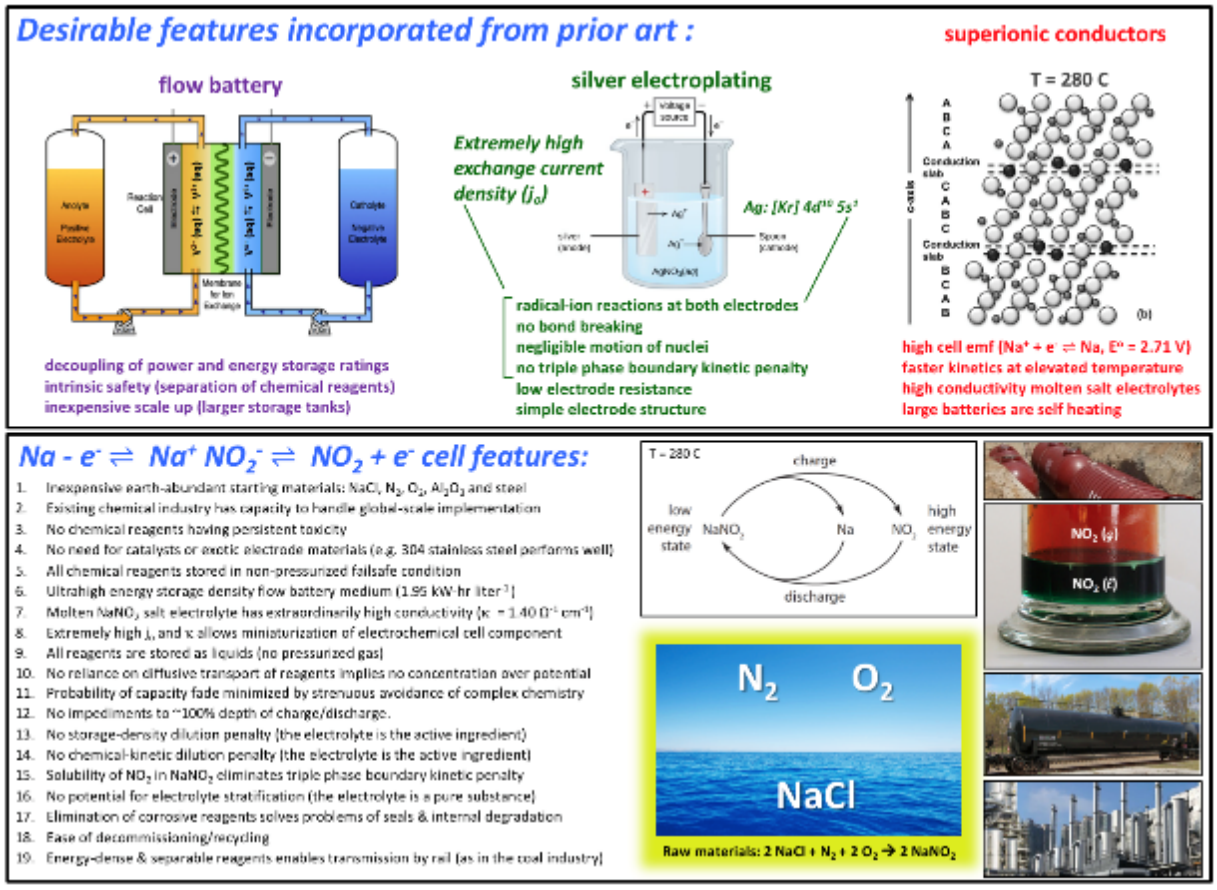

Figure 110: Condensed overview of logic underlying the Radical-Ion Flow Battery architecture.

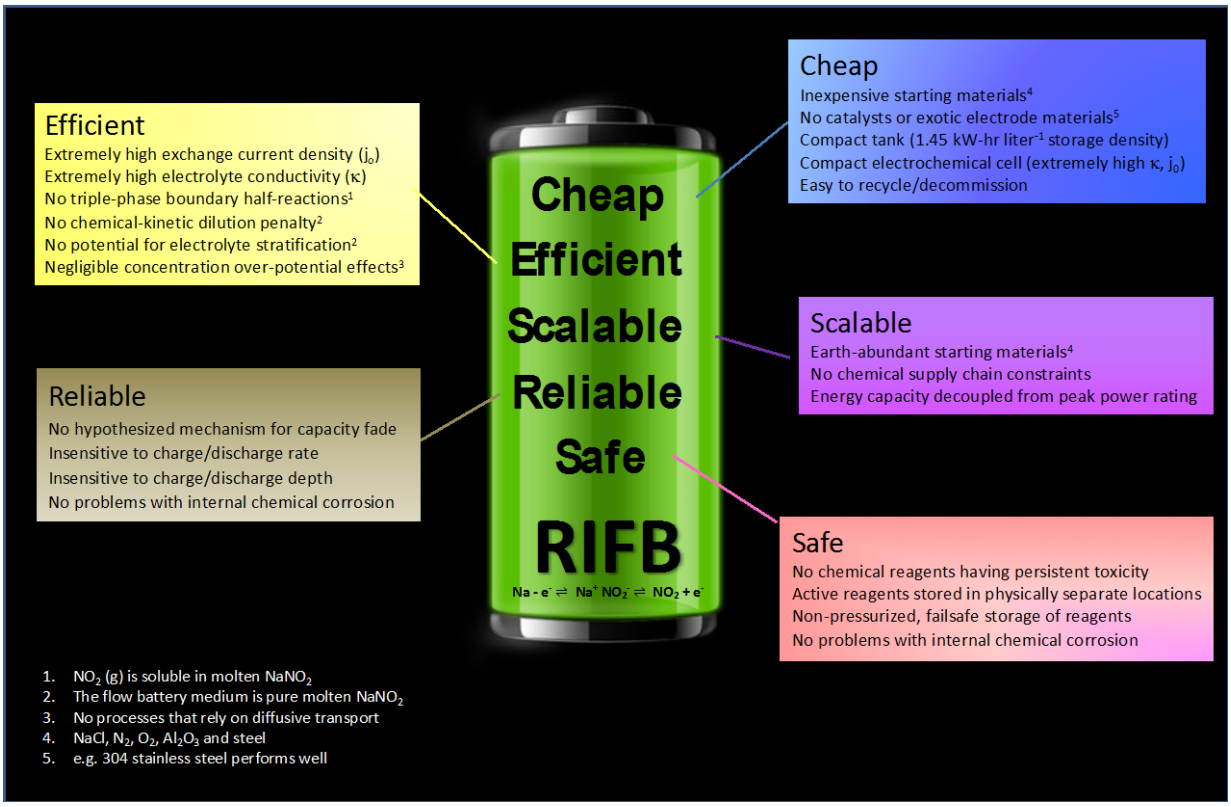

Figure 111: RIFB value proposition map. Attempting to achieve all objectives in a single device

6.3. Formal recommendations

It is the formal recommendation of this report that both the proposed hydrogen peroxide cycle and Radical-Ion Flow Battery should enter the next phase of R&D de-risking. Both of these proposed energy storage solutions survived numerous red teaming sessions under the scrutiny of a wide range of subject matter experts, and no showstoppers were identified for either technology. On the other hand, as described in this report, there are still many questions related to technology de-risking that constitute uncharted territory. Nonetheless, based on the technical due diligence completed to date, it would not be shocking if either of the two proposed SSIR energy storage solutions ultimately turns out to be competitive. At a minimum, the author hopes that this report serves to illustrate the advantages of using a first-principles-based, technology-agnostic problem solving methodology. In particular, the author has found this methodology effective for solving longstanding problems that have proven resistant to a monodisciplinary approach.

REFERENCES

[1] See for example, https://en.wikipedia.org/wiki/Photovoltaics#Efficiency

[2] Source: https://en.wikipedia.org/wiki/Energy_density_Extended_Reference_Table

[3] See for example, https://aziz.seas.harvard.edu/files/azizgroup/files/mja240.pdf

[4] See for example, https://en.wikipedia.org/wiki/High-test_peroxide

[5] H. Miyaoka, T. Ichikawa, and Y. Kojima, "Thermochemical energy storage by water splitting via redox reaction of alkali metals", Energy Procedia 49 (2014) pages 927-934.

[6] *Fuel Cell Fundamentals*, R. O'Hayre, S. Cha, W. Colella, and F. Prinz, John Wiley and Sons (2006).

[7] H. Darling, "Conductivity of Sulfuric Acid Solutions", Journal of Chemical Engineering Data, Vol. 9, No. 3, pg. 421 (1964).

[8] http://batteryuniversity.com/learn/article/what_causes_lithium_ion_to_die

[9] S. Zhang, "A review of electrolyte additives for lithium-ion batteries", Journal of Power Sources, Vol. 162, Issue 2, pg. 1379 (2005).

[10] http://www.greencarcongress.com/2015/11/20151105-jcesr.html

[11] R. Whitwam, "Doping lithium-ion batteries could prevent overheating and explosion", www.extremetech.com, June 25, 2015.

[12] http://batteryuniversity.com/learn/article/lithium_ion_safety_concerns

[13] https://blogs.wsj.com/digits/2011/07/07/fanfare-for-a-new-way-to-fan-computer-chips/

[14] A. Kisza, J. Kazmierczak, B. Borresen, G. M. Haarberg, and R. Tunold, "The kinetics of the sodium electrode reaction in molten sodium chloride", J. Electrochem. Soc., Vol. 142, No. 4, page 1035-1040, April 1995.

[15] http://www.wiredchemist.com/chemistry/data/entropies-inorganic

[16] http://www.ne.anl.gov/eda/ANL-RE-95-2.pdf

[17] L Kourkova, R. Svoboda, G Sadovska, V. Podzemna, and A. Kohutova, "Heat Capacity of $NaNO_2$", Thermochimica Acta, 491, Pg. 80 (2000).

[18] G. Rayner-Canham, T. Overton, Descriptive Inorganic Chemistry, W. H. Freeman and Company (2006).

[19] It is possible that a two-step reaction mechanism involving some degree of adsorption of NO_2/NO_2^- on the surface of the electrode is involved, but to the extent that the kinetics of the NO_2/NO_2^- interconversion process illustrates no sensitivity to the composition of the electrode surface, the distinction between a one-step and two-step process is not particularly important.

[20] http://www.wiredchemist.com/chemistry/data/bond_energies_lengths.html

[21] G. Janz, U. Krebs, H. Siegenthaler, and R. Thompkins, "Molten Salts: Volume 3, Nitrates, Nitrites, and Mixtures, Electrical Conductance, Density, Viscosity, and Surface Tension Data", J. Phys. Chem. Ref. Data, Vol. 1, No. 3 (1972).

[22] *Fuel Cell Fundamentals*, R. O'Hayre, S. Cha, W. Colella, and F. Prinz, John Wiley and Sons (2006).

[23] https://en.wikipedia.org/wiki/Lithium-ion_battery

[24] https://en.wikipedia.org/wiki/World_energy_consumption#cite_note-EIAIES2015-17

[25] See for example, R. Naam, "Solar + Wind, More than the Sum of Their Parts", April 28, 2015, http://rameznaam.com/2015/04/28/solar-wind-more-than-the-sum-of-their-parts/

[26] "Chlorine Market is Fastest Growing Chemical Sector to 2019 - Due to Increased Demand From the Chemical/EDC/PVC Industries", http://www.prnewswire.com/news-releases/chlorine-market-is-fastest-growing-chemical-sector-to-2019---due-to-increased-demand-from-the-chemicaledcpvc-industries-496966741.html

[27] M. Martins, A. Calandra, A. Arvia, "Kinetics and mechanism of anodic oxidation of nitrite ion in nitrate melts on platinum electrodes", Electrochemica Acta, Vol. 15, p. 11 (1970).

[28] http://encyclopedia.airliquide.com/images_encyclopedie/VaporPressureGraph/Nitrogen_dioxide_Vapor_Pressure.GIF

[29] K. Mazloomi1,*, N. Sulaiman1, H. Moayedi, "Electrical Efficiency of Electrolytic Hydrogen Production", Int. J. Electrochem. Sci., 7, 3314 – 3326 (2012).
[30] U.S. Energy Information Administration: http://www.eia.gov/tools/faqs/faq.cfm?id=427&t=3
[31] "Impacts of Coal Power: Water Use", Union of Concerned Scientists, http://www.ucsusa.org/clean_energy/coalvswind/c02b.html#.Vq-urLIrJaQ
[32] "Particulates and coal", http://www.sourcewatch.org/index.php/Particulates_and_coal
[33] "Sulfur dioxide and coal", http://www.sourcewatch.org/index.php/Sulfur_dioxide_and_coal
[34] "Heavy metals and coal", http://www.sourcewatch.org/index.php/Heavy_metals_and_coal
[35] B. Sorensen, *Renewable Energy*, 2nd edition, Elsevier (1998).
[36] Table 4-17: "Class I Rail Freight Fuel Consumption and Travel", U.S. Department of Transportation website, http://www.rita.dot.gov/bts/sites/rita.dot.gov.bts/files/publications/national_transportation_statistics/html/table_04_17.html
[37] U.S. Energy Information Administration: https://www.eia.gov/tools/faqs/faq.cfm?id=667&t=2
[38] M. Mintz, C. Saricks, A. Vyas, Argonne National Laboratory, "Coal-by-Rail: A Business-as-Usual Reference Case", http://energy.gov/sites/prod/files/2015/04/f22/QER%20Analysis%20-%20Coal-by-Rail%20Business-as-Usual%20Reference%20Case.pdf
[39] M. Mintz, C. Saricks, A. Vyas, Argonne National Laboratory, "Coal-by-Rail: A Business-as-Usual Reference Case", http://energy.gov/sites/prod/files/2015/04/f22/QER%20Analysis%20-%20Coal-by-Rail%20Business-as-Usual%20Reference%20Case.pdf
[40] See for example http://www.hazmat101.com/hazmat/docs2/silhoutes.pdf
[41] See for example http://www.hazmat101.com/hazmat/docs2/silhoutes.pdf
[42] 49 CFR 173.314 - Compressed gases in tank cars and multi-unit tank cars. https://www.law.cornell.edu/cfr/text/49/173.314
[43] See for example https://www.youtube.com/watch?v=BvTkefJHfC0
[44] J. Sudworth, A.R. Tiley, *The Sodium Sulfur Battery*, Chapman and Hall Ltd, London (1985).
[45] G. Janz, U. Krebs, H. Siegenthaler, and R. Thompkins, "Molten Salts: Volume 3, Nitrates, Nitrites, and Mixtures, Electrical Conductance, Density, Viscosity, and Surface Tension Data", J. Phys. Chem. Ref. Data, Vol. 1, No. 3 (1972).
[46] "Cost of transporting coal to power plants rose almost 50% in decade", U.S. Energy Information Agency, November 19, 2012, https://www.eia.gov/todayinenergy/detail.cfm?id=8830
[47] Please see http://www.eia.gov/forecasts/aeo/electricity_generation.cfm
[48] U.S. Energy Information Administration: https://www.eia.gov/tools/faqs/faq.cfm?id=667&t=2
[49] http://www.ne.anl.gov/eda/ANL-RE-95-2.pdf
[50] L Kourkova, R. Svoboda, G Sadovska, V. Podzemna, and A. Kohutova, "Heat Capacity of $NaNO_2$", Thermochimica Acta, 491, Pg. 80 (2000).
[51] http://webbook.nist.gov/cgi/cbook.cgi?ID=C10102440&Type=JANAFG&Plot=on
[52] http://encyclopedia.airliquide.com/Encyclopedia.asp?GasID=25
[53] *"Costs of storing and transporting hydrogen Pag.50" (PDF). www1.eere.energy.gov. Retrieved* 2015-04-06.
[54] See for example: http://www.psmag.com/nature-and-technology/why-californias-solar-power-could-soon-be-curtailed
[55] http://www.fueleconomy.gov/feg/Find.do?action=sbs&id=35980&id=36009&id=36008&id=35994
[56] http://www.roperld.com/science/TeslaModelS.htm
[57] Edelstein, Stephen (2015-09-24). "Tesla Model 3 Will Benefit From Lowest Battery Costs of Any Maker: Jefferies". *Green Car Reports*. Retrieved 2015-11-06.
[58] http://www.greentechmedia.com/articles/read/Why-Lithium-Isnt-the-Big-Worry-for-Li-ion
[59] J. Ohi, "Environmental, Health and Safety Issues of Sodium-Sulfur Batteries for Electric and Hybrid Vehicles", Volume 1: Cell and Battery Safety, http://www.nrel.gov/docs/legosti/old/4678.pdf, NREL/TP-262-4678 (1992).

[60] http://batteryuniversity.com/learn/article/bu_210a_why_does_sodium_sulfur_need_to_be_heated
[61] http://www.wiredchemist.com/chemistry/data/entropies-inorganic
[62] https://en.wikipedia.org/wiki/Lithium_nitrite
[63] See for example: http://phys.org/news/2013-12-scientists-ion-selective-membrane-ultra-stable-lithium.html
[64] http://www.wiredchemist.com/chemistry/data/entropies-inorganic
[65] http://www.nist.gov/data/PDFfiles/jpcrd11.pdf
[66] See for example: http://www.ionotec.com/conductive-ceramics.html
[67] K. Stern, *High Temperature Properties and Thermal Decomposition of Inorganic Salts with Oxyanions*, CRC press (2001).
[68] K. Stern, *High Temperature Properties and Thermal Decomposition of Inorganic Salts with Oxyanions*, CRC press (2001).
[69] https://en.wikipedia.org/wiki/Diagonal_relationship
[70] https://en.wikipedia.org/wiki/Calcium_nitrite
[71] See for example: http://www.sisweb.com/vacuum/o-rings/viton.htm
[72] C. Bale, "The K-Li (Potassium-Lithium) System", Bulletin of Alloy Phase Diagrams, Vol. 10, No. 3, pg. 262 (1989).
[73] T.Bauer, D.Laing, and R.Tamme, "Recent Progress in Alkali Nitrate/Nitrite Developments for Solar Thermal Power Applications", Molten Salts Chemistry and Technology Conference, MS9, Trondheim, Norway, 5 - 9 June 2011, Page 1 / 10
[74] T.Bauer, D.Laing, and R.Tamme, "Recent Progress in Alkali Nitrate/Nitrite Developments for Solar Thermal Power Applications", Molten Salts Chemistry and Technology Conference, MS9, Trondheim, Norway, 5 - 9 June 2011, Page 1 / 10.
[75] *Lu, X.; Li, G.; Kim, J. Y.; Mei, D.; Lemmon, J. P.; Sprenkle, V. L.; Liu, J. (2014). "Liquid-metal electrode to enable ultra-low temperature sodium–beta-alumina batteries for renewable energy storage". Nature Communications 5. doi:10.1038/ncomms5578.*
[76] F. Lalere et al, "All solid state NASICON sodium battery operating at 200° C", Journal of Power Sources, Volume 247, 1 February 2014, Pages 975–980.
[77] D. Pysz et al, "Stack and draw fabrication of soft glass microstructured fiber optics", BULLETIN OF THE POLISH ACADEMY OF SCIENCES TECHNICAL SCIENCES, Vol. 62, No. 4 (2014).
[78] M. Pellow, C. Emmott, C. Barnhartd and S. Bensonaef, "Hydrogen or batteries for grid storage? A net energy analysis", Energy Environ. Sci., Vol. 8, pgs. 1938-1952 (2015).
[79] See for example, F. Krok, Influence of sintering conditions on chemical composition of NASICON, Solid State Ionics, Volume 24, Issue 1, June 1987, pages 21-28.
[80] M. H. Braga, A. J. Murchison, J. A. Ferreira, P. Singh, J. B. Goodenough, (2016), "Glass-amorphous alkali-ion solid electrolytes and their performance in symmetrical cells," *Energy and Environmental Science,* **9**, 948-954.
[81] See for example, S. Dai, M. Rodriguez, and J. Griego, "Sealing Glass-Ceramics with Near Linear Thermal Strain, Part I: Process Development and Phase Identification", Journal of the American Ceramic Society, Vol 99, No 11, pages 3718-25, Nov 2016.
[82] https://www.nde-ed.org/GeneralResources/MaterialProperties/ET/Conductivity_Misc.pdf
[83] M. H. Braga, A. J. Murchison, J. A. Ferreira, P. Singh, J. B. Goodenough, (2016), "Glass-amorphous alkali-ion solid electrolytes and their performance in symmetrical cells," *Energy and Environmental Science,* **9**, 948-954.
[84] RADICAL-ION BATTERY AND OPERATION THEREOF, J. P. Koplow, U. S. Patent Application filed February 16, 2017, claiming priority to United States Provisional Patent Application No. 62/297,022, filed on February 18, 2016, and entitled "Novel Battery for Large-scale, Low-cost, Electrochemical Storage of Energy".

[85] See for example page 8 of "Lazard's Levelized Cost of Storage – Version 2.0", December 2016, https://www.lazard.com/media/438042/lazard-levelized-cost-of-storage-v20.pdf
[86] R. O'Hayre, S. Cha, W. Colella, and F. Prinz, Fuel Cell Fundamentals, John Wiley and Sons (2006). The best electrolytes in fuel cells have conductivities of order 0.1 Ω-1 cm-1, and typical conductivities of electrolyte mixtures used in lithium ion batteries are ~0.01 Ω-1 cm-1 at room temperature (increasing by approximately 30–40% at 40 °C and decreasing slightly at 0 °C).
[87] See for example: https://www.alibaba.com/showroom/sodium-nitrite-price.html
[88] In the U.S. molten sodium metal is transported by rail in DOT 105J300W tank cars having a name plate capacity of 33,600 gallons. See for example http://www.hazmat101.com/hazmat/docs2/silhoutes.pdf; In the U.S. liquefied nitrogen dioxide is transported in DOT 105A500W tank cars with a name plate capacity of 20,500-gallons. See for example: 49 CFR 173.314 - Compressed gases in tank cars and multi-unit tank cars. https://www.law.cornell.edu/cfr/text/49/173.314
[89] The most comprehensive study was conducted in 1970 using a platinum electrode: M. Martins, A. Calandra, A. Arvia, "Kinetics and mechanism of anodic oxidation of nitrite ion in nitrate melts on platinum electrodes", Electrochemica Acta, Vol. 15, p. 11 (1970).
[90] R. P. T. Tomkins, Gases in Molten Salts, IUPAC Solubility Data Series, Volume 45/46 (1991).
[91] There is extensive fuel cell literature on the topic of gaseous diffusion electrode design. See for example: S. C. Yang, "Simulation and Optimization of porous gas-diffusion electrodes used in hydrogen/oxygen phosphoric acid fuel cells." UMI Publishing (1980).

DISTRIBUTION

2 DOE Solar Energy Technology Office
OFFICE of ENERGY EFFICIENCY & RENEWABLE ENERGY
Forrestal Building
1000 Independence Avenue, SW
Washington, DC 20585

1	MS 9052	Wayne Staats	08366
1	MS 9052	Arthur Kariya	08366
1	MS 9102	Justin Vanness	08736
1	MS 9052	Amanda Dodd	08366
1	MS 9054	Chris Moen	08360
1	MS 9054	Robert Hwang	08300
1	MS 1033	Abraham Ellis	08812
1	MS 1138	Charlie Hanley	08810
1	MS 0613	Travis Anderson	02546
1	MS 0734	Chad Staiger	08824
1	MS 1411	Leo Small	01874
1	MS 1217	David Wheeler	05864
1	MS 0736	Pat Brady	08840
1	MS 9291	Anup Singh	08600
1	MS 9153	Michael Hardwick	08200
1	MS 1169	Charles Barbour	01300
1	MS 9033	David Farley	08648
1	MS 9033	Scott Bisson	08648
1	MS 9161	Vitalie Stavila	08341
1	MS 9161	Christian Mailhiot	08340
1	MS 1188	Craig Lawton	08834
1	MS 1108	Babu Chalamala	08811
1	MS 1104	Amy Halloran	08820
1	MS 0721	Carol Adkins	08800
1	MS 0359	Greg Frye-Mason	01171
1	MS 9403	LeRoy Whinnery	08200
1	MS0899	Technical Library	9536 (electronic copy)


Sandia National Laboratories